THE ISOLATION OF HUMAN ROD AND CONE PHOTORECEPTOR ACTIVITY COMBINING ELECTRORETINOGRAPHY AND SILENT SUBSTITUTION TECHNIQUES

J. MAGUIRE

Ph.D

2017

The Isolation of Human Rod and Cone Photoreceptor Activity combining Electroretinography and Silent Substitution Techniques

John Charles MAGUIRE

Submitted for the degree of

Doctor of Philosophy

Department of Optometry and Vision Science

University of Bradford

2017

Abstract

The Isolation of Human Rod and Cone Photoreceptor Activity Combining Electroretinography and Silent Substitution Techniques

John Charles Maguire

Keywords: electroretinography, human vision, retina, photoreceptors, rods and cones

Aims: The electroretinogram (ERG) can be used to independently assess the function of rod and cone photoreceptors within the human retina. The work in this thesis sought to investigate an alternative method of recording the ERG, using the silent substitution paradigm (Estevez and Spekreijse 1982). The aims are separated into two parts, firstly, the isolation and characterisation of the non-dark adapted rod photoreceptor response, and secondly, characterising the ERG response from L-, M- and S-cones.

Methods: Rod, L-, M- and S-cone isolating as well as non-isolating sinusoidal flicker and transient square-wave stimuli were generated on a 4 primary LED ganzfeld stimulator to elicit ERGs from non-dark adapted participants with normal and compromised rod or cone function.

Results: The results from the rod experiments showed that ERGs elicited by rod isolating silent substitution stimuli exhibit low-pass temporal frequency response characteristics with an upper response limit of 30Hz and saturate beyond 1000ph Td. Responses are optimal between 5 – 8 Hz and between 10-100 photopic Td. There is a significant correlation between the response amplitudes obtained with the silent substitution method and current standard clinical protocols. The results from the cone experiments showed that the L-, M- and S-cone stimulation produced ERGs with very different morphologies. L- and M-cone stimulation is of limited use as an objective measure of colour vision deficiency.

Conclusion: Silent substitution provides an effective method for the isolation of human rod and cone photoreceptor function in subjects when stimuli are used within appropriate parameter ranges.

Table of Contents

List of Figures

Chapter 1

Anatomy and Physiology of the Retina

1.1 The Retina

Light is essential for vision. We see the surrounding world when light is reflected from our immediate environment and enters our eyes. The lens in the eye focuses the light onto the retina at the back of the eye. The retina is a laminar structure with a thickness of 0.5mm (Kolb 1991). Within that 0.5mm are ten well defined layers made up of many different cell types (Figure 1.1).

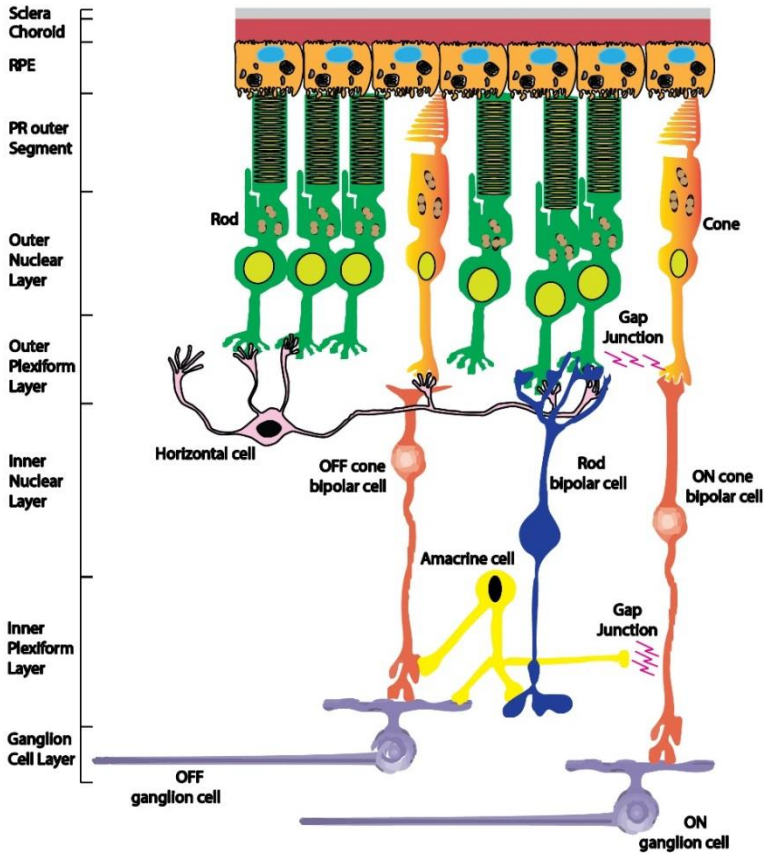

Figure 1.1. The laminar structure of the human retina and the major individual types of cells. The retina is structured in such a way that light has to pass through all of the cells before it comes into contact with the photoreceptors.

1.2 Photoreceptors

Photoreceptors are light sensitive neurons within the retina. There are five types of photoreceptor in the human retina: rods, three types of cones (long- (L), middle- (M) and short- (S) wavelength sensitive) and the relatively recently discovered intrinsic photosensitive ganglion cells (Berson et al. 2002; Hattar et al. 2002). This introduction will focus primarily on the rod and cone system.

The reason we have rods and cones is because our vision has to operate over a 12 log range unit range of natural light levels from absolute darkness to bright sunlight. To deal with such a wide range we have two systems; a rod system for scotopic light levels (10^{-6} – 10^{-3} cd.s.m^{-2}), and a cone system for photopic light levels (10 – 10^{8} cd.s.m^{-2}) where the rods become saturated. In between these levels exists a mesopic range of light levels (extending between 10^{-3} – $10^{-0.5}$ cd.s.m^{-2}) over which we use both the rod and cone system. The rod system is optimised for night vision and therefore possesses a high sensitivity to light, but at the expense of good visual acuity and colour detection. Cones, on the other hand, are optimised for daytime vision, enabling the perception of fine detail and coloured images, but with reduced light sensitivity (Figure 1.2).

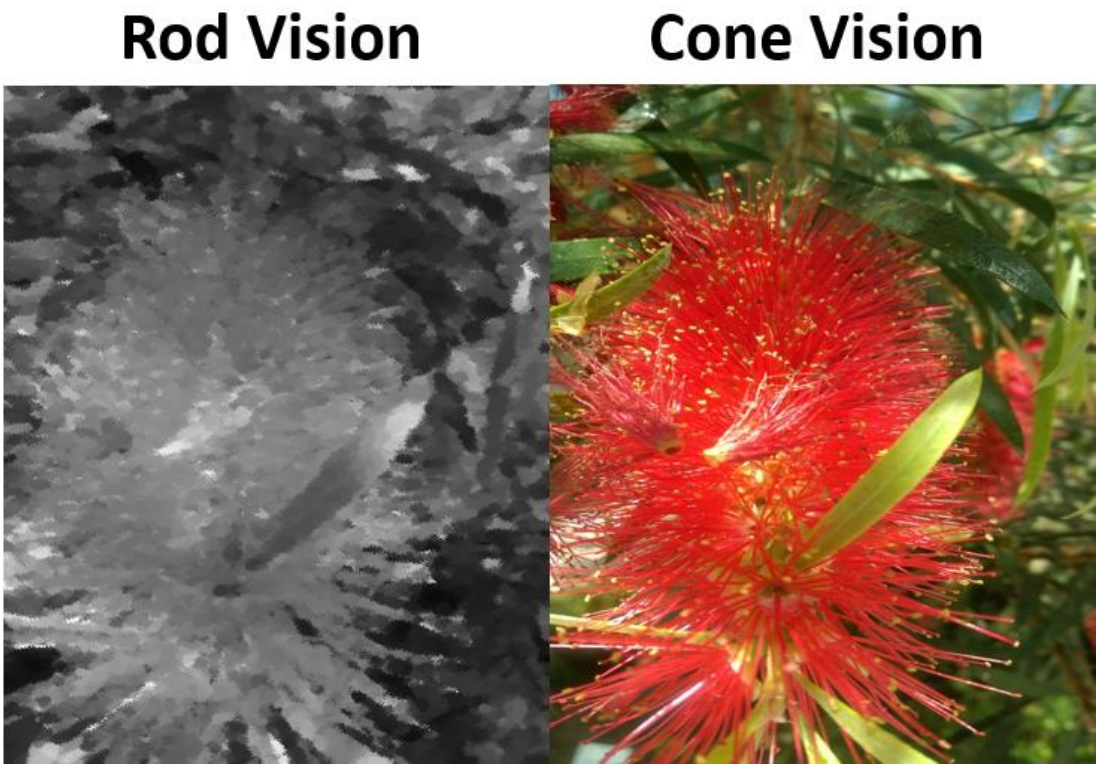

Figure 1.2. Image of the same scene viewed using achromatic rod vision with poor visual acuity on the left compared to the fine detail, chromatic vision of the cone system

There are approximately 95-115 million rods in the human retina, with peak density at an eccentricity approximately 20 degrees to the fovea (Curcio et al. 1990; Ahnelt 1998) and approximately 5-6 million cones (Curcio et al. 1990) with the highest density per mm^2 seen in the fovea and decreasing rapidly towards the peripheral retina (Figure 1.3), however in absolute terms the periphery contains the majority of cones. Rods are completely missing from the fovea centralis, a central portion of the fovea with a diameter of approximately 0.3mm.

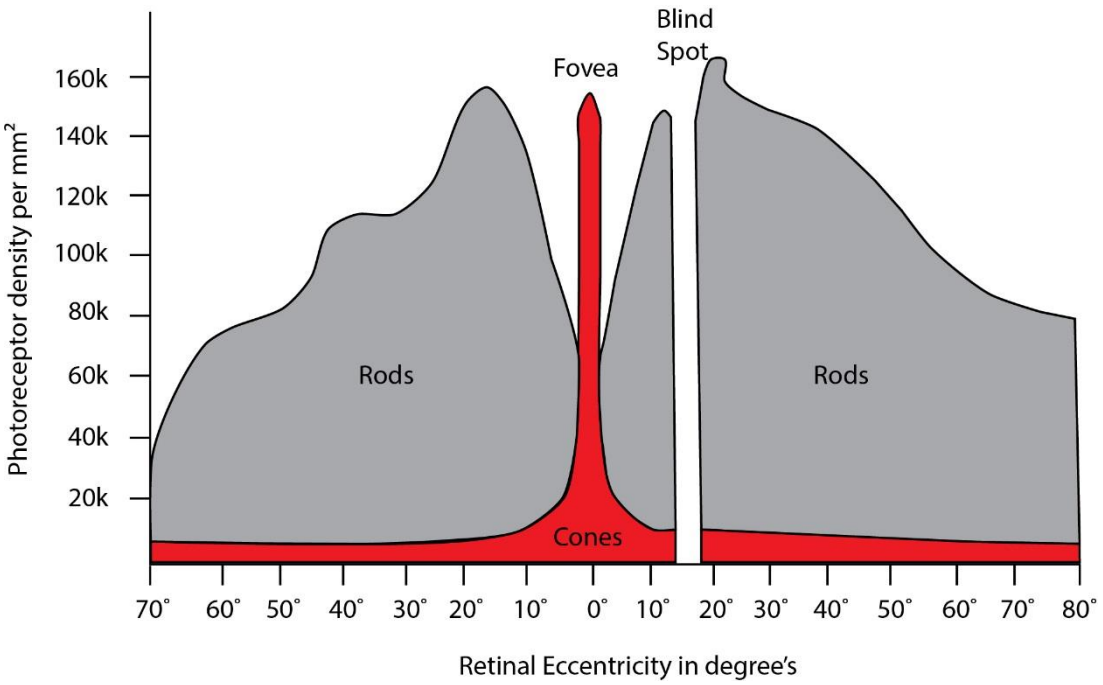

Figure 1.3. The spatial distribution of the rod and cone photoreceptors in the human retina. The density of cones in central vision is high, however the large retinal area assigned to peripheral vision means that there are far more cones in peripheral retina. Modified from Rodieck 1988

1.2.1 Rod and cone structure

Rod photoreceptors are approximately 2 microns in diameter and can be anatomically divided into an outer segment and an inner segment. The outer segment contains approximately 1000 disc like structures, stacked tightly together. These discs are derived from and are contained within, the plasma membrane (Cohen 1968; Cohen 1972). Each disc contains a double layer of the light sensitive visual pigment rhodopsin (Lamb and Pugh 1992). The inner segment contains two sub regions, the myoid and the ellipsoid region, which serve to maintain and distribute metabolites and nutrients throughout the cell. The cilium is a long, thin structure joining both sections and facilitating enzymatic and protein transport (Kanski and Bowling 2011).

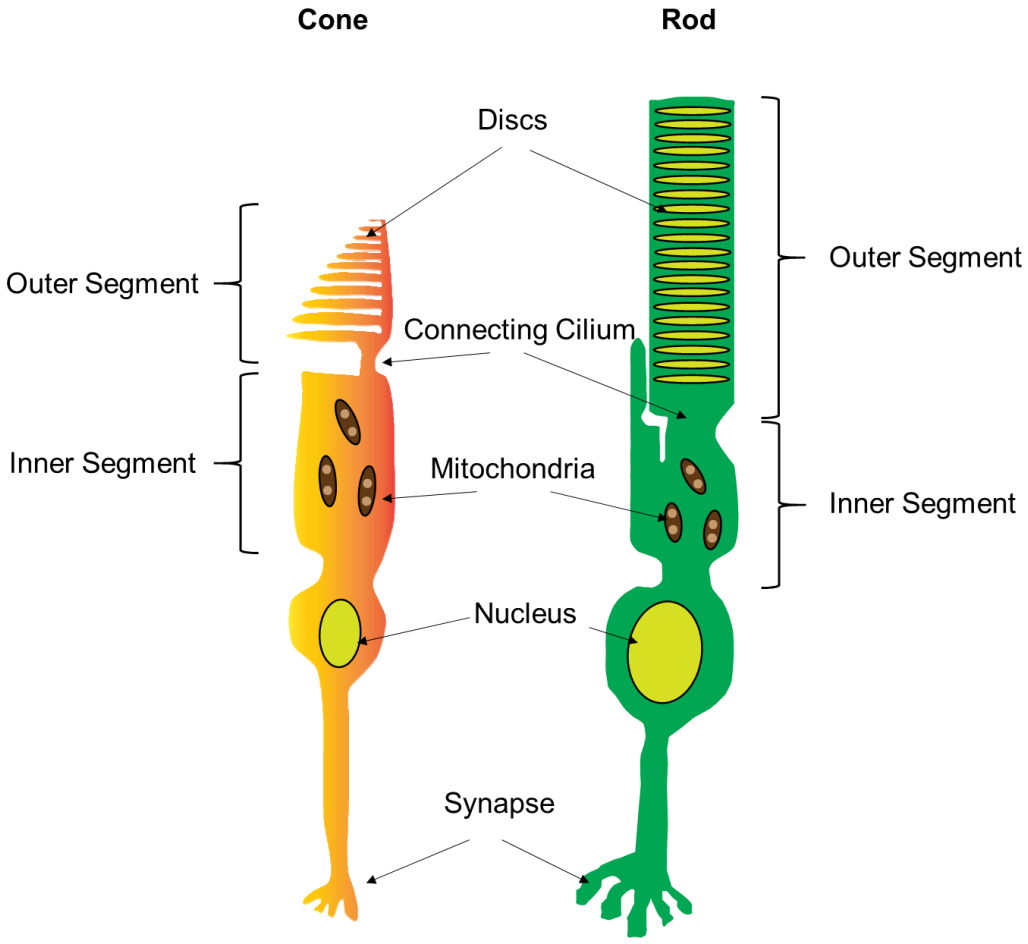

Figure 1.4. Illustration of the cone and rod photoreceptors detailing the general internal and external cellular structures.

The basic cone structure is similar to that of the rod photoreceptors, in that they have both an inner and outer segment. The main differences between cones and rods are: 1) cones possess a larger diameter than the rods, typically 6µm compared to 2µm (Curcio et al. 1990). 2) The cone outer segment consists of invaginations culminating in a conical peak (Figure 1.4) whereas the rod outer segment contains separate discs neatly stacked on top of one another. 3) The rods and cones possess different visual pigments.

1.2.2 Photoreceptor Pigments

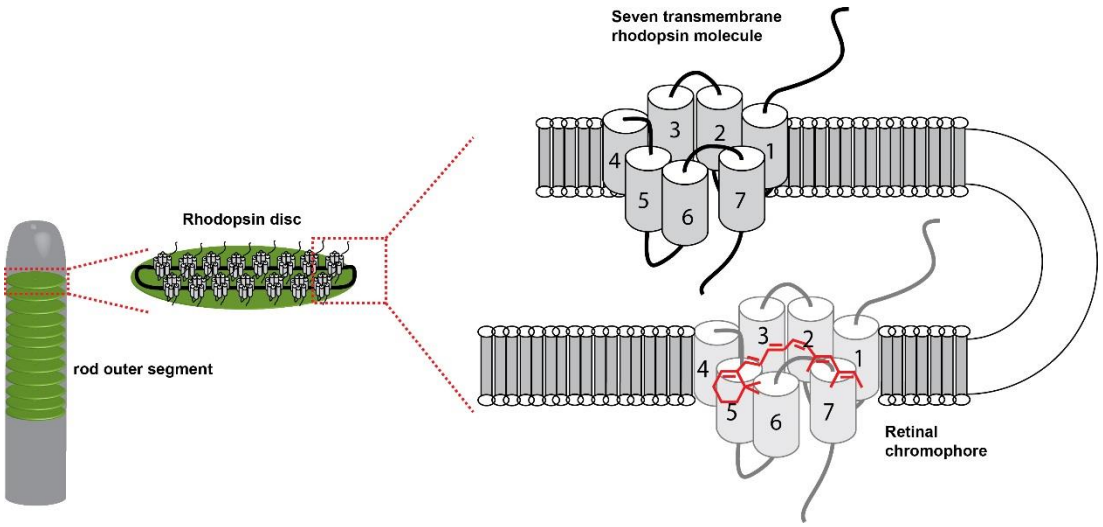

Figure 1.5. Illustration of the disc structure in the rod outer segment (left) along with an enlarged representation of a single disc (middle) and a further enlarged representation of the rhodopsin structure (right)

In rods the visual pigment is rhodopsin, which is a seven transmembrane protein, made up of 348 amino acid residues, surrounding the chromophore retinol (Hargrave 2001). The chromophore is the light catching portion of the molecule, called 11 cis retinal. It is a 15 carbon molecule with a twist at the 11th carbon. There is a double bond at this point made up of σ bond and π bond to prevent rotation (Pugh and Lamb 2000; Lamb and Pugh 2006). When a photon of light is absorbed by the molecule (Figure 1.7 stages 1 and 2), the energy of the photon causes the π bond to be raised to a higher level, allowing rotation about the σ bond and a subsequent conformational change from 11-cis-retinal to All-trans-retinal. The energy that it takes to complete the conformational change is directly related to the spectral sensitivity of the photopigment. This is the initial stage in a series of electrochemical changes in the process of phototransduction (Figure 1.7) (Fu and Yau 2007).

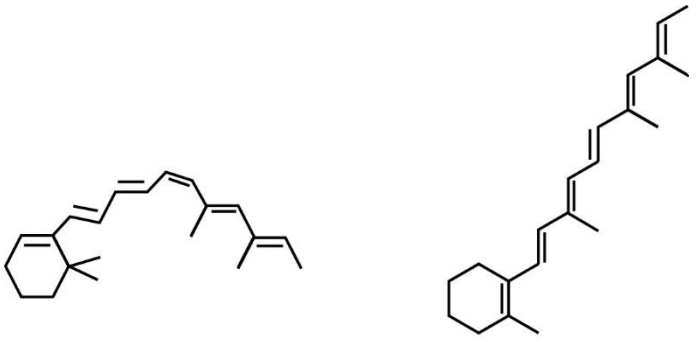

Figure 1.6. The chemical structure of the retinal chromophore before (left) and after (right) absorption of a photon.

The rhodopsin molecule undergos several transitional changes (Forrester 2002) and plays an important role by triggering signalling pathways (Figure 1.7). It does this by acting on the G protein transducin (Figure 1.7 stage 3), a three sub unit protein, alpha, beta and gamma ($G_t\alpha\beta\gamma$) (Hargrave and McDowell 1992; Pugh and Lamb 2000), which plays a vital part in cellular activity, predominantly in signal transmission. This causes the alpha sub-unit ($G_t\alpha$) to disassociate (Figure 1.7 stage 4), thereby inactivating transducin $G_t\beta\gamma$ (Hargrave and McDowell 1992; Pugh and Lamb 2000). The active $G_t\alpha$ will then go on to activate phosphodiesterase 6 (Figure 1.7 stage 5). Phosphodiesterase 6 is an effector molecule which means that its primary role is to bind to certain proteins and regulate their biological output.

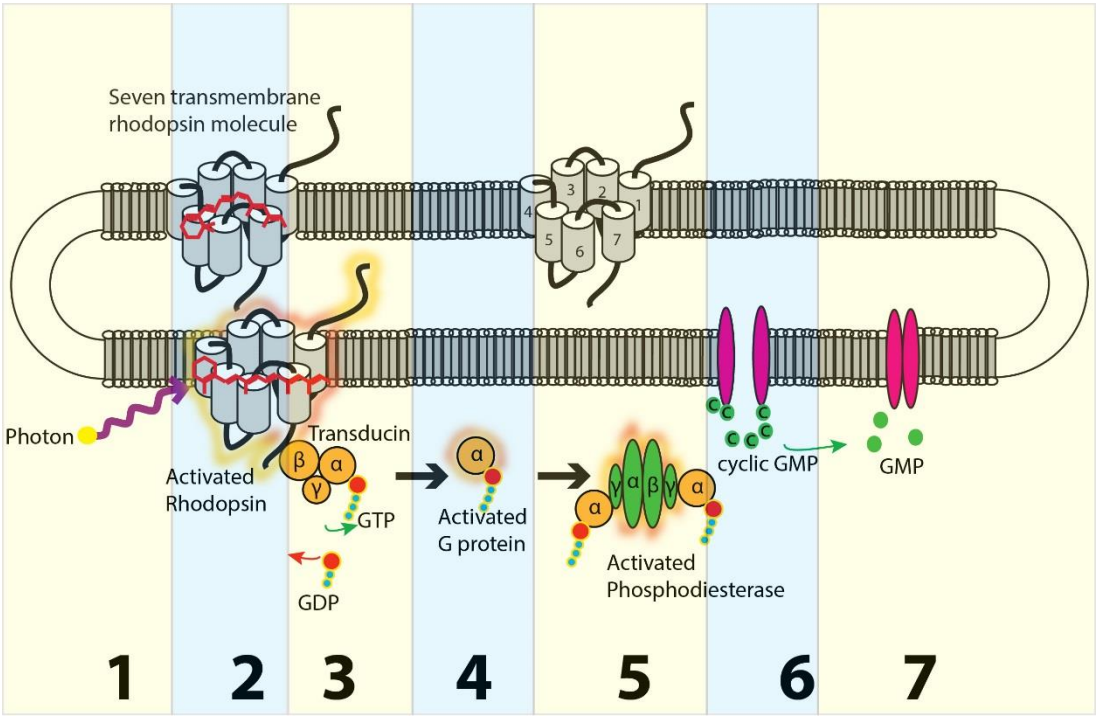

Figure 1.7. Illustration of the disc membrane containing rhodopsin molecules. The phototransduction cycle and the cascade of reactions which occur following a photon of light striking a rhodopsin molecule in the human rod cell is demonstrated. The numbers at the bottom and the highlighted regions indicate the various stages. Guanisine mono phosphate (GMP), guanisine di phosphate (GDP), guanisine tri phosphate (GTP), Alpha (α), Beta (β), Gamma (γ)

In this instance the activated phosphodiesterase 6 (PDE 6*) will catalyse cyclic guanisine mono phosphate (cGMP), thus abolishing its cyclic formation Figure 1.7 stage 6). The role of cGMP is to maintain the cGMP ion gates open, allowing the flow of positively charged sodium (Na^+) and calcium (Ca^{2+}) into the cell maintaining its positivity. Once PDE 6* catalyses cGMP to GMP, this reduces the cGMP concentration in the cell, leading to the closing of the cGMP gates (Figure 1.7 stage 7). The positively charged molecules of Na^+ and Ca^{2+} are unable to enter the cell, leading to a hyperpolarisation of the cell.

Every photon that is absorbed will always have the same effect on the retinal chromophore independent of its wavelength, this is the foundation of the principle of univariance (Donner and Rushton 1959), the implications of this concept are explained in greater detail in a later section. If we only possessed one type of photoreceptor the probability of a photon being absorbed by that particular type of photoreceptor is described by its spectral sensitivity curve (Figure 1.8). Any two different wavelengths of light can be matched with each other by simply altering the intensity as shown in Figure 1.8, therefore the identity of colours cannot be determined based on wavelength alone with just a single photoreceptor.

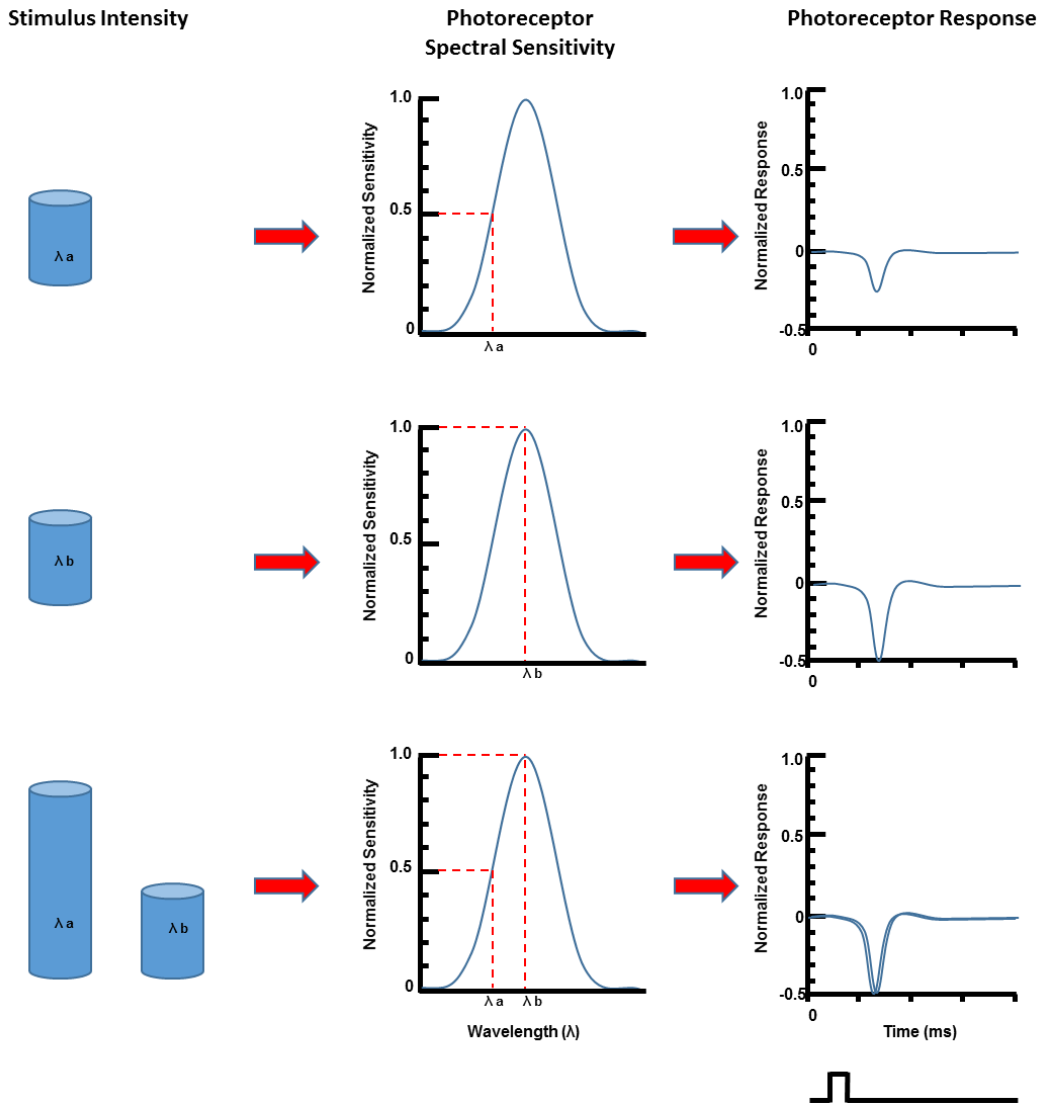

Figure 1.8. Top and middle rows show how two monochromatic light stimuli with different wavelengths will affect the excitation response of the same photoreceptor. The bottom row shows that the excitation of the photoreceptor can be matched by just altering the intensity of one light stimulus.

In order to be able to distinguish colours based on wavelength, more than one photoreceptor type is required. Human retinas contain three different cone types, long- (L), middle- (M) and short- (S) wavelength sensitive cones each with their own photopigment (Figure 1.9).

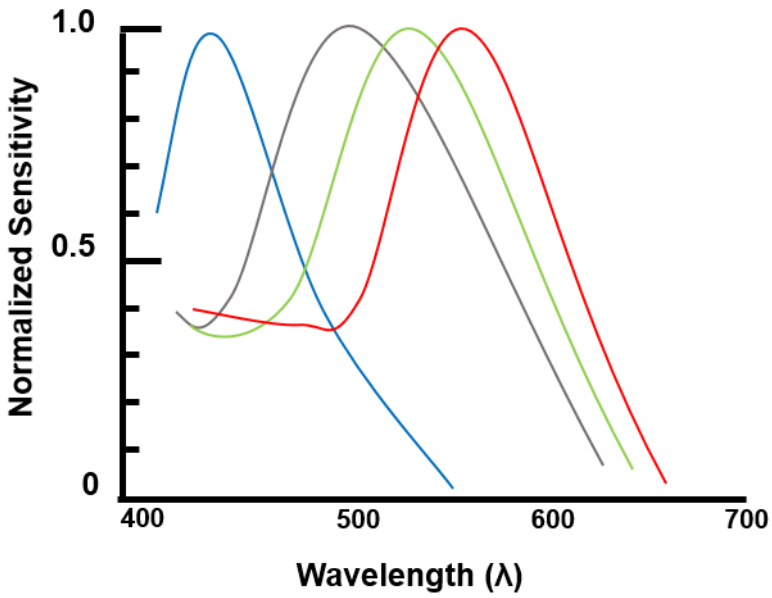

Figure 1.9. Graph displaying the spectral sensitivity functions of the four photoreceptors. Rods in grey, L cones in red, M cones in green and S cones in blue.

L and M cones make up 90% of the cone population with S cones making up the remaining 10%. The ratio of the L to M cones is typically 2:1 but this can vary from 0.33:1 to 10:1 in individuals with normal colour vision (Kremers et al. 2000). There are no S cones contained in the fovea centralis (Castańo and Sperling 1982).

Absolute changes in the electrical potential of the photoreceptors produced upon absorption of light photons from our surrounding environment are passed on to both the horizontal and bipolar cells through a series of highly complex and selective synaptic connections in the outer plexiform layer. It is from here that the addition and subtraction of relative differences in cone

inputs is performed, processing which ultimately provides the primate visual system with the ability to signal a wide array of colours.

1.3 The outer plexiform layer

The outer plexiform layer is the region that contains the photoreceptor synaptic terminals and the dendritic connections from the both horizontal and bipolar cells (Kolb 1970). These connections between the photoreceptors and horizontal and bipolar cells are the initial steps in the processing of photoreceptor inputs. The formation of the synaptic structure is highly conserved at all photoreceptor pedicles and is known as a triad. It consists of a central bipolar cell dendrite flanked by two horizontal cell dendrites. The triad process is repeated multiple times at a single photoreceptor pedicle and increases as a function of retinal eccentricity (Kolb 1970; Kolb 1974) with each receptor pedicle making over 500 synaptic contacts and thus creating multiple pathways where the input signal from the photoreceptors is fed forward, backwards and modulated before it reaches the inner plexiform layer (Wässle 2004).

1.3.1 Horizontal cells

There are two types of horizontal cells in the retina, HI and HII cells (Kolb 1974; Ahnelt and Kolb 1994b; Kolb et al. 1994) and both make invaginating connections with the photoreceptor. The horizontal cell has a dendritic arbor close to the cell body, a long thick axon and a structure termed the telodendritic arbor towards the end of its axon. The arbors are extensive

clusters which branch out laterally and have the ability to make contact with hundreds of photoreceptors (Kolb 1974; Ahnelt and Kolb 1994a; Dacey et al. 1996). Horizontal cells form lateral connections with both photoreceptors and bipolar cells. The lateral connections that the HI and HII cells make are unique and selective (Ahnelt and Kolb 1994a).

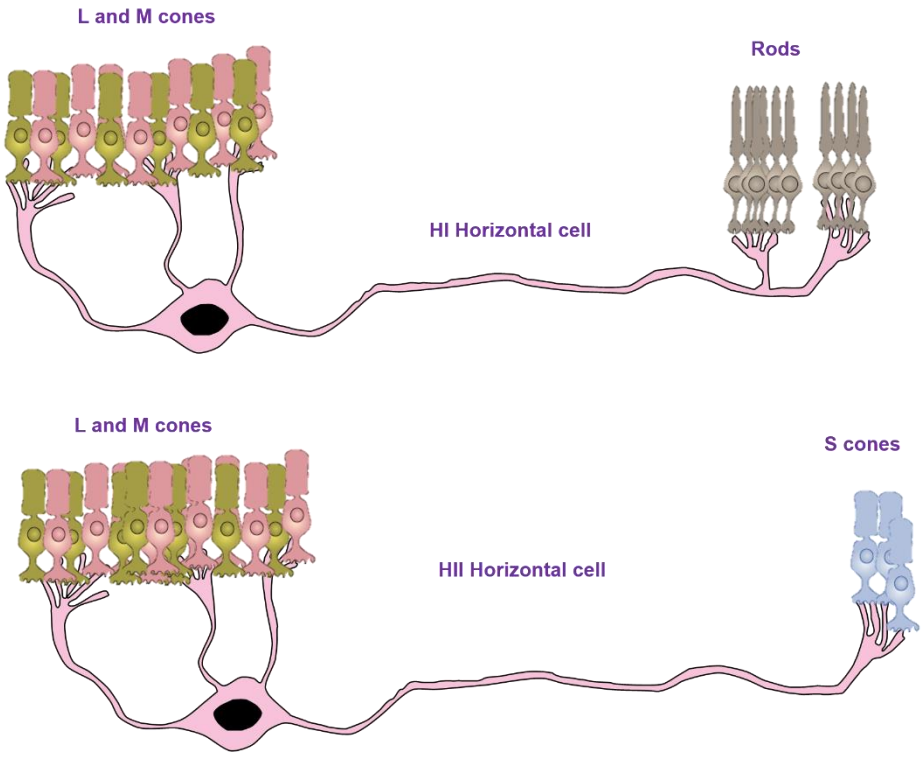

Figure 1.10. Illustration of the HI horizontal cell showing multiple synaptic connections with L and M cones at its dendritic arbor and multiple rod connections at the telo-dendritic arbor at the end of its axon (top). The HII horizontal cell with multiple synaptic connections with L and M cones at its dendritic arbor and dense connections with S cones at the telo-dendritic arbor (bottom)

HI dendrites connect almost exclusively with L and M cones, with few S cone connections observed (Figure 1.10). HII dendrites, in contrast, connect with all three cone pedicles but selectively favour S cone pedicles (Dacey et al. 1996). The telo-dendritic arbor of the HI cell is connected to the rod pedicle

and the rod bipolar cell (Kolb 1974; Ahnelt and Kolb 1994b; Kolb et al. 1994; Rodieck 1998). The telo-dendritic arbor of the HII cell connects S cones and S cone bipolar cells exclusively. The HII cell forms dense synaptic connections at the S cone pedicle but relatively few at L and M cone pedicles. This gives the S cone a greater gain relative to the L and M cones. (Dacey 1999)

The main function of horizontal cells is to provide inhibition to both photoreceptor and bipolar cells. This is performed through a series of feed-back and feed-forward networks, respectively (Lasater et al. 1984; Dorgau et al. 2015) and enables the retina to regulate its sensitivity to light as well as forming the basis for centre-surround and lateral inhibition (Abd-El-Barr et al. 2009), this will be discussed in a later section. Although the HII horizontal cells are not suspected of providing any kind of spectral opponency, they do retain the information gathered by the photoreceptors for transmission and further processing (via the small bistratified ganglion cells) where this information is important for S/(L+M) opponency.

1.4. The inner nuclear layer

1.4.1. Bipolar cells

There are 12 different types of bipolar cell which have been identified in the human retina. Of these 12 bipolar cells, one is a rod bipolar cell which only contacts rods (Boycott and Wassle 1991) and the remaining 11 types are cone bipolar cells which are further classified into groups by their physical

and physiological features (Figure 1.11). The bipolar cell dendrites will synapse with either one (midget) or many photoreceptors (diffuse), this will determine the level of their stratification (Boycott and Wassle 1991).

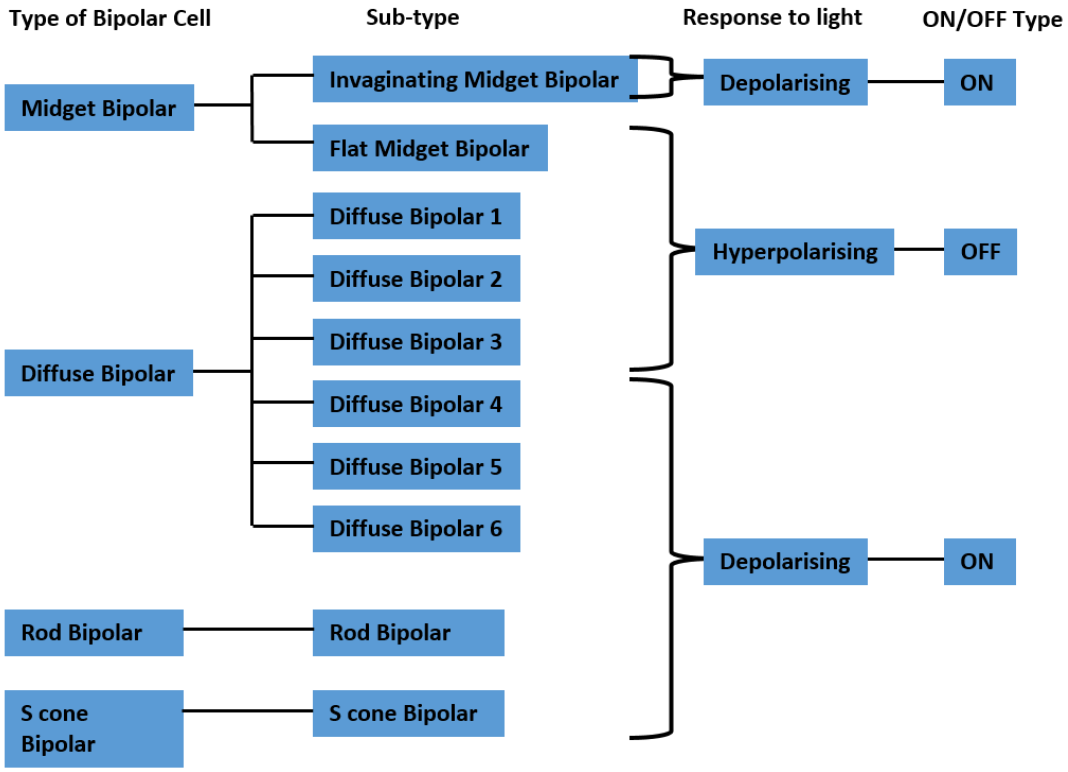

Figure 1.11. Diagram detailing the main types and subtypes of bipolar cells and their response to the neurotransmitter glutamate

Unlike ganglion cells, horizontal cells and bipolar cells do not communicate using trains of electrical impulses, instead they alter the electrical potential of their cell membrane in response to the changes in neurotransmitter at their dendrites. All photoreceptors respond to light by hyperpolarising and decreasing the amount of glutamate at their synapse (Figure 1.12).

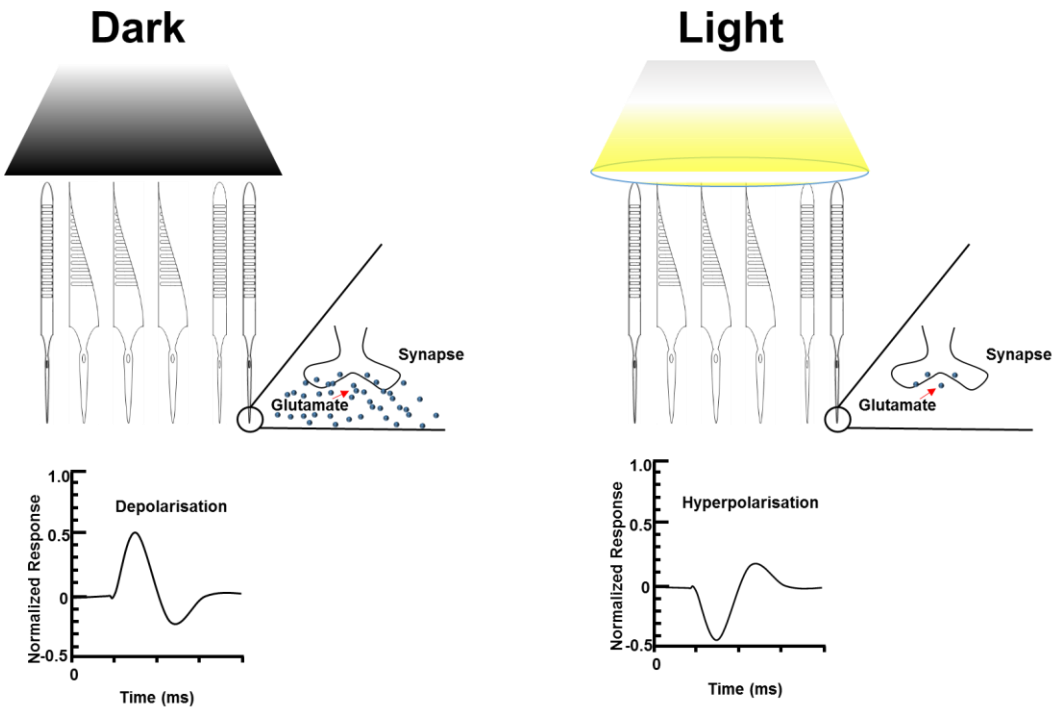

Figure 1.12. Illustration of the synaptic and outer segment electrical changes for retinal photoreceptors in dark (left) and light (right) conditions.

Both bipolar and horizontal cells are glutamergic meaning they respond to the presence of the neurotransmitter glutamate. The type of response recorded from a cell is dependent on the type of receptor it possess and the means by which it connects to the photoreceptor pedicle, i.e. flat or ribbon connections (Slaughter and Miller 1981; Slaughter and Miller 1983). A cell that conserves the photoreceptor response (hyperpolarisation) is termed an OFF cell whereas any cell that inverts the photoreceptor response is said to be an ON cell. Horizontal cells always conserve the photoreceptor response and are therefore OFF type cells (Dacey et al. 1996) whereas bipolar cells vary depending on the type of bipolar (Figure 1.13). Bipolar cells possess a centre surround mechanism, meaning the cells connected to the surrounding field will behave in an antagonistic manner relative to the centre (Werblin and

Dowling 1969; Schwartz 1974). They can either have an ON centre with an OFF surround, or vice versa. Photoreceptors, via horizontal cell connections, form the basis for the surround mechanism (Burkhardt 1993). Specific stimulation of the receptors connected to the central field of an ON bipolar cell will cause it to depolarise whereas stimulating the receptors connected to the surrounding field of the bipolar cell will cause it to hyperpolarise.

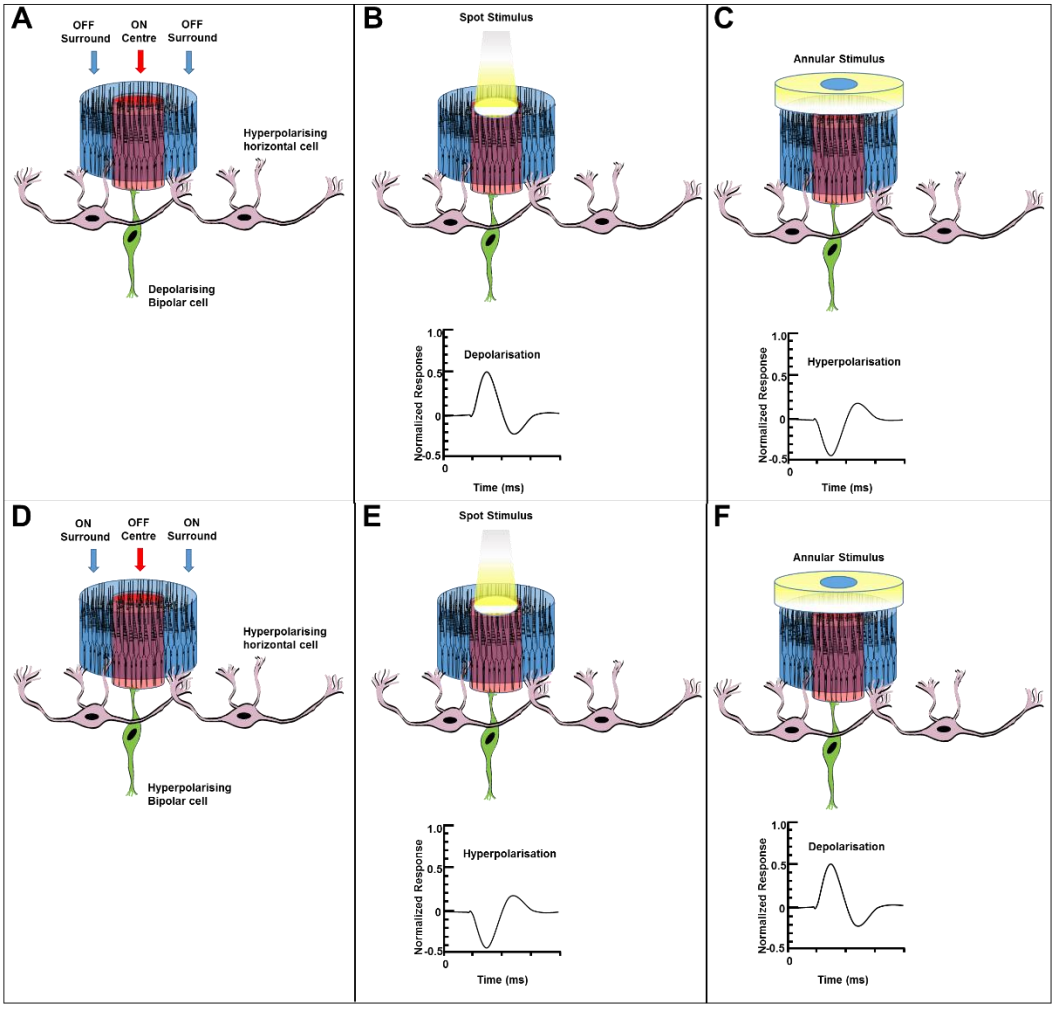

Figure 1.13. (Top row) Illustration of the synaptic formation of the ON bipolar and horizontal cells to create a centre (ON) - surround (OFF) organisation (A) and the typical recorded electrical potential following centre stimulation with a small spot of light (B) and surround stimulation with an annular stimulus (C). (Bottom row) Synaptic formation of an OFF bipolar cell and horizontal cells to create a centre (OFF) - surround (ON) organisation (D) and the typical recorded electrical potential following centre stimulation with a small spot of light (E) and surround stimulation with an annular stimulus (F).

The nomenclature given to the different groups of bipolar cells is often related to what cellular inputs they receive and how many of them. For example, midget bipolar cells typically receive inputs from single cones, diffuse bipolars from many cones, rod bipolars from rods and S cone bipolar from S cones.

1.4.2. Midget bipolar cells

There are 5 types of midget bipolar cells; L on, L off, M on, M off and S off (Boycott and Wassle 1991; Rodieck 1998). The midget bipolar cell has a small dendritic arbor and typically makes contact with only one cone with the exception of some peripheral midget bipolar cells which make contact with 2-3 (Figure 1.14). In turn they only synapse with one ganglion cell. Every L and M cone will have a synaptic connection to one ON and one OFF midget bipolar cell, whereas S cones will only synapse with OFF midget bipolar cells (Rodieck 1998). The specific one-to-one connections make up the basis for our high visual acuity and L/M (red/green) colour opponency.

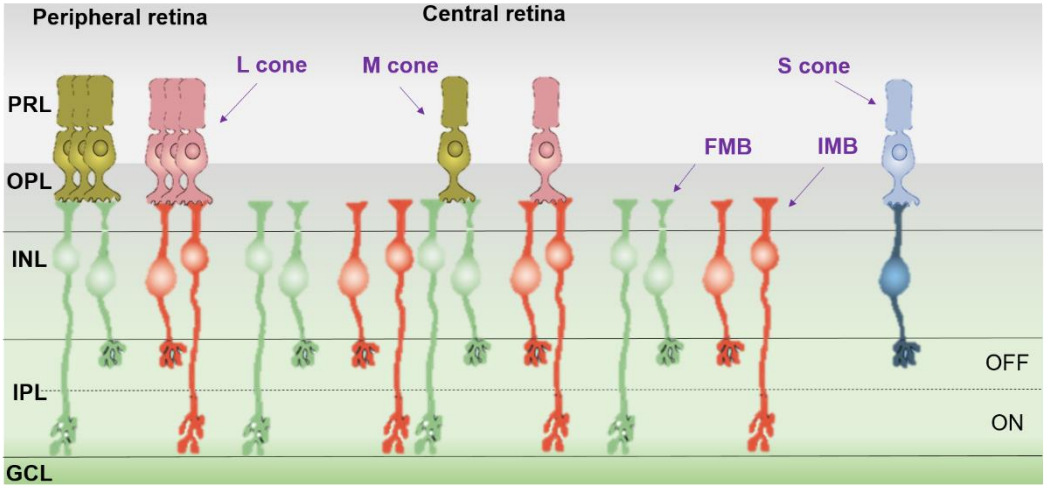

Figure 1.14. Illustration of the midget bipolars making synaptic connections in the outer plexiform layer (OPL) with single L and M cones in the centre and typically two – three in the periphery. The type of midget bipolar cell is determined by the level of axon termination. Invaginating midget bipolars (IMB) terminate in the lower ON level of the inner plexiform layer (IPL), whereas the flat midget bipolar (FMB) axons terminate in the OFF level of the inner plexiform layer. Photoreceptor layer (PRL), Outer plexiform layer (OPL), Inner nuclear layer (INL), Inner plexiform layer (IPL), Ganglion cell layer (GCL).

1.4.3. Diffuse bipolar cells

There are 6 types of diffuse bipolar cells (DB 1-6).They are suitably named as they have extensive dendritic branching which allows them to contact multiple photoreceptors (approximately 5-10) (Boycott and Wassle 1991; Rodieck 1998). Typically, DB 1-3 have stratification in the OFF layer of the inner plexiform layer (Figure 1.15) and are termed OFF diffuse bipolars, DB 4-6 having stratification in the ON layer and termed ON diffuse bipolars (Biersdorf and Armington 1957; Rodieck 1998).

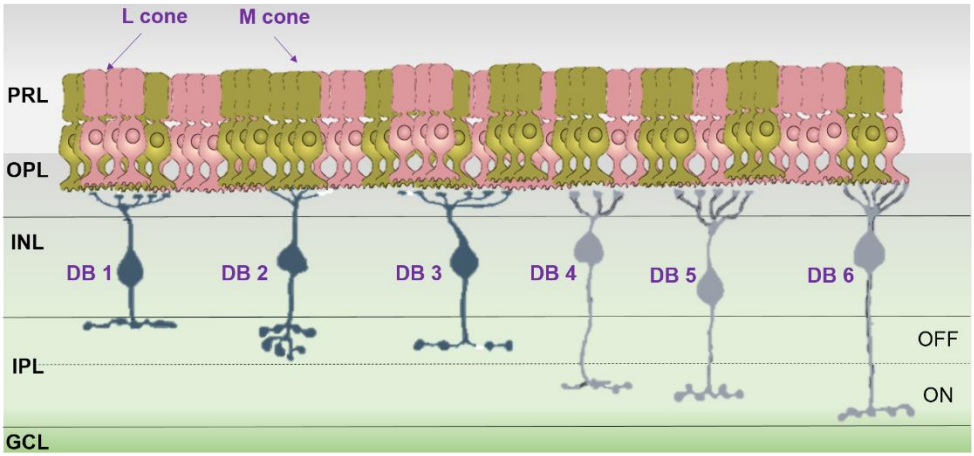

Figure 1.15. Illustration of the diffuse bipolar cells (DB1-6) making synaptic connections in the outer plexiform layer (OPL) with multiple L and M cones. The type of bipolar cell is determined by the level of axon termination. DB 1-3 terminate in the upper OFF level of the inner plexiform layer (IPL), whereas DB 4-6 terminate in the lower ON level of the inner plexiform layer. Photoreceptor layer (PRL), Outer plexiform layer (OPL), Inner nuclear layer (INL), Inner plexiform layer (IPL), Ganglion cell layer (GCL)

1.4.4. Rod bipolar cell

The rod bipolar typically receives inputs from 15 to 20 rod photoreceptors (Kolb and Nelson 1983) (Figure 1.16). It has an invaginated synaptic base as opposed to flat, connecting synaptically to rods by projecting a ribbon-like connection inside the rod spherule (Kolb 1970; Boycott and Wassle 1991). The receptors at the synaptic end of the rod bipolar cell are metabotropic glutamate receptors (mGlur). These are typically only seen in the ON bipolar cells and hyperpolarise to the presence of glutamate (Dhingra and Vardi 2012).

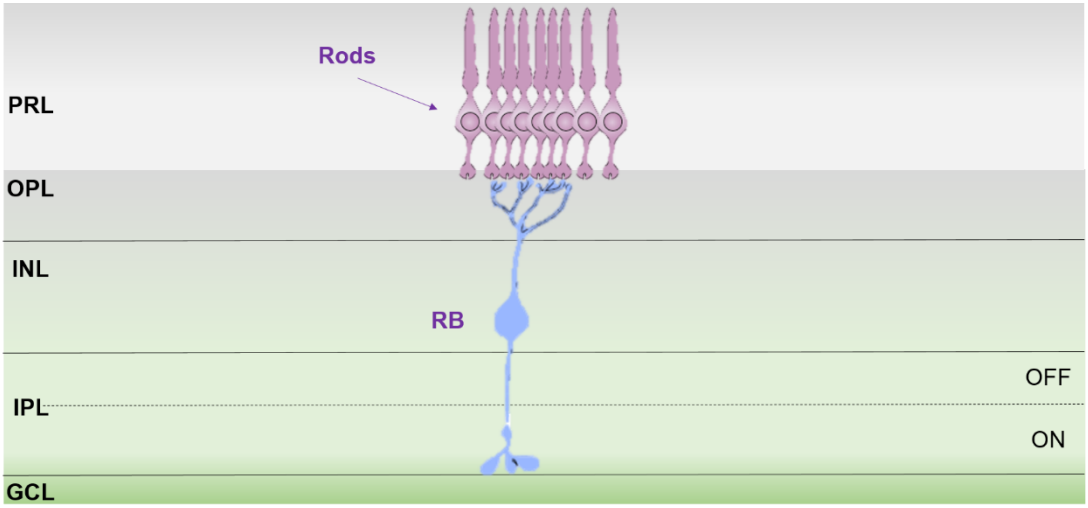

Figure 1.16. Illustration of a rod bipolar (RB) cell making multiple synaptic connections with rods. The rod bipolar cell only receives inputs from rods and can receive up to 20 rod inputs. The rod bipolar cell is an ON bipolar cell with its axon terminating in the ON layer of the inner plexiform layer (IPL). Photoreceptor layer (PRL), Outer plexiform layer (OPL), Inner nuclear layer (INL), Inner plexiform layer (IPL), Ganglion cell layer (GCL).

There are no direct rod to OFF bipolar cell connections in the human retina (Stockman and Sharpe 2006). Rods do however make connections with OFF bipolar cells and 'piggyback' on the cone pathways using gap junctions and connections to the amacrine cell network.

1.4.5. S cone bipolar cells

This particular type of bipolar cell exhibits very specific connectivity. It only receives connections from S cones, typically one to one in the central regions and two or three in the more peripheral retina (Dacey and Lee 1994; Rodieck 1998). The connection is an invaginating one, making it an ON bipolar cell with synaptic connections in the ON layer of the inner plexiform

layer (Figure 1.17). Its synaptic connections are also very specific as it only connects to the one type of ganglion cell, the small bistratified ganglion cell (Dacey and Lee 1994; Rodieck 1998).

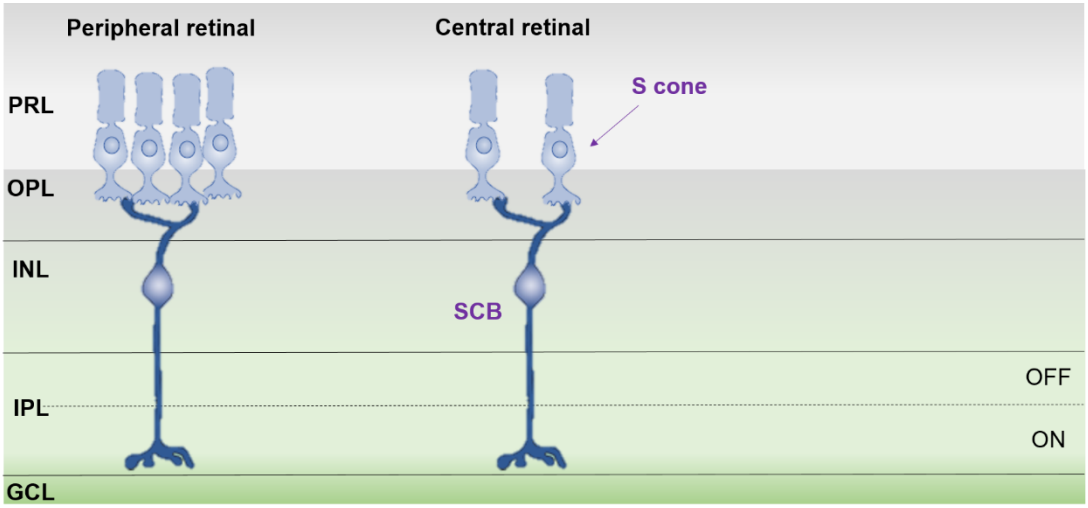

Figure 1.17. Illustration of the S cone bipolar (SCB) cells making synaptic connections in the outer plexiform layer (OPL) with single L and M cones in the centre and typically two – four in the periphery. The SCB axon terminates in the lower ON level of the inner plexiform layer (IPL). Photoreceptor layer (PRL), Outer plexiform layer (OPL), Inner nuclear layer (INL), Inner plexiform layer (IPL), Ganglion cell layer (GCL).

1.5. The inner plexiform layer

The inner plexiform layer is where information from bipolar cells of the outer plexiform layer is conveyed to ganglion cells via amacrine cell connections. This is done through direct connections but also by gap junctions. Like bipolar cells, amacrine cells hyperpolarise or depolarise to light depending on the type of cell. Of the amacrine cells involved in cone vision, the starburst and A1 amacrine cell are the most common. The A2, A17 and A18 appear to play a larger role in rod vision but crossover to both rod and cone system is observed frequently (Kolb et al. 1981; Kolb and Nelson 1996; Kolb 1997).

Through their myriad of lateral, vertical and feedback connections they contribute to motion, contrast and sensitivity modulation. The majority of amacrine cells are inhibitory and likely contribute to the formation of antagonistic surrounds in ganglion cells.

1.5.1. The ganglion cell layer

There are three main retinal pathways that project to the lateral geniculate nucleus (LGN). The LGN is a six layered structure with inter laminar layers, which receives visual input via ganglion cell axons (Levin et al. 2011). These are the parvocellular, magnocellular and koniocellular pathways and are made up from the axonal projections of midget ganglion cells, parasol ganglion cells and small bi-stratified ganglion cells, respectively (Dacey 1999).

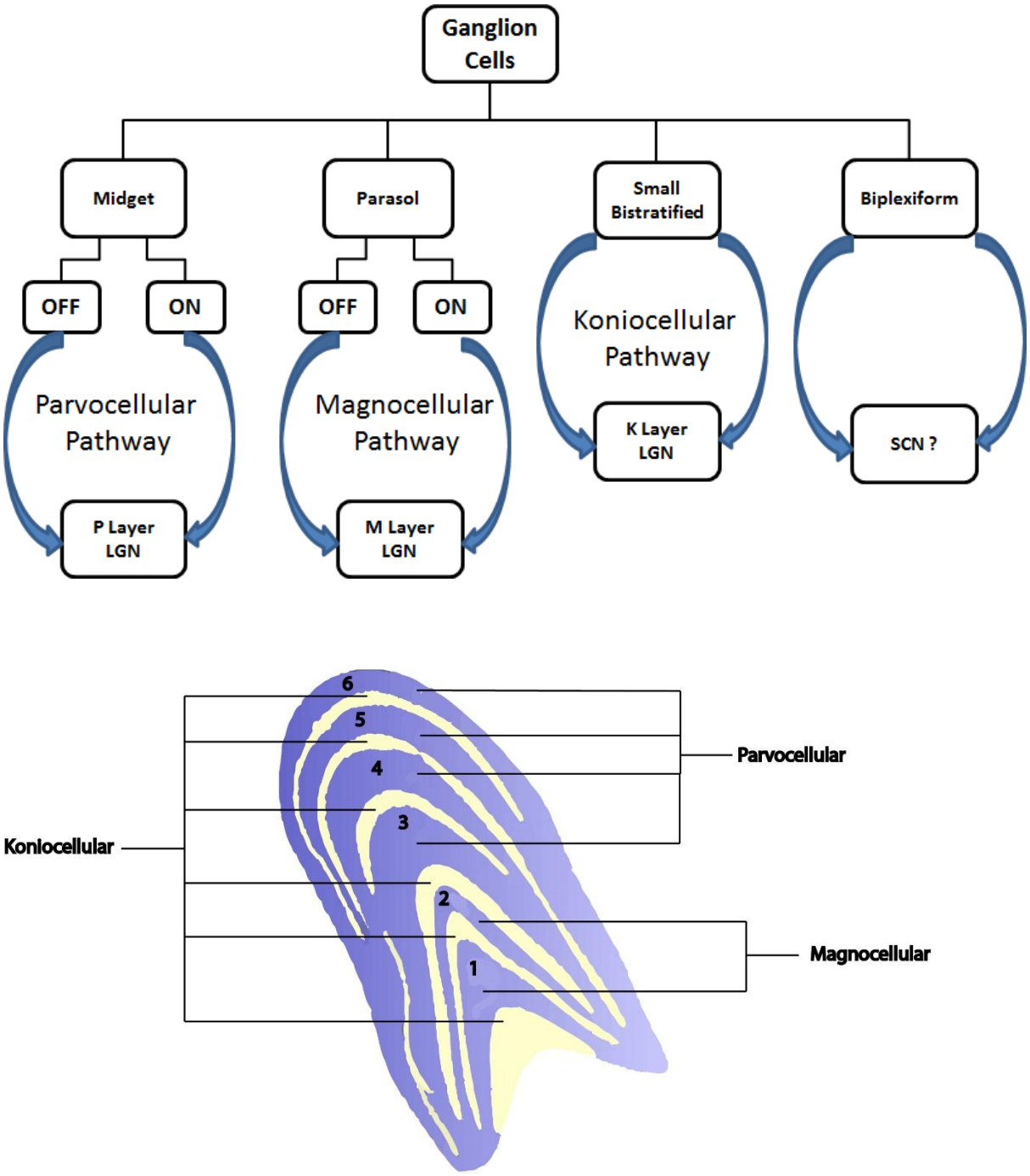

Figure 1.18. Different types and sub types of ganglion cell directly involved in vision and their cortical pathway to their respective laminae of the LGN. The layers of the LGN denoted by P, M and K are abbreviations for parvocellular, magnocellular and koniocellular respectively. The melanopsin ganglion cell has been excluded from this diagram. (Below) The laminar structure of the LGN

1.5.2. Midget ganglion cells

Midget ganglion cells (MGC) account for approximately 70% of the ganglion cell population (Perry et al. 1984; Shapley and Perry 1986). They tend to receive input from only one midget bipolar cell in the central retina but show greater divergence towards the more peripheral eccentricities. There are two types of MGC, ON centre and OFF centre, which receive input from L and M on midget bipolar cells, which in turn receive from L and M cones (Figure 1.19).

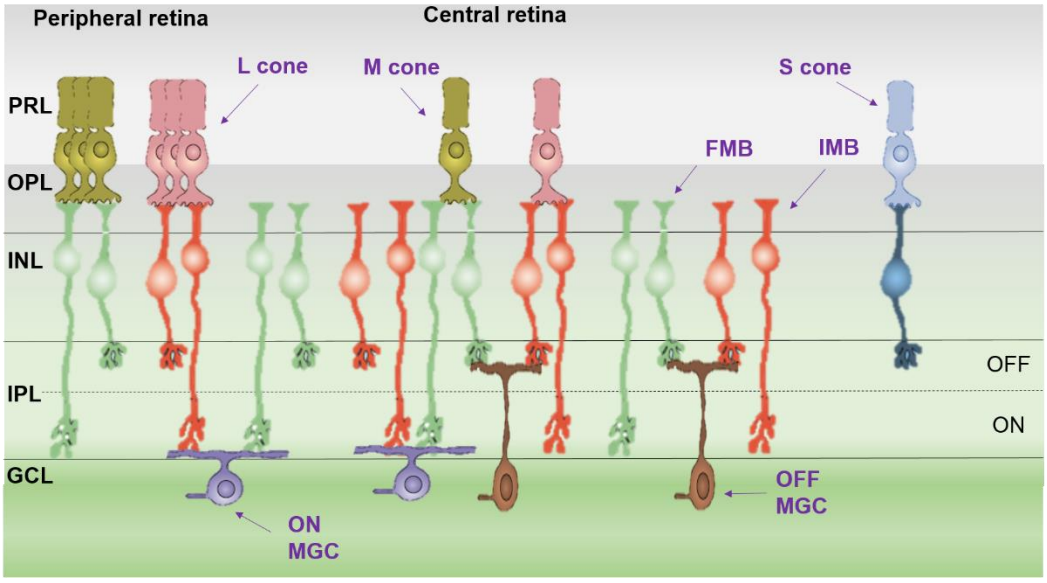

Figure 1.19. The various cone inputs via bipolar cells to the midget ganglion cells. Each midget ON bipolar cell will connect to one ON midget ganglion cell and each midget OFF bipolar cell will connect to one OFF midget ganglion cell.

1.5.3. Parasol Ganglion cells

Parasol ganglion cells (PGC) account for about 8% of the ganglion cell population and receive their input from diffuse bipolar cells. There are two types of PGC, ON centre and OFF centre (Figure 1.20). The parasol ganglion cells have extensive dendritic branching and are known to have several connections to each other but also connect with certain types of amacrine cells (Shapley and Perry 1986; Rodieck 1998).

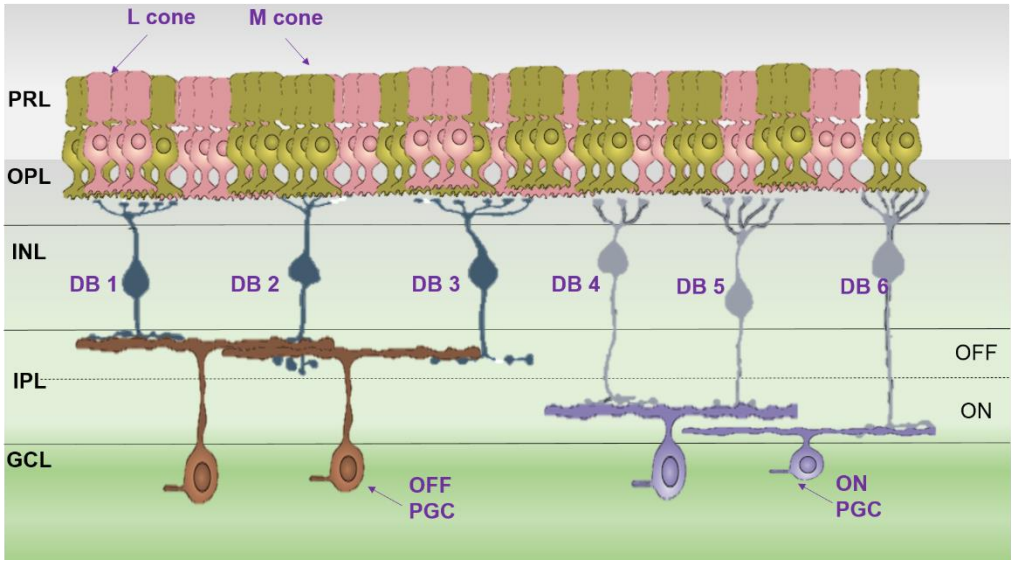

Figure 1.20. Cone inputs to the parasol ganglion cells via the diffuse bipolars. The input from the L and M cones is summed together and the OFF and ON channels provide luminance information.

1.5.4. Small bistratified ganglion cells

The small bistratified ganglion cells makes up approximately 10% of the ganglion cell population and receive signals from all three cone types. This is underpinned by synaptic connections in both the ON and OFF levels of the inner plexiform layer.

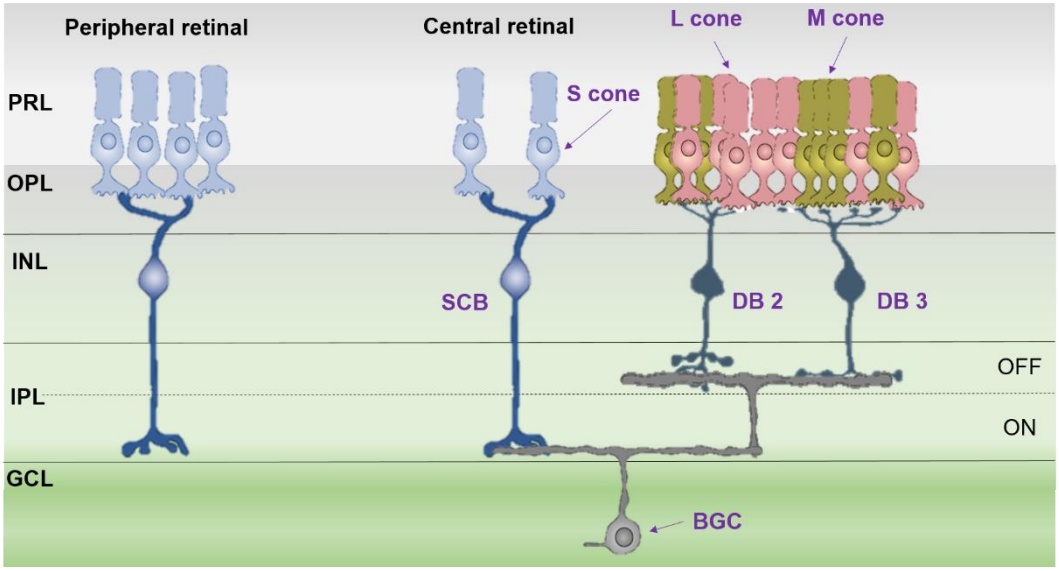

Figure 1.21. Cone input to the small bistratified ganglion cell via the S ON bipolars and diffuse bipolars 2 and 3. Their structure is different to that of the other ganglion cells in that they do not exhibit a classic centre surround, rather an S ON centre and LM OFF centre from their dendritic tree lying in both the inner and outer plexiform layers. This enables the blue – yellow comparison by subtracting from the LM input from the S input.

It connects with OFF diffuse bipolar cells, receiving input from L and M cones in the OFF layer and ON S cone bipolar cells in the ON layer (Figure 1.21).

1.5.5. Biplexiform ganglion cells

Not much is known about the biplexiform ganglion cell. Its input structure is very different from the other ganglion cells, in that it receives input directly from rod photoreceptors as well as connections to both rod bipolar and amacrine cells via gap junctions (Zrenner et al. 1983). There is also some evidence to suggest that they convey cone signals also, which may be through the receptoral gap junction mechanisms. They have a large axon and synaptic connections in both the inner and outer plexiform layer.

1.6 Cone Pathways

This section shifts in emphasis from the individual cell types and focuses on the pathways that they constitute and the flow of visual information.

The functions of cone-mediated vision are complex as it facilitates photopic luminance vision as well as red/green and blue/yellow chromatic discrimination. This requires three separate physiological retinal pathways termed, Magnocellular, Parvocellular and Koniocellular, according to their laminar projections to the LGN.

1.6.1. Magnocellular pathway

The magnocellular pathway receives additive input from multiples of L and M cones with connections to both ON and OFF diffuse bipolar cells which in turn connect to ON and OFF parasol ganglion cells (Wässle 2004). These ganglion cells project to layers 1 and 2 of the LGN (Kaplan and Shapley 1986). They typically possess large receptive fields, which respond to achromatic stimuli by either hyperpolarising or depolarising depending on whether they are ON or OFF. They possess little or no cone opponency.

1.6.2. Parvocellular pathway

The parvocellular pathway receives input from L or M cones making one to one connections with single midget bipolar cells (often 2-3 connections in the

periphery) which in turn will synapse with single midget ganglion cell (Wässle 2004). As previously outlined in the section 1.5.2, there are four types of midget bipolar cells. The type is determined by their cone wiring, +L-M, -L+M, +M-L, -M+L and a similar arrangement also exists for midget ganglion cells. This highly specific arrangement is the foundation of red/green chromatic opponent processing. The midget ganglion cells project to the parvocellular layers (3 - 6) of the LGN and exhibit colour opponency (Shapley et al. 1981). The dorsal layers are typically populated with ON centre cells whereas the OFF centre cells typically project to the ventral layers (Wiesel and Hubel 1966b).

1.6.3. Koniocellular pathway

The small bistratified ganglion cell receives input from S-cone bipolars cells which in-turn receive input from S cones. The small bistratified ganglion cell also receives an antagonistic synaptic input from specific diffuse bipolar cells connected to L and M cones. This creates an S-(L+M) opponency and forms the basis of blue/yellow colour discrimination (Martin 1998). The small bistratified ganglion cell projects to the inter-laminar Koniocellular layers of the LGN (Martin et al. 1997).

1.7. Cone opponency

The theory of Colour Opponency, first proposed by Herring in 1878, suggested that our colour discrimination was underpinned by an opponent or comparative process rather than an additive one (Hurvich and Jameson

1957). Herring suggested that there were three opponent processes, red/green, blue/yellow and black/white. DeValois et al. were the first to provide electrophysiological evidence that supported Herring's theory (DeValois et al. 1957). They demonstrated that cells in the LGN exhibited excitatory and inhibitory responses to different wavelengths using monochromatic light. Improved techniques by Derrington and co-workers and later by Lee et al, revealed that the cells displaying opponent features to wavelengths near red and green were all parvocellular cells (Derrington et al. 1984; Lee et al. 1987). Similarly, the cells displaying an opponent response to blue and yellow wavelengths were koniocellular ganglion cells.

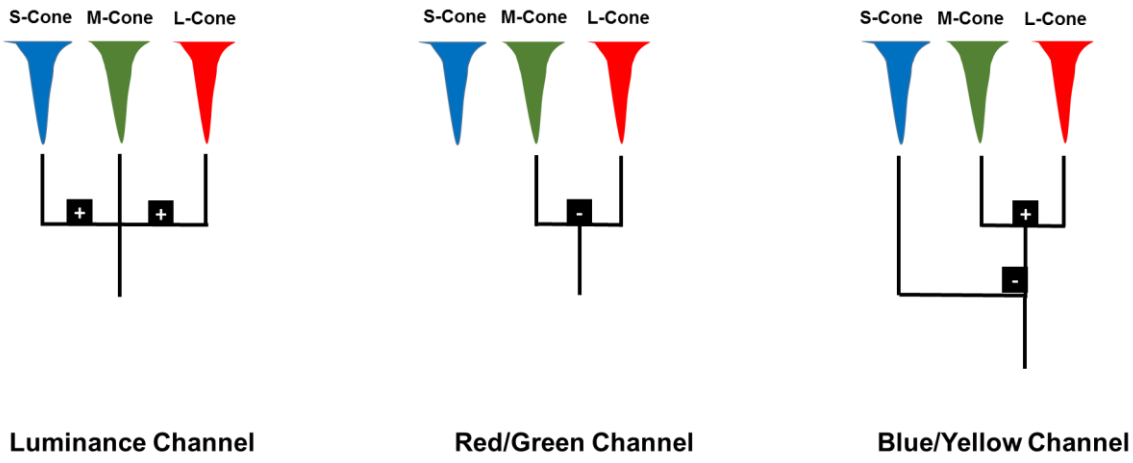

Figure 1.22. The three types of opponent processing which takes place in the human retina, forming the basis of luminance and chromatic vision.

1.8. Rod pathways

It is now well established that rods in the primate retina transmit signals via two separate pathways (Kolb and Nelson 1983; Wassle and Boycott 1991; Wässle et al. 1991). The first major pathway, involves rod signal

transmission to rod bipolars, then to the AII amacrine and then to the ON and OFF bipolar and ganglion cells (Kolb and Famigilietti 1974; Kolb and Nelson 1983; Kolb 1991). The second pathway involves the use of gap junctions between rod and cone pedicles. This allows connections to both ON and OFF bipolar cells and the ON ganglion cell pathway (Nelson 1977; Kolb and Nelson 1983).

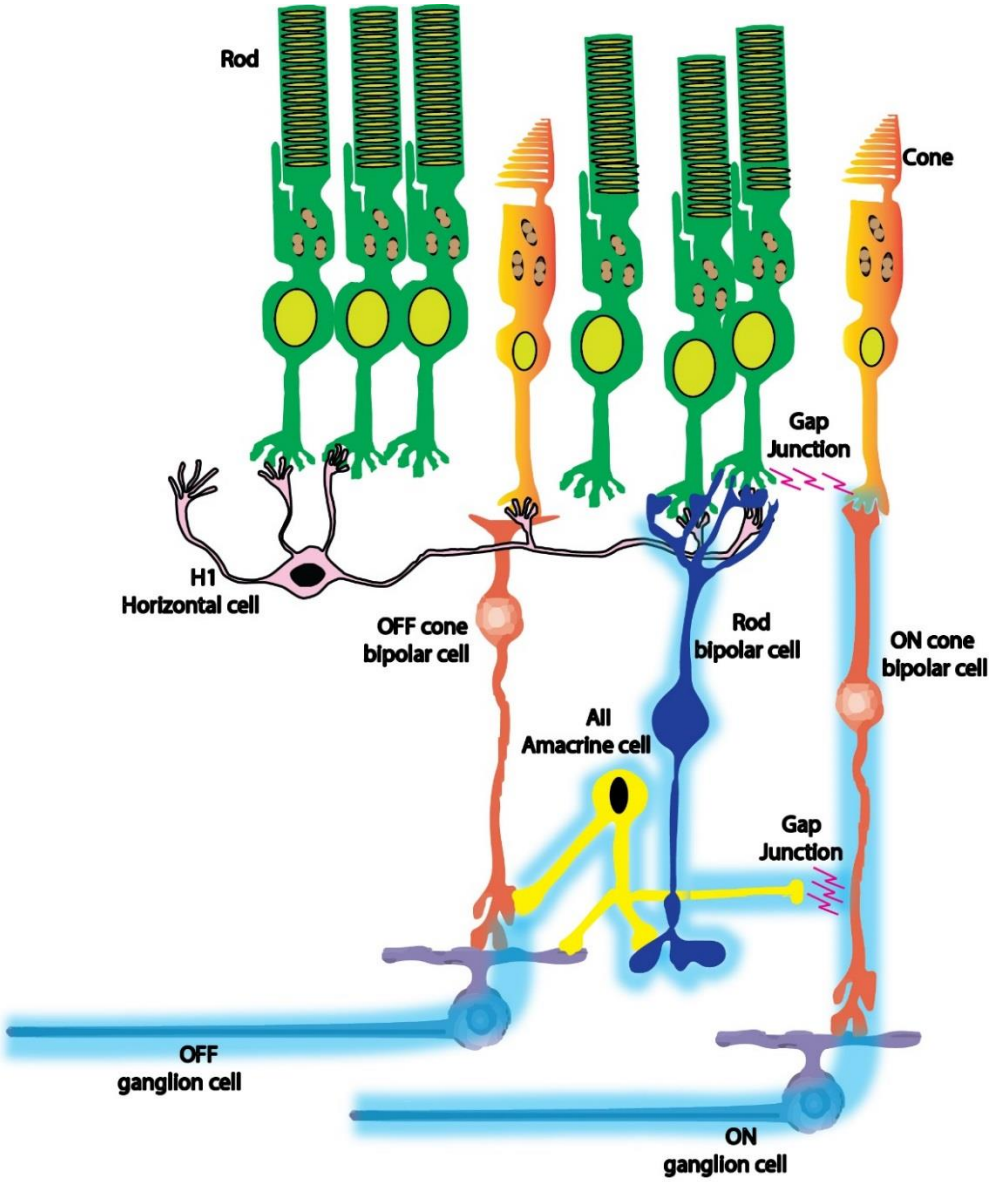

Figure 1.23. Illustration of the dual rod pathways. The blue outline represents the slow pathways: rod phototoreceptor - rod bipolar cells - AII amacrine cell and the fast pathway rod - cone gap juntion connection – cone bipolar cell. Modified from LT Sharpe and A Stockman 1999.

The first pathway is for transmission of signals during scotopic conditions. Since the secondary pathway uses gap junctions with cone pedicles it has been suggested that it is most active in high scotopic/mesopic conditions (Muller et al. 1988; Sharpe et al. 1989). Several electrophysiological studies using human participants have shown physiological evidence of a luminance dependent, two pathway model. (Sharpe et al. 1989; Stockman et al. 1995; Sharpe and Stockman 1999; Nusinowitz et al. 2007).

Regardless of the pathway taken, the rod signal has access to both ON and OFF ganglion cell pathways. The signal is then transmitted to the various levels of the LGN. Evidence of rod signal sharing has been shown to varying degrees on all of three pathways but predominantly through parasol ganglion cells to the magnocellular layer (Lee et al. 1997; Cao et al. 2010). Evidence of rod signals in parvocellular pathway was demonstrated. However the responses were weak, not recorded in all cells and only recorded to stimuli over 2 trolands, compared to strong rod mediated signals in the magnocellular pathway which were recorded at 0.2 trolands (Lee et al. 1997; Cao et al. 2010). Cao showed that the rod temporal response in the magnocellular pathway varies with light level and retinal eccentricity while remaining relatively stable with regards to changes in gain. Interestingly, Cao found no evidence of simultaneous dual retinal pathway activation in using mesopic stimulation (Cao et al. 2010).

The general consensus is that the Koniocellular pathway is not involved in the transmission of rod signals, despite a limited amount of studies which

suggesting otherwise (Wiesel and Hubel 1966a; Lee et al. 1997). It was not until 2009 that it was shown that rod signals do in fact use small bistratified cells of the Koniocellular pathway (Field et al. 2009). At near threshold levels to approximately 10 trolands rod signals are present in the rod bipolar → AII amacrine pathway and somewhere in between 2–10 trolands both rod and blue-yellow opponent systems are in operation (Field et al. 2009).

1.8. The Electroretinogram

Having examined the anatomy and physiology of the retina we now turn to the electroretinogram (ERG). This can be defined in its most basic form as an electrical response elicited from the retina in response to stimulation by light. The electrical currents produced, as a result of changes in potential across the membrane of photoreceptor, following the absorption of a photon of light have been previously outlined. Although these voltages are small, the response can be recorded using microscopic electrodes (Baylor et al. 1984). When a sufficiently large stimulus is used then a large population of cells are synchronously stimulated. In this instance the voltage produced is relatively large and spreads throughout the retina. This mass trans-retinal potential can then be recorded as the electroretinogram by placing electrodes on or near the eye.

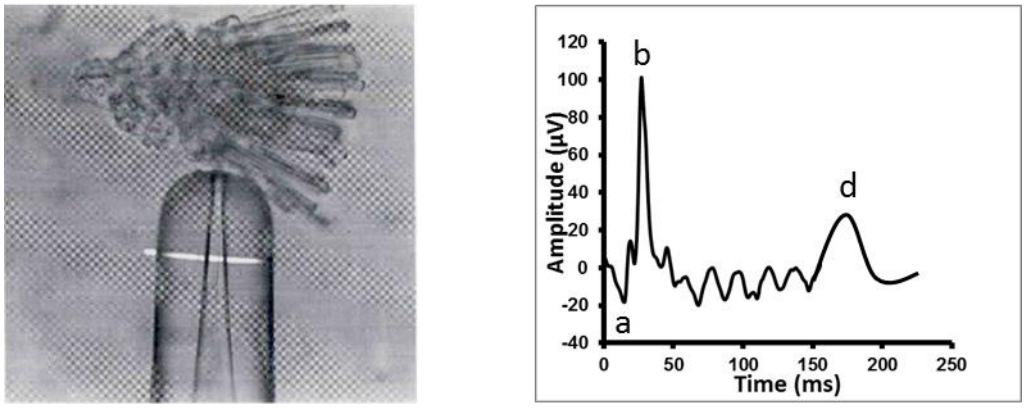

Figure 1.24. Image (left) of the micropipette used to record the ERG from a single photoreceptor. (Right) The mass potential ERG recorded using a high luminance stimulus with the modern day waveform nomenclature of the a, b and d-wave labels. Image taken from Baylor et al. 1984.

1.9. Origins of the Electroretinogram (ERG)

In 1865 Holmgren first demonstrated that the light from a candle (and later with light from the moon so as to exclude temperature related factors) caused a change in the electrical potential of an excised amphibian retina using a galvanometer. This was later performed in an in-situ animal eye in 1877 by Dewar, (Henkes 1984; Heckenlively and Arden 2006) and in 1924 Kahn and Lowenstein were the first to publish a human ERG, recorded using a complicated setup, which was later refined by Hartline, Riggs and Granit. In 1908 Einthoven and Jolly had put forward the idea that this complex waveform was made up of three main waveform components. However it wasn't until 1933 that a series of investigations on cats by Granit showed that the ERG could be divided into three main components using various levels of anaesthesia. He called the waveforms PI, PII and PIII in the order that they disappeared with increasing levels of anaesthesia (Henkes 1984; Heckenlively and Arden 2006).

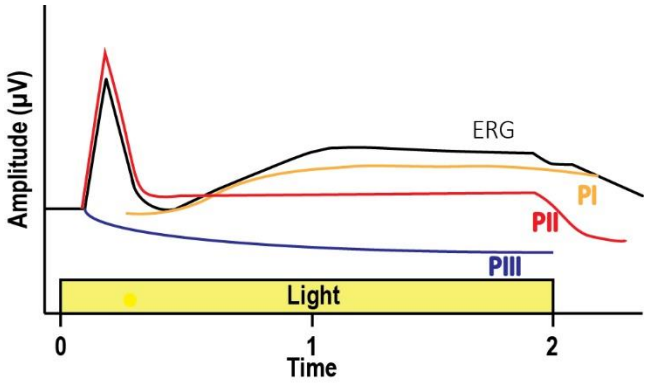

Figure 1.25. The graph shows the three individual components of the ERG from Granit's studies on cat retinas. Modified from webvision.med.utah.edu

The PI waveform, a positive slow waveform, disappeared first following the introduction of anaesthesia. The PII waveform, which exhibited a faster more prominent positivity, disappeared second and was thought to originate somewhere between the photoreceptors and ganglions cells. The PIII waveform, a negative waveform, which occurred first and remained negative for the duration of the flash stimulus was thought to originate in the photoreceptor layer (Heckenlively and Arden 2006). Today the PII and PIII components makes up part of the b-wave and a-wave respectively. Both of these components will be discussed later in more detail. This classical work was the beginning of isolating the ERG into its individual components. In 1950, the invention of the microelectrode really advanced this region of research as it allowed the recording of small electrical signals from a much smaller area within the laminar regions. This was initially performed in cold blooded vertebrates (Tomita 1950), however, this was later adapted for studying cats and primates by Brown and Wiesel. Their purpose-built three microelectrode system consisted of one recording electrode, one reference

electrode and a third electrode to clamp blood vessels (Brown and Wiesel 1959). In experiments they showed that the a-wave amplitude was at its maximum near the retinal side of the RPE and was therefore likely to originate in the photoreceptors (Brown and Wiesel 1961b; Brown and Wiesel 1961a). In 1954, Noelle demonstrated through the administration of pharmacological blockade in rabbits, that the ERG Granit's PI component (what is now referred to as the c-wave) originated in the RPE as a result of light-induced ionic transfer (Rodieck 1972). Noelle also utilised the fact that the RPE and photoreceptors are maintained by choroidal circulation and the neural retina is supplied by the central retinal artery. By clamping the retinal circulation and later examining the histological slices of the retina he demonstrated that the neural retina had atrophic changes while the RPE and receptors were spared (Rodieck 1972). This technique was also adopted by Brown and Wiesel with their microelectrode system which showed an abolished b-wave and diminished d-wave response (figure 1.24) when the central retinal artery was clamped (Brown and Watanabe 1962). Thus providing evidence that the origins of the b-wave were somewhere in the inner nuclear layer and that the PIII component was very likely to be generated by the receptors (Brown 1968). In 1969 definitive evidence for the origin of the a-wave in the outer segment of the photoreceptor was demonstrated by Penn and Hagins by recording the spatial distribution of the rod photocurrent in the rat retina (Penn and Hagins 1972).

One of the problems encountered in using the microelectrode technique was that the vitreous has such a low electrical resistance. Electrical

contamination from other retinal regions often affected the response, leading to inconsistencies in the origins of the signal. In 1965, Arden and Brown overcame this by replacing the vitreous fluid in cats with a non-conducting heavy oil (Arden and Brown 1965). This allowed only the local ERG response at the microelectrode tip to be recorded, the so-called local ERG. By examining the polarity and amplitude changes of the local ERG b-wave with respect to retinal depth, the bipolar cell was suggested as a likely candidate to fit the electrical profile. The discovery of better glutamate agonists and antagonists allowed greater precision in the isolation of individual retinal components (Slaughter and Miller 1981). Gurevitch and Slaughter showed that the metabotropic glutamate antagonist APB selectively abolished the b-wave, thus suggesting that its origins were specifically from ON bipolar cells (Gurevich and Slaughter 1993). Sieving and co-workers showed that in primates the OFF bipolar cells have an opposing affect which counteract the sustained ON bipolar cell response and when summed together account for the shape of the b-wave (Bush and Sieving 1994). They also demonstrated that the a-wave of the photopic ERG is made up from an OFF bipolar cell postreceptoral element as well cone receptors. Similarly, Robson and Frishman as well as others showed that dark adapted cones and hyperpolarising bipolar cells significantly contributed to the amplitude of the dark adapted ERG a-wave (Robson and Frishman 1995; Hood and Birch 1996; Pepperberg et al. 1997; Robson and Frishman 1998). Similar methods also revealed the d-wave to originate in OFF bipolar cells at stimulus offset (Xu and Karwoski 1994).

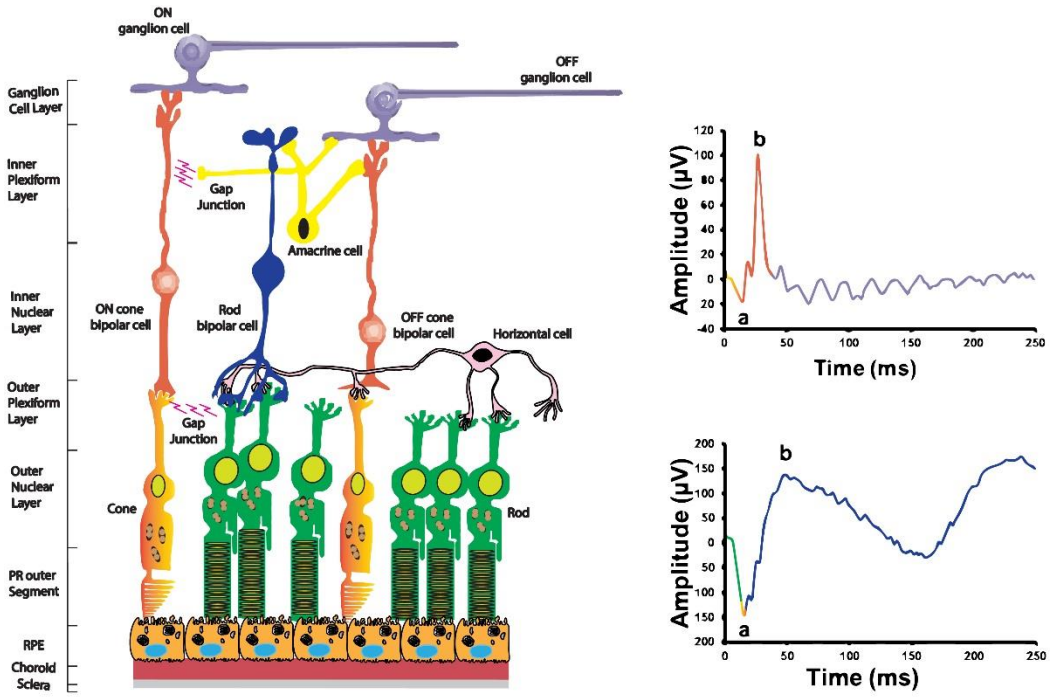

Figure 1.26. A representation of the retina and the light adapted 3.0 flash ERG (top) and dark adapted 3.0 flash ERG (bottom). Regions of both ERGs have been colour coded to provide a graphical indication of the component origins.

1.10. Methods of isolating the ERG

The above research that led to the identification of the cellular origins of the various components of the ERG has been invaluable. This has led to our ability to use the ERG to independently assess cone and rod function within the human retina, making it a powerful clinical tool. This is accomplished by altering parameters such as retinal adaptation, stimulus intensity and stimulus frequency.

1.10.1. Adaptation

Controlling the level retinal adaptation is probably the most important parameter when it comes to separating rod and cone function on the ERG.

Dark adaptation serves to increase the sensitivity of the rod system. In the duplex retina Granit noted that dark adaptation reduces the d-wave component (Brown 1968). Brown and Wantanabe showed that dark adaptation significantly increased the a-wave and b-wave amplitude in the cynomologus monkey (Brown et al. 1965). In humans, dark adaptation typically brings about a fourfold increase in amplitude compared to no dark adaptation. Psychophysically determined measures show that it takes approximately 20 - 40 minutes to achieve full dark adaptation. However several studies suggest that a reliable maximum rod response can be achieved in a significantly shorter time frame (Cameron et al. 2008; Hamilton and Graham 2016).

Light adapting the duplex human retina increases the relative sensitivity of the cone system. The rod system quickly becomes saturated in photopic conditions (Aguilar and Stiles 1954) so its overall sensitivity is reduced. Granit noted that by light adapting the duplex retina, responses resembled that of the cone ERG (Brown 1968). In humans the amplitude of the a-wave and b-wave will on average increase by 75% compared to non-light adapted conditions (Peachey et al. 1989).

1.10.2. Stimulus temporal frequency

Altering the stimulus frequency can also be used to isolate response from the rod and cone system. This is based on differences in their temporal frequency response characteristics. Dodt showed that under scotopic

conditions the maximum flicker fusion frequency had a maximum of 15Hz but increasing to 50Hz at photopic levels (Dodt 1951). It is now known that the cone system has an upper flicker fusion range of 60-100Hz compared to a maximum of 28Hz from the rod system (MacLeod 1972). This is partly due to a very fast integration time of the cones (Baylor et al. 1984; Demontis and Cervetto 2002).

1.10.3 Stimulus Intensity

The intensity of the stimulus used to elicit a response is an important factor. However, a scotopic stimulus on a dark adapted retina or a photopic stimulus on a light adapted retina will provide greater isolation of the rod and cone system respectively.

1.10.4. The ISCEV Clinical ERG

The clinical ERG is a non-invasive test which encompasses all of the three techniques mentioned previously to isolate and test the rod and cone systems (McCulloch et al. 2015). This highly standardised set of tests, put in place by the International Society for Clinical Electrophysiology of Vision (ISCEV), is the gold standard in assessing retinal function. A brief outline of the testing procedure is detailed below.

1.10.5. Isolating ERGs from the cone system.

To successfully isolate ERGs representative of the cone system, the participant is initially light adapted for a period of ten minutes. This is designed to supress the rod system and maximise the sensitivity of the cone system (Gouras and MacKay 1989). While light adapted, two tests are performed. The first test using a brief photopic flash which elicits the classic photopic response (Figure 1.27), consisting of a negative deflection, termed the a-wave, followed by a positivity termed the b-wave. From this waveform alone, inferences on the function of the cone photoreceptor (a-wave) (Bush and Sieving 1994) and postreceptoral (b-wave) function (Sieving et al. 1994) can be drawn based on the amplitude and implicit time of these components. The second test uses a fast flickering (30Hz) stimulus, both delivered on a photopic background. This produces a steady-state response. Information on cone inner retinal system function (Bush and Sieving 1996) can be determined by measuring the peak to trough amplitude and implicit time of the first peak. Implicit time is defined as the time taken from stimulus onset at t=0 to the peak/trough of the waveform component.

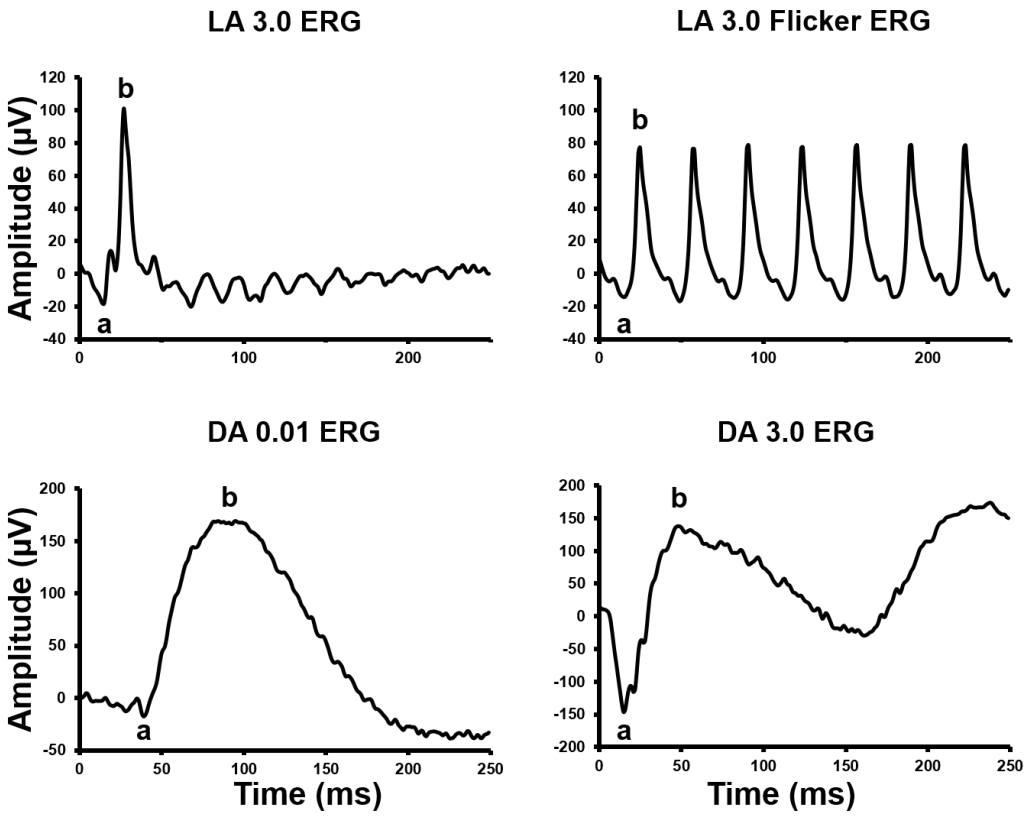

Figure 1.27. Graphical representations of the ISCEV clinical ERG waveforms. The top left graph is the photopic single flash response. Top right graph is the photopic 30Hz flicker. Bottom left is the scotopic rod response. Bottom right is the dark adapted ERG using a photopic stimulus. The DA 10.0 and oscillatory potential (OP's) are also part of the protocol (waveforms not shown).

1.10.6. Isolating the rod system

When testing the rod system, the patient is dark adapted for a period of 20 minutes to achieve maximum sensitivity of the rod system. Two tests are performed while the patient is dark adapted. The first uses a brief dim flash, whereas the second uses a brief bright flash. Both are delivered on a dark background. The first stimulus triggers a response from the rod system only. This is a high amplitude slow waveform driven mainly by the ON bipolar system (Gurevich and Slaughter 1993). The second test stimulus produces the archetypal dark adapted ERG, largely facilitated by the rod receptor and

postreceptoral contributions but with input from the dark adapted cone system also (Robson and Frishman 1998). A very detailed outline on procedures are outlined in the ISCEV ERG standards 2015 (McCulloch et al. 2015).

1.11. Photoreceptor isolation

The previous sections have described how using scotopic and photopic white light stimuli at various frequencies and adaptation levels can effectively separate the rod and cone ERG. By measuring the amplitude and implicit time of the a-wave of the ERGs it is then possible to obtain an estimation on the combined cone photoreceptor (L+M+S) or combined cone and rod photoreceptor (L+M+S+rod) input depending on the test. However, in some instances of retinal pathology, it may be of benefit to be able to assess the ERG from individual photoreceptor classes as opposed to the overall cone or overall rod and cone contribution. One potential example of this is the characterisation and diagnosis of the cone dysfunction syndromes (Aboshiha et al. 2015). Initially achromatopsia and blue cone monochromacy (BCM) can appear to be clinically similar however these may be separated by the presence of an S cone ERG in the BCM patients (Arden et al. 1999; Scholl and Kremers 2001; Kuchenbecker et al. 2014). Another benefit of the being able to separate the individual photoreceptor ERG is in colour vision research. There are still many unknowns about how colour is processed at post-receptoral and higher levels. To isolate the ERG of individual photoreceptor sub-populations a different approach is required. There are two methods that can produce isolation of responses from individual cone

populations: chromatic adaptation (Biersdorf and Armington 1957; Padmos and Van Norren 1971) and silent substitution (Estevez and Spekreijse 1982).

1.11.1 Chromatic Adaptation

Chromatic adaptation is achieved by using two different light stimuli, a continuous background light for adaptation and a pulsed light stimulus to stimulate. The photoreceptors which we do not want to stimulate are exposed to a continuous background light stimulus with a wavelength similar to their spectral peak, thereby selectively bleaching them and reducing their overall sensitivity. A second stimulus with a different wavelength is then presented transiently to selectively stimulate the population of photoreceptors we are interested in. (Biersdorf and Armington 1957) Typically long wavelength light (647nm) was used to supress the L and M cones while using a short wavelength light (467nm) to record the S cone response or vice versa (Padmos and Van Norren 1971; Arden et al. 1999).

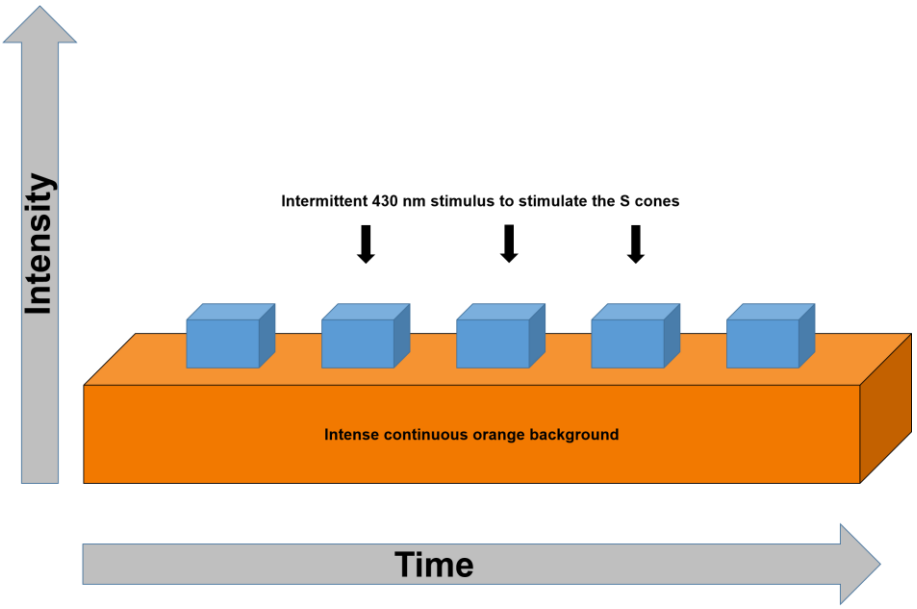

Figure 1.28. Illustration demonstrating the technique of chromatic adaptation to isolate the S cone ERG. A high intensity, long wavelength light is continuously on in the background (orange) to desensitize the L cone, M cone and saturate the rod response. Intermittent brief pulses of short wavelength light are presented (blue boxes) at an intensity above background to selectively stimulate the S cones.

However this method is not without its disadvantages. Firstly, it is not possible to separate the L and M cone response using this method because of their similar spectral profile. Secondly, the continuous background stimulus will affect the adaptation of all photoreceptors not just the sub-population we wish to supress. This will lead to non-linearities in the recorded response (Kremers et al. 2003). Finally, pre-retinal absorption as result of lenticular changes and macular pigment density need to be accounted for as they vary between individuals.

The second and more refined method used to isolate the individual photoreceptor sub populations is the silent substitution technique. This is the method that is used throughout this thesis and is described in detail in the following chapter.

Chapter 2

Methods and Materials

2.1 Introduction

Silent substitution is a method that will be utilised throughout this thesis. It is based on the principle of univariance advanced by Rushton (Estevez and Spekreijse 1982) and Young's trichromatic colorimetric theory. The principle of univariance states that a change in the visual pigment following the absorption of a photon of light is always the same regardless of the wavelength of that light (Estevez and Spekreijse 1982). A silent substitution occurs when a stimulus of a specific spectral composition is alternated with another stimulus of a different spectral composition which creates an overall net effect of zero excitation of a particular photoreceptor. By varying the intensity of the light sources in these different spectral compositions it is possible to create this effect for 3 out of the 4 human photoreceptor sub-populations; thereby only registering a change in one sub population. An example is shown in figure 2.1, where in this case it is the rods that have been selectively stimulated and the other photoreceptor populations having been silenced. Such a stimulus allows us to record ERGs that selectively reflect the activity rods free from cone intrusions (Shapiro et al. 1996; Usui et al. 1998; Kremers and Meierkord 1999; Pokorny et al. 2004; Cao et al. 2011).

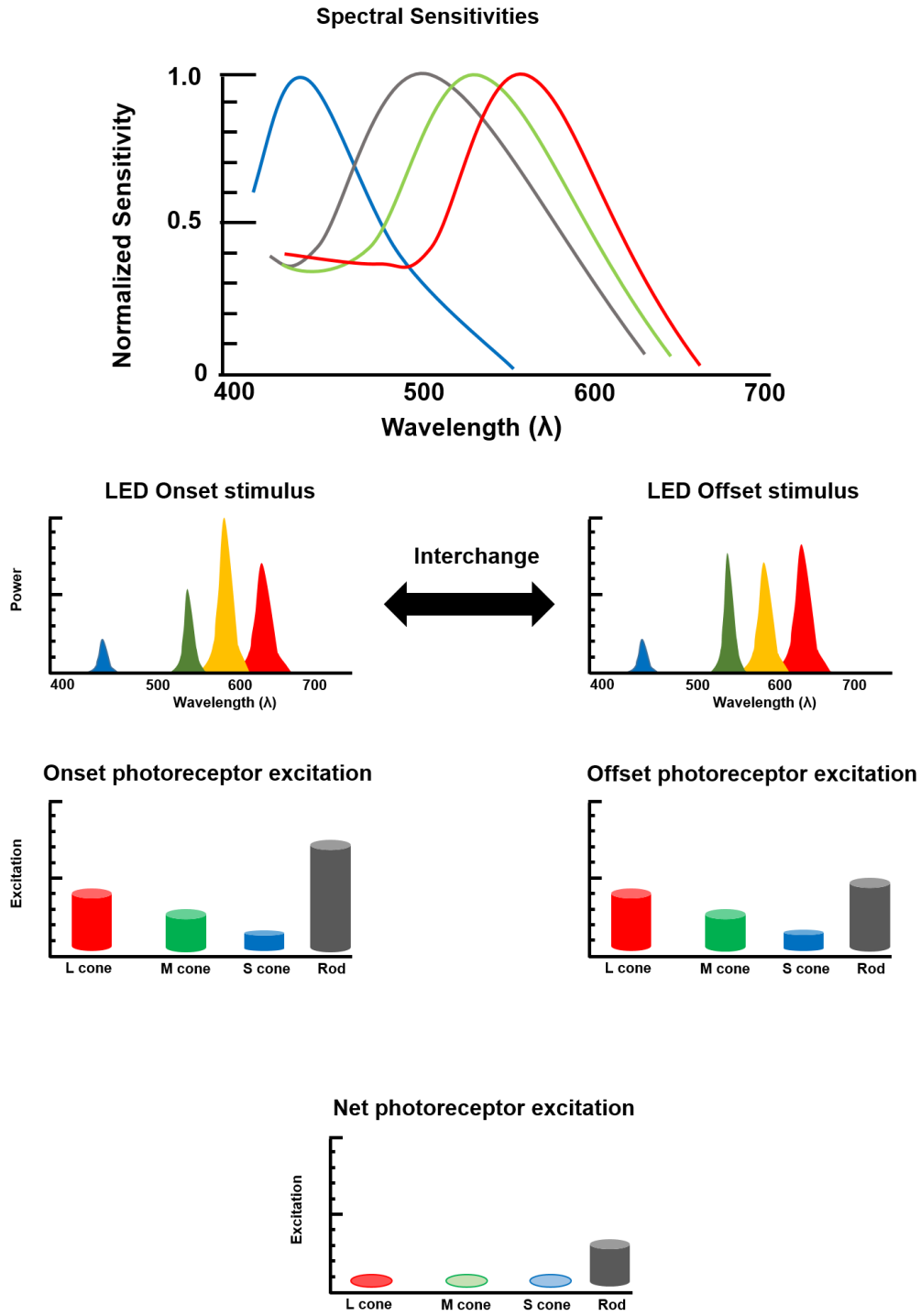

Figure 2.1. A graphical representation of the silent substitution process. The top graph shows the typical spectral sensitivity of the four human photoreceptors types. The second row of graphs details the different spectral compositions of two light stimuli. The third row shows the individual photoreceptor excitation produced in response to the above stimuli. The bottom graph shows the net change in excitation produced in each photoreceptor class following modulation of both stimuli. The net change in excitation is effectively zero for three of the four photoreceptor classes. Therefore this stimulus selectively stimulates the rod photoreceptors which in turn is recorded as the rod isolated ERG.

Of course, in order to achieve a silent substitution we must also know the cone spectral sensitivity characteristics or fundamentals. They are defined as the relative sensitivity of each cone class across the visible spectrum. The first set of complete cone fundamentals were determined in 1971 (Vos and Walraven 1971) with revisions of the estimates performed by several other groups (Smith and Pokorny 1975; Stockman and Sharpe 1998; Stockman and Sharpe 2000). The cone fundamentals used in this thesis are taken from the work by Stockman and Sharpe (2000) and are based on Stiles and Burch's 10^0 colour matching functions (CMFs) (Stiles and Burch 1955). The rod fundamentals are obtained from work by Wysecki and Stiles (1967).

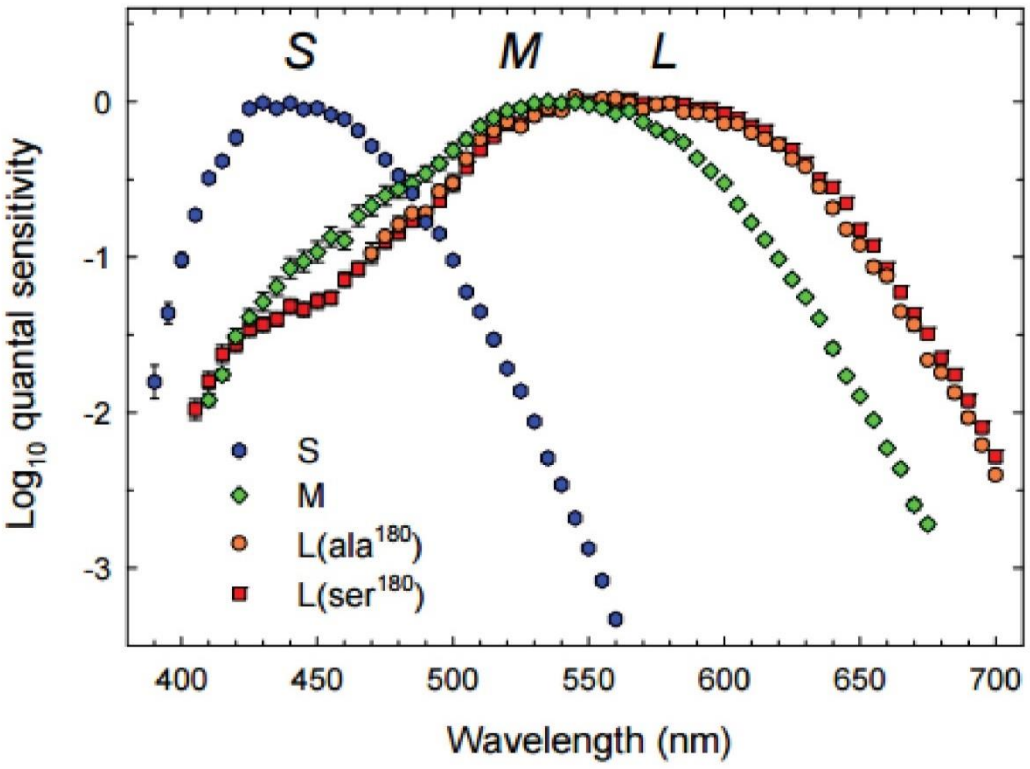

Figure 2.2. Spectral sensitivity measurements using heterochromatic flicker photometry (HFP) for two common variations of L cone pigment along with the M and S cone recorded by Stockman and Sharpe (Stockman 2008).

2.2 Experimental equipment

All of the photoreceptor isolation experiments were carried out using the Espion E2 Ganzfeld stimulator™ (Colordome; Diagnosis LLC, Lowell, MA) (See Figure 2.3). It is a sphere shaped stimulator with an opening to place the participants head allowing them full field stimulation. It contains an integral Xenon flash tube with a luminance range from 3000 cd.s.m^{-2} down to below 0.009 cd.s.m^{-2} as well as red (632nm), green (514nm) amber (592nm) and blue (460nm) LEDs with a nine order of magnitude luminance range and half bandwidths of approximately 30nm. It provides illumination as close to uniform as possible also allowing precision control of stimulus duration, intensity and wavelength.

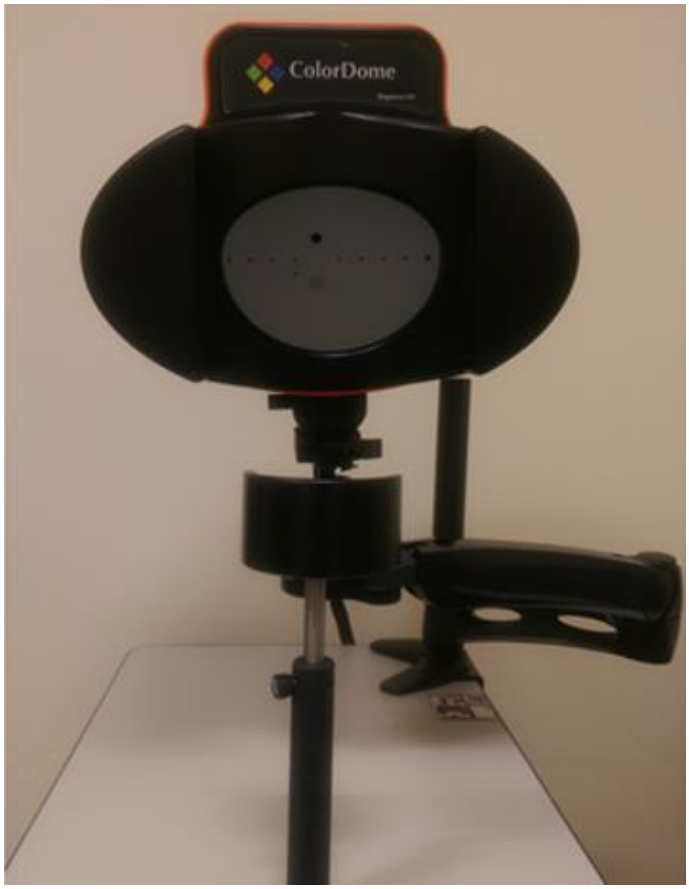

Figure 2.3. The four primary Colordome ganzfeld stimulator used to deliver the ERG stimuli.

2.3 Calibration

Calibration of the ganzfeld stimulator was performed using the PR-650 Spectrascan Spectral Colorimeter (Photo Research Inc., Chatsworth, California). This was performed through the 'Ganztest' feature specific to the Espion system, which allows the operator control of the individual sets of LEDs. The linearity of each type of LED was measured, comparing measured luminance (using the photometer) with theoretical luminance (the luminance quantity inputted to the software). The linearity of the LEDs up to 200 cd.s.m^{-2}, (the maximum luminance used in our experiments) is shown in figure 2.4. The LEDs maintain good linearity over the luminance range tested. Towards the upper end of the range the blue, red and amber begin to slightly stray from the ideal linearity. This potentially could have an effect on some of the high luminance stimuli, however the majority of the stimuli are well within the linear region.

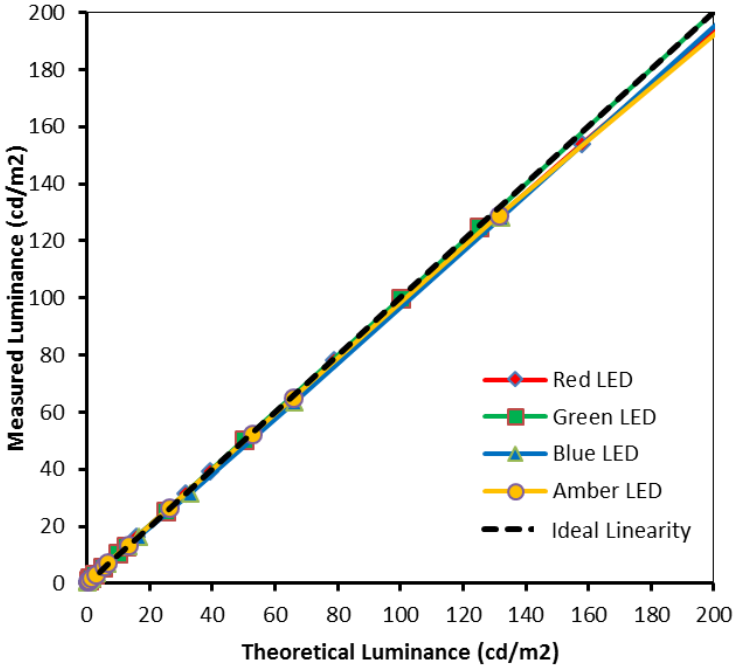

Figure 2.4. Linearity of the four types of LEDs in the ganzfeld stimulator.

The emission spectra of each set of bright and dim LEDs were measured at intervals of 5 nm ranging from 380 to 780nm and graphed as shown in figure 2.5. These values are required to create the silent substitution stimuli. The range at which the LEDs can be driven at ranges from 0 - 64000. This is an arbitrary range. Both radiometric and luminance measurements of the bright LEDs were obtained along with the peak wavelength and the CIE coordinates at a setting of 1000 or one 64th of the total power (Table 2.1). Both the radiometric and photometric measurements were then multiplied by 64 to obtain their maximum value. All values were relatively stable with a variation of <1%.

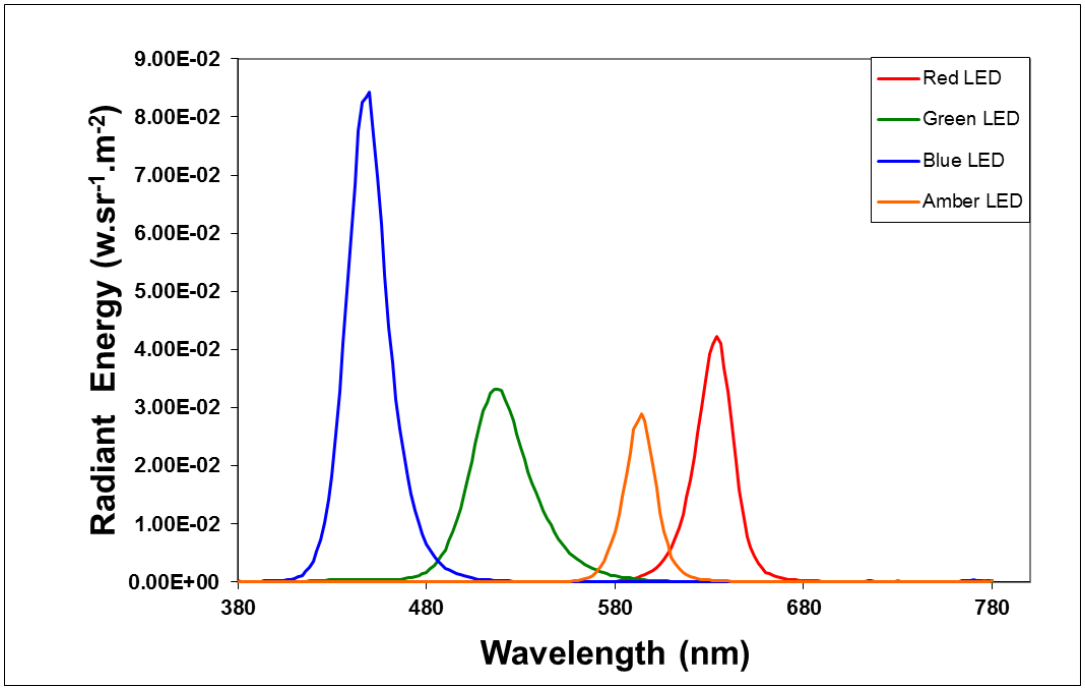

Figure 2.5. The LED spectral radiance measurements from the ganzfeld stimulator using a PR650 spectrophotometer.

LED	Peak Wavelength (nm)	Radiometric Measurement ($w.sr^{-1}.m^{-2}$)	Luminance Measurement ($cd.s.m^{-2}$)	CIE Coordinates (x and y)	$w.sr^{-1}.m^{-2}$ for 1 $cd.s.m^{-2}$
Bright Red	**632**	**0.216**	**38.4**	**x= 0.695 y=0.301**	**0.00562**
Bright Green	**516**	**0.266**	**120**	**x=0.154 y=0.695**	**0.00221**
Bright Blue	**448**	**0.46**	**15.6**	**x=0.154 y=0.026**	**0.02948**
Bright Amber	**592**	**0.133**	**63.9**	**x=0.583 y=0.416**	**0.00208**

Table 2.1. Calibration measurements of the bright sets of LEDs in the ganzfeld stimulator.

2.4. Generation of stimuli

As outlined in the introduction to this chapter, silent substitution can be used to selectively stimulate a single photoreceptor class. There are four different classes of photoreceptors in the human retina directly involved in vision. In order to selectively stimulate a single class of photoreceptor only, the number of primaries required are equal to n, where n is the number of photoreceptor populations we wish to silence. The Colordome ganzfeld, four primary LED stimulator as described in section 2.2 was used to create a triple silent substitution. Stimulus intensity and wavelength combinations were used that produced no change in the net excitation of three of the four photoreceptors classes, thereby selectively stimulating the remaining photoreceptor class. To generate silent substitution stimuli the spectral characteristics of the 4 LED spectra were multiplied by each of the four photoreceptor fundamentals,(Shapiro et al. 1996; Stockman and Sharpe 2000) integrating across the visible spectrum of wavelengths (see Equation 1). Equation 1 shows the calculation of the excitation of the rod photoreceptors by the red LED:

$$E_{r,R}(t) = F_R * L_R(t) * \sum_{\lambda} I_R(\lambda) A_r(\lambda) \quad (2.1)$$

where $E_{r,R}$ is the excitation of the rod by the red LED, changing as a function of time t. F_R is a conversion factor for the red LED relating to photometric measurements obtained from the relevant row of the last column in table 2.1, L_R is the luminance of the red LED, $I_R(\lambda)$ is the emission spectrum of the red LED and $A_r(\lambda)$ is the V'(λ) 10º function (Stockman and Sharpe 2000). When the above calculation is carried out for all four photoreceptors and each of the individual LEDs the resultant is **A**, a 4x4 matrix (Equation 2.2). This is effectively the sensitivity for a photoreceptor for a given luminance of an LED.

$$\mathrm{A} = \begin{matrix} \begin{bmatrix} E_{lR}(t) & E_{mR}(t) & E_{sR}(t) & E_{rR}(t) \\ E_{lG}(t) & E_{mG}(t) & E_{sG}(t) & E_{rG}(t) \\ E_{lB}(t) & E_{mB}(t) & E_{SB}(t) & E_{rB}(t) \\ E_{lA}(t) & E_{mA}(t) & E_{SA}(t) & E_{rA}(t) \end{bmatrix} \\ \mathrm{Total} \quad \mathrm{E_{lRGBA}(t)}\ \mathrm{E_{mRGBA}(t)}\ \mathrm{E_{sRGBA}(t)}\ \mathrm{E_{rRGBA}(t)} \end{matrix} \quad (2.2)$$

The subscripts R, G, B, A represent the four LEDs (red, green, blue, and amber) and l, m, s, r the L-, M-, S-cone, and rod photoreceptors, respectively. To calculate maximal and minimal excitation, and then cone or rod Michelson contrast from LED Michelson contrast, a further step is required. With sine-wave stimuli, the maximal or minimal excitations coincide with the time-point t where LED luminance is maximal or minimal. Thus, from

matrix **A** maximal and minimal excitations are calculated for each photoreceptor. From that we can calculate the photoreceptor contrast from LED contrast (RCd, GCd, BCd, and ACd). Matrix B is the relative sensitivity for a photoreceptor for a given luminance of an LED.

$$\mathrm{B} = \begin{bmatrix} E_{lR}(t)/\mathrm{E}_{\mathrm{lRGBA}}(\mathrm{t}) & E_{mR}(t)/\mathrm{E}_{\mathrm{mRGBA}}(\mathrm{t}) & E_{sR}(t)/\mathrm{E}_{\mathrm{sRGBA}}(\mathrm{t}) & E_{rR}(t)/\mathrm{E}_{\mathrm{rRGBA}}(\mathrm{t}) \\ E_{lG}(t)/\mathrm{E}_{\mathrm{lRGBA}}(\mathrm{t}) & E_{mG}(t)/\mathrm{E}_{\mathrm{mRGBA}}(\mathrm{t}) & E_{sG}(t)/\mathrm{E}_{\mathrm{sRGBA}}(\mathrm{t}) & E_{rG}(t)/\mathrm{E}_{\mathrm{rRGBA}}(\mathrm{t}) \\ E_{lB}(t)/\mathrm{E}_{\mathrm{lRGBA}}(\mathrm{t}) & E_{mB}(t)/\mathrm{E}_{\mathrm{mRGBA}}(\mathrm{t}) & E_{SB}(t)/\mathrm{E}_{\mathrm{sRGBA}}(\mathrm{t}) & E_{rB}(t)/\mathrm{E}_{\mathrm{rRGBA}}(\mathrm{t}) \\ E_{lA}(t)/\mathrm{E}_{\mathrm{lRGBA}}(\mathrm{t}) & E_{mA}(t)/\mathrm{E}_{\mathrm{mRGBA}}(\mathrm{t}) & E_{SA}(t)/\mathrm{E}_{\mathrm{sRGBA}}(\mathrm{t}) & E_{rA}(t)/\mathrm{E}_{\mathrm{rRGBA}}(\mathrm{t}) \end{bmatrix}$$

(2.3)

For example, to generate a rod-isolating stimulus that produces a 0.25 modulation of rod excitation. Our desired photoreceptor contrast setting (PCd) would be 0% for L cone, 0% for M cone, 0% for S cone, and 25% for rods:

$$\mathrm{PC_d} = \begin{bmatrix} 0 \\ 0 \\ 0 \\ 0.25 \end{bmatrix} = \mathrm{B} \times \begin{bmatrix} RCd \\ GCd \\ BCd \\ ACd \end{bmatrix} \tag{2.4}$$

We then can multiply our desired photoreceptor contrast with the inverse of **B** ($\mathbf{B^{-1}}$), to obtain the desired LED contrast (LCd) required to achieve our level of photoreceptor isolation.

$$\mathrm{LCd} = \mathrm{PCd} * \mathrm{B} - 1 \quad (2.5)$$

An Excel spreadsheet was used to generate a script file which specified details of phase, modulation depth and mean luminance required for each LED on a millisecond-by-millisecond basis for the full duration of the stimulus. This script file was then used by the Espion E^2 system to drive the stimulus on Ganzfeld stimulator. Specific stimulus characteristics for each experiment are detailed in each of the experimental chapters.

2.5 Stimulus Description

Both transient and steady-state stimuli are used in this thesis. The transient stimuli typically consisted of a square-wave temporal profile (flash) with an initial ON period for 250ms followed by an OFF period for 250ms. The steady-state stimuli took the form of temporal sinusoids (flicker) which varied in both amplitude and frequency, depending on the experiment. This section describes the temporal profiles for each of the stimuli used as well as their spectral characteristics.

2.5.1 Steady-state stimuli

Steady-state stimuli are used in chapter 3 and chapter 5. Depending on the experiment, we varied the temporal frequency (5-60Hz) and luminance (1-10000 ph.Td) of rod and cone isolating stimuli as well as rod + L cone and

non-isolated stimuli. The temporal profiles of the steady-state stimuli used are shown in figure 2.6.

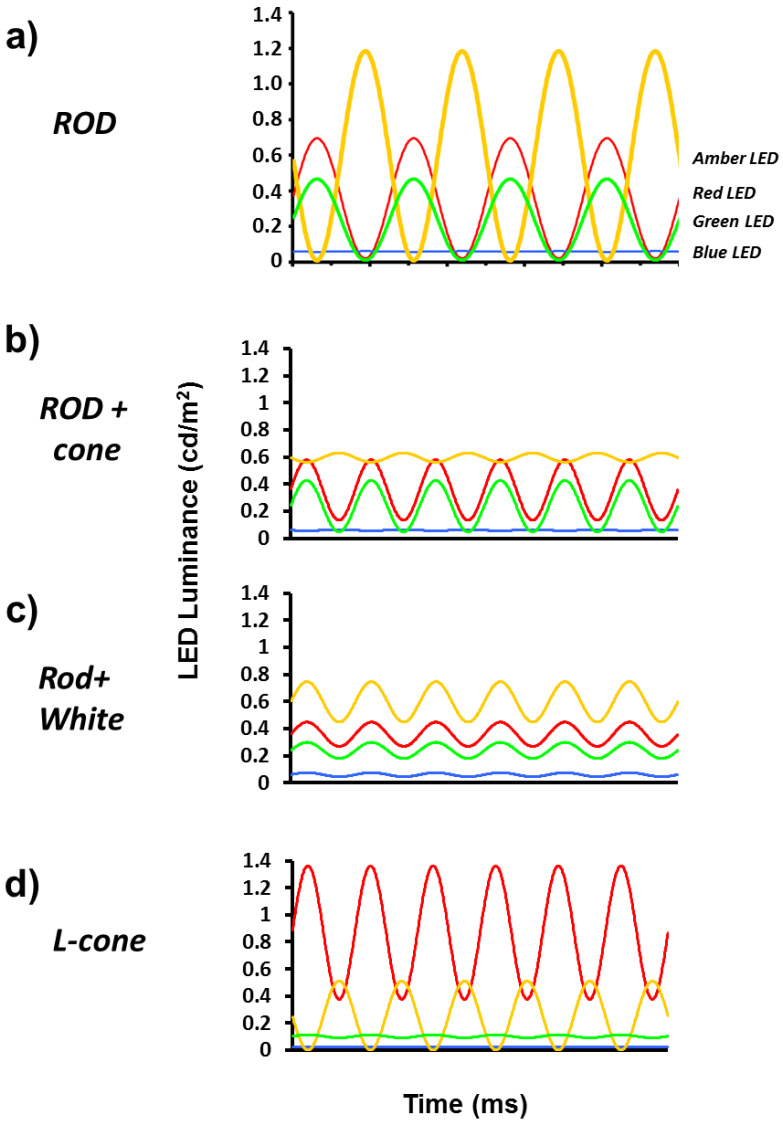

Figure 2.6. The luminance profiles and relative phases of the blue (B), green (G), amber (A) and red (R) LEDs that are required to generate a) a rod isolating stimulus, b) mixed rod and L- and M-cone stimulus, c) rod and 'white' stimulus and d) L-cone stimulus.

2.5.2 Transient stimuli

Transient rod and cone isolating stimuli are used in chapters 4, 5, and 6. Examples of their onset and offset luminance temporal profiles are shown below.

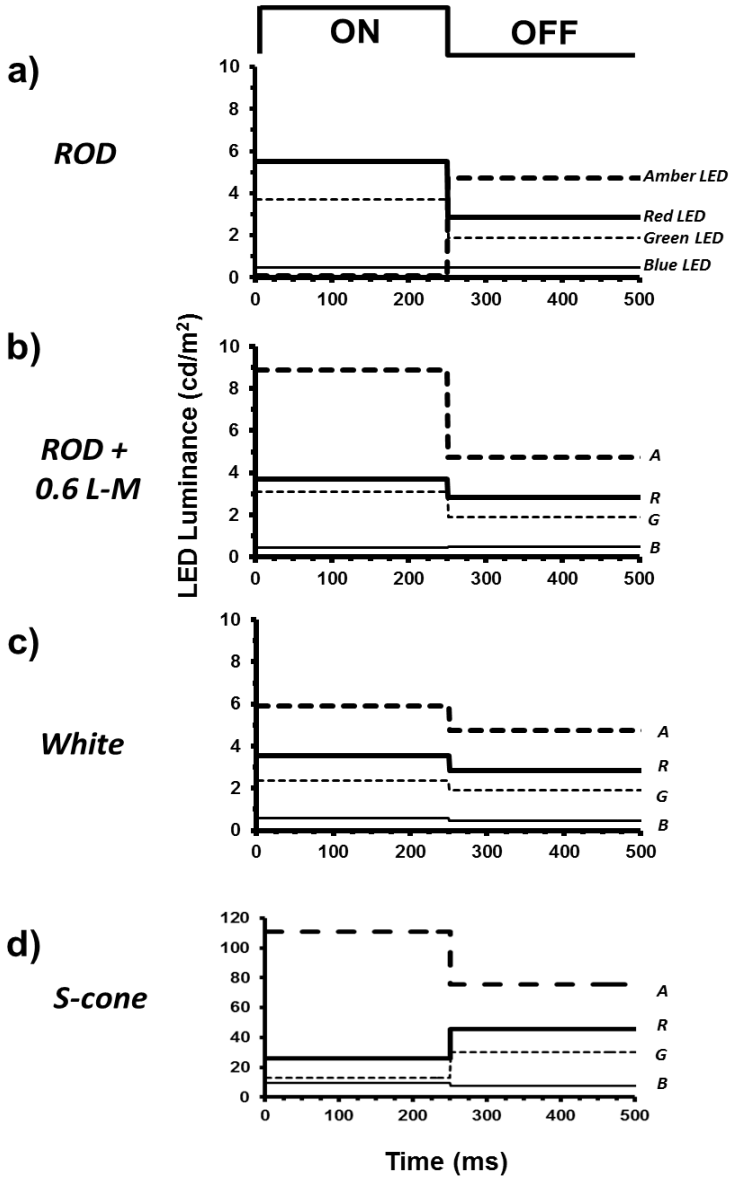

Figure 2.7. Temporal profiles of the square-wave pulse stimulus used to generate isolated ERGs. The plots show the luminance variation of the four LED primaries required to generate: a) a rod isolating stimulus, b) a mixed rod and L- and M-cone stimulus (cone modulation = 0.6), c) 'white' stimulus and d) S-cone stimulus. In each case the initial 0 - 250ms is the onset period followed by the offset period (250-500ms).

2.5.3 Stimuli emission spectra

The emission spectra of both the onset and offset stimuli (or maximum and minimum for steady-state stimuli) were measured using the PR-650 Spectrascan Spectra Colorimeter (Photo Research Inc., Chatsworth, California). The resulting graph for each stimulus used is shown in figure 2.8.

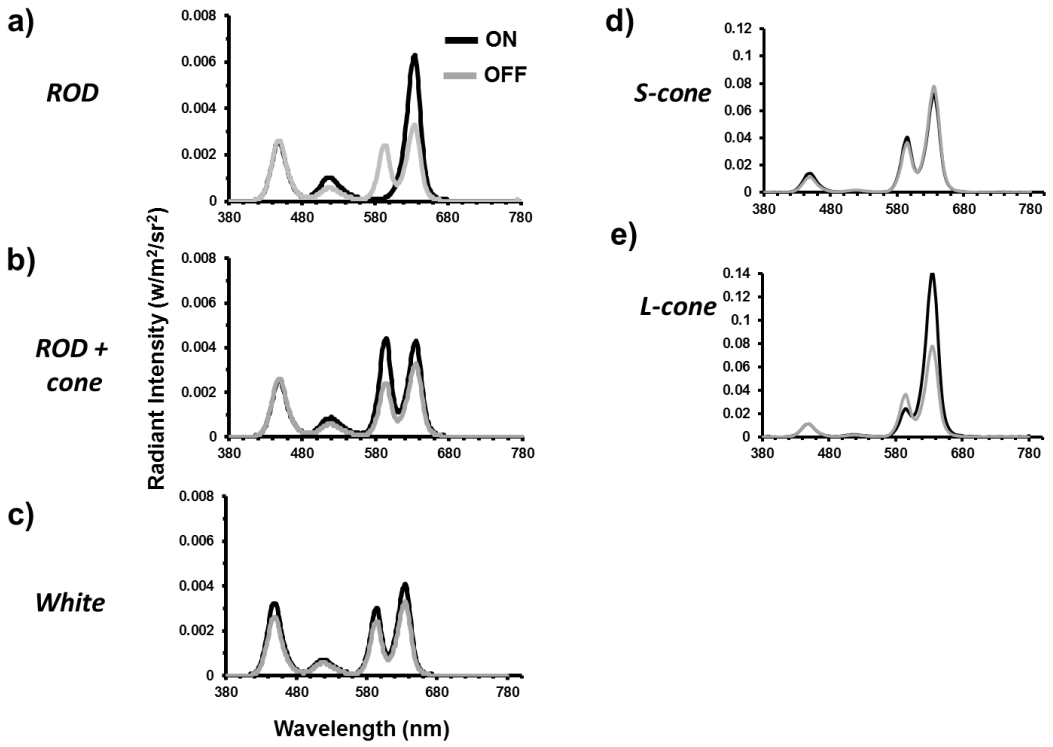

Figure 2.8. Spectral characteristics of the stimuli used to generate a) the rod isolating stimulus, b) the mixed rod and L- and M-cone stimulus, c) the 'white' stimulus, d) the S-cone stimulus and e) the L-cone stimulus. The plots show the spectral characteristics of the onset (black lines) and offset (grey lines) phases of each of the stimuli.

2.6 Participant preparation

Informed consent was received from all participants. An examination of the anterior chamber was then performed by a registered optometrist before administration of Tropicamide (1%). Tropicamide was used to dilate the

participant pupil. Pupil diameter was measured when the participant reached full dilation after approximately 20 minutes. The participant was positioned in front of the ganzfeld stimulator using the chin rest and asked to fix on the red LED at the centre subtending approximately 0.5 degree of angle to reduce eye movement. The fellow eye was patched to reduce artefact and increase participant viewing comfort.

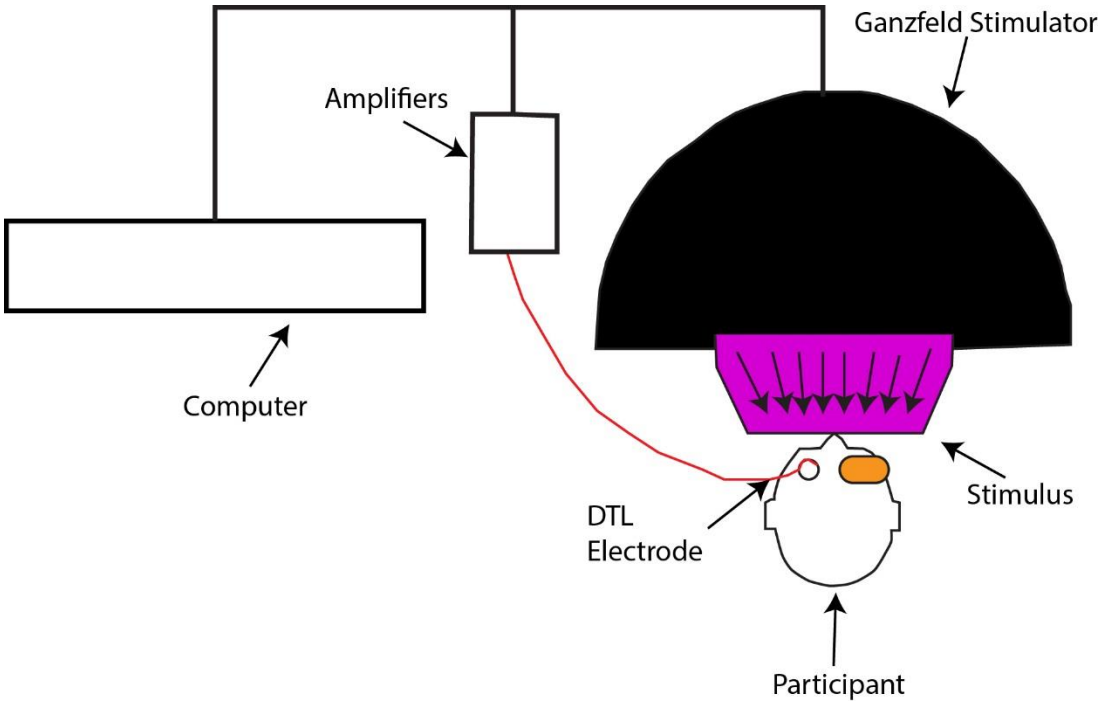

Figure 2.9. Illustration of the experimental set up. The participant's head is situated in front of the Ganzfeld stimulator. The recording electrode is attached to the eye and connected to the amplifier box which is then connected to the PC. The isolating stimulus (purple) is presented to the participant.

2.6.1 The electrodes

The ERGs were recorded from the corneal DTL electrode (Diagnosys LLC, Lowell, MA) and silver-silver chloride (Biosense Medical, Chelmsford UK) reference electrode. A silver-silver chloride electrode was also used for the ground. The DTL electrode was placed across the sclera, close to the lower limbus. The reference electrode was placed at the outer canthus and the ground electrode was placed on the forehead at the Fpz position consistent with the 10-20 electrode placement system (Sharbrough et al. 1991). A gritted exfoliation paste was used to lightly abrade the skin before placement. This ensures low skin impedance and contributes to the overall quality of the signal to noise ratio. For the VEP experiment the active electrode was placed in the Oz position consistent with the 10-20 electrode placement system.

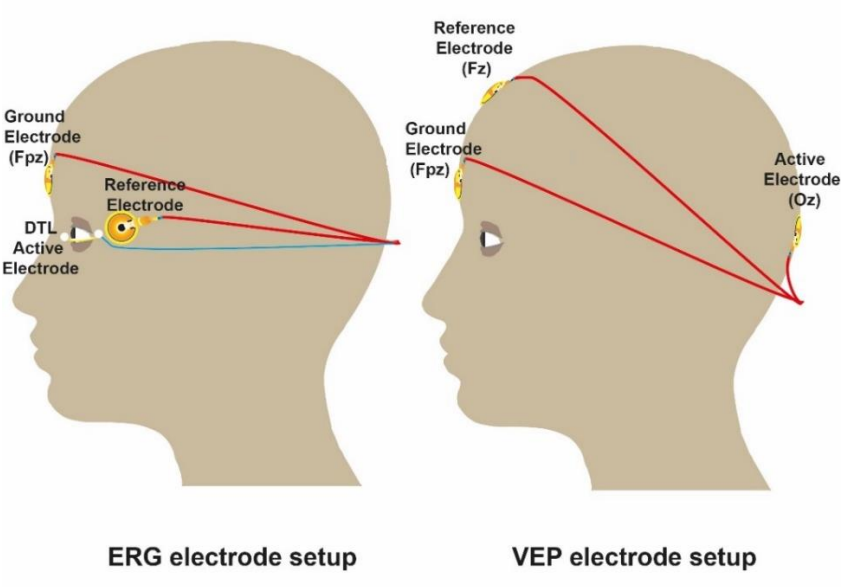

Figure 2.10. Electrode montage used to perform an ERG (left image) and VEP (right image) measurements. The ground electrode is placed on the forehead in the Fpz position for both tests. The reference electrode for the ERG is placed at the outer canthus. The reference electrode for the VEP is placed in the Fz position along the anterior midline of the head. The ERG DTL active electrode is a corneal surface fibre electrode which sits on the sclera just below the cornea. The VEP active is placed at the Oz position at the posterior midline of the occipital cortex.

2.7 Data Analysis

2.7.1 Steady-state analysis

The ERG responses were amplified and the bandwidth was set at 0.3-300Hz with a sampling rate of 1000Hz with an epoch of 4000ms for all steady state stimulus protocols. In post analysis, Fast Fourier Transform (FFT) plus interface running Signal (version 2.16) software (Cambridge Electronic Design, Cambridge, UK) was used to extract amplitude and phase information from the raw steady state data. The FFT used a sampling rate 1024Hz, therefore some simple interpolation was required to resample the data timings to produce 4096 data points from the 4000ms epoch.

Amplitude and phase measurements of the fundamental frequency (f), the 2^{nd} harmonic (f_2) and the noise (average of f+1 and f-1) were measured as shown in figure 2.11. An acceptable signal to noise ratio (SNR) was determined as 2.82 which gives a statistical significance of p=0.05 (Meigen and Bach 1999).

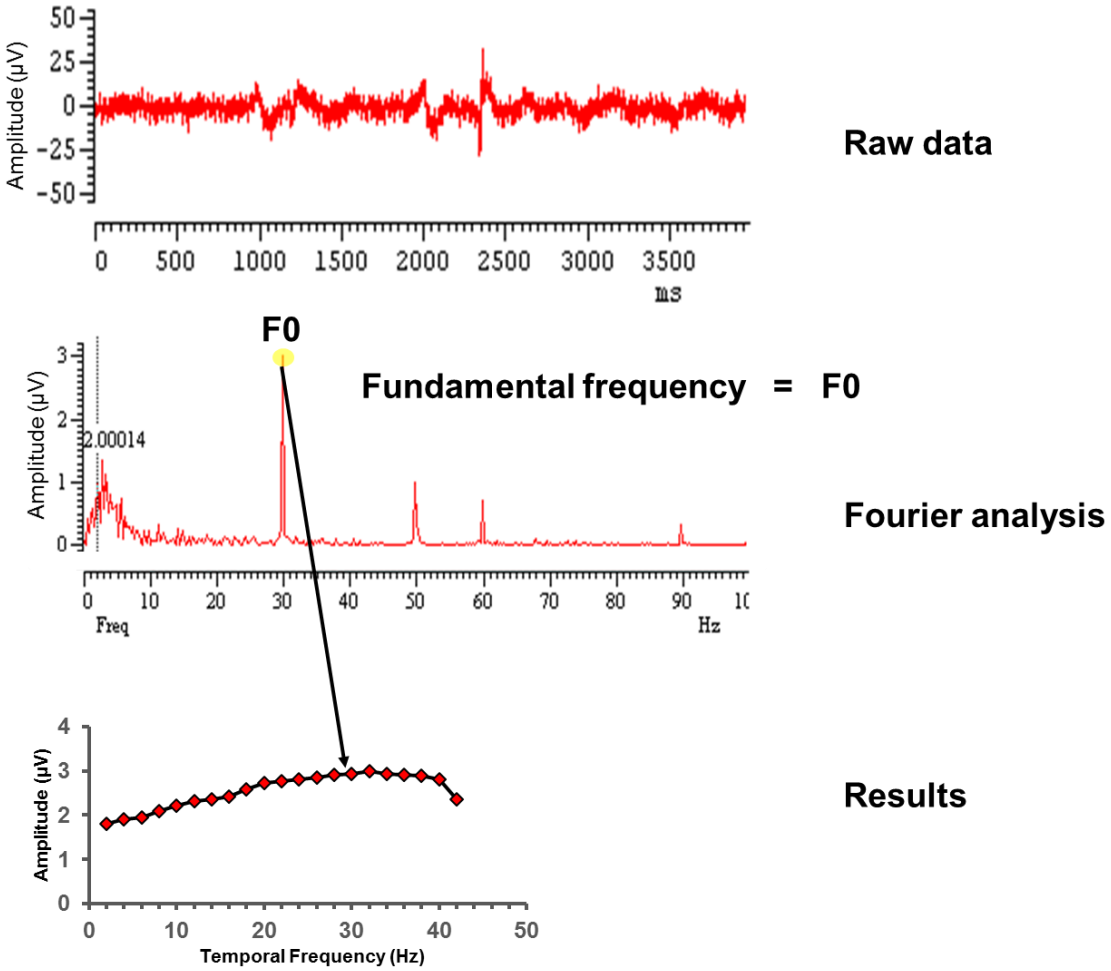

Figure 2.11. (Top graph) raw data from a steady state stimulus. (Middle graph) The Fast Fourier Transform of the signal, displaying the magnitude of the fundamental frequency with the noise measured as the average of the magnitude of the signal at the integer frequency either side of it. (Bottom graph) example of how the overall result is compiled using individual data points as a function of temporal frequency.

2.7.2 Transient data analysis

The ERG responses were amplified and the bandwidth was set at 0.3-300Hz with a sampling rate of 1000Hz with an epoch of 500ms for all steady state stimulus protocols. The transient square-wave stimuli produced ERG responses in which the amplitude and implicit time of the relevant peaks and

troughs were measured. The implicit time of a waveform component which was produced following an onset stimulus was defined as the time difference (t) from stimulus onset, where t=0 ms, to the peak or trough of the component in question. The implicit time of a waveform component which was produced following an offset stimulus was defined as the time difference (t) from stimulus offset, where t=250 ms, to the peak or trough of the component in question. Waveform specific amplitude and other timing measurements are outlined in more detail in the relevant data chapters.

2.8 Participants

Colour vision in all subjects (except the participant with ESCS) was assessed using CAD colour test from City University and the Ishihara test plates.

2.8.1 Chapter 3 experiments

Experiments 1 and 2.

5 colour normal trichromats (3 males; mean age: 28 yrs., age range: 35 yrs.) were used.

Experiment 3.

A sub-set of the cohort from experiment 1, consisting of 3 colour normal trichromats (2 males; mean age: 39 yrs., age range: 19 yrs.).

2.8.2 Chapter 4 experiments

Experiment 1.

20 normal trichromatic observers *(*mean age: 31.5 yrs., age range: 53 yrs.)

Experiments 2 and 3

A sub-set of the cohort from experiment 1, consisting of 5 colour normal trichromats (3 males; mean age: 32 yrs., age range: 24 yrs.).

2.8.3 Chapter 5 experiments

Experiment 1.

5 colour normal trichromats (3 males; mean age: 28 yrs., age range: 35 yrs.) and 3 members of a family (ACR 1 (31 yrs.), ACR 2 (38 yrs.) & ACR 3 (34 yrs.)) & with a homozygous p.T383fsX mutation in CNGB3 causing rod monochromacy

Experiment 2.

The 20 normal trichromatic observers from chapter 4 (mean age: 31.5 yrs., age range: 53 yrs.), along with the 3 subjects with rod monochromacy (previously described) and 2 subjects (NB1 (17 yrs.) and NB2 (27 yrs.)) with congenital stationary night blindness (CSNB 1).

Experiment 3.

The three members diagnosed with rod monochromacy, previously described.

2.8.4 Chapter 6 experiments

Experiments 1 and 2.

15 colour normal trichromats (5 males, 10 females; mean age: 33 yrs, age range: 40 yrs).

11 participants with a colour vision deficiency; including 9 dichromats (6 deuteranopes, 3 protanopes) and 3 anomalous trichromats (2 deuteranomalous, 1 protanomalous) all males; mean age 32yrs, age range: 38 yrs.

Experiment 3.

A subset of the participants from experiments 1 and 2, consisting of 13 colour normal trichromats (5 males, 10 females; mean age: 33 yrs, age range: 40 yrs).

9 participants with a colour vision deficiency including 6 deuteranopes, 3 protanopes, all males; mean age 36yrs, age range: 38 yrs.

1 participant diagnosed with blue cone monochromacy (BCM).

1 participant diagnosed with enhanced S cone syndrome (ESCS).

The participant diagnosed with BCM had an L opsin gene, with a novel point mutation p.Pro196Ala, predicted to account for the phenotype. The participant with ESCS has bi-allelic loss of function mutations in NRL. This is a transcription factor which positively regulates is NR2E3 and the loss of function is likely to cause the phenotype.

2.9 Colour vision assessment

Colour vision testing was performed on all participants.

2.9.1 The CAD test

The colour assessment and diagnosis (CAD) test was developed by City University. It is a computer-based test which measures the participant's red/green and blue/yellow colour signal sensitivity required to discriminate a moving chromatic stimulus on a background of random dynamic luminance contrast noise (Rodriguez-Carmona et al. 2005). The stimulus moves in a diagonal manner from corner to corner on a square background of noise (Figure 2.12). The participant is given a four alternative, forced choice to select the direction in which the stimulus is moving using arrows on a keypad e.g. bottom left to top right, bottom right to top left and vice versa. The test employs 16 different directions in colour space on the 1931 CIE chromaticity diagram. The participant's chromatic sensitivity for each coordinate, is measured as the distance in colour space away from the neutral grey background (Rodriguez-Carmona et al. 2005) shown in figure 2.13.

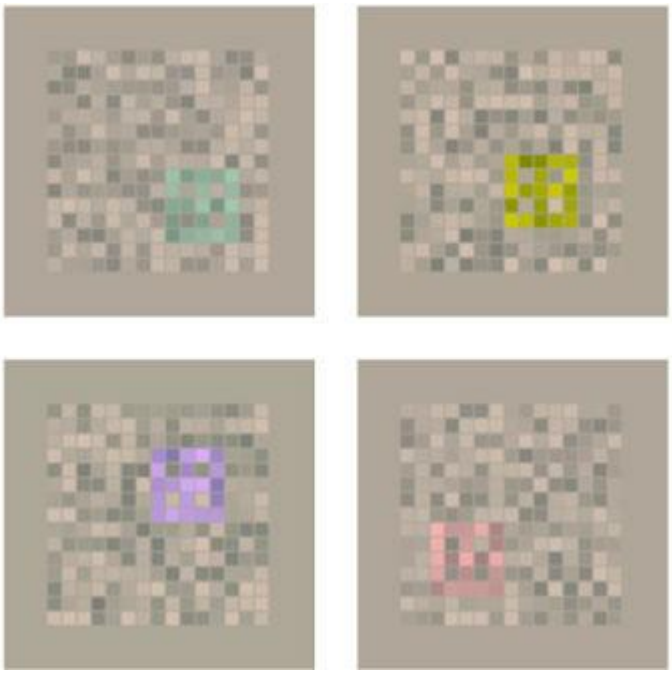

Figure 2.12. Example of the different chromatic stimuli on the background of noise used in the CAD test.

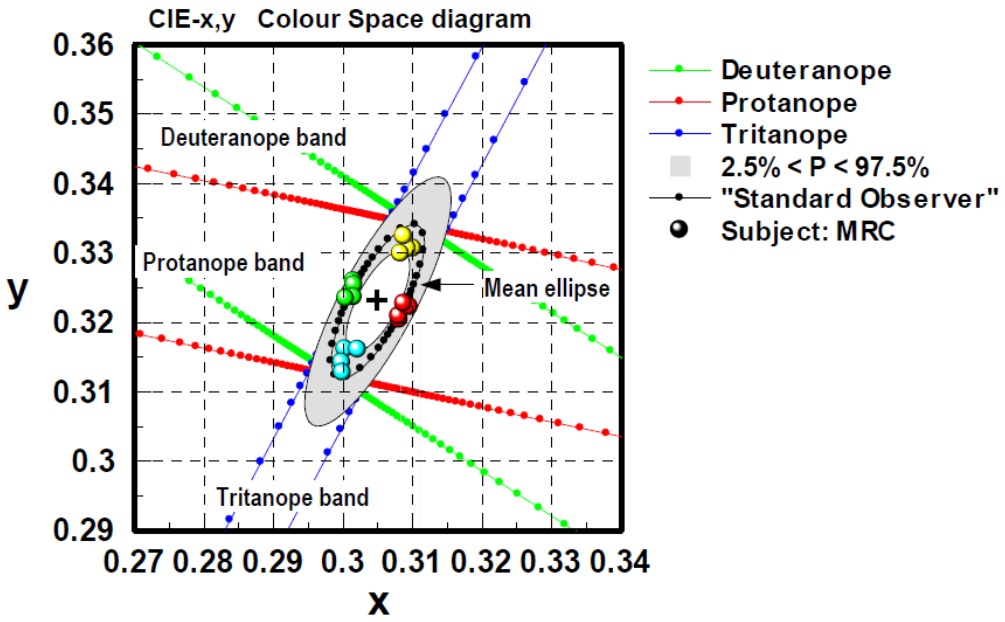

Figure 2.13. Graphical representation of the results from the CAD system. The results are presented on the 1931 colour space diagram. The inner and outer grey ellipse represents the colour normal variability. The black markers represent the response from a typical observer. The red, green and blue lines represent the protanope, deuteranope and tritanope axis. The large yellow, green, red and cyan dots represent the 16 different colour directions tested. Image taken from ML Rodriguez-Carmona 2005

The participant's results are compared to a large normal and colour deficient database, enabling not only a diagnosis but a severity rating (Rodriguez-Carmona et al. 2005).

2.9.2 Ishihara test plates

Ishihara test plates are used for quick diagnosis of protan and deutan or red/ green colour deficiencies. They consist of a number of test plates each with a background of coloured dots of different sizes and colour in which the shape of a number, in the centre of the plate is visible to those with normal red/green colour vision (with the exception of the hidden digit plate). The number only differs in colour, not saturation, dot size or luminance. There are four different types of plates; Transformation where individuals with a colour vision deficiency will see a different number compared to people with normal colour vision, vanishing plates, where only colour normal individuals can see the number, hidden digit plates, where individuals with a colour deficiency can see the number and diagnostic plates, which are used to specify the type of colour deficiency.

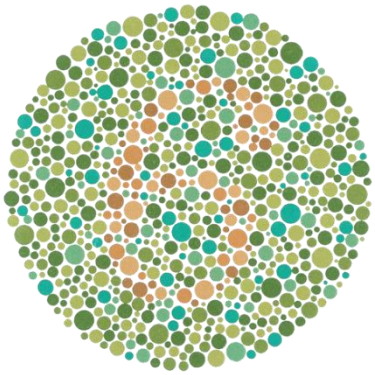

Figure 2.14. Example of an Ishihara plate with the background of randomly coloured dots and the number in the middle. Taken from www.wikipedia.org.ishihara. Accessed /29/06/20117.

2.10 Ethics

All participants gave informed consent prior to the commencement of the experiments which were conducted in accordance with the Declaration of Helsinki and were approved by the University of Bradford Ethics Committee.

Chapter 3

Rod Electroretinograms Elicited by Silent Substitution Stimuli from the Non-Dark-Adapted Human Eye.

3.1 Introduction

The flash electroretinogram (ERG) is an electrical response elicited from the retina in response to stimulation by light. The ERG is generated by contributions from many different retinal cells types, but with appropriate manipulation of the temporal, chromatic and luminance characteristics of the stimulus, as well as the subject's adaptational state, it is possible to selectively stimulate and assess the functional characteristics of discrete populations of retinal neurons (Kremers and Link 2008; Parry et al. 2012). In particular, the isolation of rod photoreceptor activity has long been considered important from a clinical perspective as many congenital and acquired visual disorders can differentially affect rod relative to cone function. The ability to elicit ERGs that selectively reflect the activity of rods has played a key role in the diagnosis and monitoring of conditions such as retinitis pigmentosa, congenital stationary night blindness (CSNB) and vitamin A deficiency (Berson et al. 1968; Berson et al. 1969; Perlman et al. 1983; Scholl et al. 2001; Petzold and Plant 2006). In age-related macular degeneration (ARMD) some of the earliest pathological and functional changes occur in rod–mediated vision in geographically localised regions of the retina (Owsley et al. 2000). In addition, it has been shown that normal younger individuals who carry a high genetic risk of developing ARMD in later life exhibit subtle changes in rod-mediated mesopic vision (Feigl et al.

2011). Thus there are compelling clinical reasons for methods that selectively assess rod function in humans.

The most frequently employed method of isolating rod function has centred on the use of stimuli of low light intensity after rod sensitivity has been maximised by a 20-30 minute period of dark adaption (McCulloch et al. 2015). An alternative, but less frequently employed, means of isolating ERGs from rods involves the method of silent substitution (Estévez and Spekreijse 1974; Estevez and Spekreijse 1982) which is based on the principle of univariance (Donner and Rushton 1959). The isolation of rod photoreceptor activity requires alternation between two stimuli which contain mixtures of wavelengths at different intensities. The alteration elicits no overall change in excitation in the L-, M- and S-cone classes, but does elicit a change in rod excitation. The basic rule is that the isolation of 1 out of n classes of photoreceptor requires a minimum of n primaries tuned to different wavelengths. Theoretically, any desired combination of photoreceptor excitation modulation can be achieved without changing the state of adaptation, a major advantage of this approach. With the increased commercial availability of LED ganzfeld stimulators containing at least 4 primaries, researchers now have the prospect of more precise control of ERG stimuli. This improved precision, coupled with our knowledge of cone and rod spectral characteristics, enables better control of photoreceptor excitation (Kremers 2003). Stimuli based on the silent substitution method have already been applied in previous ERG studies of rod function (Kremers et al. 2009; Cao et al. 2011; Kremers and Pangeni 2012; Mcanany et al.

2015; Park et al. 2015). However, despite the possible advantages afforded by silent substitution, there is a clear need to demonstrate that the ERGs elicited by such rod isolating stimuli do in fact selectively reflect rod function and are free from intrusions from cone photoreceptors which normally predominate at higher mesopic and photopic light levels in the non-dark-adapted human retina (Stockman and Sharpe 2006; Zele and Cao 2014).

The aim of this chapter is to demonstrate that stimuli generated using the silent substitution method enable the functional assessment of rods without the confounding effects of cone intrusion. Specifically, we will examine ERGs obtained using rod isolating stimuli in terms of temporal frequency and luminance characteristics as well as post bleach recovery timings. Rod vision has a lower temporal resolution limit than that mediated by cones (Ives 1922; Hecht and Shlaer 1936; MacLeod 1972; Conner and MacLeod 1977; Conner 1982; Hess and Nordby 1986; Odom et al. 1992). At high scotopic levels of illumination rod temporal resolution can reach up to 28 Hz (Conner and MacLeod 1977; Conner 1982; Hess and Nordby 1986). Cones, by comparison, can support a temporal resolution limit in excess of 60 Hz (Conner 1982) and previous work has demonstrated that the cone flicker ERG can be recorded at frequencies up to 100 Hz in visually normal subjects (Tyler and Hamer 1990). We therefore wanted to exploit this difference to test the selectivity of our rod isolating stimuli. We will also assess retinal illuminance response characteristics. Rod ERGs are typically measured using low intensity stimuli at scotopic levels of illumination (Gouras and Gunkel 1964; Stockman et al. 1995; Scholl and Kremers 2001; Bijveld et al.

2011a; Bijveld et al. 2011b). This allows the study of rod responses free from the cone intrusions which become increasingly more predominant as the stimuli increase to mesopic and photopic light levels (Stockman and Sharpe 2006; Zele and Cao 2014). However, in the non-dark-adapted eye, stimuli of higher intensity need to be used and this will require caution as we have to ensure rod selectivity is maintained and that cone intrusions are minimised. Measuring the ERG response as a function of retinal illuminance will help us to gauge the extent of such intrusions. Finally, we will take advantage of the inherent kinetic differences between the rod and cone photoreceptors to validate our stimulus. Following a full retinal bleach the cones recover significantly quicker than rods (Lamb and Pugh 2004; Mahroo and Lamb 2004). By separately tracking the post bleach recovery of an L cone and rod isolating stimuli, we hope to show that they are being driven by two different systems.

By examination of the temporal and retinal illuminance response characteristics we will assess the suitability of ERGs generated by silent substitution for the assessment of rod function in humans. In doing so this study will attempt to define stimulus conditions for which rod responses can be optimised and identify parameter ranges beyond which the effects of cone intrusion can be demonstrated. Overall, this approach may lead to the development of better clinical testing protocols for the acquisition of rod mediated ERGs for which there will be improved selectivity and reduced clinical testing times.

3.2. Methods

3.2.1. Stimuli

Sinusoidal, full-field flicker stimuli with temporal frequencies ranging between 5 – 100Hz were presented using a ColorDome (Diagnosys LLC, Lowell, MA, USA) four primary ganzfeld stimulator with blue (460 nm), green (514 nm), amber (592 nm) and red (632 nm) LEDs. The spectral characteristics, chromaticities and luminances of each class of LED were measured and calibrated using a PR650 spectrophotometer (Photo Research Inc., Chatsworth, CA, USA). In order to obtain silent substitution stimuli photoreceptor excitations were calculated by multiplying the emission spectra of the LEDs with cone fundamentals and the V'λ 10° function (Wysecki and Stiles 1967; Stockman et al. 1999) (see section 2.3 and 2.4). Wavelength and intensity combinations were used which produced no changes in net excitation in three out of the four photoreceptor populations; thus these were triple silent substitution stimuli (Estévez and Spekreijse 1974; Estevez and Spekreijse 1982; Shapiro et al. 1996). Figure 3.1 shows how the luminance output of the four LEDs vary as a function of time in order to produce a silent substitution rod-isolating stimulus (8 Hz, 63 Td). Contrast was defined as the Michelson contrast of rod excitation and was set at 0.25 for all stimuli. Retinal illuminance varied between 1 – 12,000 photopic trolands (Td). We also used L-cone isolating stimuli (c = 0.25) to compare ERGs mediated by the two photoreceptor populations. In addition, we also generated non-selective, non-isolating stimuli that elicited simultaneous excitation of both rods and cones. These stimuli were generated by the same method described in sections 2.3 and 2.4, except that L- and M-cone

modulations were added to the standard rod isolating stimulus. Another non-selective 'white' stimulus was also used and this was generated by modulating all of the LEDs in phase, the resultant stimulus generating the same excitation (0.25) across all four photoreceptors. A 3000cd/m^2 white light was used in the bleaching experiment. We have used photopic as opposed to scotopic trolands throughout the study since it would be arbitrary to change units when going from high to low stimulus intensities and would also confuse the examination of ERGs across mesopic-photopic illumination transitions. For the stimulus set used in this particular study, conversion from photopic to scotopic trolands is achieved by multiplying by a factor of 2.489 (Stockman et al. 1993).

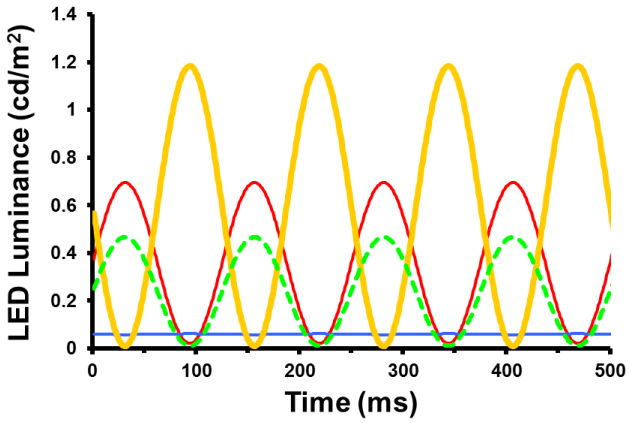

Figure 3.1. The luminance profiles and relative phases of the blue (B), green (G), amber (A) and red (R) LEDs that are required to generate a 63 Td, 8 Hz rod isolating silent substitution stimulus. The modulation of rod excitation for the resultant stimulus = 0.25.

3.2.2. ERG Recording

ERGs were recorded from the right eye using a silver/nylon corneal fibre electrode (Dept. of Physics and Clinical Engineering, Royal Liverpool University Hospital, UK) referenced to a 9mm Ag/AgCl electrode (Biosense Medical, Chelmsford, UK) on the outer canthus; a similar electrode was affixed to the forehead to serve as ground. Impedance was maintained below 5 kΩ. Signals were recorded using the Espion E^2 system (Diagnosys LLC, Lowell, MA, USA) which amplified and filtered (bandwidth = 1 to 300 Hz) the ERGs and digitised them at a rate of 1000Hz. Retinal responses to the flicker stimuli were acquired over 4 sec epochs with subsequent offline analysis being performed on an average of a minimum of 8 of these epochs. Participants viewed the stimuli monocularly and fixation was maintained on a central point which subtended approximately 0.5^0. Participants underwent pupillary dilation (1% Tropicamide), the mean (dilated) pupil diameter across the 7 subjects was 8mm (S.D. = 1.78) and this value was used in the computation of retinal illuminance. Prior to each recording session they sat in the testing room, which had an illumination level of 500 lux, for 5 minutes.

3.2.3. Data Analysis

Following acquisition, the averaged traces were subjected to a two-stage offline analysis involving, firstly, resampling of the traces and then, secondly, subjecting these re-sampled traces to Fourier analysis. The first stage was necessary because the Espion system samples at 1000 Hz producing 4000 points over the recording epoch. In order to perform a Fast Fourier

Transform (FFT) 2^n data points (where n = integer value) are required, so a method of interpolation was used to resample the averaged traces to give 4096 data points. The resampled traces were then imported into Signal software (version 2.16; Cambridge Electronic Design, Cambridge, UK) and subjected to a FFT. This analysis provided a measure of the amplitude and phase of the response at the stimulation frequency (i.e. the fundamental, F) as well as higher harmonics (2F). The phase values generated by the FFT can provide values that cycle in multiples of 360°. In order to 'unwrap' these phase values we either added or subtracted multiples of 2π radians (360°) in order to minimise the phase differences measured between the adjacent sampled temporal frequencies. Noise (N) was defined as the mean amplitude (A) of the response at the stimulus frequency minus 1 Hz and plus 1 Hz:

$$N = (A_{(F-1Hz)} + A_{(F+1Hz)})/2 \quad (3.1)$$

A response was considered significant if the measured ERG amplitude was a least 2.82 times greater than the computed noise amplitude for that frequency (Meigen and Bach 1999).

3.2.4. Participants

In this study where the objectives were to: 1) characterise the response properties of the rod mediated ERGs and 2) optimise stimulus parameters, a total of 5 colour normal trichromats (3 males; mean age: 28 yrs, age range: 35 yrs) were used. Colour vision in all subjects was assessed using the City

University Colour Vision Test (2nd Edition), the Farnsworth Munsell 100 Hue test and the HMC Anomaloscope (Oculus, Wetzlar, Germany). All participants gave informed consent prior to the commencement of the experiments which were conducted in accordance with the Declaration of Helsinki and were approved by the University of Bradford Ethics Committee.

3.3. Results

3.3.1. Temporal Frequency Response Characteristics

Figure 3.2 shows the variation in ERG amplitude and phase as a function of temporal frequency for a 63 Td rod isolating stimulus. The data shown are the group (vector) averaged responses (n = 5) and were obtained without dark adaptation. These results are similar to previous studies (e.g. (Gouras and Gunkel 1964)). The data describe a low-pass temporal function and, consistent with psychophysically obtained estimates of the temporal resolution limit of rods (Conner and MacLeod 1977), the ERG amplitude relative to noise falls below significance between 26 and 30 Hz.

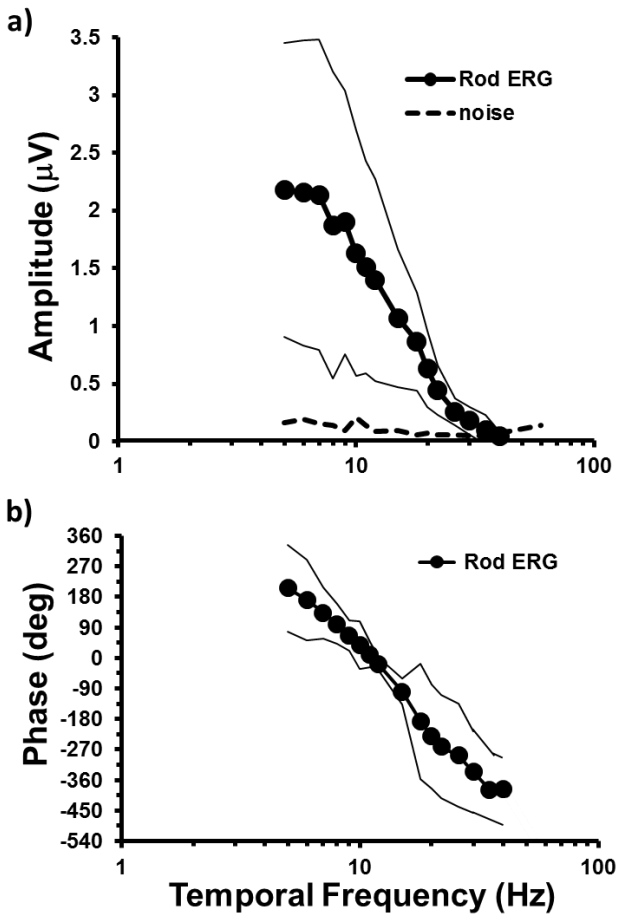

Figure 3.2. ERG amplitude (a) and phase (b) of the fundamental component as function of temporal frequency obtained for a 63Td rod isolating silent substitution stimulus (C=0.25). The data shown are the group (n = 5) averaged results and the thin solid lines represent +/- 1 S.D. from the mean. The thick dashed line (a) plots the measure of noise (see methods).

We compared the temporal frequency response functions obtained using silent substitution rod isolating stimuli with those obtained using non-isolating stimuli. Figure 3.3 shows the amplitude (3.3a) and phase (3.3c) of the ERG response fundamental obtained using a dim (63Td) white light stimulus. Compared to those obtained with the rod isolating stimuli (also shown in Figure 3.3) the temporal response functions elicited by the non-isolating stimuli are very different. In terms of amplitude, ERGs elicited by the dim white stimulus are reduced at low temporal frequencies (< 15 Hz) whilst at

frequencies normally considered beyond the range of rod photoreceptors (> 30 Hz) responses are still obtainable. The phase plots show that beyond 18 Hz there is a discontinuity in response which is likely to reflect contributions from other (presumably cone based) mechanisms at higher temporal frequencies. Figures 3.3b & 3.3d show the temporal response functions obtained from rod isolating stimuli to which we have intentionally added L-cone modulation (C = 0.30), via manipulation of the luminance outputs and relative phases of the four LEDs. The addition of cone modulation to the erstwhile rod isolating stimulus again has characteristic effects on the amplitude and phase responses as a function of temporal frequency. In terms of amplitude, the addition of cone modulation generates a more band-pass temporal response function, compared to the low-pass function obtained using a purely rod isolating stimuli, with response amplitude being markedly reduced at low temporal frequencies. Similar reductions for combined rod/cone stimuli have been noted previously (Mcanany et al. 2015) and have been attributed to destructive interference between signals emanating from the different photoreceptor populations. The addition of cone modulation leads to a gradual phase advance of the response relative to that of the isolated rod response at higher temporal frequencies.

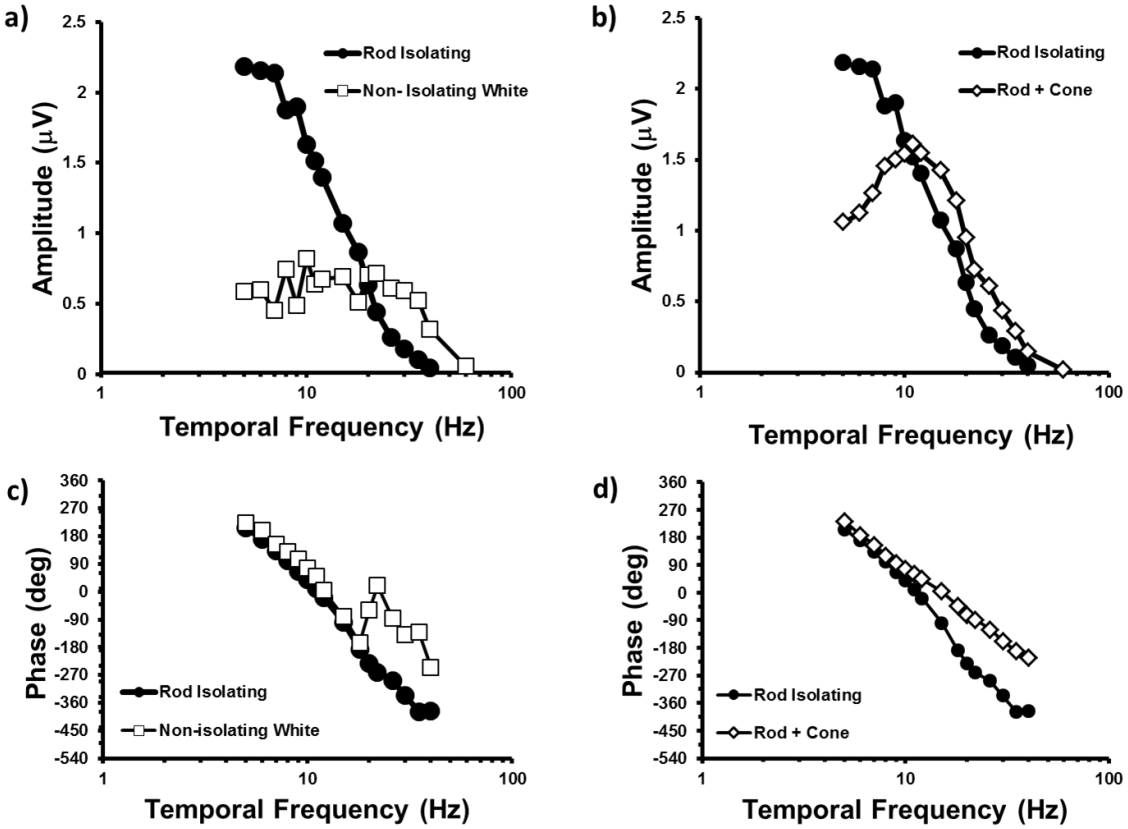

Figure 3.3. Left panels: comparison between the variations in ERG (fundamental) amplitude (a) and phase (c) as function of temporal frequency obtained for a 63Td rod isolating (filled circles) and a 63 Td non-isolating white stimulus (empty squares). Right panels: comparison between the variations in ERG (fundamental) amplitude (b) and phase (d) as function of temporal frequency obtained for a 63Td rod isolating (filled circles) and a 63 Td stimulus which modulates both rods (0.25) and L-cones (0.30) (empty diamonds).

In order to eliminate intrusions from cones, rod ERGs have typically been elicited using low intensity scotopic stimuli (e.g. (Scholl and Kremers 2001)). To what extent does the use of silent substitution stimuli free the experimenter from this constraint? Figure 3.4 shows the amplitude and phase variation of the ERG fundamental as a function of temporal frequency obtained using rod isolating stimuli with retinal illuminances extending well into the photopic range. Increasing the retinal illuminance of stimulus up to

120 Td decreases the response amplitude at low temporal frequencies but the limit of temporal response is similar to that obtained at 63 Td as signal amplitude relative to noise falls below significance between 26 – 30 Hz. When stimulus illuminance is increased to high photopic illumination levels (12,000 Td) the temporal response function of the ERG takes on a very different form and becomes more band-pass in appearance, peaking around 30 Hz. In addition the temporal response limit extends to higher frequencies. The function in effect becomes more like the cone temporal response function (Gouras and Gunkel 1964; Kommanapalli et al. 2014) and clearly indicates a loss of rod selectivity in the ERG at these light levels.

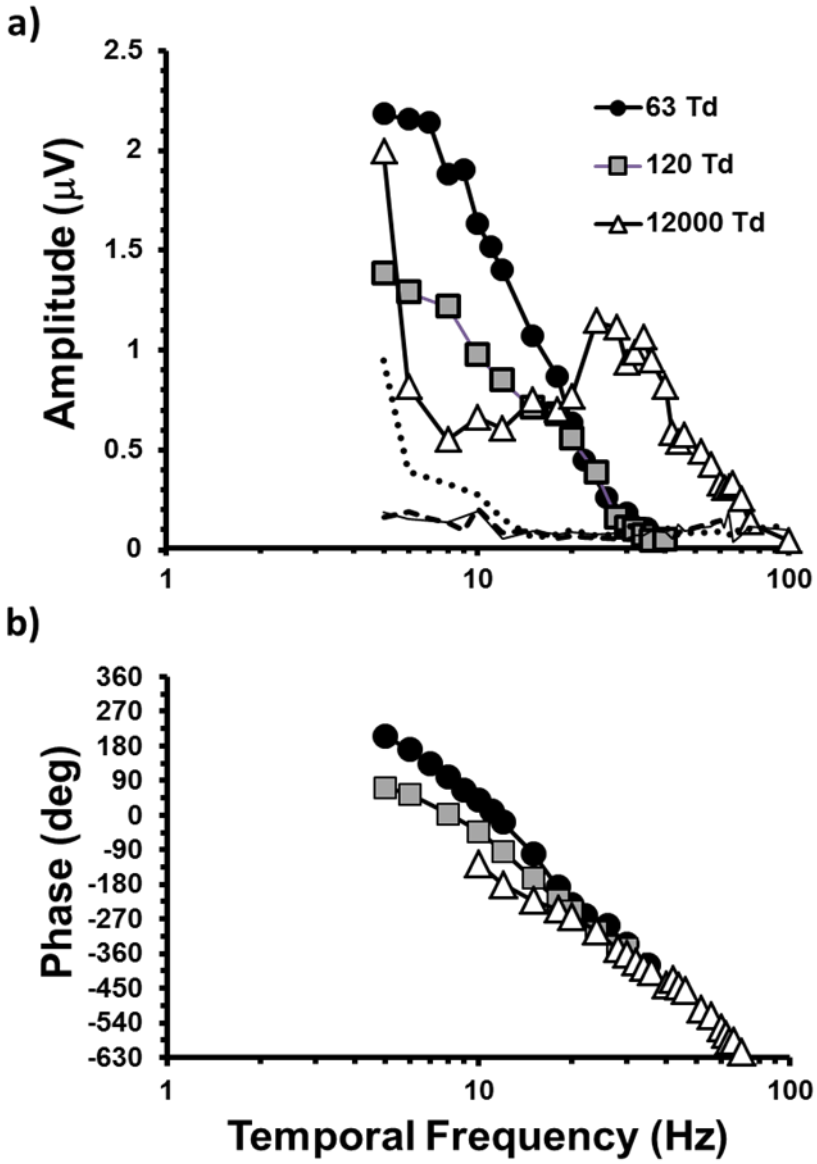

Figure 3.4. ERG temporal response functions for a) amplitude and b) phase of the fundamental obtained using rod isolating stimuli at retinal illuminances equal to 63, 120 and 12000 Td. The data represent the group vector average (n = 5). The thick dashed line, the solid thin line and the dotted line represent the noise for 63, 120 and 12000 Td conditions, respectively and phase is plotted only for temporal frequencies where signal was 2.82 x greater than noise.

To examine more closely the stimulus intensity range over which the transition from rod- to cone-like temporal frequency response characteristic occurred, we measured a series of temporal response curves in four subjects. These were sampled less frequently in the temporal domain

compared to the previous experiment but used a larger range of retinal illuminances (8, 63, 500, 1200, 3000 & 10000 photopic trolands). The results are shown as a three dimensional plot in figure 3.5. The temporal functions generated by the stimuli of lower (8, 63 & 500 Trolands) and higher (1200, 3000 & 10,000 Trolands) illuminance are qualitatively very different; the former are low-pass in nature contrasting with the latter which have more band-pass shape where responses can still be obtained for frequencies greater than 30 Hz.

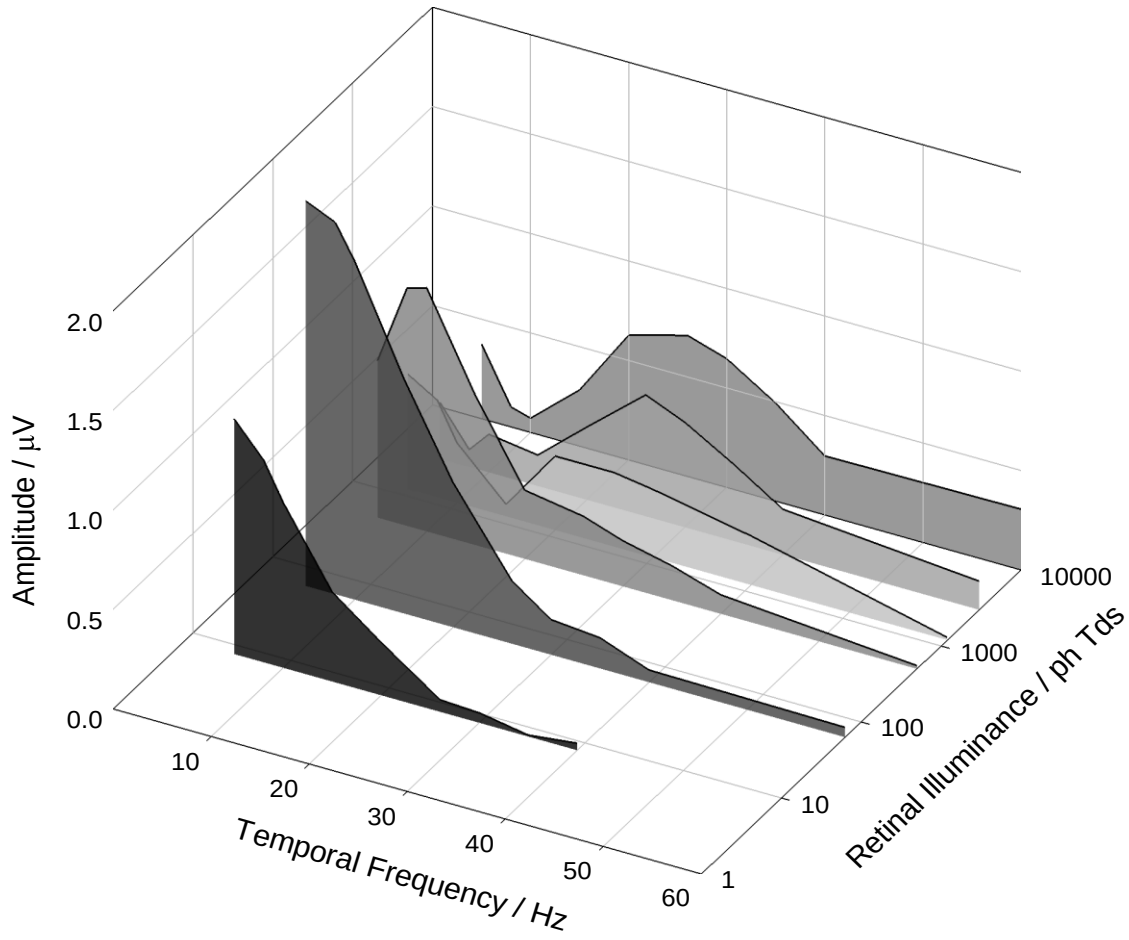

Figure 3.5. ERG (fundamental) temporal response functions obtained using rod isolating stimuli at retinal illuminances: 8, 63, 500, 1200, 3000 & 10000 photopic trolands. The data represent vector averaged group (n=4) responses.

In figure 3.6 a measure of the temporal response limit of the ERG is plotted as a function of stimulus illuminance. This value was computed as the temporal frequency at which signal amplitude fell below the criterion for significance (i.e. 2.82 x noise amplitude). ERG temporal response functions were obtained for a single subject using rod isolating stimuli ranging from 8 Td up to 12,000 Td and the ERG temporal response limit was calculated for each condition. The resultant plot shows that, at high illuminance levels (> 2000 Td), the temporal response limit of the ERG is in excess of 60 Hz – a level that is incompatible with rod function but is more in keeping with the properties of cone photoreceptors(Bijveld et al. 2011a; Bijveld et al. 2011b). Below 500 Td the temporal response limit falls to between 20-30 Hz, a value that is consistent with psychophysical measures of rod temporal properties obtained at higher scotopic illumination levels (Conner and MacLeod 1977; Conner 1982; Hess and Nordby 1986).

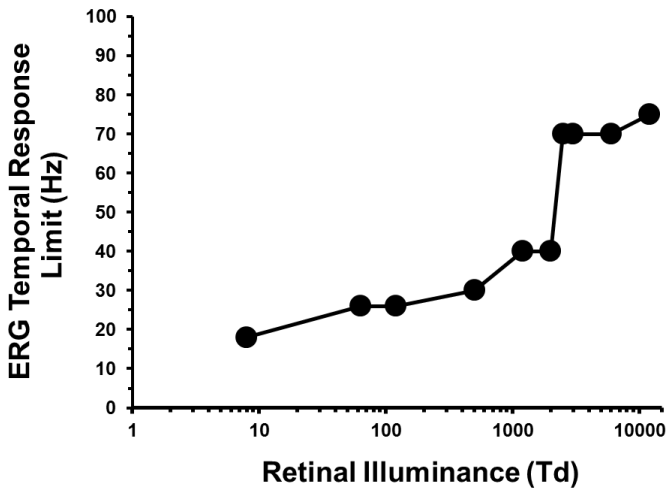

Figure 3.6. The temporal response limit of the ERG elicited by a rod isolating stimulus as a function of retinal illuminance (see text for calculation).

The phase data plotted in figure 3.4b for the 63, 120 and 12000 Td stimuli are useful as they can provide information about the temporal characteristics of the neuronal mechanisms that underpin the generation of the response. Specifically, the slope of the function provides a measure of what is known as apparent latency and provides a measure of response delay (Van der Tweel and Lunel 1965; Regan 1966). Apparent latency (τ) is given by:

$$\tau = -1/360 * (\Delta\phi/\Delta ft) \quad (3.2)$$

Where ϕ is response phase and ft the temporal frequency of the stimulation. In figure 3.7 the apparent latency is plotted as a function of temporal frequency for the 63, 1200 and 12000 Td 'rod isolating' stimuli. Each data point is calculated from the slope of a linear regression line fitted to 5 adjacent data points on the phase versus linear temporal frequency function. Constant values of apparent latency imply that physiological mechanisms that underpin the generation of the response have similar temporal response properties (Kommanapalli et al. 2014). In this respect, the function derived from the 12000 Td phase data is the simplest in that a relatively constant value for apparent latency is returned across the temporal frequency range tested. This suggests that a common mechanism with a short response delay (i.e. fast temporal response characteristics) underpins the ERG response to this stimulus. In view of the temporal response functions shown above for such high intensity stimuli it would seem likely that cone-based mechanisms are the most likely generators of these responses. For the 120

Td and 63 Td stimuli the apparent latency functions have two regions where a constant value is returned; the first is between 22-30 Hz where apparent latency values converge on a value similar to ERGs elicited by the 12000 Td stimuli, implying that they are generated by mechanisms with common temporal response properties. A second constant region, indicating a different temporal mechanism, is found between 10-15 Hz. Between the two lies a transitional region (15 – 22 Hz) where the function has a non-zero slope. For the 63 Td stimuli there is also an additional transitional region below 8 Hz which points to the possible existence of a third even slower mechanism (i.e. with increased apparent latency) that operates across low stimulus intensities and low temporal frequencies. The existence of multiple mechanisms with different temporal properties which contribute to the generation of rod mediated ERG is consistent with previous studies (Gouras and Gunkel 1964; Conner and MacLeod 1977; Sharpe et al. 1989; Stockman et al. 1991; Stockman et al. 1995; Sharpe and Stockman 1999).

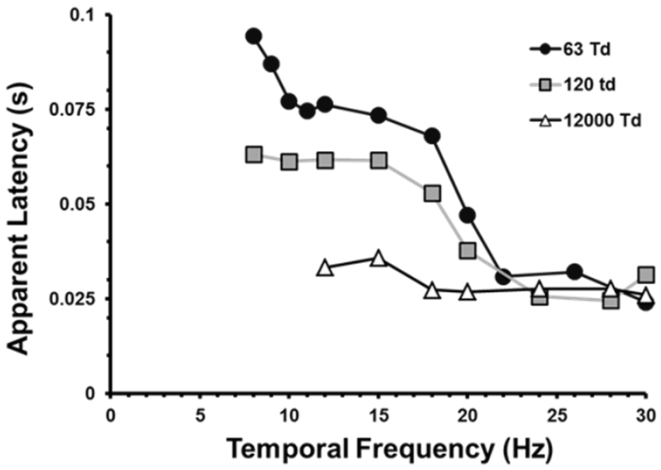

Figure 3.7. Apparent latency plotted as a function of temporal frequency for ERGs elicited by rod isolating stimuli of retinal illuminance equal to 63, 1200 and 12000 Td.

3.3.2. Retinal Illuminance Response Characteristics

Figure 3.8 shows the group averaged data where ERG amplitude measured with an 8 Hz rod isolating stimulus is plotted as a function of retinal illuminance. ERG response amplitude increases as a function of illuminance reaching a peak between 10-100 Td where the response is significantly greater than noise. Response amplitude then falls towards noise levels at 1000–2000 Td: there may be a small increase for higher illuminances but this rarely exceeds our criterion for significance (> 2.82 x noise).

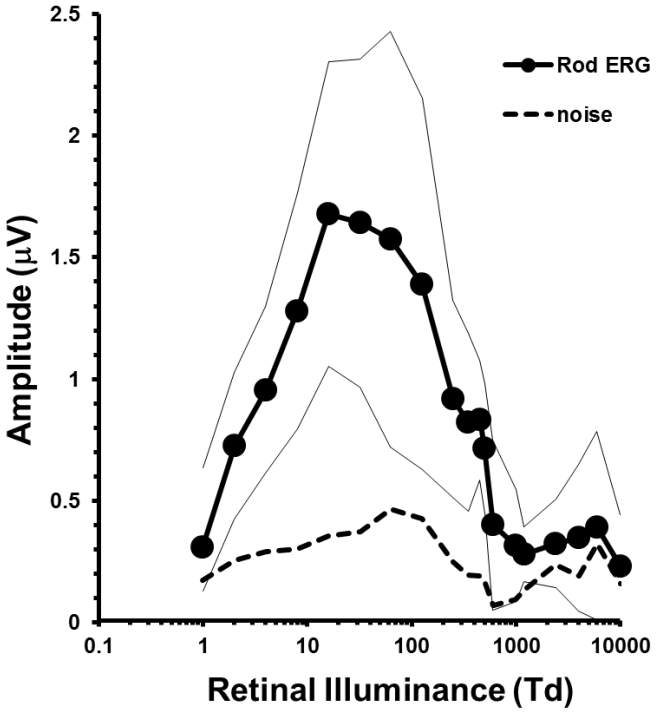

Figure 3.8. ERG (fundamental) response amplitude for an 8 Hz sinusoidal rod isolating flicker stimulus plotted as a function of retinal illuminance (photopic trolands). The dashed line plots the measure of noise as a function of stimulus illuminance. The data shown (thick solid line filled circles) are the group (n = 5) averaged data and the thin solid lines represent +/- 1 S.D. from the mean.

By way of comparison, figure 3.9 shows ERG amplitude as a function of retinal illuminance for an 8 Hz L-cone isolating stimulus of the same temporal

frequency and with a cone contrast of 0.25. The data plotted were obtained from a subset (n=2) of the main experimental group and demonstrate that the cone mediated response behaves very differently from that of the rod ERG. Unlike the rod mediated ERG the L-cone response exhibits an increase in response amplitude with increasing retinal illuminance showing no sign of the peak response between 10-100 Td. Another key point is that, in the region where the rod response reaches its maximum (~ 30 Td) the cone response barely rises above noise levels.

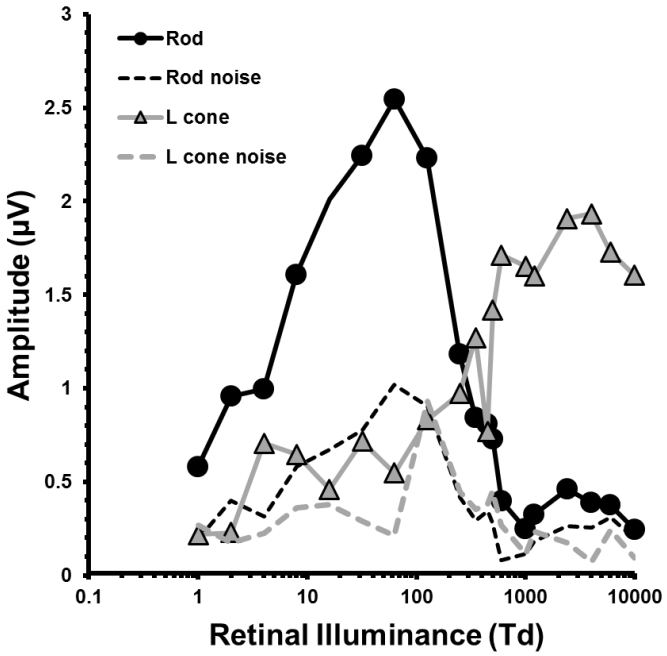

Figure 3.9. ERG (fundamental) response amplitude for 8 Hz sinusoidal rod (black circles) and L-cone (grey triangles) isolating flicker stimuli plotted as a function of retinal illuminance (photopic Trolands). The dashed lines plot the measure of noise as a function of stimulus illuminance. The data shown are averaged data from a sub-set of 2 subjects.

In addition to 8Hz stimulation we also examined ERG amplitude as a function of retinal illuminance (less densely sampled) at other stimulation frequencies. Figure 3.10 shows the averaged data from 4 subjects for rod-isolated ERGs elicited by stimulation frequencies of 5, 10, 15 and 30 Hz. For all but the highest stimulation frequency the responses are similar to the 8 Hz data in that the responses all reach maximum amplitude at approximately 100 Td then decrease with increasing illuminance. The data obtained from the 30 Hz stimulus follow a different response pattern; below 1000 Td it is barely recordable above noise levels but exhibits a steady increase in amplitude with increasing retinal illuminance, similar to the L cone isolated response shown in figure 3.9.

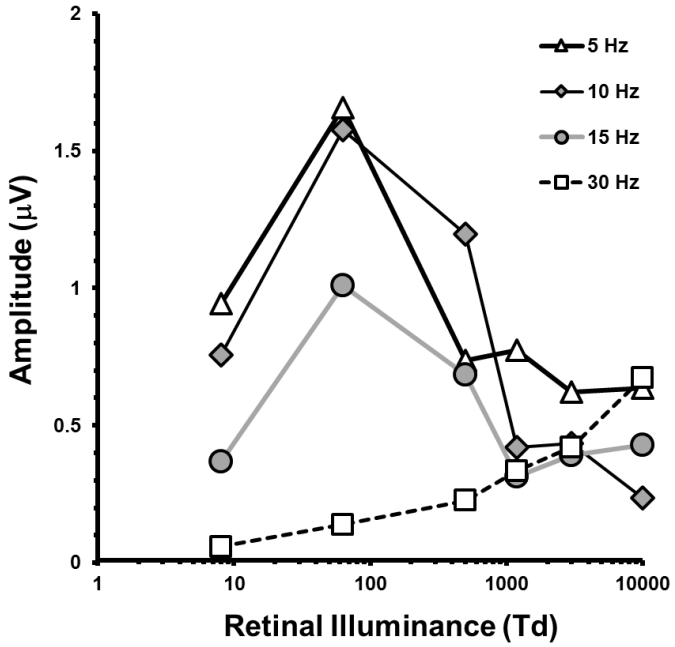

Figure 3.10. ERG (fundamental) response amplitude sinusoidal rod isolating flicker stimuli plotted as a function of retinal illuminance (photopic Td) for stimuli of temporal frequency = 5, 10, 15, and 30 Hz. The data represent the group average from n=4 subjects.

3.3.3. Post Bleach Recovery Response Characteristics

To further demonstrate the selectivity of our isolation we performed a full retinal bleach using a 3000cd/m^2 flash for 60 seconds (Mahroo and Lamb 2004) and tracked the recovery of the both rod and cone ERG amplitude. Figure 3.11(a) shows ERG amplitude recovery as a function of time for an 8 Hz L-cone (6000Td) and rod (63Td) isolating stimulus of the same temporal frequency and with a cone contrast of 0.25. The data plotted were obtained from a subset (n=3) of the main experimental group and demonstrate that the cone mediated response recovers rapidly (<2 mins) compared to the rod response, taking 12 minutes to reach its pre bleach baseline. Constraints in the methodology (epoch duration and number of trials per each average) meant that the earliest we could obtain an amplitude measurement was after one minute had elapsed. By this time, most of the cone ERG amplitude had almost completely recovered. Figure 3.11 (b) shows the post bleach b-wave amplitude recovery function of the LA 3.0 single flash (cone) and the DA 0.01 scotopic flash (rod) from a single participant. Both rod and cone functions exhibit similar recovery times to the responses in figure 3.11 (a). Figure 3.11 (c) illustrates the recovery of the rod ERG following a bleach at one minute intervals. The data in figure 3.11 clearly indicates that the L cone stimuli and rod stimuli are modulating two different systems.

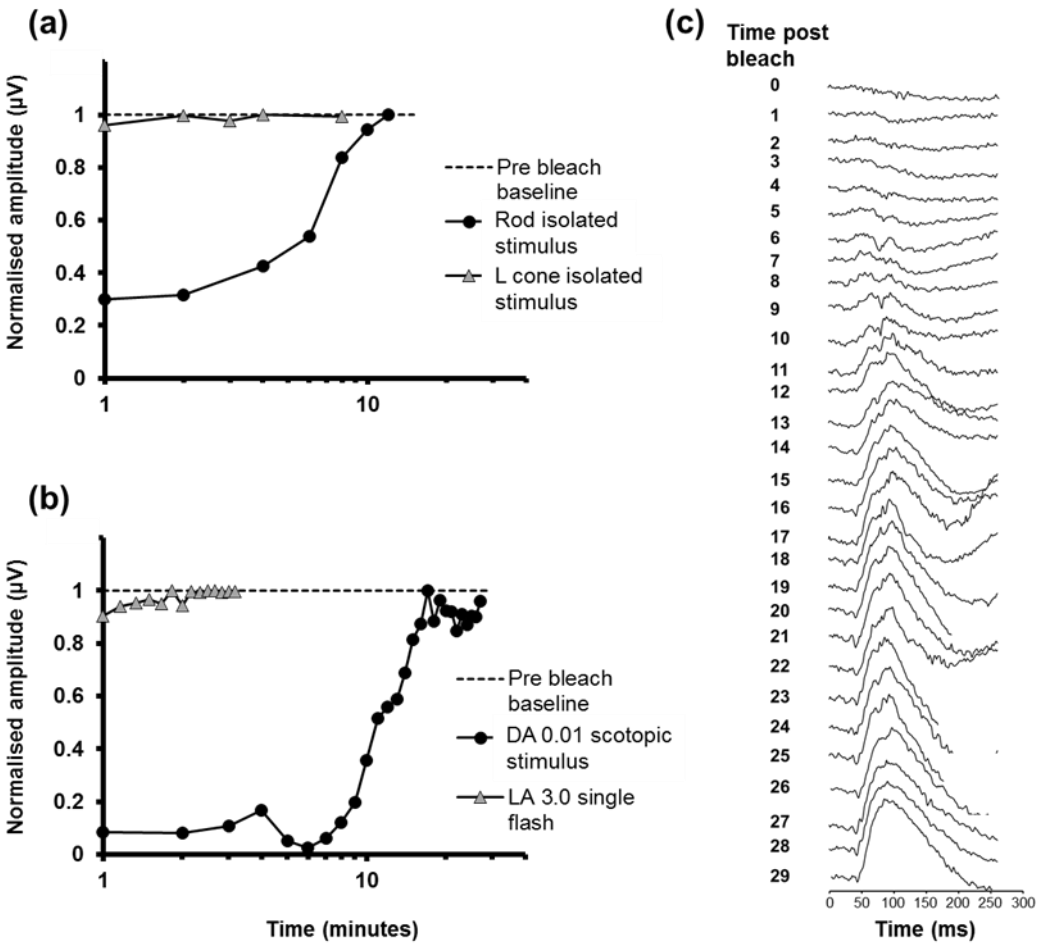

Figure 3.11. Post bleach recovery times of rod and cone system. (a) Group averaged data showing the recovery of the normalised ERG amplitude (fundamental) as a function of time following a full retinal bleach from n=3 subjects using 8Hz 6000Td L-cone (grey triangles) and 8Hz 63Td rod (black circles) isolated stimuli. (b) Data from a single participant showing the recovery of the normalised b-wave ERG amplitude using the LA 3.0 cd/m^2 single flash (grey triangles) and DA 0.01cd/m^2 single flash (black circles) following a full retinal bleach. (c) Raw data recorded from the single participant showing the recovery of the normalised b-wave ERG amplitude using a DA 0.01cd/m^2 scotopic stimulus. A 3000 cd/m^2 xenon flash was used to bleach the retina. Time on the Y axis is in minutes

3.4. Discussion

In this study we have demonstrated that, using silent substitution stimuli, it is possible to elicit ERGs with response characteristics that are consistent with known properties of rod mediated vision. Rod ERGs are optimal for stimuli of temporal frequencies between 5 – 8 Hz and retinal illuminances between 10 – 100 photopic Td. Importantly, isolation of rod function can be achieved without prior dark adaptation and without the need for stimuli restricted to low scotopic light intensities. The low-pass, low resolution (< 30Hz) ERG temporal frequency response functions generated by rod isolating stimuli constitute a key piece of evidence supporting the fact that silent substitution stimuli provide a selective assay of rod mediated visual function (Gouras and Gunkel 1964). Importantly, our measures of the temporal response limit of the rod ERG are consistent with psychophysical measures of rod function obtained at high scotopic light levels (Conner and MacLeod 1977; Conner 1982). Whilst this functional selectivity for rods is maintained for ERG responses elicited by silent substitution stimuli at mesopic and low photopic intensity levels, it is absent at levels of retinal illumination greater than 1000 Td. Above this level ERG temporal frequency response curves take on a more band-pass form and responses can be elicited by stimuli of frequencies in excess of 60Hz. Such properties are incompatible with rod function. They are more consistent with their mediation by cone photoreceptors (Gouras and Gunkel 1964; Hess and Nordby 1986) and indicate that ERGs elicited beyond this parameter range are no longer rod selective. In the final experiment of this chapter we showed that the recovery of the ERG elicited by our rod isolating stimulus was much slower to recover than the ERG

elicited by the L cone stimulus. The reason for such discrepancies in recovery time is related to opsins (Lamb 1981). Free opsins released into the extracellular space are a bi-product as a result of rhodopsin being bleached. Even after the bleaching light has ceased, these opsins continue to replicate the chemical processes produced by light, therefore keeping the sensitivity threshold elevated. These opsins eventually combine to 11-cis retinaldehyde and are depleted (Lamb 1981). This process occurs much quicker in the cone system, and is the basis behind the quicker recovery of theses photoreceptors (Mahroo and Lamb 2004). Psychophysical measure of full recovery of the rod system following a full bleach typically is noted at 40 minutes (Lamb and Pugh 2004). However, electrophysiology often involves the use of a suprathreshold stimulus to elicit a mass electrical response and therefore will reach a plateaux sooner compared to threshold stimuli used in psychophysics (Hamilton and Graham 2016). The fact that our isolated L cone and rod ERG recovery data shows clear similarities with published rod and cone recovery times (Lamb and Pugh 2004; Mahroo and Lamb 2004; Hamilton and Graham 2016), provides further validation of the selective ability of the individual stimuli.

A number of studies have demonstrated the existence of separate pathways for the transmission of temporal information by rods (see (Sharpe and Stockman 1999) for a review). The existence of these pathways has been revealed by changes in the temporal resolution of the rod system with increasing stimulus intensity as well as phase dependent interactions observed in both psychophysical and electrophysiological experiments

(Hecht et al. 1948; Gouras and Gunkel 1964; Conner and MacLeod 1977; Conner 1982; Hess and Nordby 1986; Sharpe et al. 1989; Stockman et al. 1991; Sharpe and Stockman 1999; Stockman and Sharpe 2006). These multiple processing pathways are based on the fact that rod signals have at least two, but probably more (see (Völgyi et al. 2004)), routes via which they can pass from outer to inner retina (Bloomfield and Miller 1982). One route is via rod bipolar cells to AII amacrine cells (Famiglietti Jr and Kolb 1975; Dacheux and Raviola 1986; Demb and Singer 2012). This forms the so-called 'slow' rod pathway which operates over scotopic levels of illumination. A 'fast' rod pathway, which operates at higher intensity levels, is thought to be mediated anatomically by gap junctions which allow the passage of rod signals directly to cones and then via cone bipolar cells to ganglion cells (Raviola and Gilula 1973; Nelson 1977; Bloomfield and Miller 1982; Dacheux and Raviola 1986; Schneeweis and Schnapf 1995). A key question is whether ERGs elicited by silent substitution stimuli show evidence of similar temporal mechanisms. Examination of the apparent latency data (Figure 3.7) would indicate that this is indeed the case. The plots of apparent latency versus temporal frequency exhibit distinct lobes for low intensity rod isolating stimuli, indicating the existence of multiple generators of the ERG response with different temporal characteristics. Furthermore, an important transitional region between one mechanism and the other occurs between 15-20 Hz. This is consistent with psychophysical studies where the measurements of critical fusion frequency versus intensity also show this to be a key region in the transfer from slow to fast rod pathways (Hess and Nordby 1986; Sharpe and Stockman 1999). Previous studies that have employed silent substitution

to generate rod isolating stimuli have found that rod function can be assessed over a wider range of stimulus intensities than that which might be expected using non-isolating flash stimuli (Kremers and Pangeni 2012; Park et al. 2015). However, with the use of more intense stimuli comes the need for re-assurance that, despite the employment of intensities that extend well beyond the scotopic range, rod selectively is maintained and is free of confounding contributions from cones. Hence the emphasis in this study has been on defining parameter boundaries within which we can be confident about the selective stimulation of rod function. Our data show that rod-isolating silent substitution stimuli generate ERGs that rise to a maximum amplitude between 10-100 Td then decrease with increasing stimulus intensity. This 'band-pass' shaped function is similar to rod ERG amplitude versus intensity functions obtained in previous studies that have used either low intensity (scotopic) stimuli (Bijveld et al. 2011a; Bijveld et al. 2011b) or rod isolating silent substitution stimuli in dark-adapted participants. For comparison, in figure 3.12 we have re-plotted rod ERG amplitude versus intensity functions obtained by Bijveld and colleagues. Using a 15 Hz flickering stimulus they measured ERGs in patients with either absent or reduced cone function (rod monochromats) or defective rod pathways (CSNB) (Bijveld et al. 2011a; Bijveld et al. 2011b). Alongside these data we show 8 Hz amplitude versus intensity functions obtained in this study for rod- and L-cone isolating stimuli.

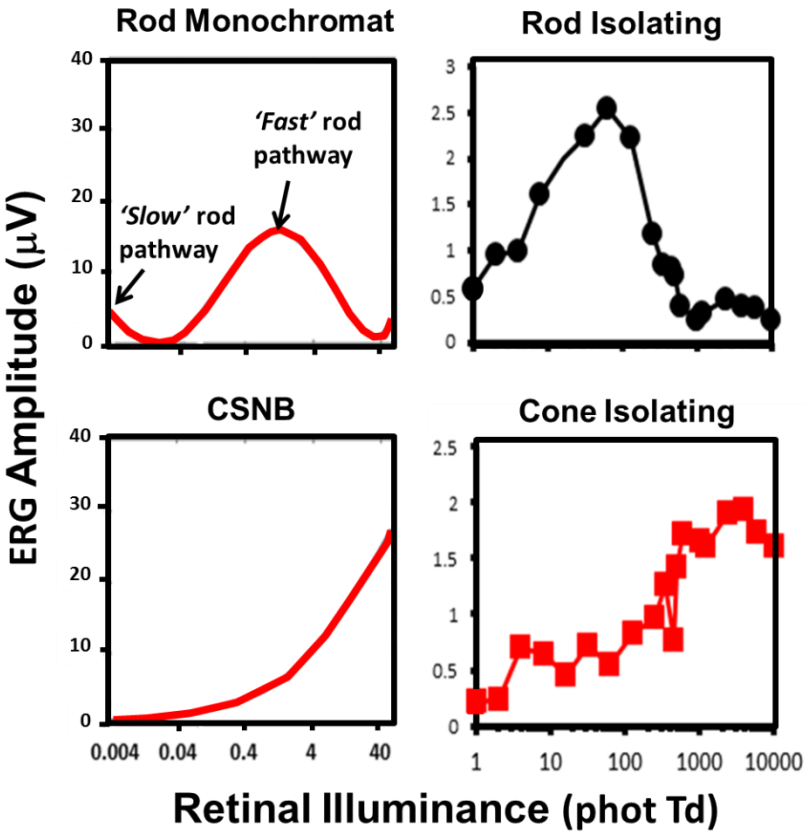

Figure 3.12. Left hand column – ERG amplitude as a function of stimulus intensity recorded from rod monochromats (upper left panel) and CSNB patients (lower left panel). These data are replotted from Bijveld et al., (Bijveld et al. 2011b) and were generated using 15 Hz flickering white light stimuli of low scotopic intensity. Right hand column – ERGs recorded from normal trichromats in this study which were elicited using an 8Hz flickering rod isolating stimulus (upper right panel) and an 8 Hz L-cone isolating stimulus (lower right panel).

There are clear qualitative similarities between the different datasets. Importantly, the band-pass amplitude versus intensity function for the ERG obtained using rod isolating silent substitution stimuli can be directly linked to rod activity on the basis that a similarly shaped response function is evident in ERG recordings from rod monochromats (Bijveld et al. 2011a; Bijveld et al. 2011b; Kremers and Pangeni 2012). Rod ERGs obtained within this optimal intensity region are purported to reflect the activity of the fast rod pathway (Scholl et al. 2001; Bijveld et al. 2011a; Bijveld et al. 2011b). At higher

illuminance levels our data show a reduction in rod ERG amplitude where responses fall to a minimum around 1000 Td. This minimum at higher intensities has been attributed to destructive interference between rod and cone signals (Sharpe et al. 1989; Stockman et al. 1991; Sharpe and Stockman 1999; Bijveld et al. 2011a; Bijveld et al. 2011b). The data from CSNB patients (who have dysfunctional rod signalling pathways) and normal trichromats using L-cone isolating ERG responses, show that cone responses behave in a different manner, clearly increasing in amplitude with increasing stimulus intensity. At higher intensities the temporal frequency response functions of the silent substitution rod ERGs become more 'cone-like' in terms of their properties – i.e. they take on a more temporally band-pass form and support high (> 60 Hz) temporal response limits. This increase in cone activation to ostensibly rod isolating stimuli may arise from a number of possible sources. Firstly, the anatomy of the rod signalling pathway itself provides multiple points of contact between the rod and cone systems. Studies have demonstrated a high degree of complexity in the extent to which rod signals can gain access to cone signalling pathways via direct photoreceptor coupling as well as via multiple connective pathways that are found in the inner retinal layers (Völgyi et al. 2004; Demb and Singer 2012). The increases observed in the ERG amplitude at the high stimulus intensities could in theory be mediated by any of these pathways. Secondly, increased cone contributions at high stimulus intensities could be the result of small departures from complete rod isolation by our stimuli. Such departures from isolation could arise as a result of inter-individual variations in photoreceptor fundamentals and as well as differences in pre-retinal absorption

characteristics (Kremers 2003). The responses elicited at high stimulus intensities (> 1000 Td) therefore are not rod selective and are contaminated by intrusions from cone activation that potentially may be derived from a number of separate physical as well as physiological sources.

The reduction in rod ERG amplitude for stimuli above 100 Td is interesting because it coincides with illumination levels over which rod saturation begins (Aguilar and Stiles 1954; Stockman and Sharpe 2006). Earlier studies have referred to this as 'rod insensitivity' at higher intensities (Park et al. 2015). But what is the mechanism for this reduction? Previously, observed decreases in flicker ERG amplitude with increasing stimulus intensity have been accurately modelled on the basis of destructive interference and cancellation between rod and cone signals that are delayed with respect to one another (Sharpe et al. 1989; Stockman et al. 1991; Sharpe and Stockman 1999). Such interactions have been clearly demonstrated when ERGs have been elicited using non-isolating luminance flicker stimuli (Stockman et al. 1995). However, with the use of silent substitution stimuli to isolate rod function, the extent of cone modulation should be minimal. Thus the potential for interference between rod and cone signals is likely to be reduced for silent substitution stimuli. Furthermore, the decrease in rod ERG for stimuli > 10-100 Td is observed at all the temporal frequencies that we have tested (see Figure 3.10). Stimulus frequencies at and around 7.5Hz are important for revealing interactions between rods and cones because, at this frequency, the delay between rod and cone signals (66 ms) produces a 180° difference in phase between the rod and cone mediated responses, leading

to almost complete cancellation between the two signals (Sharpe et al. 1989; Stockman et al. 1995; Sharpe and Stockman 1999). However, at higher and lower temporal frequencies there should be constructive interference between the two signals which should augment the ERG signal. Figure 3.10 shows that, below 30Hz, decreases in rod ERG amplitude occur regardless of the stimulation frequency suggesting that another mechanism must be responsible for this rod insensitivity at high illuminance levels. One possibility is that rod polarization remains essentially constant during the stimulus, therefore generating no response to the silent substitution. Another is that the decrease in rod ERG amplitude is the result of a generalised suppression of rod activity that occurs abruptly with increasing illumination. Such a mechanism has been described in the mouse retina where a retinal circuit has been described which mediates rapid switching from rod to cone mediated vision at illumination levels where cone bipolars become activated (Farrow et al. 2013). We speculate that a similar suppression of rod function may also exist in the human retina and that the decreases in rod ERG amplitude that occur at high light intensities, regardless of the temporal frequency, may constitute a non-invasive electrophysiological correlate of this suppression in humans.

The assessment of rod mediated visual function is becoming increasingly clinically relevant with the growing realisation that some of the earliest pathological and functional changes that occur in age-related macular degeneration (ARMD) are found in rod photoreceptors (Owsley et al. 2000). In addition, rod function may also constitute an important biomarker in the identification of individuals who carry a high genetic risk of developing ARMD

in later life (Feigl et al. 2011). Thus there are growing clinical demands that are driving the need for the development and improvement of methods that selectively assess rod function in humans. Our data demonstrate that it is possible to elicit ERGs with response characteristics that are consistent with known properties of rod mediated vision using silent substitution stimuli. Furthermore, we have delineated parameter ranges over which these responses can be optimised. From a clinical perspective our approach offers potential advantages over current standard methods of assessing rod function. Importantly, the use of silent substitution stimuli provide an opportunity for the assessment of human rod function without the need for subjects having to undergo time-consuming periods of dark adaptation, offering the prospect of more time-efficient testing protocols. A second advantage is that the adaptation state is constant throughout the test session. Specifically, rods are maximally sensitive immediately following dark adaptation and begin to lose sensitivity following repeated stimulation. This can result in much larger responses at the beginning of the test session compared to the end. Excluding dark adaptation largely obviates this problem. The data presented here provide an important translational link between basic and clinical research and demonstrate that silent substitution stimuli can efficiently and effectively isolate rod function in humans and provide a possible additional approach to current standard clinical protocols. However, we acknowledge that the diagnostic/ clinical aspect of this method is yet to be fully proven.

Chapter 4

The Morphology of Human Non Dark-Adapted Rod ERGs obtained by Silent Substitution Stimulation.

4.1 Introduction

The human electroretinogram (ERG), when elicited by a diffuse flash of light, constitutes a global electrical response from the retina which reflects the neural activity of a number of different retinal cell populations. However, with careful choice of the temporal, chromatic and luminance characteristics of the stimulus, it is possible to generate responses that have a greater degree of specificity in terms of the retinal cell populations from which they originate (Kremers 2003). The isolation and selective stimulation of rod photoreceptor activity forms an important part of clinical electrodiagnostic assessment routines. There is a variety of congenital and acquired visual pathologies that can differentially affect rod relative to cone function (Gouras and Gunkel 1964; Berson et al. 1968; Berson et al. 1969; Perlman et al. 1983; Scholl et al. 2001; Petzold and Plant 2006). The International Society for Clinical Electrophysiology of Vision (ISCEV) has outlined a detailed set of standards governing all aspects of clinical electroretinography (McCulloch et al. 2015) which covers scotopic (and photopic) retinal assessment. However, in recent years, other non-standard test methods have been developed and these have proven to be useful in providing extra information about retinal function. One method that has become popular, following the wider availability of four and five primary LED stimulator systems, is silent substitution (Donner and Rushton 1959; Estevez and Spekreijse 1982). This method provides a means by which ERGs from any one of the retinal photoreceptor populations

can, in theory, be isolated from the other photoreceptor classes. In the case of rod isolation, four-primary stimulators allow the creation of stimuli which, when modulated in time, produce a constant level of photoisomerizations in the three types of cone photoreceptors, but not in the rods (Shapiro et al. 1996; Cao et al. 2011). Thus cone modulation is effectively kept at zero while the rods are selectively stimulated.

In the previous chapter, we demonstrated that it is possible to isolate rod mediated steady-state (8 Hz) ERG responses using the silent substitution method without the need for dark adaptation (Maguire et al. 2016). We were able to show that ERGs elicited by this technique were selective for rods by the demonstration of a correspondence between temporal frequency and illuminance response characteristics and previously reported psychophysical properties of rod mediated vision. In this chapter we have used the same silent substitution technique to generate transient ERGs using stimuli with square–wave temporal profiles. This approach facilitates examination of rod mediated responses in the time domain and enables characterisation of the morphology of the ERG waveform and its constituent components. The primary aim of this study was to describe the basic morphological features of the ERG associated with rod function in the normal trichromatic retina generated by silent substitution stimuli. In addition, we also wanted to explore how the rod ERG waveform morphology is affected by the use of less selective stimuli that modulate cone as well as rod photoreceptors. To this end we compared isolated rod ERGs, elicited by silent substitution, with responses obtained using non-selective broadband ‘white’ stimuli and stimuli

to which we intentionally introduced varying degrees of cone modulation. Such stimulus manipulations allow us to identify key changes in the ERG waveform that might be attributable to the intrusion of cone activity. We also wanted to explore interactions between rod and cone responses using stimuli of varying intensities. Of particular interest is the way the rod ERG waveform is influenced by the use of stimuli that span the mesopic illumination range. This range is important as it marks the main transition between rod- and cone-mediated visual function and it would be useful to ascertain whether the rod ERG reflects this transition in the human retina, as has been previously demonstrated in the mouse (Allen and Lucas 2016).

4.2 Methods

4.2.1 Stimuli

Rod isolating stimuli were presented using a ColorDome (Diagnosys LLC, Lowell, MA, USA) four primary ganzfeld stimulator with blue (460 nm), green (514 nm), amber (592 nm) and red (632 nm) LEDs. The spectral characteristics, chromaticities and luminances of each class of LED were calibrated using a PR650 spectrophotometer (Photo Research Inc., Chatsworth, CA, USA). In order to create silent substitution stimuli, photoreceptor excitations were calculated by multiplying the emission spectra of the LEDs with cone fundamentals and the V'$_\lambda$ 10° function (Wysecki and Stiles 1967; Stockman and Sharpe 2000) and integrating over a range of wavelengths [see: section 2.3 and 2.4 for a fuller description of stimulus generation]. The stimuli used in these experiments were triple silent

substitutions in which intensity and wavelength combinations were used which produced no change in the net excitation of L-, M- or S-cones, but did produce excitation modulation of rod photoreceptors. Figure 4.1a illustrates an example of a rod isolating stimulus. In these experiments, the modulation of rod excitation was kept constant at C_{rod} = 0.25 (Michelson contrast) for all stimuli. The retinal illuminance produced by the stimuli was varied between 40 and 10,000 photopic trolands (ph Td). In order to obtain the stimuli with the lowest retinal illuminances (40 & 63 ph Td) a 0.9 neutral density filter was placed in front of the stimulator which attenuated the stimuli to the required levels with little or no distortion of the spectral characteristics.

Prior to the start of each experimental session the participants underwent a 5 minute adaptation period under ambient room illumination (500 lux). The stimuli were then delivered as continuous trains of pulses (only 1 cycle is shown in the figure 4.1 for clarity) with each waveform the average of at least 256 cycles (on-off presentations) of the stimulus.

In addition to the rod isolating stimuli, we employed two other types of non-isolating stimuli which were designed to elicit excitation of both rod and cone photoreceptors. For one stimulus type we introduced varying amounts of L- and M-cone modulation, ranging from 0.0 – 0.6, into our basic rod stimulus (Figure 4.1b). The second kind of non-selective stimulus was produced by the modulation in phase of all four LEDs (Figure 4.1c). This so-called ‘white’ stimulus (which actually appeared purple to the normal trichromats)

produced the same modulation (0.25) across all four classes of photoreceptor.

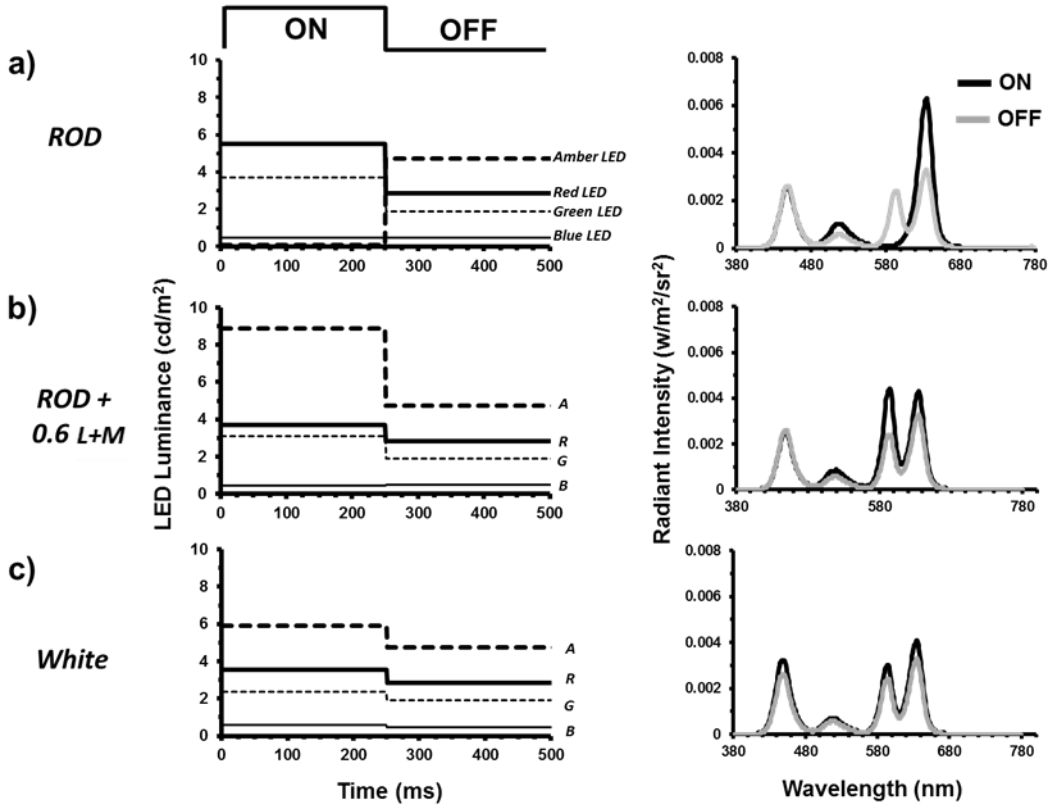

Figure 4.1. Temporal profiles of the square-wave pulse stimulus used to generate rod ERGs. The plots on the left show the luminance variation of the four LED primaries required to generate: a) the rod isolating stimulus, b) the mixed rod and L- and M-cone stimulus (cone modulation = 0.6) and c) the 'white' stimulus. In each case the initial 0 - 250ms is the onset period followed by the offset period (250-500ms). This sequence was then repeated with the stimuli presented as continuous trains of on-off pulses (256 cycles in total). The graphs on the right hand side show the spectral characteristics of the onset (black lines) and offset (grey lines) phases of each of the stimuli.

4.2.2 ERG Recording

ERGs were recorded from the right eye using a silver/nylon corneal fibre electrode (Dept. of Physics and Clinical Engineering, Royal Liverpool University Hospital, UK) referenced to a 9mm Ag/AgCl electrode (Biosense Medical, Chelmsford, UK) on the outer canthus; a similar electrode was affixed to the forehead to serve as ground. Impedance was maintained below 5 kΩ. Signals were recorded using the Espion E^2 system (Diagnosys LLC, Lowell, MA, USA) which amplified and filtered (bandwidth = 1 to 300 Hz) the ERGs and digitised them at a rate of 1000Hz. Retinal responses were acquired over 500 ms epochs with each response being composed of an average of a minimum of 256 epochs. Participants viewed the stimuli monocularly with a dilated pupil (1% Tropicamide) from a distance of 10 cm and both a chin and head rest were used. Fixation was maintained on a central point which subtended approximately 0.5^0.

4.2.3. Participants

In experiment 1 a total of 20 normal trichromatic observers *(*mean age: 31.5 yrs, age range: 53 yrs) acted as participants, whilst in experiments 2 and 3 a sub-set of this cohort consisting of 5 colour normal trichromats (3 males; mean age: 32 yrs, age range: 24 yrs) took part. Colour vision in all normal subjects was assessed using the City University Colour Test (2nd Edition) and the HMC Anomaloscope (Oculus, Wetzlar, Germany).

Ethical approval for this study was obtained from the local ethics committee and all participants gave informed consent prior to the commencement of the

experiments which were carried out in accord with the tenets of the Declaration of Helsinki.

4.3. Results

4.3.1 Morphology of the Transient Rod system ERG

Figure 4.2 shows ERGs obtained from 20 normal trichromatic observers in response to a silent substitution rod isolating stimulus with a square-wave temporal profile comprising an onset (i.e. rod excitation increment) duration of 250ms and a 250ms offset (rod excitation decrement) period. Rod contrast, C_{rod} = 0.25 and the stimulus had a mean retinal illuminance of 63 ph Td. In normal trichromats the ERG produced by this stimulus had a consistent appearance across all participants exhibiting a waveform with an initial prominent positive peak, which we have termed P_{Ri}, which has a peak implicit time of 85.95ms (±95% CI = 7.88ms). The offset response is dominated by a negative component (termed N_{Rd}) which has a mean peak implicit time of 95.18ms (±95% CI = 7.85) after the offset of the stimulus.

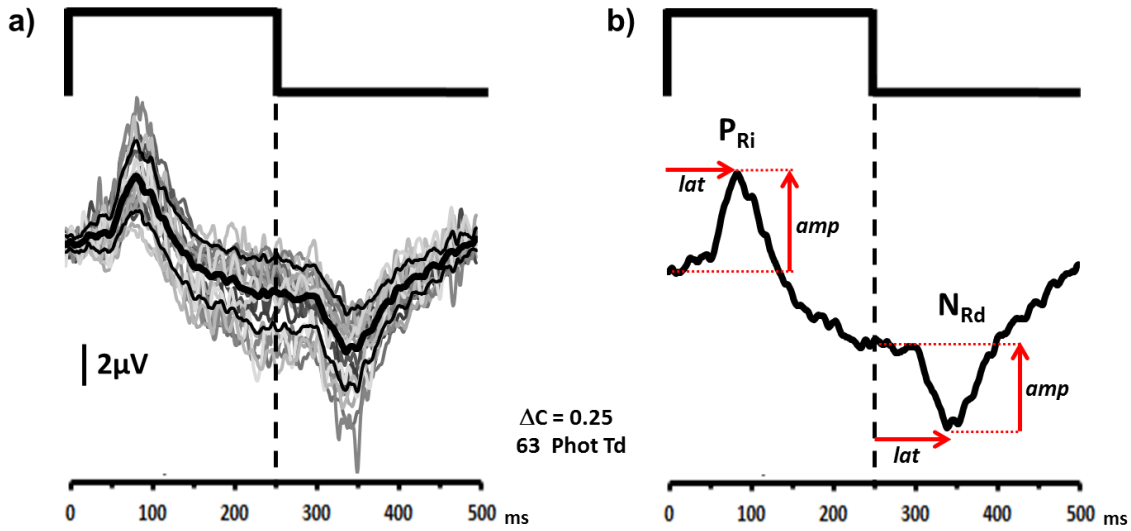

Figure 4.2. (a) The individual (grey lines) and group averaged (thick black line) ERGs elicited from 20 normal participants by a silent substitution rod isolating stimulus. The thin black lines represent +/- 1 S.D. from the mean. For clarity we have shown the group averaged rod ERG in (b), this response consists of an initial positive peak (P_{Ri}) at stimulus onset followed by a negative response component (N_{Rd}) after stimulus offset. The amplitude measurements for the P_{Ri} component was taken from the amplitude at time zero to the peak. The amplitude measurements for the N_{Rd} component was taken from the amplitude at time 250ms to the peak of the trough.

4.3.2. Rod system ERGs as a Function of Retinal Illuminance

ERGs mediated by rods are usually elicited from the dark-adapted eye (McCulloch et al. 2015) using low intensity (scotopic) stimuli (Gouras and Gunkel 1964; Stockman et al. 1995; Bijveld et al. 2011a; Bijveld et al. 2011b; McCulloch et al. 2015). However, the use of silent substitution stimuli to isolate rod activity potentially provides an opportunity to record rod responses at higher stimulus intensities. Examination of the responses elicited by stimuli that extend from mesopic to photopic levels of illumination, in particular, provide the opportunity to observe the effects of the ERG waveform as the transition from rod- to cone-mediated vision takes place. To

this end we generated a series of rod isolating square-wave pulse stimuli which produced retinal illuminances ranging from 40 to 10,000 ph Td with a rod contrast of 0.25. Figure 4.3 shows the changing morphology of the averaged (n = 5) rod ERGs as a function of retinal illuminance. For the low intensity stimuli (40-100 ph Td) the ERGs have a distinct waveform similar to the responses shown in figure 4.2 with a prominent positive onset response (P_{Ri}) and a negative offset (N_{Rd}). As retinal illuminance increases from 100-1000 ph Td, the response becomes highly attenuated with hardly any discernible ERG waveform elicited by rod isolating stimuli within this intensity range. At stimulus intensities above 1000 ph Td a response does appear to re-emerge but it has a very different morphology from that which is obtained at the lowest stimulus intensities. Under these conditions the response exhibits a negative component (upward arrows in figure 4.3) with an implicit time of between 20 – 30 ms, followed by a small positive going peak at approximately 40ms (downward arrows in figure 4.3). These components resemble those observed in the non-selective single flash photopic response. Later components (both positive and negative) are also observed between 75-100ms and give the response obtained at these high illuminance levels a very different morphology to that which is observed for low illuminance levels.

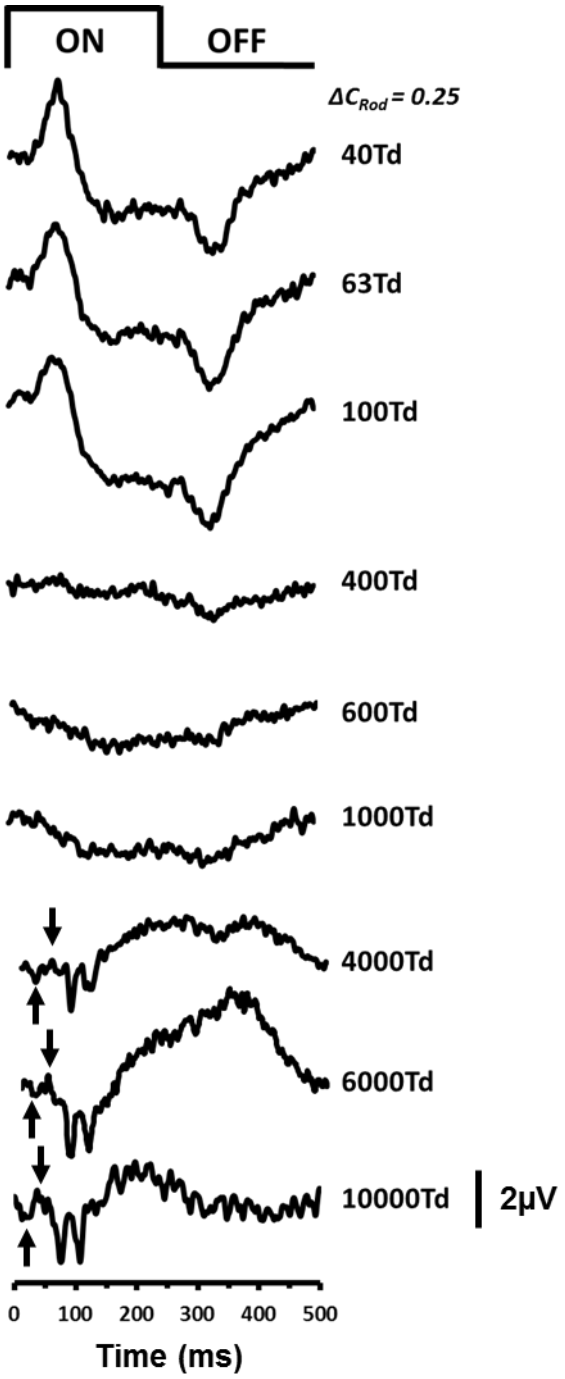

Figure 4.3. Group averaged (n = 5) transient rod ERG as a function of retinal illuminance. For all stimuli the modulation of rod excitation was 0.25. Black upward and downward arrows indicate a small negativity and positivity more consistent with the cone response.

4.3.3. ERGs Elicited with Non-Isolating Stimuli

Having examined the morphology of the ERG generated by rod isolating silent substitution stimuli, we wanted to examine the extent to which this waveform was affected by the use of non-selective stimuli that induce excitation of cone as well as rod photoreceptors. We employed two groups of stimuli: the first were broad-band flash stimuli which modulated all photoreceptors to the same extent (0.25). These stimuli were presented over a range of different retinal illuminances. The second group comprised a series of nominally rod isolating stimuli at 63 ph Td to which varying degrees of L- and M-cone modulation were added, ranging from 0% (i.e. rod isolating) to 60% cone modulation. All stimuli had the same temporal profile as those used in experiments 1 and 2 (Figure 4.1 b & c).

Figure 4.4 shows the ERG responses elicited using the first non-isolating (white) group of stimuli. For comparison, the rod isolating responses are also shown for the same stimulus intensities (grey traces). When we compare the rod isolated responses with the non-isolated responses at similar stimulus intensities we see that there are qualitative differences between the responses elicited by the different stimulus types. A key difference is that, at the lowest stimulus intensities, ERGs elicited by non-isolating stimuli do not exhibit the large positive component (P_{Ri}) that is present in the rod isolating response. Instead, non-isolated responses are dominated by a broad negativity which is similar to the scotopic threshold response (STR) that has been previously reported in the dark-adapted ERG (Sieving and Nino 1988;

Robson and Frishman 1998). This later and longer duration negativity, also observed in the response elicited by the silent substitution stimuli at low illuminance, has previously been attributed to inner retinal activity (Robson and Frishman 1998) and we speculate that a similar source is responsible for the generation of this component in both the non-isolated and rod isolated ERGs.

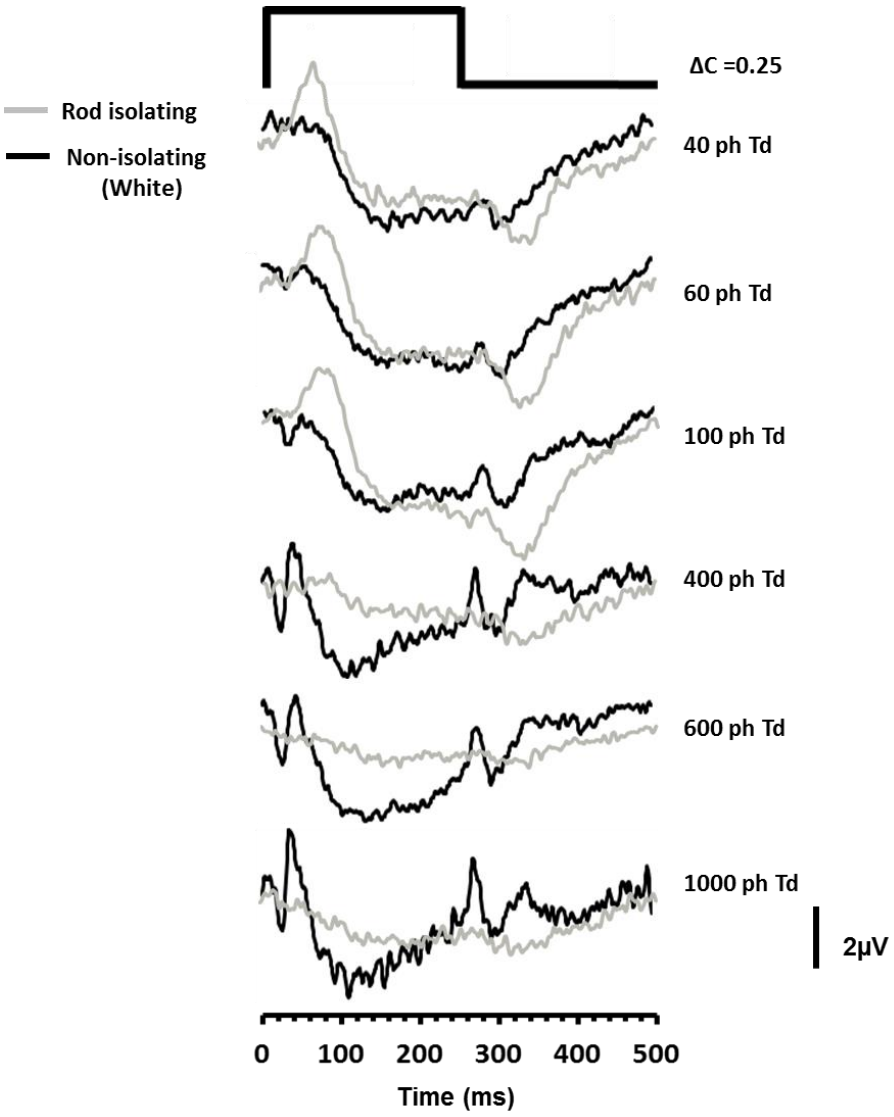

Figure 4.4. ERGs elicited by a non-isolating (white) stimulus of increasing intensity (black traces). Also shown are the responses for the rod isolating stimuli at the same levels of retinal illuminance (grey traces). The traces represent group averaged (n=5) responses and for all stimuli the modulation of each photoreceptor class. Contract = 0.25.

As retinal illuminance increases the non-isolated ERG starts to develop a prominent negative going a-wave and positive b-wave. Both these components have implicit times that are shorter than corresponding components found in the isolated rod ERG. The development of these onset response components occurs in conjunction with the increased prominence of a positive d-wave offset response in the non-isolated ERG [30]. Figure 4.5 plots the variation in the amplitude of the b- and d-waves of the ERG generated in response to the non-isolating white stimulus as a function of retinal illuminance. As can be observed, both of these onset and offset components undergo an increase in amplitude with increasing stimulus intensity. Not unexpectedly, the waveform morphology to this non-selective stimulus takes on the appearance of the photopic on-off ERG that has been described previously (see:(Sieving et al. 1994), figure 9). In contrast, the amplitude of the P_{Ri} component of the isolated rod ERG behaves very differently exhibiting a marked reduction in amplitude as a function of retinal illuminance beyond 400 ph Td.

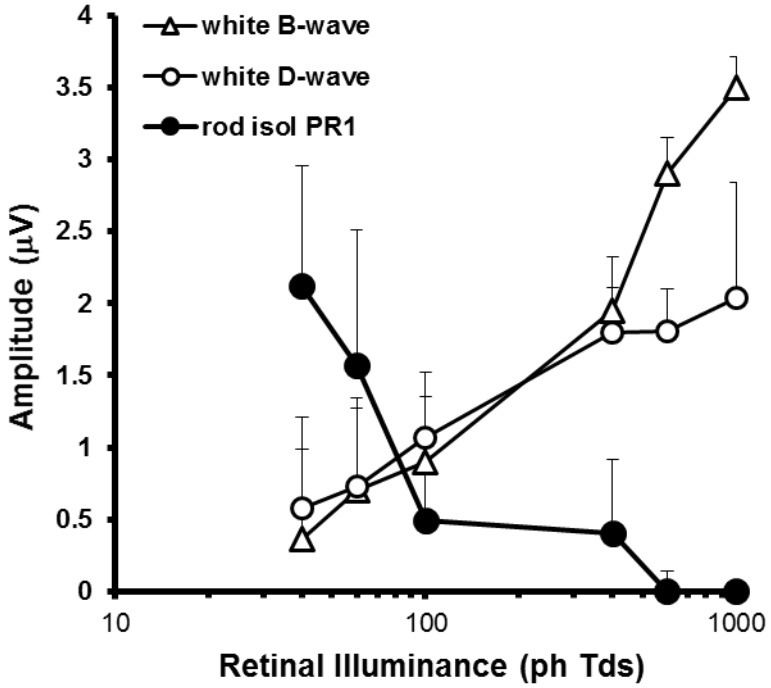

Figure 4.5. Dependency of the ERG b- (empty triangles) and d-wave (empty circles) amplitude generated by a non-selective 'white' stimulus plotted as a function of retinal illuminance. Also plotted for comparison is the amplitude of P_{Ri} (filled circles) of the rod isolated ERG in the same participants across the same illuminance range. Data are the group averages (n =5) and the error bars = + 1 S.D.

ERGs elicited by the second group of non-isolating stimuli are shown in figure 4.6. The stimuli used in this experiment modulate L- and M-cones as well as rods. The extent of cone modulation varies across the stimuli from 0.0 (i.e. rod isolating) to 0.6. As the magnitude of cone modulation increases there are clear changes in the ERG waveform morphology; there is an initial decrease in the P_{Ri} amplitude accompanied by increases in a- and d-wave amplitudes (Figure 4.7). At the highest levels of L- and M-cone modulation the ERG waveforms elicited by these non-isolating stimuli are similar in appearance to those generated by the highest intensity white stimuli shown in figure 4.4.

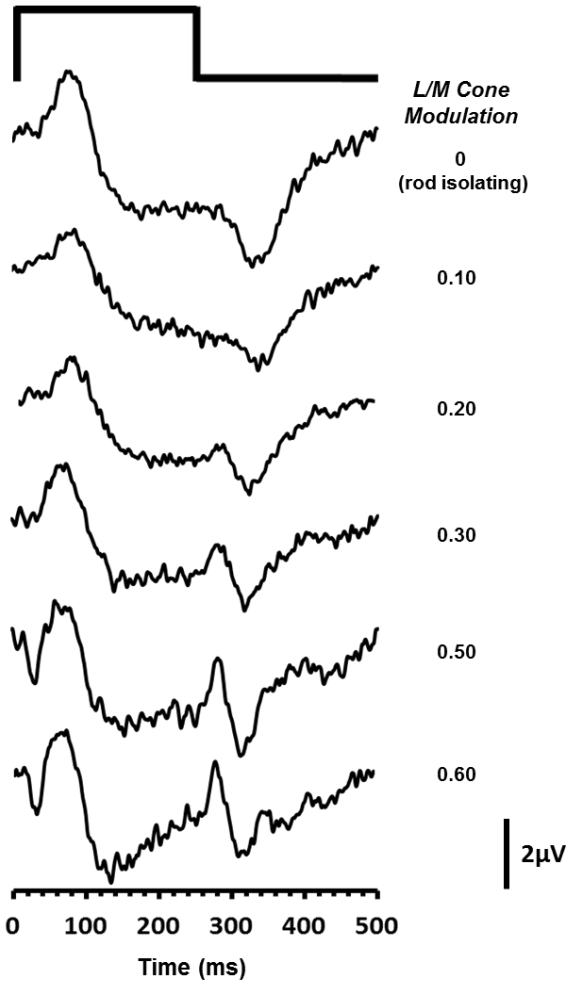

Figure 4.6. ERGs elicited by stimuli which contain increasing amounts of L- and M-cone modulation. The ERGs in the uppermost trace was generated by a stimulus that produced no L or M cone excitation and was therefore rod isolating. Each stimulus has a retinal illuminance = 63 photopic Trolands.

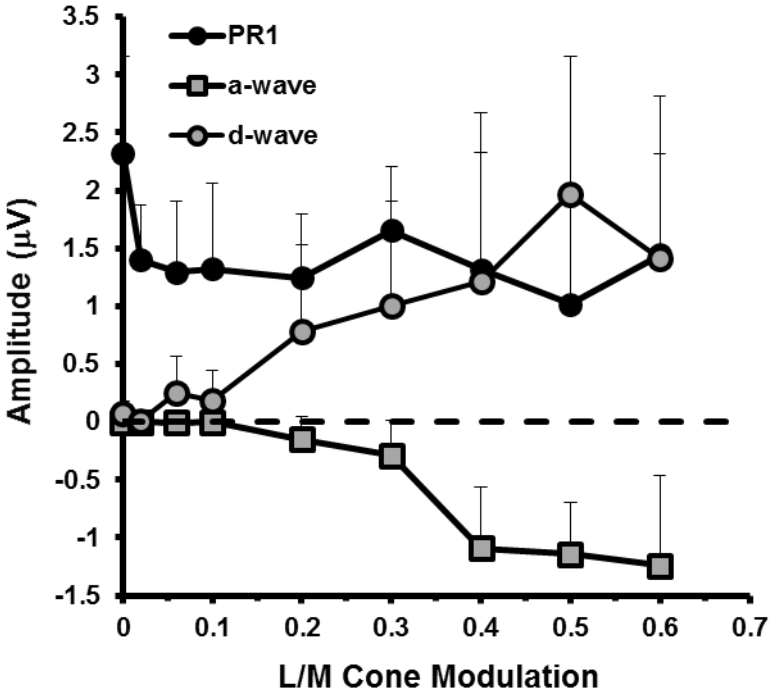

Figure 4.7. Amplitude of the a-wave (squares), d-wave (circles) and P_{Ri} (black circles) components as a function of increasing amounts of L/M cone modulation added to a rod isolating stimulus. Data are the group averages (n =5) and the error bars represent + 1 S.D.

4.4. Discussion

In this study we have used silent substitution stimuli to elicit transient ERGs from the light-adapted human retina in an attempt to generate retinal responses that selectively reflect rod mediated visual function. We have characterised the morphology of this rod ERG waveform in the normal trichromatic retina and demonstrated how non-selective stimuli induce changes in this response that arise as the result of cone photoreceptor stimulation. Importantly, we have shown that rod ERGs generated by our methodology exhibit a clear reduction in response amplitude as stimulus intensity increases from mesopic to photopic levels. This response attenuation is not observed in ERGs elicited by stimuli that are not rod-selective and is critical because it provides a clear correlation with rod photoreceptor response properties which exhibit response saturation over the same illumination range (Stockman and Sharpe 2006).

The human dark-adapted rod ERG, recorded under ISCEV standard conditions (McCulloch et al. 2015), typically comprises a positive b-wave of large amplitude with an implicit time of approximately 100 ms. The response is generated by a short duration broadband flash stimulus and the resultant waveform is in effect a composite response of both onset and offset components (though heavily dominated by the former). In the mammalian retina, low scotopic vision is mediated by a pathway based upon rods which synapse with depolarising rod bipolar cells (Smith et al. 1986; Sterling et al. 1988; Sieving et al. 1994; Bloomfield and Dacheux 2001) and numerous pharmacological studies point to the direct involvement of this pathway in the

generation of the dark-adapted ERG b-wave (Witkovsky et al. 1975; Slaughter and Miller 1983; Frishman and Steinberg 1990). ERGs elicited from the normal light-adapted human retina to the onset of a rod isolating silent substitution stimulus (<400 ph Td) also are dominated by an initial positive component, P_{Ri}, with an implicit time of 85.95ms (±95% CI = 7.88ms). Based on its peak timing and its response to changes in luminance, we propose that the origin of this component is similar to that of the dark adapted rod b-wave or the PII response (Brown 1968; Sieving et al. 1994; Robson and Frishman 1998) and is produced by the depolarization of the rod ON-bipolar cells (Robson and Frishman 1998). Further evidence supporting this position, using disease models is presented in the following chapter.

The temporally extended nature of our stimulus means that an offset response is also a feature of our rod ERG responses – something that is not usually observed in the ISCEV scotopic ERG. An intense, long duration stimulus typically evokes a positive potential or d-wave from cone-rich light-adapted retinas at stimulus offset (Granit 1950; Brown and Murakami 1967). Examples of this offset response component can be seen in the ERGs recorded in response to high intensity white stimuli and stimuli which induce cone and rod excitation (Figures 4.4 and 4.6). In comparison, offset responses elicited from dark-adapted, rod dominated retinas comprise a negative component followed by a slower positive response (Granit 1950; Brown 1968). These morphological features are more in keeping with those observed in our rod isolated ERGs which at stimulus offset exhibits a negative trough, N_{Rd}, that typically occurs at 95 ms post stimulus offset. The

rod ERG offset response was first described when assessing retinal responses to long duration stimuli in rod dominant animal models and was described as a corneal negative wave occurring after stimulus offset (Granit and Riddell 1934; Brown 1968). Brown originally suggested the offset response was a combination of the decay of ON bipolar cells plus a dc component along with the recovery of the photoreceptors (Frishman and Steinberg 1990). Further analysis in the cat confirmed that part of the negative trough is formed by repolarisation of the rod bipolar cells but that the slow positivity, immediately following it, originates in the more proximal regions of the retina (Frishman and Steinberg 1989). Literature on the rod offset response in human retina is limited (Scholl and Kremers 2001; Chen et al. 2005). In one study (Scholl and Kremers 2001) the rod offset ERG was recorded in a patient with S-cone monochromacy using silent substitution. The resultant response is qualitatively similar to the offset ERGs reported in this study. A second study (Chen et al. 2005) used scotopic rapid on/off ramp stimuli and multifocal stimuli to record the rod onset and offset responses. The elicited waveform had a positive deflection at onset and a negative dip at offset. Our speculation is that the negative offset component observed in the rod isolated ERGs recorded in this study is related to the recovery of the On-bipolars, rather than an independent entity.

A key feature of the ERGs generated by the silent substitution rod isolating stimuli is that they exhibit a decrease in amplitude with increasing stimulus intensity, the responses becoming highly attenuated above 100 ph Td. This decrease is significant because it occurs across the range of mesopic illumination levels for which the saturation of rod responses is purported to begin (Aguilar and Stiles 1954). This intensity dependent decrease in amplitude for the isolate rod ERG is in stark contrast to the increase in amplitude of the responses elicited by non-selective stimuli which not only modulate rods but also cone photoreceptors (Figures 4.3, 4.4 & 4.5). This response behaviour provides another piece of evidence which points to the selective isolation of rod function by the current stimulation protocols. Similar intensity dependent increases and decreases have been demonstrated in the mouse retina for cone and rod-mediated ERGs, respectively (Allen and Lucas 2016). Interestingly, similar to the murine responses, human rod ERGs appear to undergo a similar abrupt reduction in amplitude across a relatively narrow range of retinal illuminance. The rapid nature of the rod response attenuation, which is coupled with an increase in the ERGs generated by cone photoreceptors (Allen and Lucas 2016), has prompted speculation about the existence of retinal mechanisms which control the switch from rod- to cone-mediated vision with increasing retinal illumination. One possibility is that rod response levels are moderated by the light intensity experienced by cones (Frumkes et al. 1986; Cameron and Lucas 2009). Various mechanisms have been proposed as to how this suppression of rod function might be achieved, including mediation via gap junctions that exist between rods and cones (Heikkinen et al. 2011) or via neural switching

mechanisms involved cone bipolars (Farrow et al. 2013). These have, thus far, only been described in the mouse retina – but the behaviour of the rod isolated ERGs shown here, suggest that similar mechanisms involving the rapid suppression of rod responses by increasing cone activity exist in the human retina. The use of rod isolating silent substitution stimuli may provide a means via which these mechanisms can be studied in humans.

Our results show that whilst there is a clear attenuation of the rod isolated ERG for stimuli above 100 ph Td, some form of response does re-emerge at high stimulus illuminances (≥ 4,000 ph Td). However, the morphology of these waveforms is clearly very different from that obtained using low illuminance stimuli (see Figure 4.3). The early negative and positive components, occurring at approximately 20ms and 40ms, respectively, are similar in timing to the a- and b-waves observed in ERGs generated by non-selective stimuli. In addition, there is a later complex of negative and positive components, occurring between 75 – 110ms that is observed in the high illuminance responses. This complex is completely absent from the responses elicited by the optimal (< 100 ph Td) rod isolating stimuli. In the light of these differences in waveform morphology, our view is that the ERGs elicited by rod isolating stimuli of high illuminance no longer selectively reflect rod function and are the result of contamination from non-rod mediated sources. Previous work has demonstrated that cone photoreceptors may form one potential source of these intrusions. This is based on the fact that the temporal response limit of these high illuminance ERGs far exceeds that supportable by the rod system and lies closer to temporal response limit of

the cones (Maguire et al. 2016). These intrusions may be the result of the intrinsic anatomical connectivity that exists between the rod signalling pathway and cones (Raviola and Gilula 1973; Völgyi et al. 2004; Moskowitz et al. 2009). The inadvertent stimulation of other photoreceptor populations may also arise as a result of departures in the degree rod isolation provided by our stimuli. Silent substitution calculations are based on representative photoreceptor fundamentals (Stockman and Sharpe 2000). However, across individuals there are differences in these fundamentals, as well as variation in pre-retinal absorption characteristics. These factors are likely to increase the likelihood of stimulation of other photoreceptor classes which becomes more significant with increasing stimulus intensity (Huchzermeyer and Kremers 2016; Huchzermeyer and Kremers 2017). In addition to retinal based sources of contamination we also cannot rule out the possibility of myogenic contamination (due to blinks or blepharospasm) that is often induced by stimuli of high intensities. This could form a potential source, particularly for the later components observed in the ERGs elicited by high illuminance stimuli. Our results suggest that even with silent substitution stimuli, which in theory should elicit no cone excitation, rod isolation can no longer be assured for stimuli of illuminance above 1000 ph Td as a result of these potential physiological and physical sources of contamination.

In summary, we have described the key features of an ERG response, generated by silent substitution stimulation, which selectively reflect the operation of rod photoreceptors in the normal, light-adapted human retina. We have demonstrated how this rod ERG is affected by the use of stimuli

that vary in the extent to which they selectively isolate rod function. We propose that our methodology will prove to be useful in the respect that it provides an opportunity for the examination of human rod function, without having to subject participants to long periods of dark adaptation. Secondly, the use of rod isolating stimuli, used in conjunction with carefully generated stimuli that are less selective in terms of their rod isolation, provide a means to study interactions between rods and cones in the normal and pathological retina, particularly in the context of the control of retinal sensitivity across mesopic illumination levels.

Chapter 5

Verification and Utility of Non Dark-Adapted Rod Isolated ERGs Using Disease Control Models

5.1. Introduction

In the previous two chapters we have shown that rod ERGs obtained using triple silent substitution stimuli and without dark adaptation generate responses consistent with known characteristics of rod mediated vision. As well as examining rod mediated ERGs from the normal trichromatic human retina, we also wanted to assess responses from individuals with specific retinal pathologies. As a result this chapter has been divided into two sections; the first details experiments in which we will validate the photoreceptor-selective nature of our stimuli, whilst the second section will investigate the clinical utility of our isolating stimuli.

5.1.1. Validation

In the context of the first part of this study, individuals with specific retinal pathology constitute an important control group. This is particularly true for individuals diagnosed with achromatopsia. Such individuals lack significant cone function and effectively only possess functioning rod photoreceptors. Thus rod ERGs from these individuals can be compared to those responses obtained from normal trichromats (who still have functioning L-, M- and S-cones). If our silent substitution stimuli and recording conditions do effectively isolate rod function, then we would expect a high degree of

correspondence between the characteristics of the ERGs elicited from normal trichromats and those from achromats.

To facilitate this comparison, we recorded rod ERGs from individuals who have achromatopsia caused by a common CNGB3 gene mutation. Such mutations result in complete or highly impaired cone function which results in abnormal colour vision, reduced visual acuity and nystagmus (Alpern et al. 1960; Kohl et al. 1998; Khan et al. 2007). Conversely, other retinal pathologies, such as the complete form of congenital stationary night blindness (type 1) (CSNB1) for example, lead to severely compromised rod but preserved cone function (Zeitz et al. 2015). CSNB1 is associated with On-bipolar cell dysfunction and leads to a characteristic set of full-field ERG abnormalities including; abolished scotopic rod responses, electronegative mixed rod-cone responses and preserved, though abnormal photopic responses (Miyake et al. 1986; Dryja et al. 2005; Zeitz et al. 2015). In such cases we would expect rod responses generated by silent substitution stimuli in participants with CSNB1 to be very different from those obtained from those with normal retinal function.

In addition to the validation of our rod stimulus, we have included data obtained through further ERG testing on the three individuals with a common CNGB3 mutation. In the assessment of these individuals we discovered that all three had an unusually abnormal deficit in the rod ERG amplitude. Therefore we proffer that a more in depth assessment of their rod function,

which also includes some mathematical modelling of the a-wave, may help explain any differences observed between them and the normal trichromat group.

5.2. Methods

5.2.1. Stimuli

Rod and cone isolated stimuli

Details of the stimulator and the construction of the stimulus are detailed in sections 2.2 and 2.4 respectively. A square-wave, 250ms onset and 250ms offset pulse and sinusoidal, full-field flicker stimuli were presented using a ColorDome (Diagnosys LLC, Lowell, MA, USA) four primary ganzfeld stimulator with blue (460 nm), green (514 nm), amber (590 nm) and red (635 nm) LEDs. Wavelength and intensity combinations were chosen, which produced no net excitation in the three cone classes, only stimulating the rod photoreceptors, generating triple silent substitution stimuli (Estévez and Spekreijse 1974; Estevez and Spekreijse 1982; Shapiro et al. 1996). Figure 5.1 shows how the luminance output of the four LEDs vary as a function of time in order to produce a silent substitution 8Hz 63Td sinusoidal (5.1a) and 250ms onset, 250ms offset 63Td square-wave pulse (5.1b) rod-isolating stimulus. Contrast was defined as the Michelson contrast of rod excitation and was set at 0.25 for all stimuli. Retinal illuminance varied between 1 – 10,000 photopic trolands (Td).

ISCEV Clinical ERG stimuli

Full-field ERGs were recorded using a ColorDome (Diagnosys LLC, Lowell, MA, USA) four primary ganzfeld stimulator and were obtained using standard protocols detailed by the International Society for Clinical Electrophysiology of Vision (ISCEV) (McCulloch et al. 2015). The light-adapted (LA) single flash and 30Hz flicker stimuli (both 3.0 $cd.s.m^{-2}$) were used to assess the cone system. Following a period of 20 minutes dark adaptation, a 0.01 $cd.s.m^{-2}$ (DA0.01) and 10.0 $cd.s.m^{-2}$ (DA10.0) flash stimuli were used to elicit rod responses. In addition to the standard ISCEV stimuli we also examined rod mediated ERGs in our rod monochromat group and an age-matched control using series of stimuli that varied over a wider range (~ 6 log units) of retinal illuminance from -1.9 – 3.6 log scotopic trolands. ERGs were recorded using these stimuli which consisted of 4ms square wave white flash delivered after 20 mins of dark adaptation. Five trials were averaged for each luminance step. An inter stimulus interval of 60 seconds was employed to prevent attenuation of rod signals (Fulton and Hansen 2000).

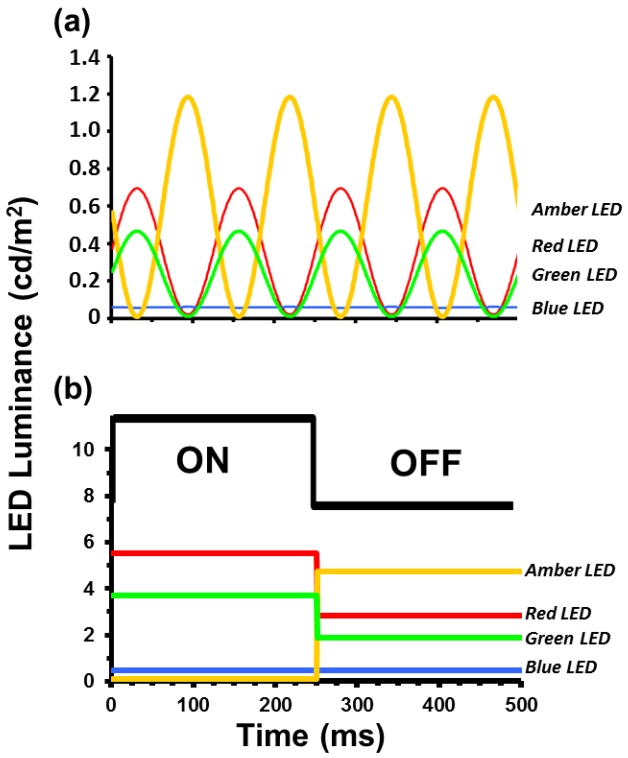

Figure 5.1. (a) Temporal profiles showing the luminance variation and relative phases of the blue, green, amber and red LEDs that are required to generate a 63 Td, 8 Hz rod isolating silent substitution stimulus. The modulation of rod excitation for the resultant stimulus = 0.25. (b) Temporal profile of the square-wave pulse stimulus used to generate rod ERGs. The plot shows the luminance variation of the four LED primaries required to generate the rod isolating stimulus. The initial 0 - 250ms is the onset period followed by the offset period (250-500ms). This sequence was then repeated with the stimuli presented as continuous trains of on-off pulses (256 cycles in total).

5.2.2. ERG Recording

ERGs were recorded from the right eye using a silver/nylon corneal fibre electrode (Dept. of Physics and Clinical Engineering, Royal Liverpool University Hospital, UK) referenced to a 9mm Ag/AgCl electrode (Biosense Medical, Chelmsford, UK) on the outer canthus; a similar electrode was placed on the forehead to serve as ground. Impedance was maintained below 5 kΩ. Signals were recorded using the Espion E^2 system (Diagnosys

LLC, Lowell, MA, USA) which amplified and filtered (bandwidth = 1 to 300 Hz) the ERGs and digitised them at a rate of 1000Hz. Retinal responses to the rod isolated flicker stimuli were acquired over 4 second epochs with subsequent offline analysis being performed on an average of a minimum of 10 of these epochs. Retinal responses to the rod isolated pulse stimuli were acquired over a 500 ms epoch consisting of 250 ms onset and 250 ms offset. Typically 200 trials were averaged. Participants viewed the stimuli monocularly with a dilated pupil (1% Tropicamide). The fellow eye of the participant was patched. Fixation was maintained on a central point which subtended approximately 0.5^0.

5.2.3. ERG Modelling

The mathematical model (Eq. 5.1) by Hood and Birch, based on a model of the phototransduction cascade by Lamb and Pugh accurately predicts the leading edge of the a-wave to high luminance stimuli (Hood and Birch 1990; Hood and Birch 1994; Hood and Birch 1996; Robson and Frishman 1998; Hansen et al. 2017).

$$P3(\mathrm{i},\mathrm{t}) = [1 - \exp(-\mathrm{i} * \mathrm{S} * (\mathrm{t} - t_d)^2)] * Rm_{p3} \qquad for\ t > t_d \qquad (5.1)$$

Where i is the number of photoisomerizations produced by the stimulus, t is the time after flash onset and $\boldsymbol{t_d}$ is a brief time delay of 2.4 – 4ms. S is a sensitivity parameter in isomerization/rod/sec^{-2} and $\boldsymbol{Rm_{p3}}$ is the estimated maximum amplitude. A conversion factor of 1 scot Troland = 8.5

isomerisations (Kraft et al. 1993) was used to calculate an estimation of the amount of photoisomerizations produced by the flash stimulus. The least squares minimisation search (Fminsearch) function in the Matlab package (MATLAB 2013a, The MathWorks Inc., Natick, MA) was used to estimate $\boldsymbol{S}$, $\boldsymbol{Rm_{p3}}$ and $\boldsymbol{t_d}$. Only the first 20 ms of the leading a-wave was fit to avoid b-wave intrusion.

5.2.4. Participants

Experiment 1. Validation of the steady-state rod isolated ERG response

A total of 5 colour normal trichromats (3 males; mean age: 28 yrs., age range: 35 yrs.) and 3 members of a family (ACR 1 (31 yrs.), ACR 2 (38 yrs.) & ACR 3 (34 yrs.)) & with a homozygous p.T383fsX mutation in CNGB3 causing rod monochromacy (see table 5.1 for clinical details) were used.

Experiment 2. Validation of the transient rod stimulus

A total of 20 normal trichromatic observers (mean age: 31.5 yrs., age range: 53 yrs.), as well as the ERG recordings from the 3 subjects with rod monochromacy (previously described) and 2 subjects (NB1 (17 yrs.) and NB2 (27 yrs.)) with congenital stationary night blindness (CSNB 1) took part in this experiment.

Experiment 3. Detailed assessment of rod function.

The three members diagnosed with rod monochromacy, previously described in experiment 1 took part in this experiment.

All participants gave informed consent prior to the commencement of the experiments which were conducted in accordance with the Declaration of Helsinki and were approved by the University of Bradford Ethics Committee.

5.3. Clinical assessment

The two subjects with CSNB 1 along with two siblings and a cousin with a molecularly confirmed *CNGB3*-associated ACHM were examined (see table 5.1 for a summary of the main features). A full clinical history and assessment of the participants was performed which included Snellen visual acuity, colour vision testing using the CAD test (City University, London), as well fundus photography (see Figure 5.2).

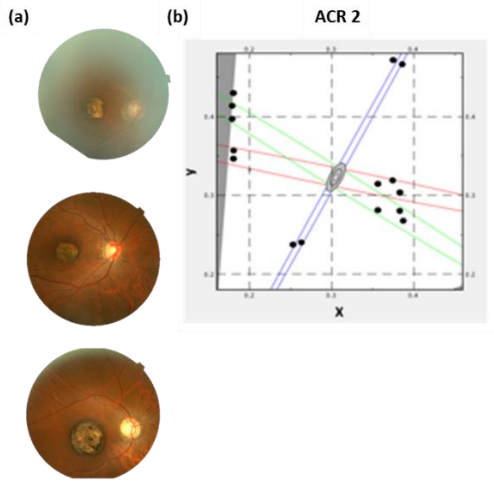

Figure 5.2. (a) Fundus photographs from the 3 rod monochromat subjects and (b) colour discrimination thresholds from the CAD test, plotted on a CIE 1931 (xy) chromaticity diagram for 16 different coloured targets along red, green, blue & yellow colour axes. Normal colour discrimination thresholds (+/- 1 SD) are indicated by the central grey ellipse. Representative data for one rod monochromat subject (ACR 2). All rod monochromats exhibited elevated discrimination thresholds consistent with severe L-, M- and S-cone dysfunction

Participants	Sex	Age	Symptoms	VA	Fundus
ACR 1	Male	28	Nystagmus Photophobia, No colour vision,	2/60(OU)	Severe macular atrophy
ACR 2	Male	34	Nystagmus Photophobia, no colour vision,	CF(OU)	Severe macular atrophy,
ACR 3	Female	38	Nystagmus, Photophobia, no colour vision,	2/60(OU)	Severe macular atrophy,
NB 1	Male	27	Nyctalopia	6/9 (OU)	Normal
NB 2	Male	17	Nyctalopia	6/9 (OU)	Normal

Table 5.1. Summary of the main clinical details of subjects with retinal pathology.

5.3.1. Genetic Assessment

One of the siblings (ACR 2) had previously been recruited to an earlier study investigating the molecular genetic basis for inherited retinal disease (IRD). As part of this study, patients' DNA was analysed by Sanger sequencing of genes known at that time to be associated with ACHM in a step-by-step procedure. The proband was found to be homozygous for a null allele in *CNGB3* (NM_019098.4; c.1148delC, p.T383Ifs*13), the most frequently reported cause of ACHM in those of European ancestry (Kohl et al. 2005). Segregation analysis confirmed that ACR 1 and 3 were also homozygous for the c.1148delC allele. Genetic testing was also performed on participants NB1 and NB2. Both were shown to have a NYX (Xp11.4) gene mutation causing CSNB1.

5.4. Electrophysiological Assessment

5.4.1. ISCEV clinical ERG

Figure 5.3 shows the standard ISCEV full-field ERG responses from the 3 rod monochromats as well as a set of responses representative of our normal data set. The light-adapted single flash and the photopic flicker responses were undetectable in all three rod monochromat subjects, consistent with the severe cone dysfunction typically reported for this condition (Khan et al. 2007).

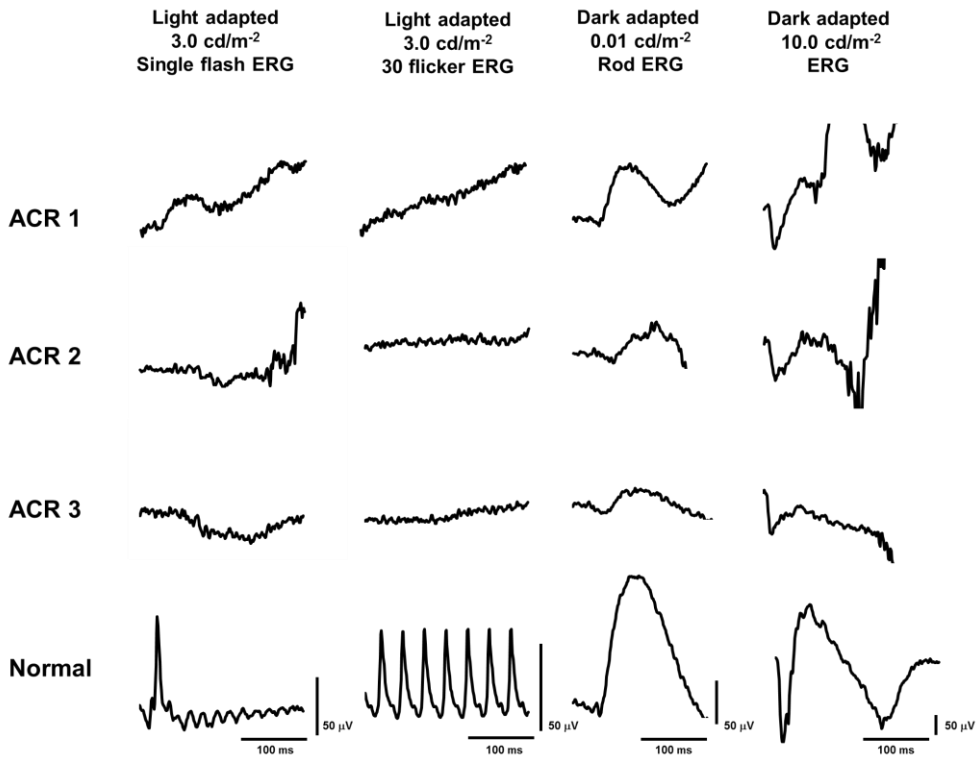

Figure 5.3. ISCEV standard full-field ERGs (RE only) recorded from 3 participants diagnosed with ACHM (rows I – III) plus a data set from a representative of our normal control group (row IV). Column 1: light adapted single flash response (3.0 cd.s.m^{-2}); Column 2: 30Hz flicker stimulus (3.0 cd.s.m^{-2}); Column 3; dark-adapted (rod only) response (0.01 cd.s.m^{-2}); Column 4: bright flash (10.0 cd.s.m^{-2}). Note: the small positivity noted in the LA 3.0 cd.s.m^{-2} is an artefact. Light adapted (LA), Dark adapted (DA)

The DA0.01 responses were also abnormal, with a severe loss of b-wave amplitude (Table 5.2). ACR 1 responses are reduced by 57%, whilst ACR 2 and 3 have lost 74% and 87% of their b-wave amplitude compared to our normal mean value. The DA10.0 waveforms also exhibit significant loss of b-wave amplitude, and for ACR 3 the waveforms are electronegative. A smaller reduction is noted in a-wave amplitude which may be explained by the loss of input from the dark adapted cone system (Robson and Frishman 2014). Implicit times of the a- and b-waves are also increased compared to normative data (see table 5.2).

Subject	Light adapted Single Flash ERG	Light adapted Flicker ERG	Dark adapted 0.01 cd.s.m^{-2} ERG	Dark adapted 10.0 cd.s.m^{-2} ERG
ACR 1				
a-wave amp	X	X	----	92
		X	69.2	165
b-wave amp	X	X	----	15
		X	97.0	60
a-wave imp T	X			
b-wave imp T	X			
ACR 2				
		X	----	85
a-wave amp	X	X	42.16	114
		X	----	16
b-wave amp	X	X	114.0	57
a-wave imp T	X			
b-wave imp T	X			
ACR 3				
		X	----	83
a-wave amp	X	X	21.25	44
		X	----	14
b-wave amp	X	X	90.0	57
a-wave imp T	X			
b-wave imp T	X			
Normal				
a-wave amp Lower limit	**9**	---	---	**76**
a-wave amp Upper limit	**33**	---	---	**217**
b-wave amp Lower limit	**59**	**34**	**102**	**173**
b-wave amp Upper limit	**176**	**121**	**314**	**433**
a-wave Imp T Lower limit	**14**	---	---	**11**
a-wave Imp T Upper limit	**17**	---	---	**16**
b-wave Imp T Lower limit	**27**	**24**	**76**	**47**
b-wave Imp T Upper limit	**31**	**29**	**112**	**56**

Table 5.2. Summary of the amplitude (amp) and implicit time (Imp T) measurements for ERGs elicited by the standard ISCEV protocols. X denotes that no data could be obtained as the waveform component was undetectable, --- denotes that no measurements were taken for that particular component. Normal values are based on n=70 subjects assessed in the University of Bradford Electrodiagnostic Unit.

The full field ERG responses for the CSNB1 participant (NB1 and NB2) along with a set of responses representative of our normal data set are shown in figure 5.4. The LA3.0 cd/m2 single flash had a normal a-wave amplitude but with the classic broad trough associated with this condition (Miyake et al. 1986). The b-wave was reduced with no oscillatory potentials, consistent with ON pathway dysfunction. The 30Hz flicker response also had a broad trough with reduced peak amplitude. The DA0.01 cd/m^2 amplitude was absent. The 10.0 cd/m^2 responses exhibited the classic electronegative response (Miyake et al. 1986; Audo et al. 2008b; Sergouniotis et al. 2012; Zeitz et al. 2015).

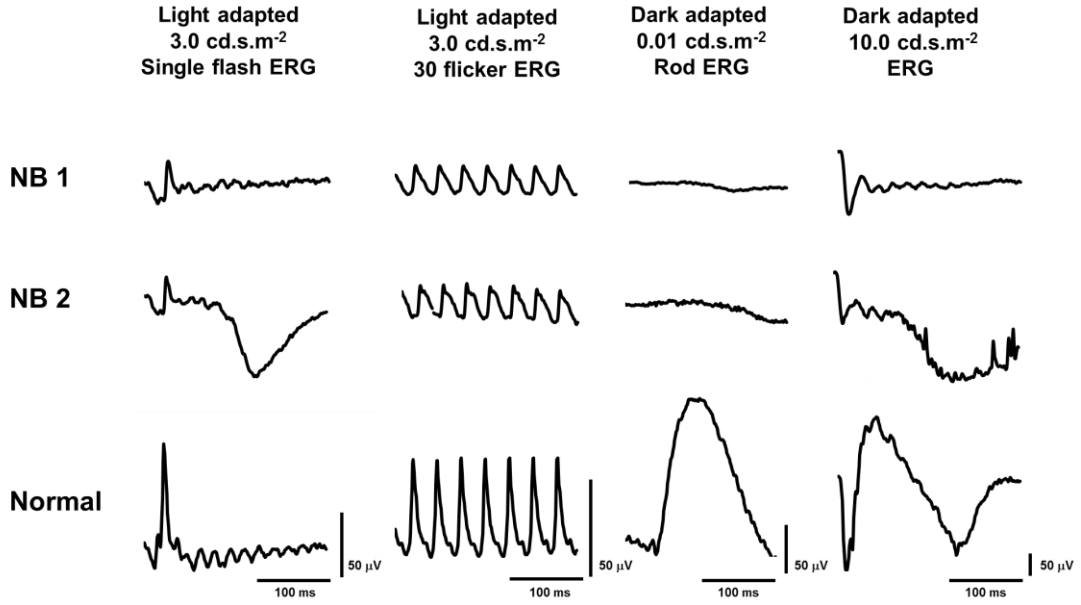

Figure 5.4. ISCEV standard full-field ERGs (RE only) recorded from the two participants diagnosed with CSNB 1 (row I and II) plus a data set from a representative of our normal control group (row III). Column 1: light adapted single flash response (3.0 cd.s.m^{-2}); Column 2: 30Hz flicker stimulus (3.0 cd.s.m^{-2}); Column 3; dark-adapted (rod only) response (0.01 cd.s.m^{-2}); Column 4: bright flash (10.0 cd.s.m^{-2}).

5.5. Results

5.5.1. Validation of the steady-state rod isolated ERG response

Temporal frequency response

Figure 5.5 shows the variation in ERG amplitude and phase as a function of temporal frequency for a 63 Td rod isolating stimulus. The data shown are the group (vector) averaged responses from the achromat group (n = 3) and the normal trichromat group data (n=5) described in chapter 3. For clarity, one standard deviation within the normal trichromat group is shown as a dotted line and as error bars from the ACR group. Both responses were obtained without subjecting the participants to a period of dark adaptation beforehand. Both averages exhibit a low pass response typical of the rod system (Gouras and Gunkel 1964). Response amplitudes were maximal at lower frequencies. From 7Hz onwards, responses decreased steadily and both groups reached noise levels between 20-30Hz. Overall the response from the ACR group was lower in amplitude and may be related to the reduced rod function previously demonstrated in figure 5.3. Both groups exhibited similar phase plots up to 20Hz. After this point the responses from the ACR group were more variable, possibly as a result of poor signal to noise.

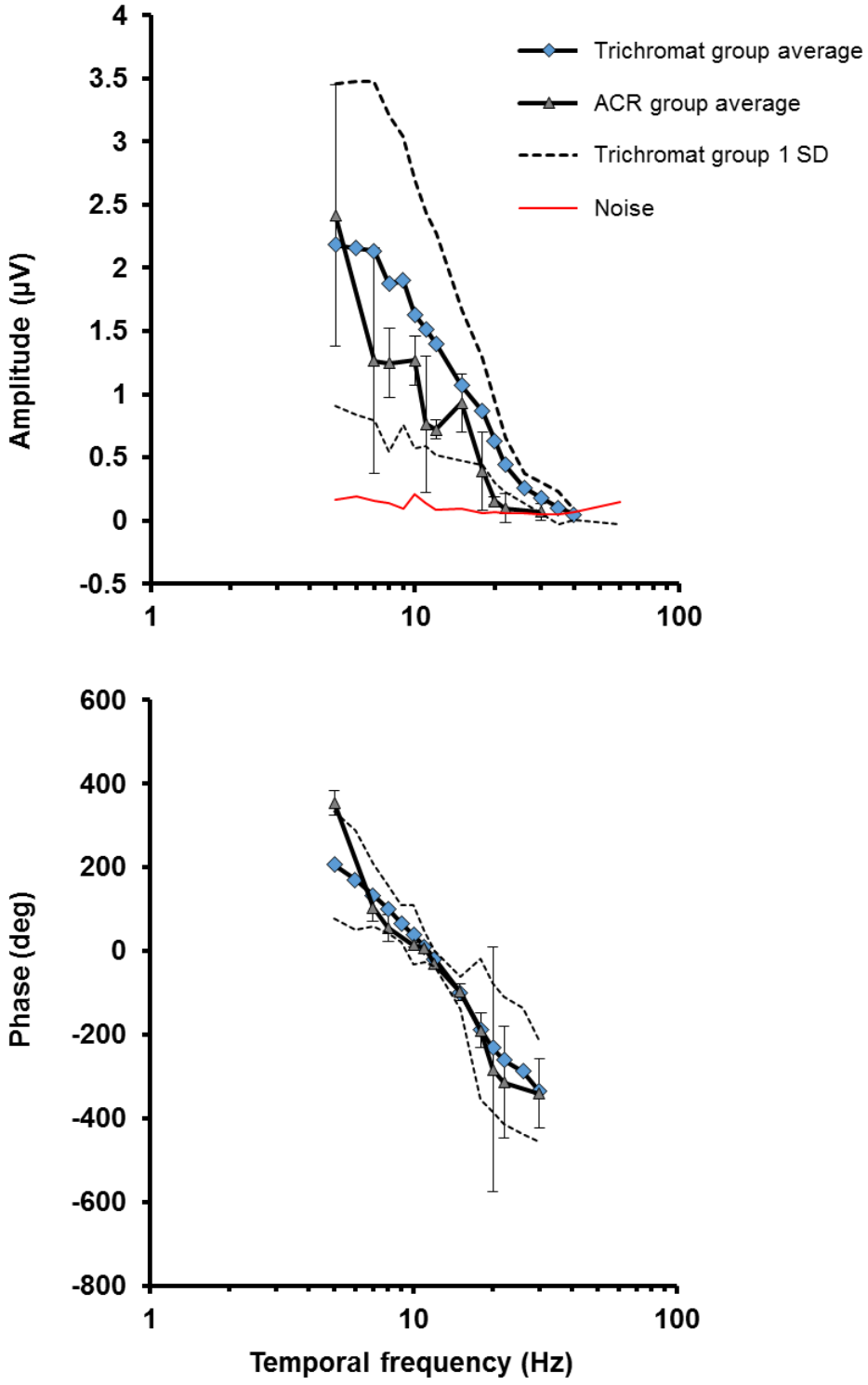

Figure 5.5. ERG amplitude (upper plot) and phase (lower plot) as function of temporal frequency obtained for a 63Td rod isolating silent substitution stimulus (C=0.25). The data shown are the group averaged results from the achromat (ACR) subjects (n=3) and the normal trichromat group (n=5).The thin dashed lines represent +/- 1 S.D. from the mean of the normal group. The error bars represent +/- 1 S.D. from the mean of the achromat group. The thin red line plots the measure of noise (see methods).

Luminance response

Figure 5.6 shows the variation in ERG amplitude and phase as a function of retinal illuminance for an 8Hz rod isolating stimulus. The data shown are the group (vector) averaged responses from the achromat group (n = 3) and the normal trichromat group data (n=5) described in chapter 3. The upper limit of the stimulus luminance was limited by photophobia and as a result did not extend to the limits recorded from the normal group. The response from the normal group shows a steady increase and has a peak between 10 and 100 ph Td. The ACR group has a lower amplitude response at lower luminances, remaining below noise levels until 10 ph Td. The phase of the ACR response is also highly variable over this region. After this point the response amplitude rises steadily, overtaking the normal group at 63 ph Td and peaking slightly later at 126 ph Td, before starting to decline.

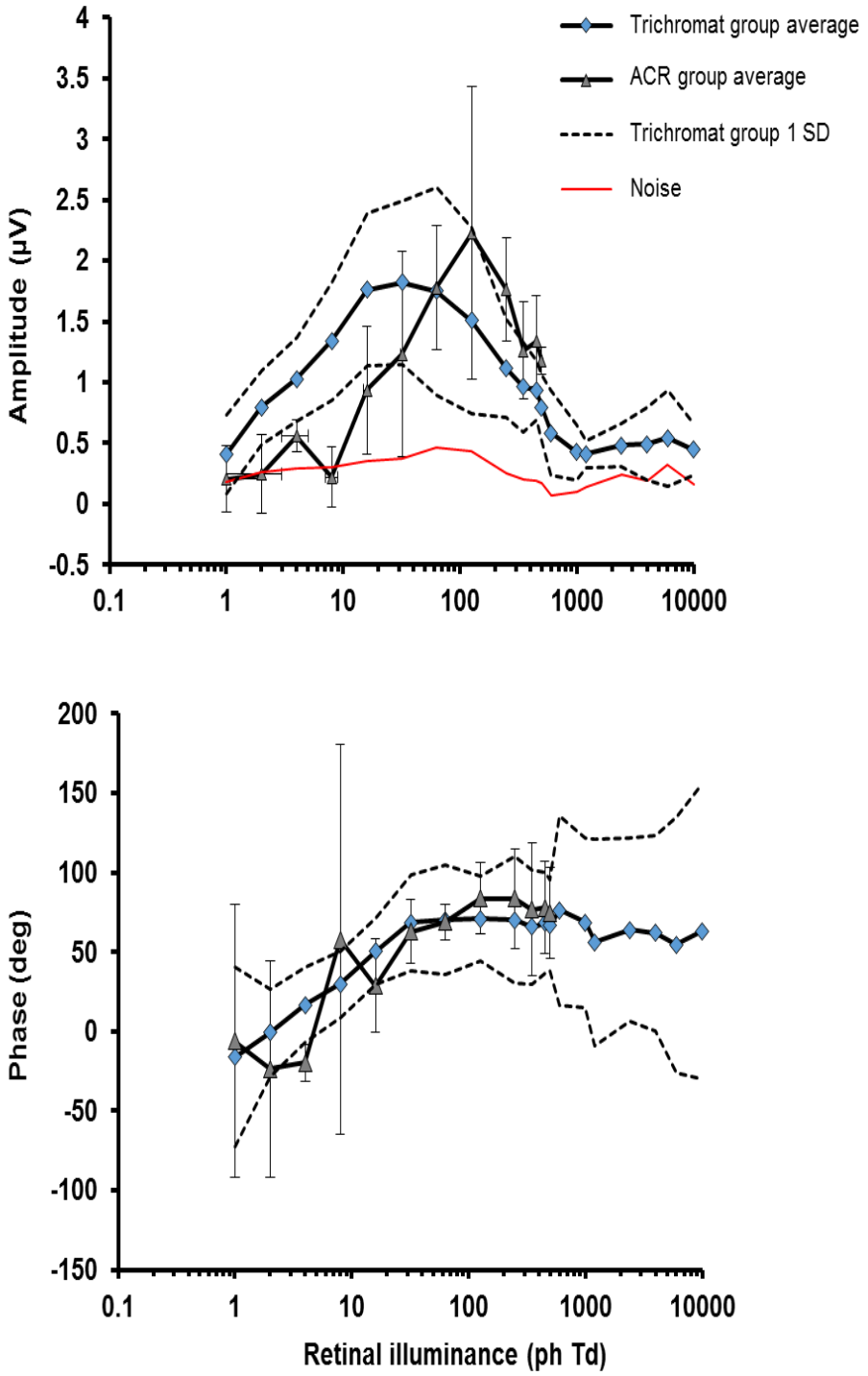

Figure 5.6. ERG amplitude (upper plot) and phase (lower plot) as function of retinal illuminance obtained using an 8Hz rod isolating silent substitution stimulus (C=0.25). The data shown are the group averaged results from the achromat (ACR) subjects (n=3) and the normal trichromat group (n=5).The thin dashed lines represent +/- 1 S.D. from the mean of the normal group. The error bars represent +/- 1 S.D. from the mean of the achromat group. The thin red line plots the measure of noise (see methods).

Transient rod isolated ERGs

Figure 5.7 shows the group averaged (n = 20) ERG obtained from the normal trichromats in response to the silent substitution, rod isolating stimulus. Also shown are the responses from the three rod monochromats and 2 CSNB1 subjects to the same stimulus. The responses elicited from the rod monochromats exhibit similar waveform morphologies to the normal rod response, with the P_{Ri} and N_{Rd} components being identifiable at stimulus onset and offset, respectively. However, response amplitudes vary across the three subjects and there is inter-subject variation in terms of the quality of waveform appearance. This is clearly seen in subject ACR 3, the P_{Ri} rises just above the baseline and is followed by a large negativity which obscures the N_{Rd} component. The reason for such variation could be due to the fact that rod function is compromised in all of these individuals. The canonical view of rod monochromacy is that it primarily leads to cone dysfunction, leaving rod function intact [see ref (Remmer et al. 2015)]. However, figure 5.3 clearly demonstrates an attenuated ISCEV DA0.01 and 10.0 responses for all three rod monochromats. This secondary loss of rod response in rod monochromats is consistent with reports from previous studies demonstrating phenotypic variability (Khan et al. 2007; Moskowitz et al. 2009; Genead et al. 2011).

In contrast, the ERGs generated by the rod isolating stimuli from the CSNB patients are markedly different. The responses lack a prominent P_{Ri} component; instead the waveform elicited by contrast increment (onset) is

dominated by a prolonged negative component. The offset response is also very different in that it shows a small positivity (NB 1) rather than a large negativity.

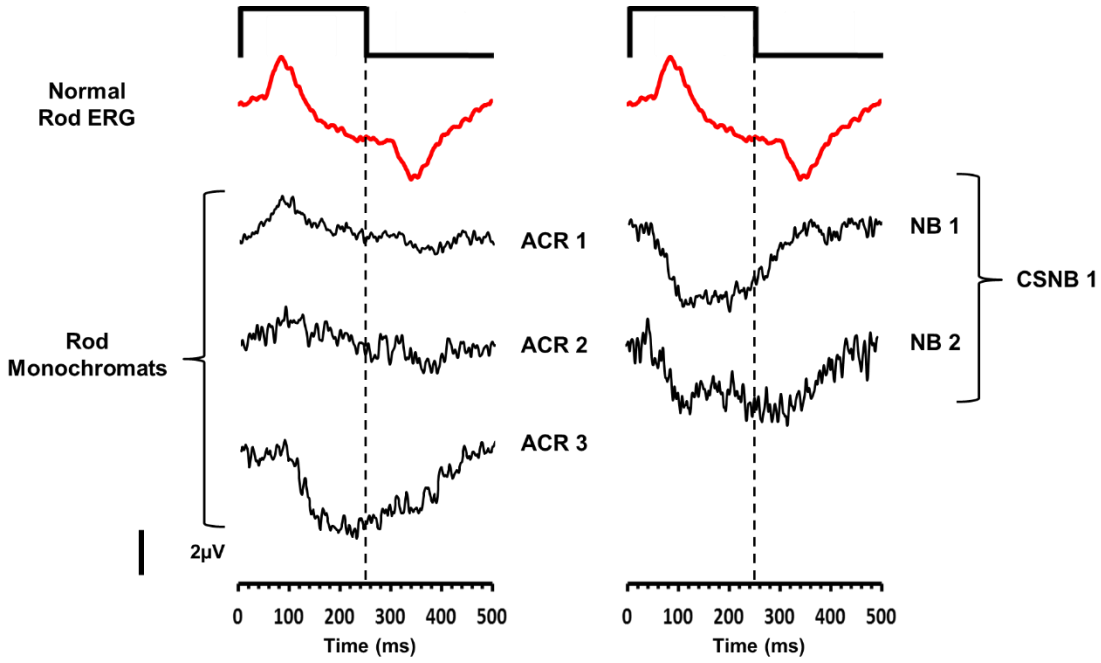

Figure 5.7. Black traces represent the ERGs elicited from the three rod monochromat's (left column) and two CSNB1 subjects (right column). The group average from the normal group (n=20) using a silent substitution rod isolating stimulus without any dark adaptation is shown at the top of each column (red trace). The stimulus was a 63 ph Td rod isolating square-wave pulse stimulus (250/250ms onset/offset).

5.5.2 Detailed assessment of rod function.

Due to the marked rod deficit noted in three participants, a more in depth assessment of rod function was conducted. Figure 5.8 shows the ERG waveforms for dark adapted ERGs, recorded as a function of retinal illuminance across a 6 log unit scale (-1.9 – 3.6 log scot trolands), from an

age matched normal participant and the three achromats using a brief (4ms) square wave white stimulus (∆C=100%).

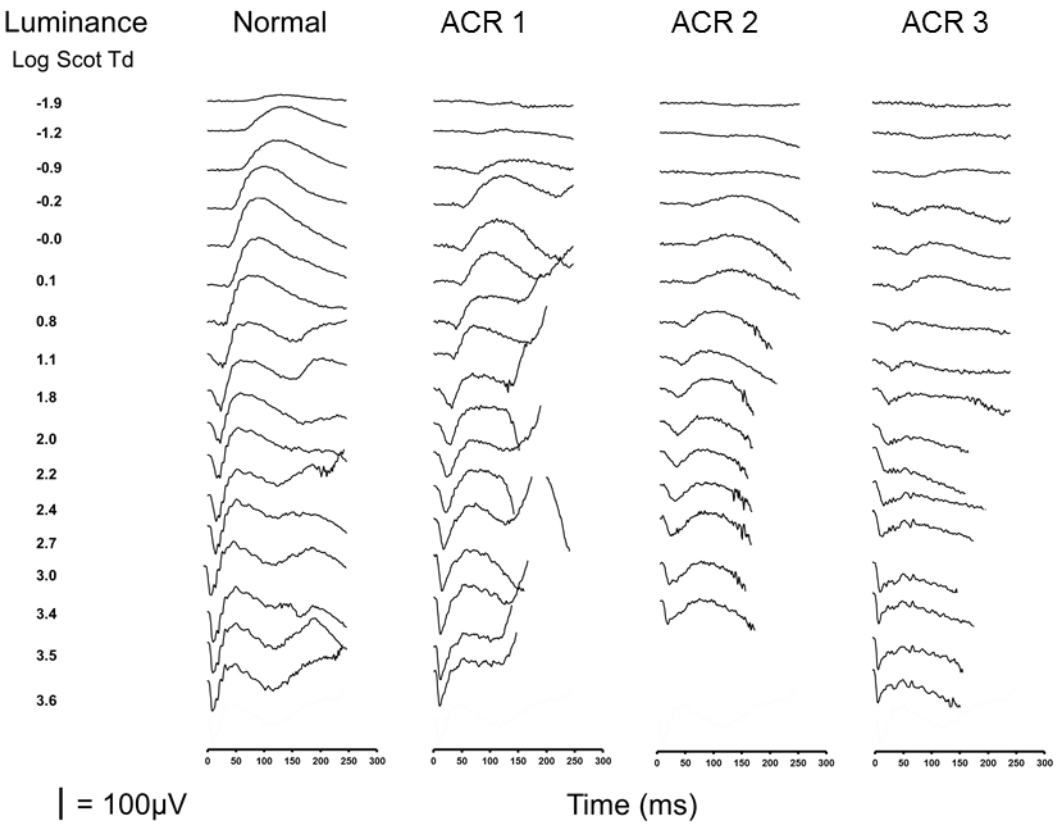

Figure 5.8. Dark-adapted ERGs generated by a series of stimuli of increasing retinal illuminance (-1.9 – 3.6 log scot trolands). ERGs from the age-matched normal control are shown in the first column with responses from the three ACHM patients shown in columns 2- 3. ERG responses were not recorded to the two highest luminance's for *ACR* 2.

The data show clear qualitative differences between the ERG waveforms obtained from an individual with normal rod function compared to those obtained from the three achromats across the same illuminance range. In particular, the responses generated at low retinal illuminances (-1.9 – -0.9 log scotopic trolands) are markedly attenuated in the achromats compared to the normal ERGs. In fact, b-wave amplitude is reduced across the whole

illuminance range in the achromats and again the development of the electronegative response in ACR 3 can be clearly observed beyond 1.1 log scot trolands.

In Figure 5.9 peak amplitudes and implicit times of the a- and b-waves have been plotted as a function of retinal illuminance for a normal control participant and the achromat subjects. As indicated by the waveforms in Figure 5.8, the greatest difference is in b-wave amplitude (fig 5.9A). The illuminance response function from the normal subject exhibits an initial steep increase in b-wave amplitude up to 1 log scotopic Troland after which it reaches saturation. This saturating response function of the dark adapted ERG has been described previously and is considered to be the result of an algebraic interaction between receptoral and post-receptoral retinal responses at higher illuminances (Peachey et al. 1989a; Wali and Leguire 1991). In contrast, the b-wave amplitude illuminance-response functions from ACR 2 and ACR 3 are markedly different; with b-wave amplitude exhibiting a much shallower, monotonic increase with increasing retinal illuminance. The response from ACR 1 sits below the normal response but retains the dual phase morphology.

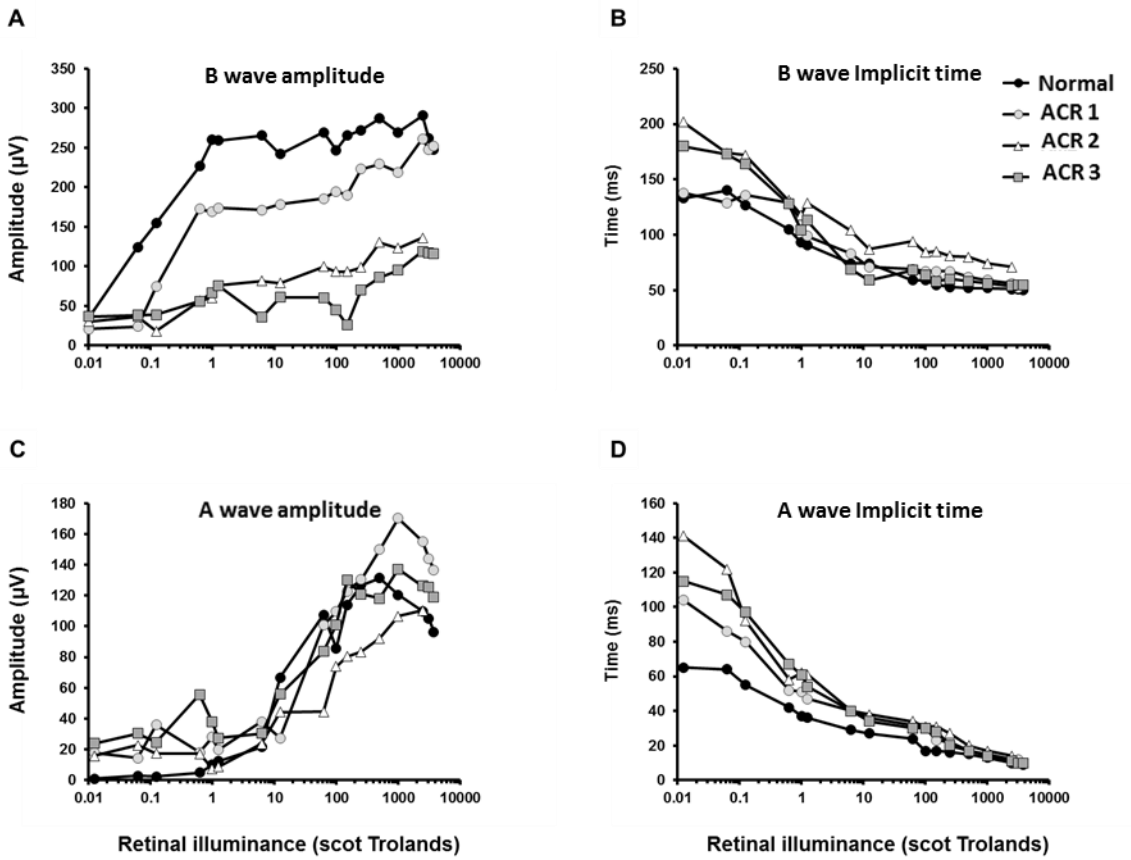

Figure 5.9. Plots of b-wave amplitude (A) and implicit time (B) and a-wave amplitude (C) and implicit time (D) as a function of retinal illuminance for the data shown in figure 5.7 for the 3 achromats and the age-matched control subject.

The illuminance response of the a-wave (Figure 5.9C), by comparison, appears to be similar across the achromats and the normal. In fact, at the upper luminance range the a-wave amplitude from ACR 1 is greater than the normal. In terms of a- and b-wave implicit times (Figure 5.9B & D) the biggest differences between the control subject and achromat subjects occur at low retinal illuminances (< 1 log scot trolands) where the ERGs from the achromats have considerably longer a- and b-wave implicit times. However, as retinal illuminance increases the differences in implicit times between the normal and the achromatopsic patients becomes less marked. Marker placement for the a-wave at lower luminance was often ambiguous. When

uncertain, the start of the b-wave was chosen. This therefore may falsely prolong the a-wave implicit time measurement.

5.5.2.1. ERG modelling

Mathematical modelling of the a-wave modelling was used to quantify any subtle change in amplitude and sensitivity with increasing luminance. The leading edge of the a-wave is dependent on the photocurrent of the rod outer-segment (Lamb and Pugh 1992; Hood and Birch 1994). The mathematical model (Eq. 5.1) by Hood and Birch, based on a model of the phototransduction cascade by Lamb Pugh, accurately predicts the leading edge of the a-wave to high luminance stimuli (Hood and Birch 1990; Hood and Birch 1994; Hood and Birch 1996; Robson and Frishman 1998; Hansen et al. 2017). The two parameters that we are most interested in are **S** and $\mathbf{Rm_{p3}}$. **S** is the sensitivity of the response and an approximation of multiple processes from photoisomerization of a single rhodopsin molecule to the closure of the channels. $\mathbf{Rm_{p3}}$ is the maximal amplitude response and is therefore dependent on the amount of channels available for closure by a high intensity light stimulus (Lamb and Pugh 1992; Hood and Birch 1994; Smith and Lamb 1997). Therefore by examining both of these parameters we can determine if there is also an abnormality at a photoreceptoral level and whether it is as a result of intrinsic problems within the outer segment of the photoreceptor or as a result of a reduction in the number of functional photoreceptors.

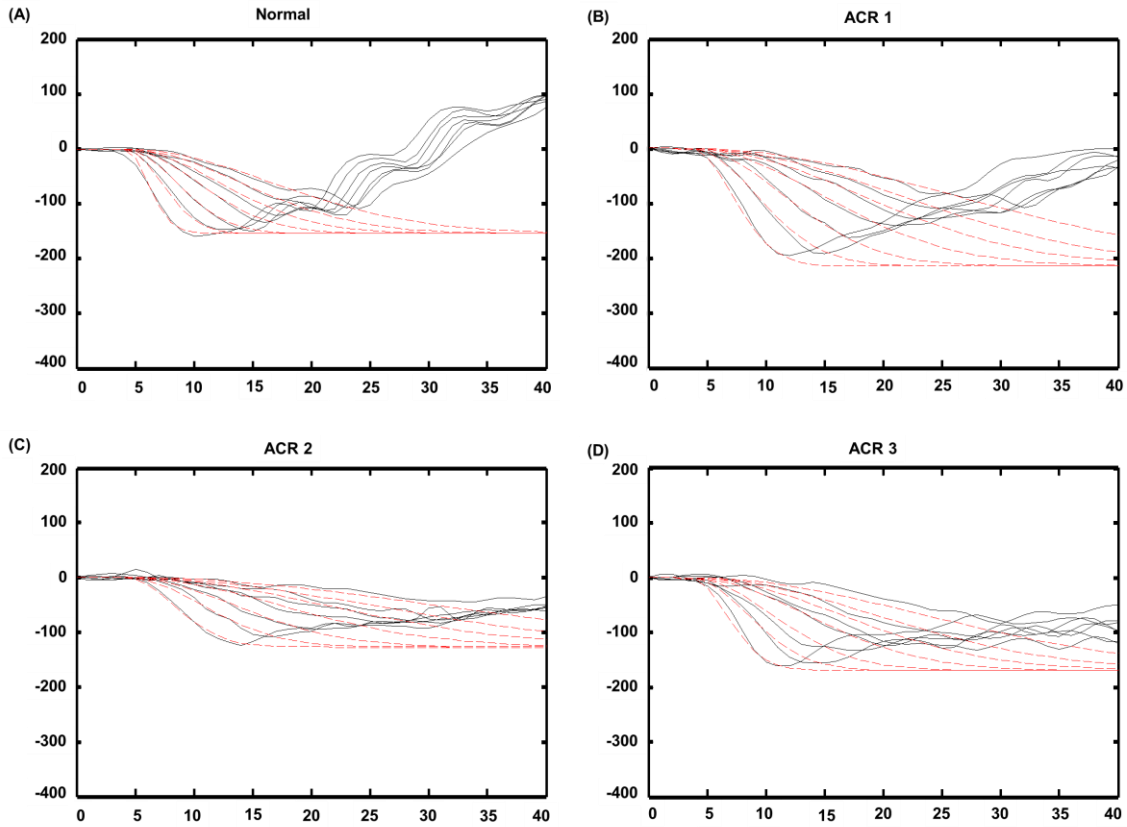

Figure 5.10. A series of a-waves (grey trace) with fitted mathematical models (dashed red trace) recorded from the three rod monochromat and one aged matched subject.

The a-wave responses (grey lines) recorded from the normal (A) and achromat (B-D) subjects to flashes of 1.8 log scot Trolands and above are shown in figure 5.10 along with the fitted model (red dashed line). The $\mathbf{Rm_{p3}}$ and **S** parameters for the normal participant and the three achromats are shown in table 5.3.

Subjects	Rmp3	S
Normal	155μV	12.15
ACR 1	213μV	3.81
ACR 2	126μV	2.75
ACR 3	168μV	4.87

Table 5.3. Rod photoreceptor parameters Rmp3 and S from the normal and achromat subjects.

The $\mathbf{Rm_{p3}}$ parameter was not decreased compared to the normal. In fact, all of the $\mathbf{Rm_{p3}}$ values from the achromat group were greater than the normal participant. Conversely, the **S** parameter was reduced in all three achromats compared to the normal participant. The **S** value recorded from the normal participant was similar to normal **S** parameters recorded by Moskowitz et al. (2009). The reduced **S** parameter may be indicative of abnormalities in phototransduction the outer segment as well as the previously noted post receptoral changes.

5.6. Assessing the clinical utility of rod isolated ERGs

5.6.1. Introduction

In the second section of this study our aim is to determine the wider clinical applicability of our non-dark-adapted silent substitution protocol in the assessment of rod function. Currently, the clinical assessment of rod function is performed using standardised methods outlined by ISCEV (McCulloch et al. 2015). This recommends a period of 20 minute dark adaptation to allow the rod system achieve maximal or near maximal sensitivity, and the presentation of a brief scotopic stimulus. The fundamental methodologies employed in the ISCEV standard and that used in silent substitution are very different, as is the elicited waveform response. However, based on data presented in the previous and this current chapter, we feel that both may have similar origins. Therefore we would expect to find a significant correlation between the amplitude of the fundamental 8Hz component of our rod isolated stimulus and the gold standard, dark adapted 0.01cd/m^2, in a cohort of participants with both normal and abnormal rod function.

5.7. Methods

5.7.1 Stimuli

Rod isolated stimuli

The 8Hz rod isolating stimulus has been previously described in section 5.2.1.

ISCEV Clinical ERG stimuli

The light-adapted (LA) single flash (3.0 cd.s.m^{-2}) and 30Hz flicker stimuli (3.0 cd.s.m^{-2}) were used to assess the cone system. Following a period of 20 minutes dark adaptation, a 0.01 cd.s.m^{-2} (DA0.01) flash was used to assess rod function.

5.7.2. ERG Recording

The ERG set up and recording method has previously been described in the section 5.2.2.

5.7.3. Participants

A cohort of 28 subjects (17 females, 11 males; mean age: 36.8 yrs, age range: 52 yrs) 18 of whom had normal rod function and 10 of whom had compromised rod function (6 diagnosed with rod or rod/cone dystrophy; 2 with congenital stationary night blindness (CSNB) type 1; 2 with CSNB type 2) took part in this study.

5.8. Results

ERGs in of group of normal participants (n=18) using our 8 Hz rod isolating stimulus were recorded and compared with ERGs obtained from the same cohort using current ISCEV standard protocols (McCulloch et al. 2015) for isolating rod- (dark-adapted; 0.01 cd.s.m^{-2}) as well as cone-mediated (light-

adapted 3.0 cd.s.m^{-2} flicker (30 Hz)) ERGs. Figure 5.11a plots the amplitude of the ERGs obtained using the 8 Hz silent substitution stimulus against those obtained for the ISCEV dark adapted 0.01 protocol. There is a significant positive correlation between these two measures of rod function (n = 18; $p < 0.005$; $R^2 = 0.39$). Figure 5.11b plots the correlation between the 8 Hz rod isolating stimulus and the ISCEV light adapted 3.0 cd.s.m^{-2} flicker response. These two measures would not be expected to exhibit a significant correlation as they purportedly separately assay rod and cone function, respectively. Our results demonstrate that this is indeed the case (n = 18; p = 0.881; $R^2 = 0.0015$). However, when a similar analysis is performed for the data collected with the ISCEV dark adapted 0.01 and light adapted 3.0 flicker protocols a significant positive correlation is found (n = 18 ; p = 0.03 ; R^2 = 0.26).

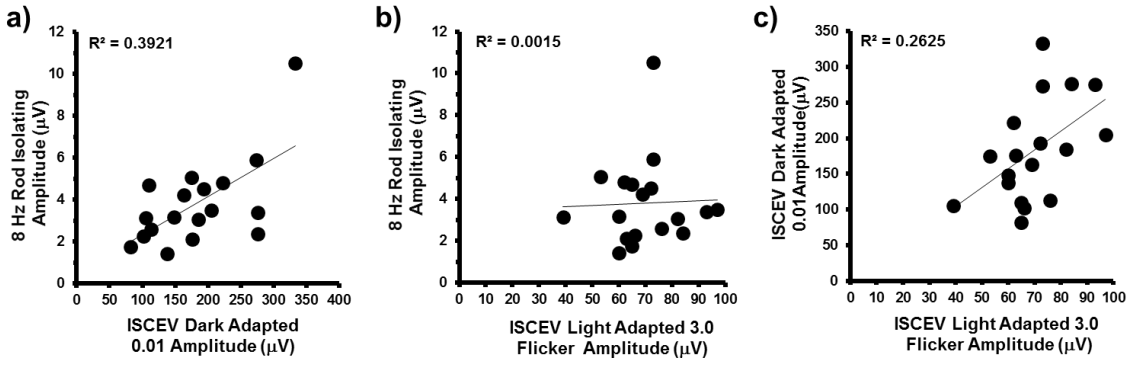

Figure 5.11. Correlation between ERG response amplitudes elicited by different testing protocols: a) compares the amplitudes of the 8 Hz silent substitution rod isolating (63 phot Td) ERGs with those obtained for the ISCEV dark adapted 0.01 protocol, b) compares the 8 Hz silent substitution with the ISCEV light adapted 3.0 flicker (30 Hz) response and c) compares the ISCEV dark adapted and light adapted responses. The data were collected from 18 normal participants.

So far we have considered the use of the non-dark adapted silent substitution protocol in participants with normal rod function. An important question is whether this new approach can be applied usefully in a clinical population with compromised rod function who may have additional issues such as reduced visual acuity or nystagmus, for example. In order to address this issue we recorded ERGs from a cohort of 10 individuals all of whom have compromised or severely reduced rod function due to rod/cone dystrophy (n=6) or congenital stationary night blindness (CSNB) (type 1 (n=2); type 2 (n = 2)). Figure 5.12 shows the full-field ERGs recorded from the participants with compromised retinal function. Figure 5.13a shows this group, now added to the normals previously shown in figure 5.11a, where response amplitude for the 8 Hz rod isolating is plotted against the ISCEV dark adapted 0.01 protocol. Analysis, now including this patient group, demonstrates a stronger correlation ($n = 28$; $p < 0.001$; $R^2 = 0.62$) between both measures of rod function.

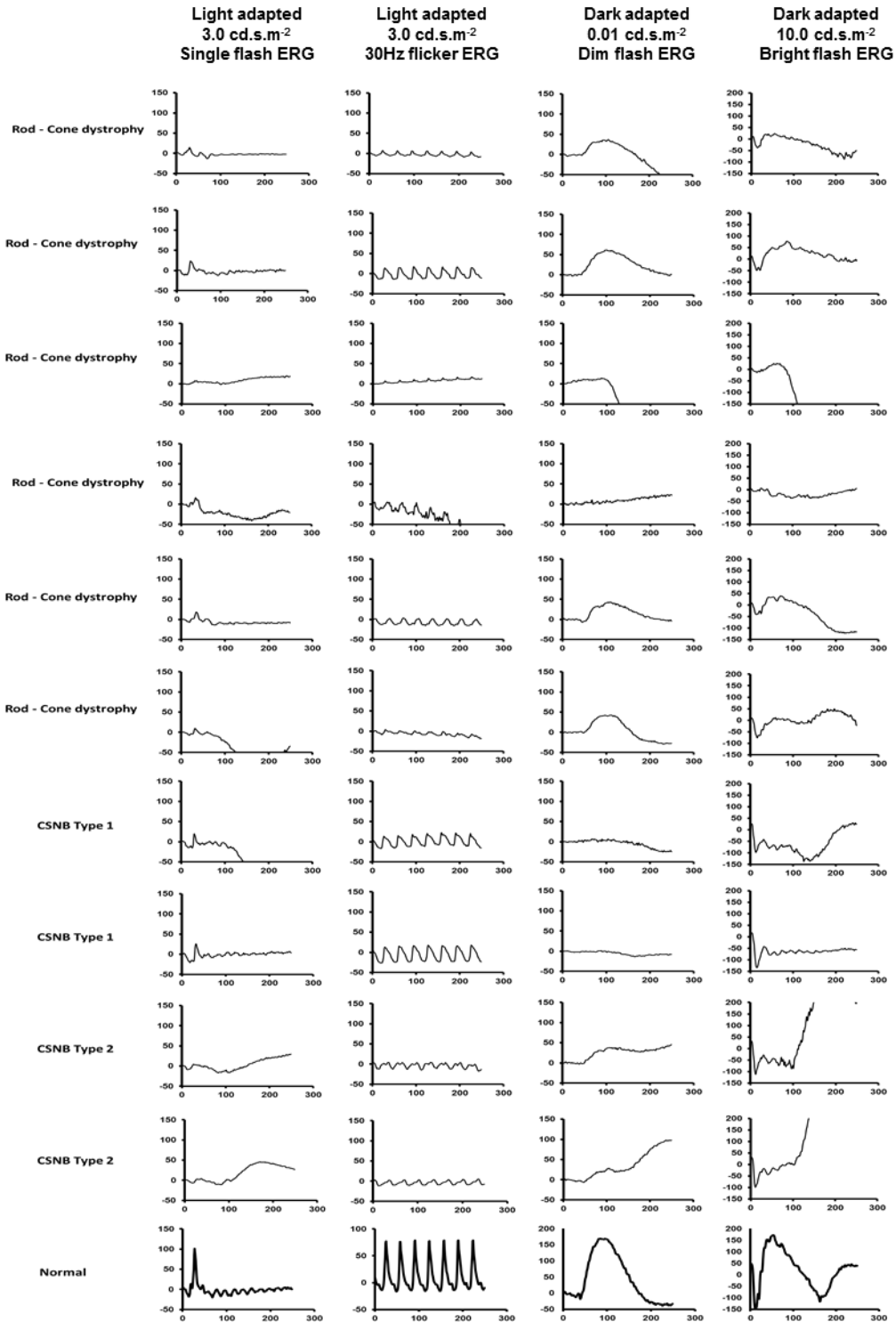

Figure 5.12 ISCEV standard full-field ERGs (RE only) recorded from the 10 individuals all of whom have compromised or severely reduced rod function due to rod/cone dystrophy (n=6) or congenital stationary night blindness (CSNB) (type 1 (n=2); type 2 (n = 2)) and a representative of our normal control group (row III). Column 1: light adapted single flash response (3.0 cd.s.m^{-2}); Column 2: 30Hz flicker stimulus (3.0 cd.s.m^{-2}); Column 3; dark-adapted (rod only) response (0.01 cd.s.m^{-2}); Column 4: bright flash (10.0 cd.s.m^{-2}).

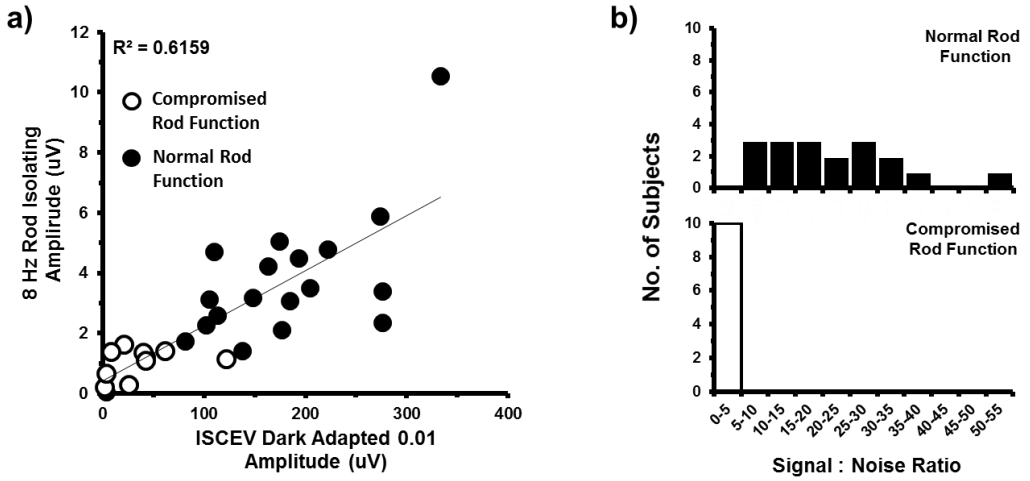

Figure 5.13. a) Correlation between ERGs obtained with a standard ISCEV dark adapted 0.01 stimulus and those obtained with an 8Hz sinusoidal rod isolating silent substitution stimulus. Recordings were made from 18 subjects with normal rod function (filled circles) and 10 subjects with compromised rod function. b) Distribution of the signal: noise ratio calculated for the 8Hz rod isolating ERG data are shown for the normal (upper panel) and compromised (lower panel) rod function groups.

Compared to the ISCEV clinical standard for generating rod ERGs, the absolute amplitude values are lower for our method. However, what is arguably more important than the absolute amplitude in this context is the signal: noise ratio (SNR). In figure 5.13b the distributions of SNR are plotted for the normal and compromised rod function groups. Comparison of these distributions (Mann-Whitney U test) shows that the SNR ratio in the normal group is statistically significantly higher than in the group with abnormal rod function ($U = 0.0$, $p < 0.001$) and demonstrates that the rod isolating silent substitution protocol has the potential to differentiate between subjects with normal and compromised rod function.

5.9. General Discussion

In this study we have compared rod isolated ERG responses from our normal group to a group of participants with various types of retinal pathology. The overall aim was twofold; firstly to provide validation of the rod-selectivity of our stimuli and secondly, to gauge the usefulness of isolated ERGs using silent substitution as a clinical diagnostic tool. Responses recorded from different pathological groups within this cohort have served as important controls and complement our observations from the normal human retina detailed in chapters 3 and 4. Of particular importance is the comparison between the steady-state rod-isolated data from the normal trichromat group and that recorded from the rod monochromats. The retina in rod monochromats typically contains only one type of functioning photoreceptor (rods). Therefore ideally we would hope to see a close degree of similarity between the rod ERGs elicited from both groups. In relation to the temporal frequency response characteristics, both groups were shown to exhibit a similar low-pass functions and almost identical phase plots. The retinal illuminance response function in the rod monochromat group showed a broad resemblance to the response from the normal trichromats, although a few differences were apparent: 1). At the lower end of the luminance range the response is relatively insensitive to changes in luminance, not rising above noise levels until after 8Td's. This may be related to the abnormal rod function noted earlier in figure 5.3 and explored further in the section 5.5.2. This is discussed in section 5.9.1 in more detail. 2). The data from the rod monochromat group peaks slightly later. A similar observation is noted in data recorded by (Park et al. 2015) albeit incorporating different stimulus

parameters (15Hz and C=0.4). In contrast to our data, their rod monochromat data (with normal ISCEV rod ERGs) elicited slightly higher amplitude rod isolated responses compared to the normal trichromat group over the full range of luminance levels. This further suggests that anomalies noted at the lower end of our luminance function may be attributable to loss of rods or reduced rod sensitivity within our rod monochromat cohort.

Despite differences in amplitude, the fact that the silent substitution rod isolating stimulus generates an ERG from these individuals that has the same basic morphology as the rod ERG obtained from the normal retina, provides verification that this response does indeed reflect rod-mediated retinal function. Both participants with CSNB1 had X-linked mutations (Xp11.4) in the Nyx gene. The Nyx gene encodes the protein nyctalopin, a protein involved in the localisation of TRPM1 to the ON bipolar cell dendrites and required for glutamate led light depolarisation (Pearring et al. 2011). This mutation directly results in ON-bipolar cell dysfunction and individuals with this condition have a characteristic set of full-field ERG abnormalities; abolished scotopic responses, electronegative bright flash ERGs, as well as abnormalities in the morphology of the photopic a-wave and flicker ERG (Miyake et al. 1986; Dryja et al. 2005; Sergouniotis et al. 2012; Zeitz et al. 2015). Recordings from the participants with CSNB1 provide further evidence to that outlined in the discussion in chapter 4 that the P_{Ri} component is similar to that of the rod b-wave. Using the rod isolating silent substitution stimuli, both participants lacked any obvious P_{Ri} component but, in keeping with previous findings e.g. (Sieving et al. 1994), exhibit an

electronegative waveform in response to the onset of a long duration rod isolating stimuli. The rod isolated ERGs obtained from the CSNB1 participants contrast with those elicited from rod monochromats and normal trichromats. The similarity between the waveform morphologies of ERGs obtained by rod isolating stimuli from normal trichromats and those from rod monochromats provides further verification that silent substitution stimuli can effectively isolate rod mediated activity in the light-adapted trichromatic retina. Furthermore, the fact that key features of our 'normal' rod ERG waveform are absent in CSNB subjects who have compromised rod function, but preserved cone function, provides another indicator that this methodology does provide a selective assay of rod photoreceptor function.

In this study we have used three participants diagnosed with *CNGB3*-associated achromatopsia as controls to validate our rod isolation. However, all three participants have demonstrated the existence of an unusually severe deficit of rod-mediated retinal function. As would commonly be expected in cases of complete achromatopsia, electroretinography reveals a complete loss of cone function. However, this deficit is also accompanied by marked abnormalities of the rod mediated dark-adapted ERG responses. Whilst *CNGB3* mutations with moderate rod dysfunction have previously been reported in the literature (Khan et al. 2007; Moskowitz et al. 2009), these three individuals demonstrate particularly poor rod responses for this particular molecular diagnosis, particularly the electronegative appearance of the dark-adapted ERGs to more intense stimuli recorded from ACR 3.

Recent advances in adaptive optics, have made it possible to examine the structure of the both inner and outer segments of the photoreceptor layer in vivo using adaptive optics scanning laser ophthalmoscopy (AOSLO) (Dubra et al. 2011; Scoles et al. 2014). Imaging in patients with rod monochromacy has shown significant loss and disruption of cone photoreceptors, but no real evidence of a decrease in the number of rods (Genead et al. 2011; Langlo et al. 2016). However, changes in rod structure have been observed. Typically, the diameter of a rod photoreceptor in a healthy retina at 10^{o} eccentricity is approximately 2.3μm. Measurements of rod diameter in patients with rod monochromacy in a similar region were shown to be on average 1μm greater (Carroll et al. 2008). This increase in diameter may be as a direct result of increased space in the retina which allows rods to expand following the loss of cone cells (Moskowitz et al. 2009). Increases in rod diameter naturally occur in the ageing retina as the overall number of rod cells is reduced (Werner 2005). It has been suggested that structural changes like these may well result in an alteration of the photo-transduction process and even post-receptoral connections (Moskowitz et al. 2009).

Our more in-depth testing of rod function in these three patients showed the particularly poor sensitivity to at lower luminances. The **S** value is an approximation of a number of phototransduction processes which take place in the rod outer segment. The low **S** value is indicative of subtle abnormality in the outer segment processing. Although it has been reported (Khan et al. 2007), such severe macular atrophy is not a common feature of achromatopsia. The atrophic region in the three participants covers a region

of the retina which contains a high density of rods (Curcio et al. 1990). At the time of assessing the three patients we were unable to determine if there was residual rod function within this region. It is possible that, given the environment, outer segment processing within any functioning rods may have affected sensitivity of the response somewhat however this is not likely.

Agreement between the ISCEV measure of rod function and the 8Hz isolated rod isolated stimulus has been demonstrated in correlation plots (Figure 5.13a). From a clinical aspect it is important that the stimulus can elicit a waveform which when measured can selectively distinguish between pathology and a healthy retina. The standard ISCEV clinical assessment provides a thorough measure of retinal function and can not only distinguish retinal disease but also on occasion provide a diagnosis based on the waveform morphology alone (Miyake et al. 1986; Vincent et al. 2013). However, a disadvantage is the prolonged dark adaptation periods needed to assess rod function, can be problematic when testing in a paediatric population. Although the characterisation of the rod isolated response elicited using the silent substitution is in its infancy, it appears to be able to provide a quick measure (2 mins) of rod function without dark adapting the patient.

5.10. Conclusion

Following on from the previous chapter, we have shown how the normal rod response generated by silent substitution stimuli is influenced by retinal pathology that differentially affects rod and cone function in humans. We propose that this methodology will prove to be useful in the respect that it provides an opportunity for the examination of rod system function in both the normal and abnormal retina.

Chapter 6

Investigation into the use of cone isolated stimuli using Silent Substitution to provide an objective measure of colour vision in the human Eye.

6.1. General Introduction

The processing of luminance and chromatic information takes place across three parallel channels in the retina. One is dedicated to luminance (L+M) processing, whilst the other two; the L-M and S/(L+M) cone-opponent channels underpin red-green and blue-yellow chromatic processing (see sections 1.6 and 1.7 for a more detailed explanation). Separation of these pathways is well maintained through to the different laminae of the LGN (De Valois et al. 1958; Hubel and Wiesel 1962; Lee et al. 1987; Dacey and Lee 1994), but the segregation becomes less distinct within higher cortical visual areas (Maunsell and Gibson 1992).

At the retinal level, the existence of these parallel chromatic and luminance channels has been demonstrated using steady-state flicker ERGs (Kremers and Link 2008; Kremers et al. 2010; Parry et al. 2012). What's more, careful selection of stimulus frequency makes it possible to separate these contributions (Parry et al. 2012). Stimuli of intermediate temporal frequency (5-12Hz), elicit ERGs with features consistent with the cone-opponent, parvocellular pathway. By comparison, ERGs produced by higher temporal frequency stimuli (>30Hz), possess properties more representative of luminance processing in the magnocellular pathway (Kremers and Link 2008;

Kremers et al. 2010). The use of cone isolated ERGs has introduced a new level of precision, allowing the independent assessment of photoreceptoral and post receptoral contributions from L, M and S cones. This also has made it possible to demonstrate evidence of cone opponent behaviour in the transient ERG. Recently, it was demonstrated in trichromats that L-cone excitation increment elicits an L ON response and an L-cone decrement elicits an OFF response. Conversely, an M-cone increment produces an OFF response and an M-cone decrement produces and ON response (McKeefry et al. 2014). This waveform polarity reversal was found to be absent in dichromats, suggesting that cone-opponent behaviour evident in the trichromat, is no longer present. In addition to this, evidence now suggests that this reversal may go beyond retinal levels as far as cortical regions (Parry et al. 2016). This is supported by psychophysical results which show that M cone increments are perceived as a brightness decrements (Parry et al. 2016). Therefore, it is conceivable that evidence of this waveform reversal is present in the cone isolated VEP and may provide information on chromatic processing at a cortical level.

In this chapter, we plan to utilise the ability of these stimuli for clinical purposes, specifically assessing their value in objective colour vision assessment. This is separated into three different experiments. In the first two experiments, we use cone isolated transient stimuli to characterise the changes in L and M cone ERG (experiment 1) and VEP (experiment 2) morphology in trichromats and dichromats, with the aim of relating specific morphology changes to a specific colour vision deficiency. In the third

experiment, we focus on characterising the morphology of the S cone ERG in trichromats and comparing the response to S cone ERGs recorded from individuals with blue cone monochromacy and enhanced S cone syndrome.

6.2. L and M cone ERG Morphology in Trichromats and Dichromats

6.2.1. Introduction

In experiment one we investigate whether cone specific ERGs generated by transient stimulation can provide an objective measure of colour vision. Previous studies in which ERGs have been used to objectively assess colour vision have either used steady-state flicker stimuli (Jacobs et al. 1996; Crognale et al. 1998; Jacobs et al. 1998) or chromatic adaptation (Norren and Padmos 1973; Gouras and MacKay 1990; Yamamoto et al. 1996; Drasdo et al. 2001). However, these methods tend to be either too time consuming to perform in a clinical setting or incapable of assessing L and M cone deficiencies separately because of high spectral overlap. The silent substitution technique provides us with the unique ability to be able to selectively stimulate each cone type independently and thus record separate L- and M-cone ERGs. The transient ON/OFF presentation also has the advantage of producing a waveform whereby the individual components can be measured, allowing analysis of both receptoral and post-receptoral contributions to both the onset and offset states (Kuchenbecker et al. 2014).

Of the limited number of studies which have adopted the silent substitution method, most have focused on S cone isolation or chosen to not to separate

the L and M response thus recording a combined L and M cone ERG (Drasdo et al. 2001; Chiti et al. 2003; North et al. 2010; Kuchenbecker et al. 2014). However, cone isolated transient stimuli have shown that L and M cone ERGs have different morphologies which are not only dependent on retinal eccentricity (Tsai et al. 2016) but also on receptoral input (McKeefry et al. 2014). The aim of this experiment is to better characterise the normal L and M cone ERG responses as well as the responses in various colour vision deficiencies. By doing so we hope to identify clear morphological waveform features which will allow discrimination between groups. To that end, the aim was to test a larger cohort of trichromats as well as colour vison deficient observers which includes anomalous trichromats as well as dichromats.

6.3. Methods

6.3.1. Stimuli

Details of the stimulator and the construction of the stimulus are described fully in sections 2.2 and 2.4, respectively. Full-field square-wave pulse temporal profile stimuli were presented using a ColorDome (Diagnosys LLC, Lowell, MA, USA) four primary ganzfeld stimulator with peak wavelengths (+/- half-bandwidth at half height) blue (460 ±15 nm), green (514 ±20 nm), amber (590 ±8 nm) and red (635 ±10 nm) LEDs. The stimuli used in these experiments constituted triple silent substitutions whereby responses from either L or M cone photoreceptors were obtained in isolation using temporal modulations of colour and luminance of the four LEDs (Estévez and Spekreuse 1974; Estevez and Spekreijse 1982; Shapiro et al. 1996)

Stimulus contrast was defined as the Michelson contrast (equation 6.1) of rod or cone excitation and was set at 0.25 for all stimuli.

$$\frac{Lmax - Lmin}{Lmax + Lmin} \tag{6.1}$$

The luminances of the LEDs were modulated with square-wave temporal profiles to generate stimuli that produced only excitation of either L or M cones.

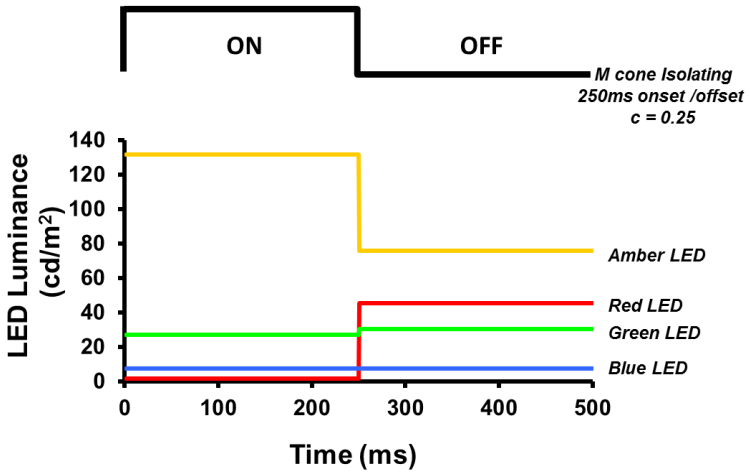

Figure 6.1. Luminance variation of the 4 LEDs over the 500ms recording epoch required to create the 250ms square-wave onset/offset. The example shown is that of an M cone isolating stimulus.

L and M cone isolated ERG responses were recorded using a transient square wave stimulus. A 250 ms onset duration was followed by a 250 ms offset period (Figure 6.1). The onset comprised either an L- or M-cone cone excitation increment with similar excitation decrement at offset. All modulations were based on the same ratio of red:green:blue:amber LED

luminances; in the unmodulated state, this ratio was 34:3:1:36 (see Figure 6.1). The retinal illuminance produced by the stimuli was 8000Td.

6.3.2. ERG Recording

ERGs were recorded from the right eye using a silver/nylon corneal fibre electrode (Dept. of Physics and Clinical Engineering, Royal Liverpool University Hospital, UK) referenced to a 9mm Ag/AgCl electrode (Biosense Medical, Chelmsford, UK) on the outer canthus; a similar electrode was affixed to the forehead to serve as ground. Impedance was maintained below 5 kΩ. Signals were recorded using the Espion E^2 system (Diagnosys LLC, Lowell, MA, USA) which amplified and filtered (bandwidth = 1 to 300 Hz) the ERGs and digitised them at a rate of 1000Hz. typically, 200 trials were averaged. Participants viewed the stimuli monocularly with a dilated pupil (1% Tropicamide). The fellow eye of the participant was patched. Fixation was maintained on a central point which subtended approximately 0.5^0.

6.3.3. Transient Analysis

Implicit time and amplitude of all three waveform components shown in figure 6.2 were measured. The implicit time of the a-wave was measured from stimulus onset at time zero to the peak of the initial negative deflection. The amplitude measurement of the a-wave was taken as the vertical distance from the peak of the first negative trough to baseline. The implicit time of the b-wave was measured from stimulus onset to the first positive peak. The

amplitude measurement of the b-wave was taken as the vertical distance from the trough of the a-wave to the peak of the first positive peak. The implicit time of the d-wave was measured from the start of stimulus offset (250ms) to the peak of the first peak after the offset response. The amplitude measurement of the d-wave was take as the vertical distance from the base of the d-wave to the peak.

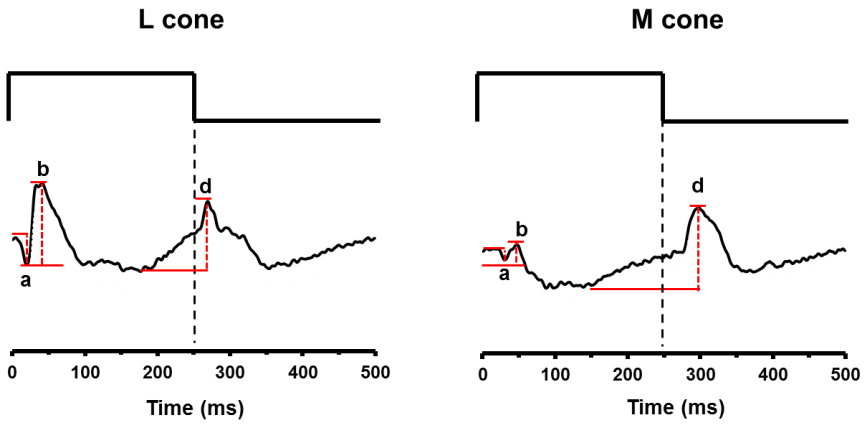

Figure 6.2. ERGs elicited using L (left) and M (right) cone stimulation with component names. Red lines denote the method used to measure amplitude and implicit time.

6.3.4. Participants

A total of 15 colour normal trichromats (5 males, 10 females; mean age: 33 yrs, age range: 20-60 yrs) and 12 participants with a colour vision deficiency; including 9 dichromats (6 deuteranopes, 3 protanopes) and 3 anomalous trichromats (2 deuteranomalous, 1 protanomalous) all males; mean age 32yrs, age range:18-56 yrs. took part in this study. Colour vision in all subjects was assessed using CAD colour test from City University.

6.4. Results

6.4.1. Transient L and M cone ERGs in the trichromat

Figure 6.3 shows the group averaged (top) and individual responses from the colour normal group (n=15).

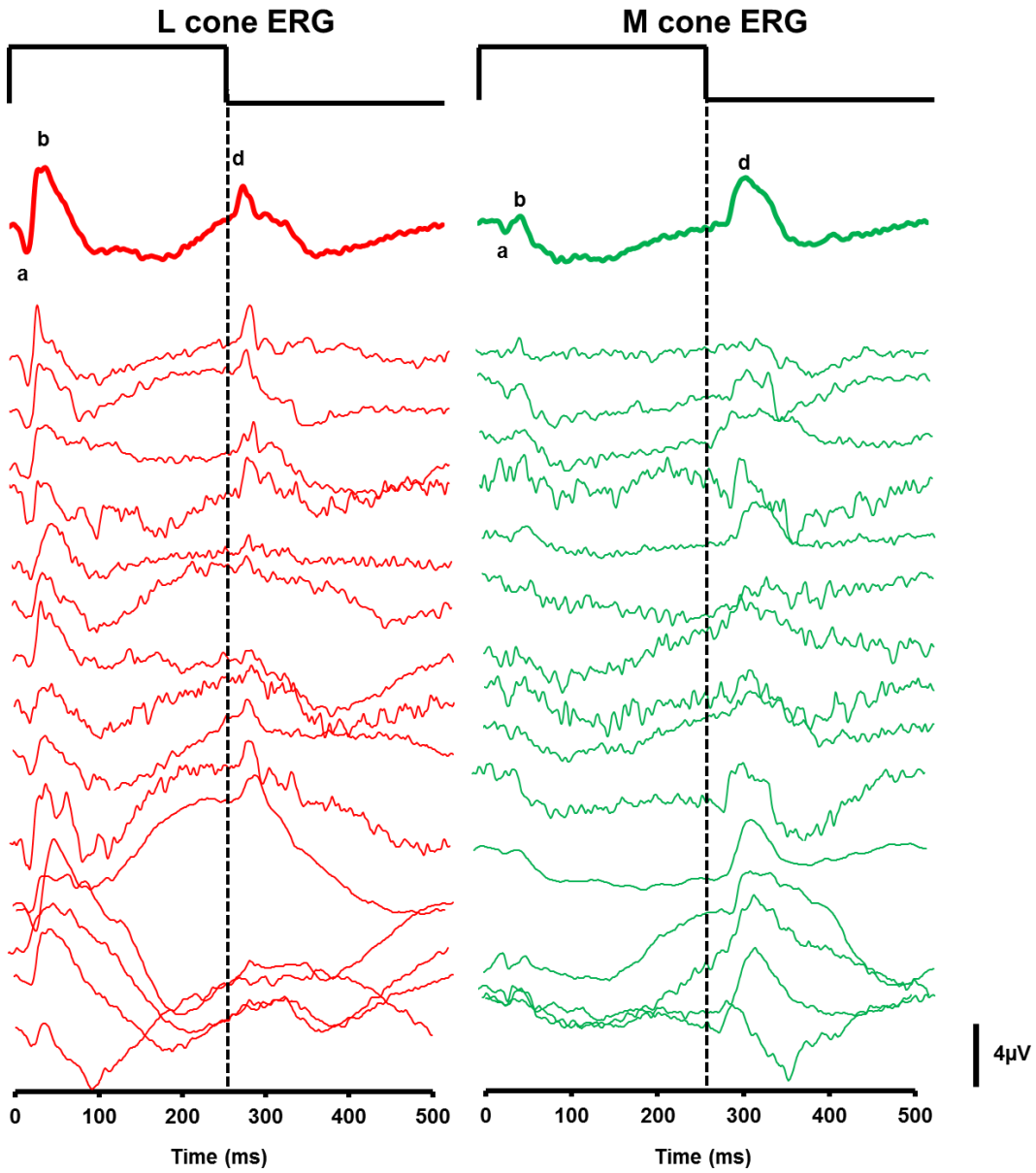

Figure 6.3. L- and M-cone ERGs elicited from the colour normal participants. The group (n=15) averaged responses are displayed as the thickened traces at the top and the individual responses are the thinner traces below. Responses were recorded using a transient square wave stimulus 250ms onset and offset with luminance of 8000 ph. Td and contrast of 0.25 stimulus. Responses to the L cone stimulus are in red and responses to the M cone stimulus are in green.

Stimulus Type	Waveform Component	Mean Peak Time (ms)	+/- 95% CI	Mean Amplitude (μV)	+/- 95% CI
L cone	a-wave	20.06	21.27/18.86	1.47	1.88/1.06
L cone	b-wave	33.25	33.95/32.55	5.73	6.61/4.79
L cone	d-wave	20.0**	21.70/18.82**	5.84	7.54/4.14
M cone	a-wave	25.31	26.90/23.73	0.90	1.10/0.70
M cone	b-wave	44.56	46.30/43.83	1.54	1.80/1.29
M cone	d-wave	45.25**	48.10/42.40**	2.69	3.89/1.49

****** denotes the time after the offset stimulus

Average noise amplitude was typically <0.5μV

Table 6.1. Amplitude and peak time measurements of L and M cone components

The L-cone ERG morphology is highly repeatable, generally well-formed for all participants and resembles the photopic luminance ERG. We used the conventional component labels for the three main waveform components. The onset response consists of a clearly defined negative trough (a-wave) with a mean implicit time of 20.06 ms (+/- 95% CI = 21.27/18.86 ms) and a mean amplitude of 1.47μV ((+/- 95% CI = 1.88/1.06μV). This is followed by a positive peak (b-wave) with a mean implicit time of 33.25 ms (+/- 95% CI = 33.95/32.55 ms) and a mean amplitude of 5.73 (+/- 95% CI = 6.61/4.79μV). A positive peak (d-wave) is noted at offset stimulus with mean implicit peak time of 20.0 ms (+/- 95% CI = 21.70/18.82 ms) and a mean amplitude of 5.84 (+/- 95% CI = 7.54/4.14μV) after the offset stimulus. The M-cone ERG onset

is smaller and slightly less repeatable for individual participants. This may be down to the fact that there are fewer M cones in comparison (Carroll et al. 2002). It consists of a small negative deflection (a-wave) with a mean implicit peak time of 25.31 ms (+/- 95% CI = 26.9/23.73 ms) and a mean amplitude of 0.9µV ((+/- 95% CI = 1.1/0.7µV), followed by a small positive peak (b-wave) with mean peak implicit time of 44.56 ms (+/- 95% CI = 46.3/43.83 ms) and a mean amplitude of 1.54µV ((+/- 95% CI = 1.8/1.29µV). The offset response (d-wave) consists of a more prominent and relatively broad positive peak with a mean peak implicit time of 45.25 ms (+/- 95% CI = 48.1/42.4 ms) and a mean amplitude of 2.69µV ((+/- 95% CI = 3.89/1.49µV) after the offset response. The 180 degree phase shift that occurs in waveform morphology when using an M cone stimulus compared to an L cone noted by McKeefry et al. (McKeefry et al. 2014) is present, although there are some subtle differences in the more recent data which are dealt with in more detail in the discussion.

6.4.2. Transient L- and M-cone ERGs in deuteranopic deficiencies

Figure 6.4 shows the group averaged (thickened traces) and individual responses from the deutan deficient group, consisting of six deuteranopes (D1-D6) and two deuteranomalous (D7 and D8) participants. The L-cone ERG recorded from both the deuteranope and deuteranomalous groups has a similar morphology and peak timings to that of the L cone response from the colour normal group with a-, b- and d-wave mean peak implicit times of 19ms, 32ms and 19ms (after the offset response) respectively. The

amplitudes were also comparable with the deuteranope mean a-wave amplitude of 1.26µV ((+/- 95% CI = 1.49/1.02µV), b-wave mean amplitude of 4.66µV ((+/- 95% CI = 5.71/3.62µV) and d-wave mean amplitude of 2.64µV ((+/- 95% CI = 3.3/1.9µV). The deuteranomalous group had a mean a-wave amplitude of 1.38µV, b-wave amplitude of 4.9µV and d-wave amplitude 1.9µV.

The M-cone ERG from the deuteranopic group exhibits a variable morphology across participants. The onset and offset components described in figure 6.3 are not present, however, a slow, broad and relatively high amplitude (in comparison to the onset response) waveform is noted for most participants in response to stimulus offset. This is more clearly seen in the averaged response. The individual M cone responses from the deuteranomalous group are similar to those described in the deuteranopes. When their responses are averaged a small positive waveform is noted at stimulus onset. In retrospect, this may also be present in the deuteranope averaged data although slightly more noisy. This feature has been previously described in the normal M cone response in an earlier study (McKeefry et al. 2014) and may be an indication of the incomplete isolation in the M cone stimulus (Kremers and Pangeni 2012; Kommanapalli et al. 2014; Kremers et al. 2014; McKeefry et al. 2014).

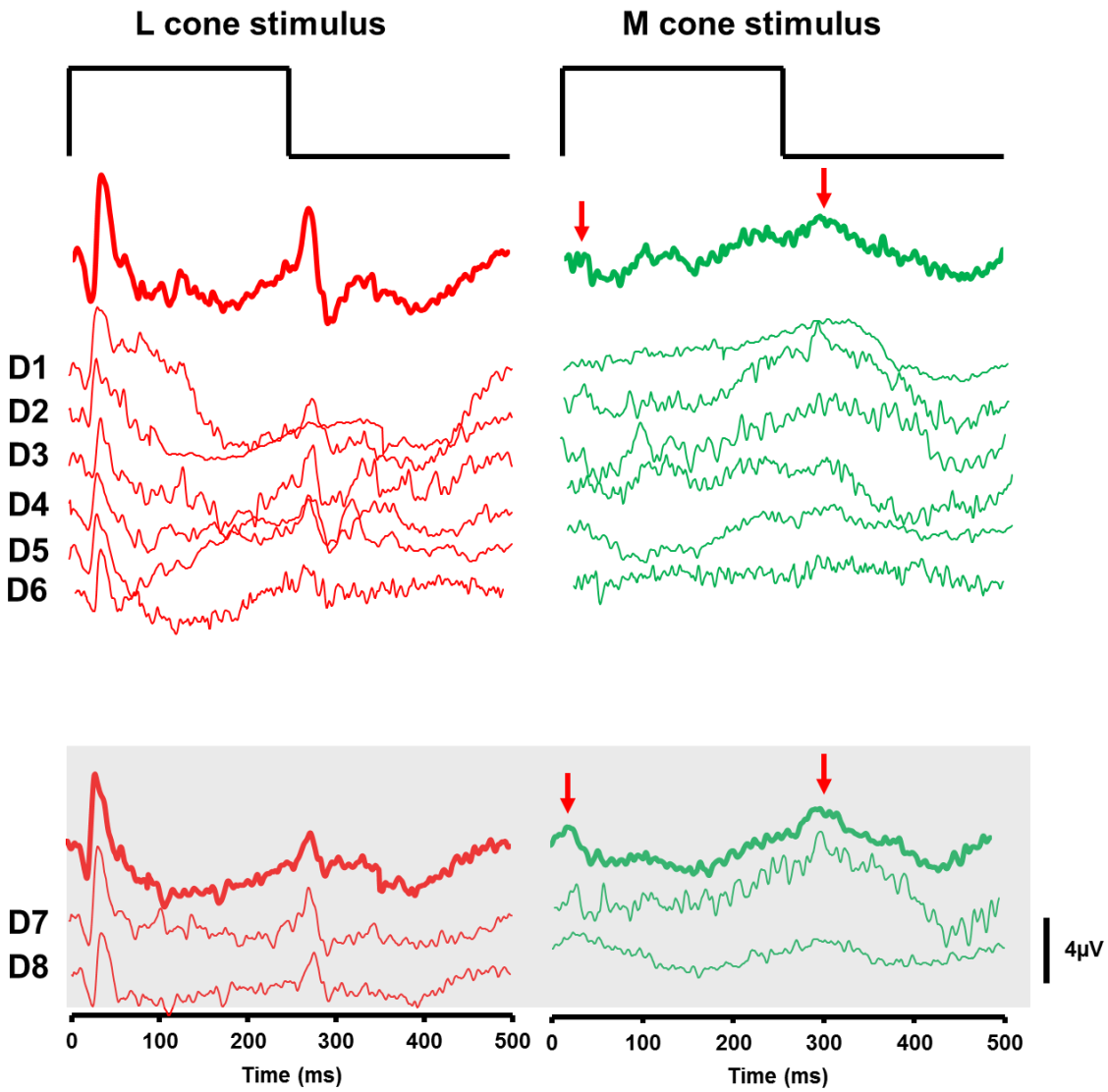

Figure 6.4. ERGs recorded from the deutan deficient group (n=8) with L and M cone isolated stimuli. Individual traces from the deuteranopic participants D1-D6 and deuteranomalous participants D7 and D8 (highlighted in grey) are shown along with the group averages (thickened traces). The red arrows highlight features consistent with both onset and offset components in the M cone ERG.

6.4.3. Transient L- and M-cone ERGs in protan deficiencies

Figure 6.5 shows the group averaged (thickened top trace) and individual responses from the protan group consisting of 3 protanopes (P1-P3) and a single protanomalous participant (P4). Both the protanopes and

protanomalous participant exhibit a minimal ERG response to L cone stimulation. None of the normal components described in figure 6.3 are present. The M cone response in protan subjects albeit with a smaller onset and offset response (mean b-wave amplitude 1.02µV (+/- 95% CI = 1.6/0.40µV), mean d-wave amplitude 2.5µV (+/- 95% CI = 3.12/2.04µV)) resembles the normal L cone ERG. The implicit peak times are also more in-keeping with the normal L cone response. The a-wave has a mean peak implicit time of 21.0 ms (+/- 95% CI = 22.3/19.6 ms). The b-wave has a mean implicit time of 34.0 ms (+/- 95% CI = 37.5/30.4 ms) and the d-wave has a mean implicit time of 20.2 ms (+/- 95% CI = 21.72/18.78 ms) after the offset stimulus.

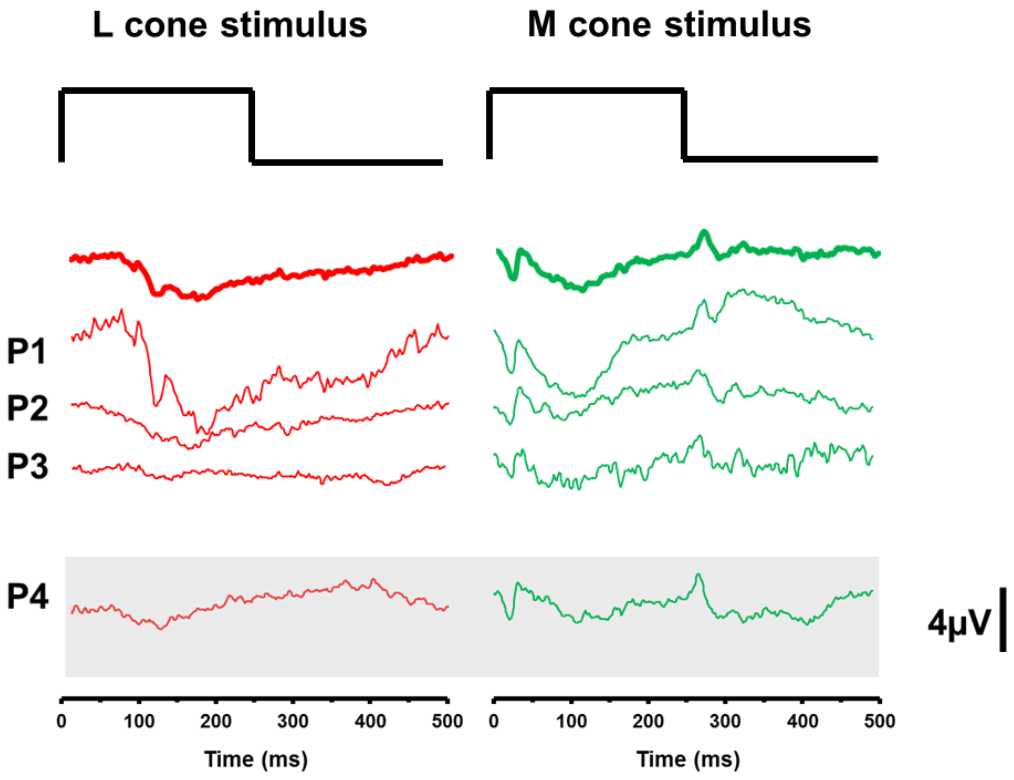

Figure 6.5. ERGs recorded from the protan deficient group (n=4) with L and M cone isolated stimuli. Individual traces from the protanopic participants P1-P3 and protanomalous participant P4 (highlighted in grey) are shown along with the group average (thickened traces) of the protanopic group.

6.5. Discussion

The morphology of the transient L- and M-cone ERGs in normal trichromats has been previously described by our group (McKeefry et al. 2014). In that study, an On/Off transient pulse stimulus was used to investigate the L- and M-cone ERGs using both in-phase and counter-phase L-cone and M-cone pulse stimuli to examine the non-opponent and opponent mechanisms. As previously mentioned, the results from that study suggested that the polarity reversal between L and M waveforms was an indication of normal opponent behaviour. Our findings from the normal trichromat group were similar, displaying the reversal of waveform polarity, and indicating normal post-receptoral chromatic processing. However, we did note some subtle differences. The differences specifically were related to the morphology of the M cone ERG as outlined in figure 6.6.

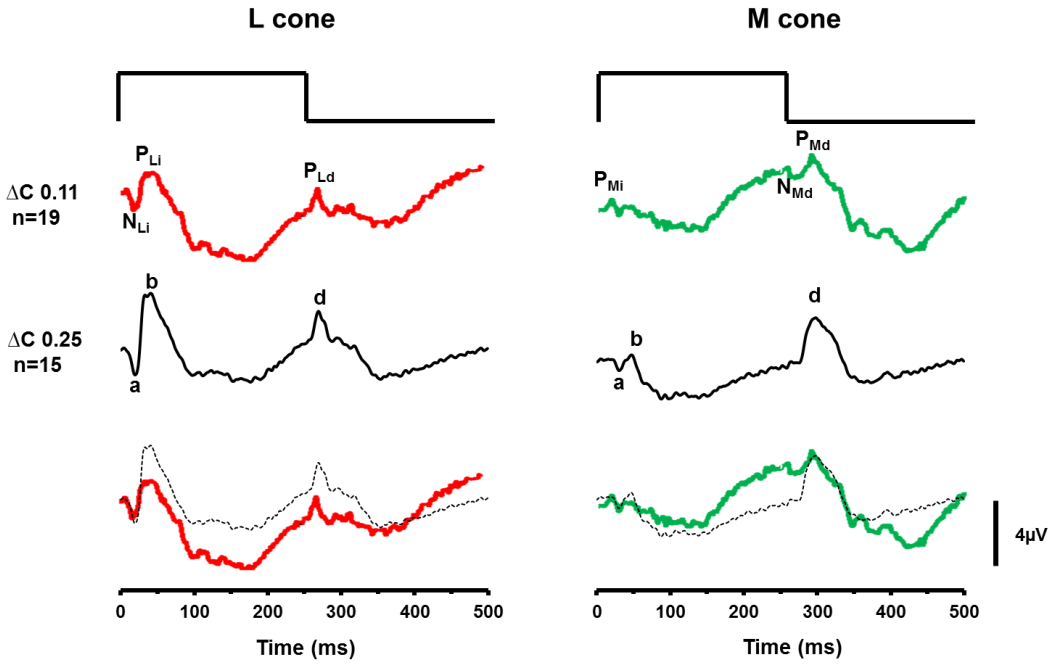

Figure 6.6. A comparison of ERG data recorded using an L and M cone isolated stimuli. The red and green traces are the group averaged responses (ΔC=0.11) taken from a previous study (McKeefry et al. 2014) and the black traces are the group averaged responses (ΔC=0.25) from the current study. The stimulus luminance for the earlier study was 12000 ph. Td versus 8000 ph.Td for the current study.

The group average of the L and M cone responses from the earlier study (McKeefry et al. 2014) (red and green respectively), along with the group average from this study (black) are displayed in figure 6.6. The earlier study used waveform component nomenclature which we have not adopted, instead choosing to opt for conventional nomenclature. The previous waveform component name is dependent on whether the waveform was positive or negative (**P** or **N**), L cone or M cone (**L** or **M**) and whether it was an excitation increment or decrement in the stimulus (**i** or **d**). In the earlier study, a small positivity ($\mathbf{P_{Mi)}}$ early in the M cone ERG was specified as the main feature of the onset response. From our M cone data (black) it now

appears that this small positivity is perhaps just the beginning of a negative deflection denoted which we have termed the a-wave. The small positive deflection, termed the b-wave, immediately following a-wave, is also not present in onset response of the earlier study. Furthermore, our M cone data does not appear to exhibit the small negative deflection immediately preceding the d-wave termed $\mathbf{N_{Md}}$ in the earlier study. Reasons for theses subtle differences may lie in the different stimulus parameters in both studies. The earlier data was recorded using a cone contrast of 0.11 and luminance of 12000 ph.Td, whereas the more recent data used a cone contrast of 0.25 but lower luminance of 8000 ph.Td. Both stimuli also differ in chromaticity. It is likely that the higher cone contrast provides a better signal to noise ratio, making it easier to distinguish smaller waveform components.

The averaged L- and M-cone data from the trichromats, protanopes and deuteranopes are shown in figure 6.7. As described previously, the reversal in on/off polarity was absent in the dichromatic participants. Based on differences in the L and M cone ERG waveform morphology, accurate discrimination between each group is possible. Both normal responses elicited by L- and M-cone stimulation have been described.

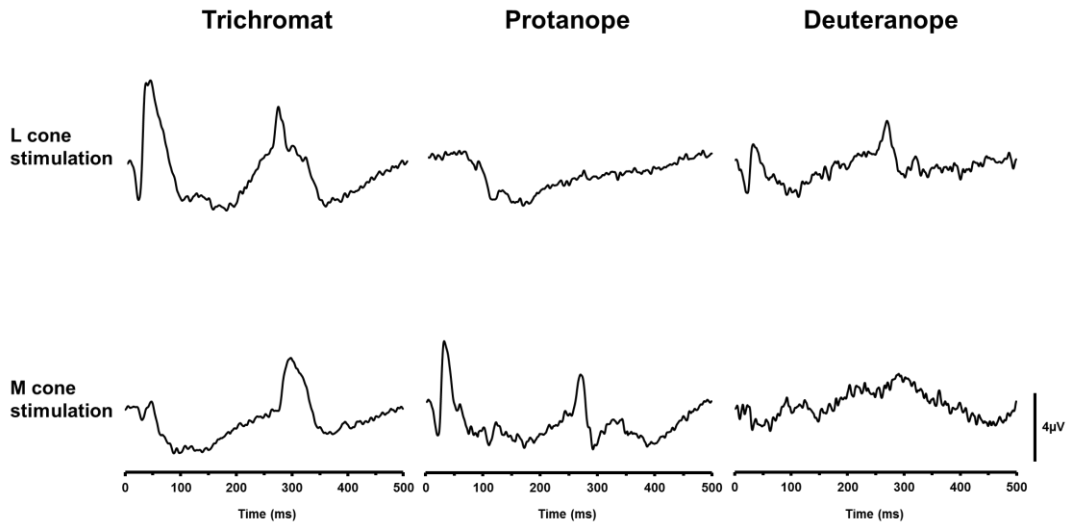

Figure 6.7. Averaged ERG data recorded using an L and M cone isolated stimuli from the trichromat, protanope and deuteranope groups.

From the data, an individual with an absent L-cone response and an M-cone ERG with a morphology similar to that of our normal L cone ERG would indicate a protan deficiency. Whereas, a deutan deficiency would be characterised by a normal L-cone ERG and an absent or very much reduced M cone ERG. As highlighted in the results, M-cone stimulation appears to elicit a residual ERG in some deuteranopic individuals. An advantage of using a transient stimulus is that the waveform components can be examined more closely and compared to the normal responses for similarities. Their morphology can sometimes indicate if input from allegedly silenced photoreceptors are present. The most notable feature of the averaged M cone response from the deutan group is the remnants of a broad, slow positivity at stimulus offset. This is not unlike the less noisy response from the deuteranomalous group (n=2) shown in figure 6.4. A second, more subtle feature, also present in the deuteranomalous group, is the early positive waveform at stimulus onset. This is highlighted in figure 6.4 and resembles

the **P_{Mi}** component from the early study (Figure 6.6). A remnant M cone ERG is not unexpected in the deuteranomalous group as it is unlikely that the hybrid M-cone pigment, with its different spectral peak, will be completely silenced (Huchzermeyer and Kremers 2016). Therefore, rather than an imperfect isolation of the M cone stimulus partially stimulating the L cones, it may be an actual M cone ERG from one or more participants. Although none of our participants were diagnosed as deuteranopes on the basis of molecular genetics, all had excessively high thresholds on the deutan axis. Alternatively, it is possible that the partial stimulation of a small population of L cones might yield a similar morphology to the M cone ERG. A more detailed overview of the factors which may affect M cone isolation are discussed in the general discussion.

6.6. Conclusion

Overall, cone isolated ERGs elicited by transient stimulation provided a relatively good objective measure of colour vision, allowing discrimination, based on waveform morphology, between trichromats and dichromats. Despite this, separation of anomalous trichromats from dichromats was not possible. The unknown spectral peak of the anomalous photoreceptor in these individuals has the potential to lead to false negative results especially among deuteranomalous individuals, and is a limitation of this method. One measure to combat this might be to create alternative sets of cone fundamentals with different spectral peaks which might provide better isolation, although this would just add to the assessment time.

6.7. L and M cone VEP morphology in trichromats and dichromats.

6.7.1. Introduction

The visual evoked potential (VEP) is the electrical response recorded from the scalp over the visual cortex following a visual stimulus. The VEP is dominated by input from the central 10 degrees of the retina with little electrical input from the periphery, making it a good indicator of central retinal function (Campbell and Kulikowski 1972; Rabin et al. 1994). The cortical projections from the fovea are represented by a relatively large region of cortex compared to the peripheral retina (Di Russo et al. 2002). These projections are located at the outer central region of the calcarine sulcus, whereas projections from the peripheral retina are located in the folds of the sulcus and further away from the scalp (Di Russo et al. 2002). Like the ERG, the VEP results from contributions from both luminance and chromatic information processed via the magnocellular and parvocellular pathways, respectively. Similarly, careful stimulus selection is required to selectively record responses from these pathways.

The use of VEPs elicited by chromatic stimuli in the assessment of parvocellular function has been well documented (Murray et al. 1987; Berninger et al. 1989; Kulikowski and Carden 1989; Crognale et al. 1993). Spatially sinusoidal gratings have generally been used as the stimulus of choice (Murray et al. 1987) as other stimuli such as checkerboard patterns, contain hard edges which have been shown to introduce luminance

contamination (Carden et al. 1985). Using a sinusoidal chromatic grating typically elicits a negative deflection at 130-140ms which becomes positive using achromatic stimulation (Kulikowski and Carden 1989). Other methods involve the use of chromatic gratings which use specifically chosen chromaticities which effectively result in a double silent substitutions, isolating individual cone responses (Crognale et al. 1993). This technique has been reported to effectively diagnose both dichromats and anomalous trichromats (Crognale et al. 1993). A similar method was used by the Kelly and co-workers in children with both cone dystrophy and cone dysfunction syndromes (Kelly et al. 2003). To investigate M- and L-cones in early infancy, Knoblauch et al. recorded a luminance series of isolated L, M and rod responses using a custom built system incorporating three primaries (Bieber et al. 1997; Knoblauch et al. 1998). This projected a 6 degree light stimulus onto a screen, and used silent substitution to isolate individual photoreceptor population responses. The exchange of homogenous light stimuli overcomes complications encountered with patterned stimuli (Givre et al. 1995) and the responses from dichromats were used to validate the level of isolation. Their results showed no L-cone VEP response when testing protanopes and a very small residual M-cone VEP when testing deuteranopes. These validation results are in agreement with more recent studies (Kremers et al. 1999; Kremers and Pangeni 2012; Kommanapalli et al. 2014; Kremers et al. 2014). We have opted for a similar technique used by Knoblauch et al, modulating two complex homogenous light stimuli, full-field on a ganzfeld stimulator. Because our stimulator has four primaries we can utilise the triple silent substitution method (Shapiro et al. 1996).

The aim of this experiment was to characterise the normal L- and M-cone VEP responses as well as the responses in various colour vision deficiencies. By doing so we hoped to identify clear morphological waveform features which will allow discrimination between groups.

6.8. Methods

6.8.1. Stimuli

The stimuli used has been previously described in experiment 1. The stimulus profile is the same as shown in figure 6.1

6.8.2. VEP Recording

VEPs were recorded from a single 9mm Ag/AgCl electrode positioned at Oz and referenced to a 9mm Ag/AgCl electrode at Fz using the International 10-20 electrode placement system (Klem et al. 1999). The VEP was recorded concurrently with the transient ERG from experiment 1. Typically, 200 trials were averaged. Participants viewed the stimuli monocularly with a dilated pupil (1% Tropicamide). The fellow eye of the participant was patched. Fixation was maintained on a central point which subtended approximately 0.5^0.

6.8.3. Participants

The subjects participating in this experiment have been previously described in experiment 1.

6.9. Results

6.9.1. Cone isolated Transient VEPs

Figure 6.8(a) (lower panel) shows the group averaged VEP produced by the L cone isolating stimulus, exhibiting a positive dual-peaked waveform at stimulus onset and a positive dual-peaked waveform at stimulus offset. Compared to the offset, the amplitude of the onset response is greater for all participants. For descriptive purposes, we termed the two most consistent peaks of the onset response L^{P1} and L^{P2} and the two most consistent peaks of the offset response L^{P3} and L^{P4}, 'L' denoting the cone type being stimulated (changed to 'M' when stimulating the M cones) and superscript ^{pn} denoting the peak number. L^{P1} has a mean implicit time of 97.6 ms (± 95% CI 3.36 ms) and L^{P2} has a mean peak implicit time of 143.67 ms (±95% CI = 5.14 ms). L^{P3} has a mean implicit time of 103 ms (±95% CI = 4.57 ms) after the offset stimulus. L^{P4} exhibited a mean implicit time of 146.8 ms (±95% CI = 4.57 ms) after the offset stimulus.

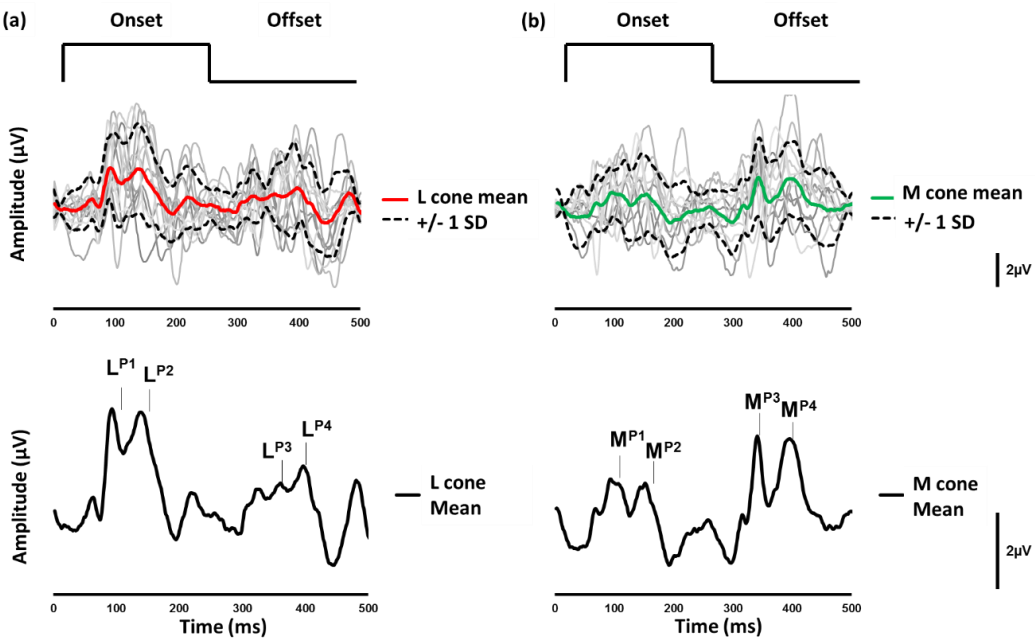

Figure 6.8. (a) (Upper graph) Individual (grey lines) and group averaged (thick red line) L cone isolated VEPs elicited from 15 colour normal participants. The dashed black lines represent the ± 1 S.D. from the mean. (Lower graph) shows the L cone VEP group averaged response on a larger scale with waveform labels. 6.8 b (upper graph) shows the individual (grey lines) and group averaged (thick green line) M0 cone isolated VEPs elicited from 15 colour normal participants. The dashed black lines represent the ± 1 S.D. from the mean. (Lower graph) shows the M cone VEP group averaged response on a larger scale with waveform labels. Both L and M isolated VEPs were elicited by a transient square wave stimulus 250ms onset and offset with luminance of 8000 ph. Td and contrast of 0.25 stimulus.

6.9.2. M-cone VEP

Figure 6.8(b) (lower panel) shows the group averaged VEP elicited by the M cone isolating stimulus. The two peaks of the onset response M^{P1} and M^{P2} have a mean implicit peak time of 96 ms and 156 ms respectively. These values were obtained by measuring the peaks of the averaged response. Although M^{P1} and M^{P2} are clearly identifiable in the averaged response, they were not always present in the individual data. Because of this, peak time confidence intervals could not be calculated. Similar to the M cone ERG, the

VEP exhibits a larger amplitude offset response compared to the onset. The offset response is a dual peaked waveform which is generally consistent across participants. M^{P3} has a mean implicit time of 98 ms (±95% CI = 7.77 ms) after the offset stimulus. M^{P4} exhibited a mean implicit time of 147.7 ms (±95% CI = 6.23 ms) after the offset stimulus. An example of the variability of peak components in the L and M cone VEP onset and offset is shown in figure 6.9.

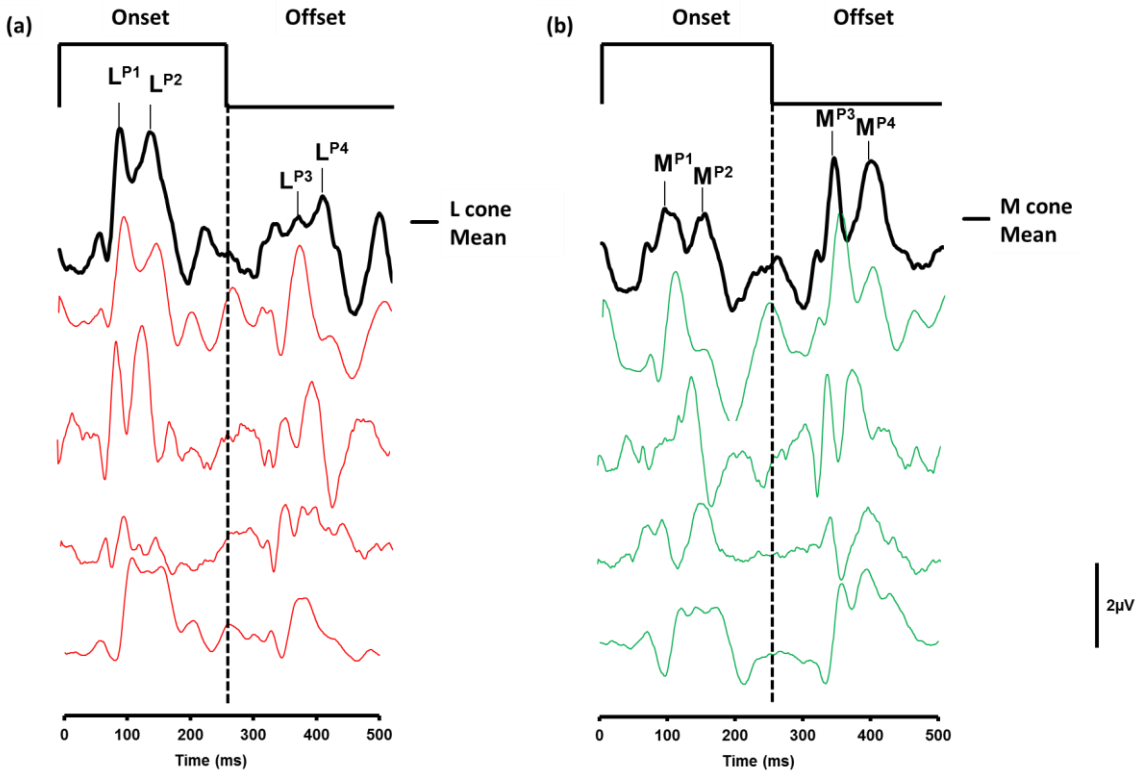

Figure 6.9. (a) Group averaged (thick black line) and four individual L cone VEPs traces (red lines) from the colour normal group. (b) Shows the group averaged (thick black line) and four individual M cone VEPs traces (green lines) from the colour normal group. The dashed black line indicates the border between the onset and the offset response.

6.9.3. L-cone VEP in colour deficiency

Figure 6.10 shows the individual and averaged (thickened traces) L cone VEP responses obtained from three protanopic (P1-P3) and one protanomalous (P4) participants. The L-cone VEP response for the three protanopes shows no clear onset or offset component as described in figure 6.8. Instead, they are dominated by background cortical activity (alpha). A possible explanation for this may be the inability of the participant to detect the stimulus modulation as a result of lacking L cones. Therefore the stimulus is effectively silent for the remaining photoreceptors, leading to no evoked potential.

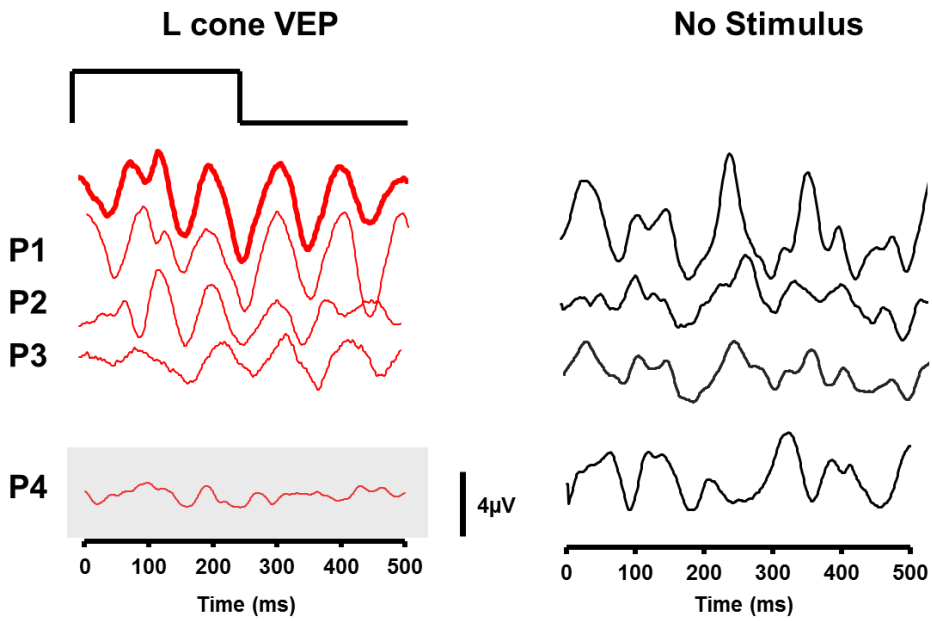

Figure 6.10. VEPs recorded from the protan deficient group (n=4) with L cone isolated stimuli. Individual traces from the protanope participants P1-P3 and protanomalous participant P4 (highlighted in grey) are shown along with the group average (thickened traces) of the protanope group. VEP responses recorded to no stimulus are shown (right) as a measure of background noise.

The L-cone VEP response from the protanomalous participant was not dominated by background cortical activity but was attenuated. The lack of alpha may indicate that some degree of stimulation is being detected, possibly by the M cone or variant L cone system.

6.9.4. M-Cone VEP in colour deficiency

Individual and averaged (thickened traces) M cone VEP waveforms of six deuteranopic (D1-D6) and two deuteranomalous (highlighted in grey) participants are displayed in figure 6.11. The averaged M cone and L cone VEP are shown in figure 6.12 from protan and deutan participants respectively.

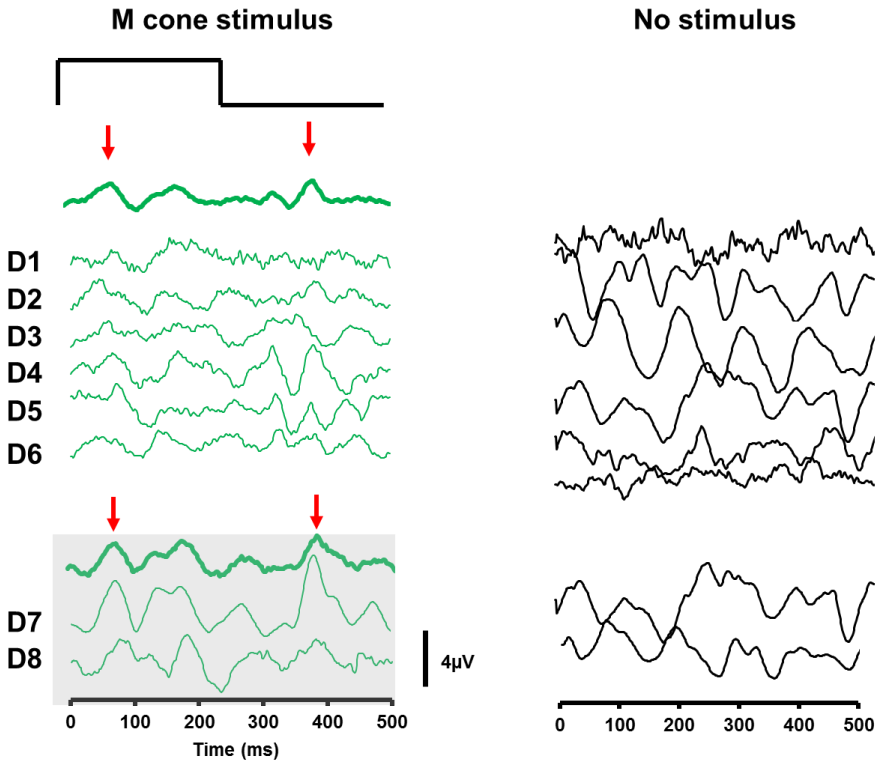

Figure 6.11. (Left) VEPs recorded from the deutan deficient group (n=8) with M cone isolated stimuli. Individual traces from the deuteranopic participants D1-D6 and deuteranomalous participants D7 and D8 (highlighted in grey) are shown along with the group averages (thickened traces). The red arrows highlight possible features consistent with both onset and offset components in the M cone VEP. VEP responses recorded to no stimulus are shown (right) as a measure of background noise.

Overall, the individual waveforms from both the deuteranopic and deuteranomalous groups are low amplitude, noisy with evidence of EEG alpha contamination and a variable morphology. The averaged M-cone VEP data group is low amplitude and exhibits none of the components previously described in figure 6.8. However, two small (~1-2 μV) positive deflections denoted by red arrows in the deuteranope and deuteranomalous slightly stand out. Given the fact that the ERG data exhibited remnants of an M cone ERG it is plausible that there may be a cortical component, although the

timings of the peaks (77ms and 133ms after the offset stimulus) are not within the range of either onset or offset peak.

6.10. Discussion

VEPs were recorded from the Oz electrode position in all participants using L- and M-cone isolating (triple) silent substitution stimuli. Figure 6.12 shows the averaged VEP data from all three groups elicited by L- and M-cone stimuli. From this experiment, we showed that two different complex VEP waveforms could be elicited by L- and M-cone stimuli from trichromats. Two prominent peaks were elicited at both onset and offset in all participants by the L-cone stimulus and in most participants by the M-cone stimulus, however the onset peaks elicited by the M cone stimulus tended to be more variable as shown in figure 6.9. The morphology of the chromatic VEP varies widely depending on the stimulus used to elicit the response (Murray et al. 1987; Rabin et al. 1994; Givre et al. 1995; Klistorner et al. 1998). Because there is no normal response for chromatic VEPs elicited using a triple silent substitution in the literature, it is difficult to be sure that what we have recorded is representative of chromatic processing. One possible indication, is that the response does bear tentative similarities with a previous study which used broadly similar methods (Paulus et al. 1986). A dual-peaked response was elicited by Paulus et al. (1986) using unstructured stimuli and double silent substitution to isolate the L and M cone system independently. The authors highlight the N87 component as possibly being related to parvocellular processing. From the averaged L and M cone VEP response in figure 6.8, a small negative component preceding the L^{P1} and M^{P1} marker is visible, exhibiting implicit times of 84ms and 93ms respectively. As this

feature was not immediately obvious it was not described in the results, however, upon close examination it does appear to be present.

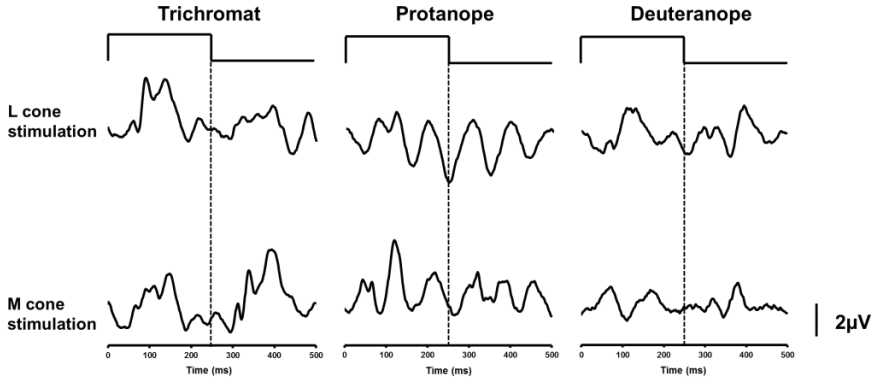

Figure 6.12. Group averaged VEP data recorded using an L and M cone isolated stimuli from the trichromat, protanope and deuteranope groups.

In that same study the authors also used red and green luminance stimuli which elicited luminance VEPs with a single positive component (P120). This also bears a qualitative resemblance with the waveform elicited by L-cone response in the deuteranope and the M cone response in the protanope groups.

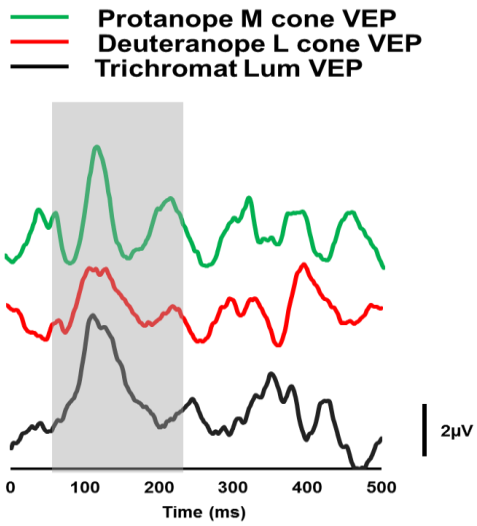

Figure 6.13. Group averaged VEPs from the protanopes elicited by an M cone stimulus (green trace), the response from deuteranopes elicited by an L cone stimulus (red trace) and the VEP recorded from the trichromats elicited by a non-isolated luminance on-off stimulus (black trace). The portion of the onset response being discussed has been highlighted in grey.

Figure 6.13 shows the comparison between the deuteranopic L-cone and the protanopic M-cone VEP. For comparative reasons, a non-isolated luminance VEP recorded from the colour normal trichromats (using the same contrast and stimulus luminance), has been also been included in this figure. The single peaked waveforms at stimulus onset bear considerable resemblance to the non-isolated luminance VEP. This may indicate that, similar to our ERG results, cone-opponency is disrupted by the missing cone class leading to a response more in-keeping with the luminance response.

6.11 Conclusion

VEP responses recorded from the trichromat group using cone isolated VEPs, did exhibit different features depending on whether it was an L or M

cone isolating stimulus. These features were very different or absent in recordings from dichromats. Although not as clear as the ERGs, they did allow for some discrimination between groups. We did however find that individual responses were more variable than cone isolated ERGs, particularly when using M cone stimuli. This could possibly lead to spurious results in a clinical situation. There are a few changes we could make for future testing to improve this, 1. For comparative purposes we used a contrast of 0.25 which may have contributed to a poor signal to noise ratio in some cases. Therefore, some of the variability may be reduced by using higher contrast stimuli. 2. Given the variation of the M cone population at different eccentricities (Kuchenbecker et al. 2008) we might have been better off to use a more spatially restricted stimulus (Jacob et al. 2015; Huchzermeyer and Kremers 2016; Tsai et al. 2016). In doing so we might have avoided non-linearities which possibly affected both isolation and M cone amplitudes. Overall cone isolated VEPs did not provide any extra information to objectively assess colour vision compared to cone isolated ERGs. They do however have the advantage of being less invasive than the ERG as corneal electrodes can be avoided. This is something that is of great benefit when testing in the paediatric population.

6.12. Characterising the S-cone ERG using triple silent substitution.

6.12.1 Introduction

The S-cone system is unique and possesses many different features to the L and M cone systems (Calkins 2001). One of the key features is that it has been shown to be more susceptible in several congenital and acquired retinal and systemic pathologies (Hood et al. 1984; Greenstein et al. 1989). This has made it an attractive system to investigate with multiple studies demonstrating selective or more severe changes in the S cone ERG compared to the L and M cone ERG in some forms of RP (Swanson et al. 1993), type 1 and type 2 diabetes (Yamamoto et al. 1996; Mortlock et al. 2005), glaucoma (Drasdo et al. 2001; Maeda et al. 2001), ocular hypertension (Aldebasi et al. 2004; North et al. 2010) and congenital tritan defects (Van Norren and Went 1981)). However, the task of isolating the S cone ERG is not an easy one and is hampered not only by the paucity of S cones within the human retina (Curcio et al. 1990) but also by the effects on short wavelength light of pre-retinal absorption by the ocular media and macular pigment (Bone et al. 1992; Shinomori and Werner 2012). Initial attempts to selectively isolate S-cone ERGs by Gouras and colleagues involved the use of a short wavelength incremental flash stimulus superimposed on a high luminance broadband background to supress L cone, M cones and rods (Gouras 1970; Norren and Padmos 1973; Gouras and MacKay 1990; Gouras et al. 1993). Sawusch et al. used a double silent substitution technique, modulating two LEDs to silence the M-cones and stimulate S cones, in conjunction with a sufficiently high luminance long

wavelength LED to supress L cones and rod responses (Sawusch et al. 1987). Simonsen et al. modified the Gouras technique by using a more selective narrow band (orange) background stimulus to supress L- and M-cone activity (Simonsen and Rosenberg 1995). Relative success was achieved by all groups in recording the S cone ERG, but overall, they failed to isolate the S-cone response completely. Studies following on from these earlier investigations used similar methods with slightly refined stimulus parameters to achieve better isolation with some success (Arden et al. 1999; Drasdo et al. 2001; Scholl and Kremers 2001; Marmor et al. 2004; Kremers et al. 2009; Kuchenbecker et al. 2014). Although two of these studies used double silent substitution and arguably sufficiently high luminances to suppress the rod (Scholl and Kremers 2001; Kuchenbecker et al. 2014), none have recorded the fully isolated S-cone ERG using triple silent substitution. The aim of the experiments described in this section is to characterise the normal S-cone ERG using triple silent substitution. To do so, S-cone ERGs are recorded from a group of normal trichromats. Comparisons are then made with S-cone ERGs recorded from a group missing either L or M cones (protanopes and deuteranopes), one individual with just S-cones and rods (blue cone monochromats) and in individual with mostly S-cones (enhanced S-cone syndrome).

6.13. Methods

6.13.1. Stimuli

The stimuli used has been previously described in experiment 1. The luminances of the LEDs were modulated with square-wave temporal profiles to generate stimuli that only produced excitation in S cones.

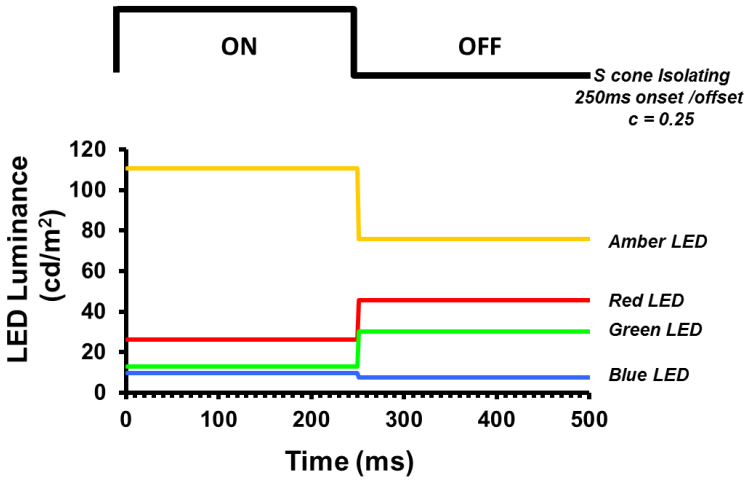

Figure 6.14. Luminance variation of the 4 LEDs over the 500ms recording epoch required to create the 8000ph Td, 250ms square wave onset/offset S cone isolating pulse stimulus.

S cone isolated ERG responses were recorded using a transient square wave stimulus. A 250 ms onset duration was followed by a 250 ms offset period (Figure 6.1). The onset comprised on an S cone excitation increment with similar excitation decrement at offset. All modulations were based on the same ratio of red:green:blue:amber LED luminances; in the unmodulated state, this ratio was 34:3:1:36 (see Figure 6.14). The retinal illuminance produced by the stimuli was 8000Td.

6.13.2. ERG Recording

The ERG recording technique has been previously described in section 6.3.2.

6.13.3. Transient Analysis

Implicit time of the a- and b-wave and amplitude of a-wave, b-wave and photopic negative response (Viswanathan et al. 1999) components were measured. The implicit time of the a-wave was measured from stimulus onset at time zero to the peak of the initial negative deflection. The amplitude measurement of the a-wave was taken as the vertical distance from the peak of the first negative trough to baseline (Figure 6.15b). The implicit time of the b-wave was measured from stimulus onset to the first positive peak. The amplitude measurement of the b-wave was taken as the vertical distance from the trough of the a-wave to the peak of the first positive peak (Figure 6.15b). The amplitude measurement of the photopic negative response (PhNR) was taken as the vertical distance from baseline to the base of the trough following the b-wave (Figure 6.15b).

6.13.4. Participants

A total of 13 colour normal trichromats (5 males, 10 females; mean age: 33 yrs, age range: 20-60 yrs) and participants with a colour vision deficiency including 9 dichromats (6 deuteranopes, 3 protanopes) all males; mean age 36yrs, age range:18-56 yrs., 1 participant diagnosed with blue cone

monochromacy (BCM) and 1 participant diagnosed with enhanced S cone syndrome (ESCS). The participant diagnosed with BCM had an L opsin gene, with a novel point mutation p.Pro196Ala, predicted to account for the phenotype. The participant with ESCS has bi-allelic loss of function mutations in NRL. This is a transcription factor which positively regulates is NR2E3 and the loss of function is likely to cause the phenotype. Colour vision in all subjects (except the participant with ESCS) was assessed using CAD colour test from City University. All subjects gave informed consent prior to the commencement of the experiments which were conducted in accordance with the Declaration of Helsinki and were approved by the University of Bradford Ethics Committee.

6.14. Results

Figure 6.15 shows ERGs obtained from 13 normal trichromatic observers in response to a silent substitution S cone isolating stimulus with a square-wave temporal profile comprising an onset (i.e. S cone excitation increment) duration of 250ms and a 250ms offset (S cone excitation decrement) period. S cone contrast (ΔC) = 0.25 and the stimulus had a mean retinal illuminance of 8000ph Td. In normal trichromats the ERG produced by this stimulus had a consistent appearance across all participants exhibited the characteristic waveform (Drasdo et al. 2001; Kuchenbecker et al. 2014) consisting of an initial small negative trough (a-wave), followed by a prominent positive peak (b-wave), then a large negative trough (PhNR). The a-wave had a mean peak implicit time of 30.69ms (±95% CI = 2.23ms) and a mean peak amplitude of 0.35µV (±95% CI = 0.17µV). The b-wave had a mean peak

implicit time of 52.30ms (±95% CI = 2.35ms) and mean peak amplitude of 0.97µV (±95% CI = 0.17µV). The photopic negative response (PhNR) peak implicit time was not measured. The mean peak amplitude was noted 2.58µV (±95% CI = 0.86µV). Unlike the L- and M-cone ERGs in the earlier experiments, no obvious d-wave offset component was evident, instead the response gradually returned to baseline. This is consistent with previous S-cone ERG studies (Sawusch et al. 1987; Drasdo et al. 2001; Chiti et al. 2003; Kuchenbecker et al. 2008) and anatomical studies which show no evidence of a direct S cone OFF pathway (Haverkamp et al. 2005).

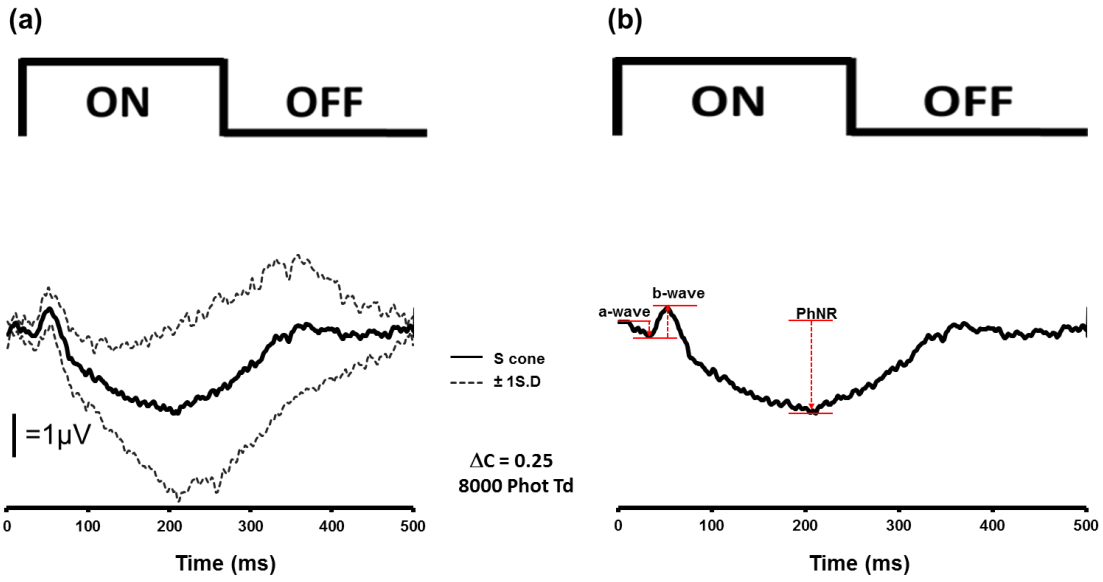

Figure 6.15. (a) Group averaged (thick black line) ERGs elicited from 13 normal participants by a silent substitution S cone isolating stimulus. The thin dotted black lines represent +/- 1 S.D. from the mean. For clarity we have shown the group averaged S cone ERG in (b), this onset response consists of a small negative trough (a-wave) followed by a prominent positive peak (b-wave) which is then followed by a large negativity (PhNR). There is no waveform component recorded to the stimulus offset.

Figure 6.16a shows ERGs obtained from 9 dichromats; 3 protanopes (lower trace) and 6 deuteranopes (upper trace) in response to the same square-wave S cone isolating stimulus. For comparison, the response from the normal participants is overlaid in figure 6.16b. The group averaged response (n=3) from the protanopes participants had an a-wave with a mean peak implicit time of 31.21ms (±95% CI = 3.12ms) and a mean peak amplitude of 0.22μV (±95% CI = 0.21μV). The b-wave had a mean peak implicit time of 49.30ms (±95% CI = 2.04ms) and mean peak amplitude of 1.12μV (±95% CI = 0.32μV). The photopic negative response (PhNR) mean peak amplitude was 2.18μV (±95% CI = 1.54μV). A similar response was recorded from the deuteranopes participants (Figure 6.4b) with an a-wave mean peak implicit time of 32.03ms (±95% CI = 2.84ms) and a mean peak amplitude of 0.41μV (±95% CI = 0.27μV). The b-wave had a mean peak implicit time of 52.30ms (±95% CI = 0.84ms) and mean peak amplitude of 1.03μV (±95% CI = 0.22μV). The photopic negative response (PhNR) peak implicit time was not measured. The mean peak amplitude was noted 2.31μV (±95% CI = 1.62μV). The protanope response, admittedly is noisier as it contains fewer averaged responses. Importantly, the responses from both the protanopic and deuteranopic participants exhibit a similar response to stimulus offset.

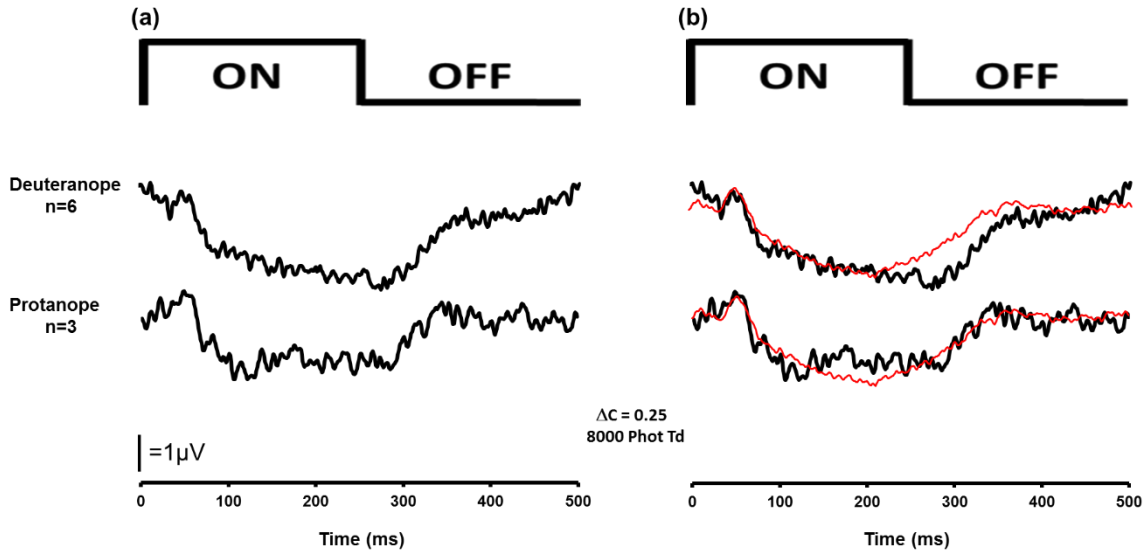

Figure 6.16. (a) black trace represents the group averaged ERGs elicited from 6 deuteranopes (top trace) and 3 protanope (bottom trace) participants using a silent substitution S cone isolating stimulus. (b) The same response is shown with the group average from the normal group (red trace) using the same stimulus, overlaid. The stimulus was an 8000phTd S cone isolating square-wave pulse stimulus (250/250ms onset/offset).

Figure 6.17 shows the full field ERGs recorded from the participant diagnosed with blue cone monochromacy (BCM) and enhanced S cone syndrome (ESCS). Responses from the BCM participant showed a very much reduced LA single flash ERG with no real evidence of the typical features seen in the normal response. The 30Hz flicker was abolished and the DA dim flash and bright flash were present but reduced in amplitude. The responses from the ESCS participant showed that both the LA single flash and flicker were present although the amplitude was reduced and the implicit timing of the a- and b-wave and flicker peak timing were prolonged. The DA dim flash elicited a small amplitude waveform and the bright flash was also reduced in amplitude with evidence of prolonged a- and b-wave timing.

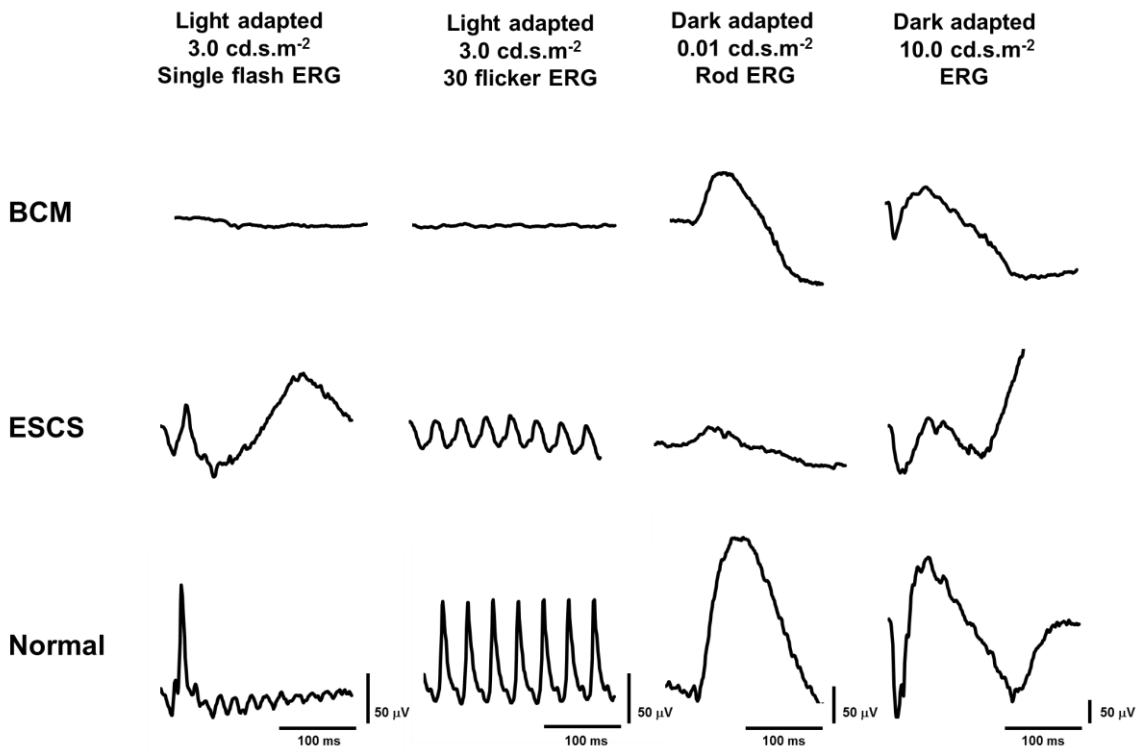

Figure 6.17 ISCEV standard full-field ERGs (RE only) recorded from the two participants diagnosed with BCM (row I) and ESCS (row II) plus a data set from a representative of our normal control group (row III). Column 1: light adapted single flash response (3.0 cd.s.m^{-2}); Column 2: 30Hz flicker stimulus (3.0 cd.s.m^{-2}); Column 3; dark-adapted (rod only) response (0.01 cd.s.m^{-2}); Column 4: bright flash (10.0 cd.s.m^{-2}).

Figure 6.18 shows the response elicited from a participant diagnosed with blue cone monochromacy (BCM) in response to the silent substitution, S cone isolating stimulus. Also shown (b) is the group averaged ERG response obtained from the normal trichromats to the same stimulus. The a-wave and b-wave responses elicited from the blue cone monochromat possess similar waveform morphology to that of the normal S cone response. However, there are some differences between the responses, the descending portion of the b-wave from the BCM participant exhibits a steep negative decline followed by a broad, low amplitude positivity. This is contrary to the typical response from the normal group which consists of a gradual negative decline into a

broad negativity. The offset response is also very different, consisting of a hyperpolarisation compared to the recovering limb of the response from the trichromats.

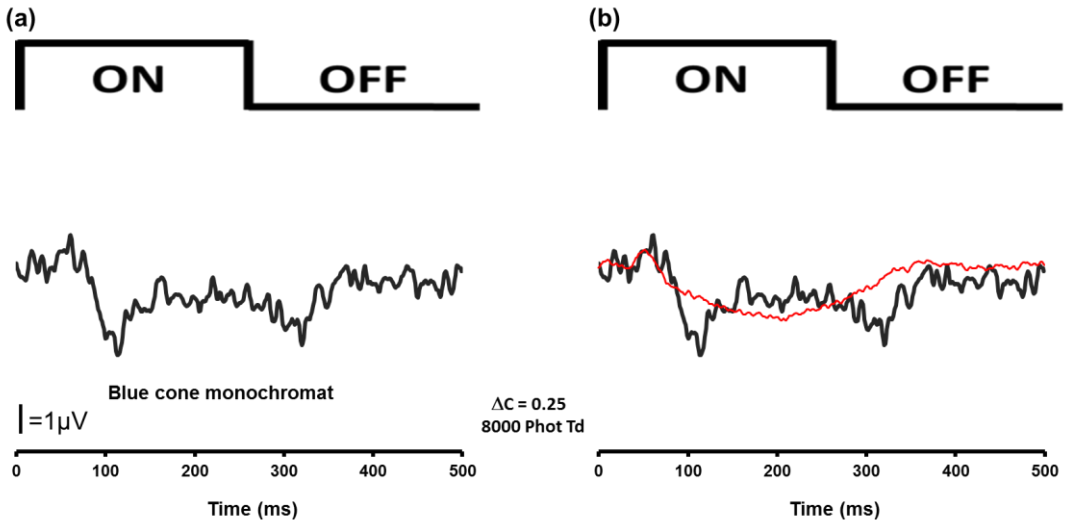

Figure 6.18. (a) An S-cone ERG elicited from a participant with blue cone monochromacy. In figure 6.18 (b) the same response is shown with the group averaged ERG obtained from the normal trichromat group (red trace) using a silent substitution S cone isolating stimulus overlaid. The stimulus was an 8000phTd S cone isolating square-wave pulse stimulus (250/250ms onset/offset).

Figure 6.19 shows the S-cone ERG elicited from a single participant diagnosed Enhanced S-cone Syndrome (ESCS) using the triple silent substitution stimulus. Also shown in 6.19(b) is the group averaged ERG response obtained from the normal trichromats to the same stimulus. This response is very different compared to the normal S cone response from the trichromat group. The first unique feature of this S cone response in ESCS is the large a-wave and b-wave, with peak amplitudes of 1.41µV and 1.28µV respectively. The ESCS a-wave is four times the amplitude of a-wave obtained from the trichromatic group. The second feature is the d-wave

(peak amplitude 2.56μV) at stimulus offset. This feature is highly unusual in the S cone ERG.

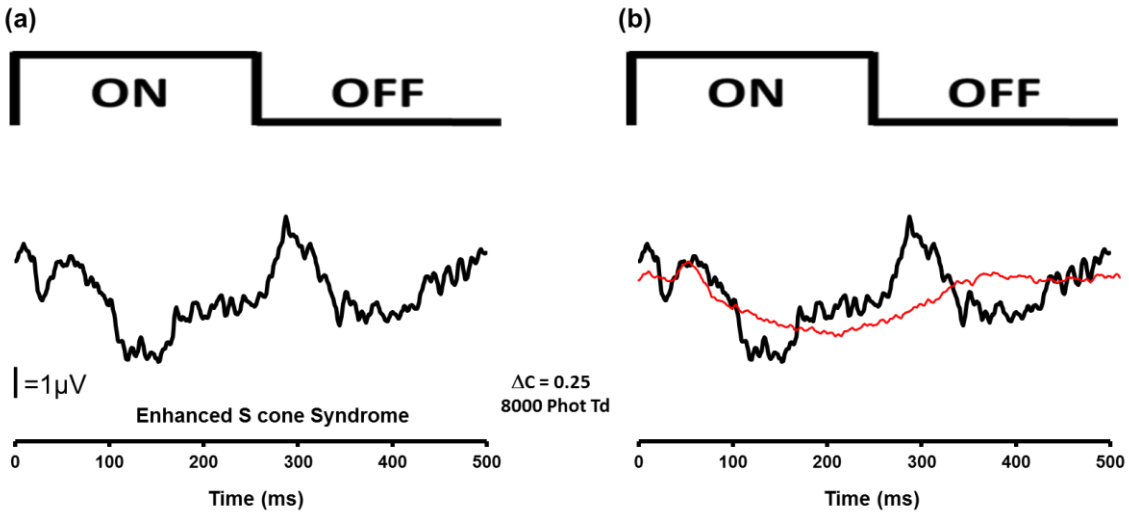

Figure 6.19. (a) ERGs elicited from a single participant with enhanced S cone syndrome (black trace) using a silent substitution S cone isolating stimulus (left). In figure 6.19 (b) the same response is shown with the group average from the normal group (red trace) using the same stimulus, overlaid. The stimulus was an 8000phTd S cone isolating square-wave pulse stimulus (250/250ms onset/offset).

6.15. Discussion

In this study, we have used triple silent substitution stimuli to elicit transient ERGs that selectively reflect S cone system function. Initially we characterised the morphology of the S cone ERG in the normal trichromatic retina. This revealed a waveform, largely in-keeping with previous studies, consisting of a small a-wave, comparatively larger b-wave and a prominent negative PhNR. Our waveform response is small, this is obviously due to the low S-cone contrast that we used and representative of the small population of S cones in the human retina. The 0.25 contrast restriction was chosen for comparative reasons with other experiments. It was the highest common contrast that we could achieve for L-, M-, S-cone photoreceptor isolation

whilst keeping our stimulus chromaticity settings constant. Despite this, amplitudes from studies using similar techniques, employing significantly higher S cone contrast (~ 90%), elicited responses within a similar range (Drasdo et al. 2001; Chiti et al. 2003; Mortlock et al. 2005; Kuchenbecker et al. 2014). One of the earlier studies also used the silent substitution technique (Sawusch et al. 1987). However, given the higher peak amplitude and longer implicit of the b-wave (16.7µV and 60-80ms respectively) it is likely that this was affected by rod intrusion. The averaged peak implicit timings of our a and b-wave components (31 ±2 and 52 ± 2ms respectively) are in-keeping with some studies (Arden et al. 1999; Drasdo et al. 2001; Chiti et al. 2003; Marmor et al. 2004; Mortlock et al. 2005) but not others (Sawusch et al. 1987; Gouras et al. 1993; Horiguchi et al. 1995; Simonsen and Rosenberg 1995; Kuchenbecker et al. 2014), who either had earlier b-wave peak times (31-46ms) or much later b-wave peak times (60-80ms). No doubt differences in stimuli account for the peak differences among groups. The longer peak times are most likely related to rod intrusion (Arden et al. 1999). The shorter peak times is more difficult to account for. Some studies show a b-wave 10ms faster than ours (Kuchenbecker et al. 2014). Higher luminance stimuli may explain some shortening of the peak time but not all of it. Earlier studies by Gouras and colleagues exhibited a peak time of 31ms (Gouras and MacKay 1990), however it is more likely that this was related to contributions from L and M cones (Kuchenbecker et al. 2014).

As previously mentioned, isolation of the S cone ERG is often complicated by certain other variables which need to be considered. The silent

substitution paradigm is based on several assumed constants, one of which is the photoreceptor spectral sensitivity. Single nucleotide polymorphisms on the X chromosome can result in significant variation of both the L and M cone spectral peak (Nathans et al. 1986; Neitz et al. 1991; Neitz and Neitz 2000). This has been shown to have a small but significant effect in M cone isolation (Huchzermeyer and Kremers 2016). Another variable is pre-retinal absorption, specifically by macular pigment density (Bone et al. 1992) and age-related lenticular changes (Pokorny et al. 1987). For the most cases these changes are less relevant for L- and M-cone isolation (Huchzermeyer and Kremers 2016), but given their effects on short wavelength light, these changes are more significant for S-cone isolation (Pokorny et al. 1987; Stockman and Sharpe 2000; Kuchenbecker et al. 2014). Part of our reasoning in developing the current S-cone stimulus was to make it easily applicable in a clinical environment. This meant that correcting for pre-retinal absorption on an individual basis was not feasible as not only was it time consuming but the psychophysics involved in such a task are difficult for a naïve observer. In our stimulus generation, we used the Stockman and Sharpe cone fundamentals (Stockman et al. 1993) which include a lens absorption correction factor but no correction for macular pigment. In the most extreme circumstances macular pigment density and lens absorption introduce rod modulation of ~5% (Huchzermeyer and Kremers 2017). The rod response is saturated at >2000 scot Td (Aguilar and Stiles 1954) and given that the mean luminance of our stimulus is well in excess of that (19,912 scot Td), rod intrusion is unlikely.

The S cone ERG is the only cone photoreceptor in the human retina that lacks a recordable offset response (Calkins 2001). Therefore, the presence of a response to stimulus offset can be used as an indicator of L- or M-cone intrusion (Zrenner and Gouras 1979). Several studies have used the attenuation of this response as a means of empirical refinement of the S cone ERG without L- or M-cone intrusion thus negating the need for correction factors or difficult psychophysical tasks (Drasdo et al. 2001; Kuchenbecker et al. 2014). Our response showed no evidence of d-wave offset response. Also reassuring is the fact that the offset portion of the response was similar to the offset responses recorded from the dichromats in figure 6.17(b), who lack either L- or M-cone contributions.

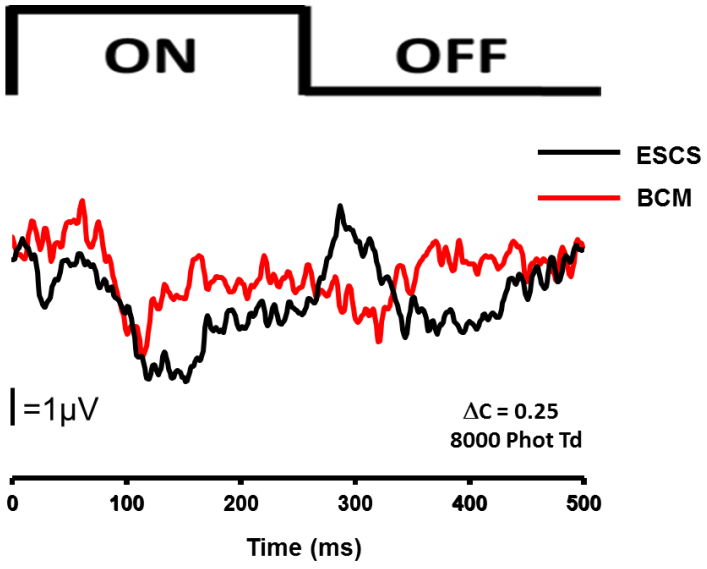

Figure 6.20. ERGs elicited from a single participant with enhanced S cone syndrome (black trace) and blue cone monochromacy (red trace) using a silent substitution S cone isolating stimulus). The stimulus was an 8000phTd S cone isolating square-wave pulse stimulus (250/250ms onset/offset).

S cone ERGs from patients diagnosed with blue cone monochromacy have been used by several studies to demonstrate isolated S cone responses in the absence of intrusions from L- and M-cones (Gouras et al. 1993; Horiguchi et al. 1995; Simonsen and Rosenberg 1995). The a- and b-wave components recorded from the participant with blue cone monochromacy had a similar morphology and amplitude to our response from normal trichromats, thus providing further validation of our isolation. However, some features of the waveform differed dramatically. Firstly, the descending portion of the b-wave/onset of the PhNR is exceptionally steep and larger compared to the gradual decline seen in the trichromats. Secondly, the response following the steep decline is positive compared to a gradual negative trough in the trichromat group. A similar response was recorded in two patients with BCM using the chromatic adaptation (Simonsen and Rosenberg 1995). Several studies in primates have shown that the second order neurons, particularly hyperpolarising bipolar cells and horizontal cells contribute largely to the negative trough following the b-wave (Sieving et al. 1994; Rangaswamy et al. 2007; Schallek et al. 2009). It's tempting to speculate that the lack of contribution from the non-functioning L- and M-cones and their respective post-receptoral OFF pathway may play a part in this polarity change. However, the data presented here are from a single participant and therefore should be treated with some caution. Finally, the offset response appears to elicit a negative deflection in the waveform compared to the positively orientated limb from the trichromat group.

When comparing our normal S cone ERG to that of the participant with ESCS we also found differences in waveform morphology. The first being a marked increase in a-wave amplitude, in line with the marked increase in S cones in the ESCS retina (Hood et al. 1995). The second difference was a large offset response. This is an unusual, although not a novel finding in ESCS (Román and Jacobson 1991; Audo et al. 2008a). It is suggested that retinal remodelling, where peripheral S cones make synaptic connections to both ON and OFF bipolar cells may explain this (Bonilha et al. 2009), although important to mention that this is not a feature of all patients with ESCS (Audo et al. 2008a). Interestingly, when we compare the S-cone ERGs recorded from the patient with BCM and the ESCS, the offsets appear to show reversed polarity (Figure 6.20). Further experiments, more thoroughly investigating these patients, are planned.

6.16. Conclusion

Triple silent substitution has proven to be a viable method to record the S cone ERG without intrusion and provide a quick and easy method to assess S cone function. The triple silencing method also means that as only S cones are being stimulated, lower luminance stimuli can be used without fear of rod intrusion. This is an advantage when testing photophobic patients, a feature often associated with BCM.

6.17. General Discussion

In the series of experiments described in this chapter we have used triple silent substitution stimuli to isolate transient L-, M- and S-cone ERGs as well

as L- and M-cone VEPs. These responses have been elicited from normal trichromats as well as from participants lacking certain cone populations. The overall aim of the study was to characterise the morphology of these cone isolated responses in normals, with the intention of implementing them into a clinical domain, specifically for the objective assessment of colour vision. It is important to note that a VEP was recorded for the S cone isolated stimulus also. However, none of the responses were reproducible and resembled noise, therefore were not included in this chapter. This may be related to the overall small population of S cones, and the potential difficulty in recording such a small signal from a scalp surface electrode.

Using group averaged waveforms we were able to successfully characterise the individual L- and M-cone isolated ERG and VEP responses. On whole, the cone isolated ERGs provided more robust responses compared to the VEPs. The cone isolated VEPs were found to be highly variable across individuals. This variability was particularly evident in the M-cone VEP. While using a homogenous full-field light stimulus provides the advantage of no edge effects often seen with patterned stimuli (Givre et al. 1995), the disadvantage is that the recorded VEP is more variable (Odom et al. 2016).

The L-cone ERG responses exhibited well defined, reproducible features among all trichromats and were completely absent in the patients with a protan colour deficiency. The S-cone ERG response was also well formed despite us using a relatively low stimulus contrast. Although we were unable

to test individuals with a tritan deficiency, tests in patients diagnosed with pathology specifically affecting L- and M-cones, as well as one patient diagnosed with ESCS, were helpful in validating the selectivity of the S-cone isolating stimuli. By comparison, the M-cone ERG was more variable (although less so than the M cone VEP). A residual M-cone ERG signal was also present in some of our deuteranopic participants, indicating poor M cone isolation.

Similar findings have been reported for the M-cone responses in multiple ERG and VEP studies that have used silent substitution to isolate M-cone activity (Bieber et al. 1997; Knoblauch et al. 1998; Kremers et al. 2003; Kremers and Pangeni 2012; Kremers et al. 2014; McKeefry et al. 2014). One of the main criticisms of silent substitution is that the calculations used to isolate photoreceptor sub-populations are based on standard sets of cone fundamental data. Therefore, anything that leads to a change in these standard measurements may affect the level of isolation. Pre-receptoral filtering, specifically age-related lens yellowing and macular pigment, selectively absorb short-wavelength light, requiring long-wavelength light to be reduced by the same amount to achieve perfect isolation. Both factors vary throughout the population. The Stockman fundamentals (Stockman and Sharpe 2000) include a lens pigmentation and macular pigment correction factor (Wysecki and Stiles 1967; Bone et al. 1992). The macular pigment spectra (Bone et al. 1992) exhibits a similar shape to previous publications (Wysecki and Stiles 1967; Vos and Walraven 1971) only the height of the curve varied depending on macular pigment concentration in individual

participants (Bone et al. 1992). It is possible to measure an individual's macular pigment concentration but such measurements were not performed for this study as it is time consuming and naïve participants may struggle with the psychophysical technique involved. For that reason we did not include the macular pigment correction factor in our calculations. However, previous work by Cao et al have demonstrated that pre-retinal filtering does not significantly affect the level of isolation (Cao et al. 2011). Furthermore, Huchzermeyer et al have shown that for L and M cone isolated stimuli, simulated lens pigmentation up to 60 years of age and macular pigment of 0.2 optical density units resulted in residual modulation of less than 1% M- or L-cone intrusion respectively (Huchzermeyer and Kremers 2016). Given relatively small region (central 2^0) occupied by macular pigment it is unlikely that it will have any effect on the full-field ERG.

Another consideration which may be detrimental to effective or complete photoreceptor isolation is the variation in their spectral sensitivity characteristics. The cone photoreceptors, for example, contain opsin proteins which determine their spectral peak. This in turn is determined by the genetic makeup of the opsin. Amino acid substitutions or polymorphisms can alter the spectral distribution by as much as 13nm in L cones and 6nm in M cones (Asenjo et al. 1994). The participants used by Stockman et al to calculate the cone fundamentals all possessed the most commonly found L- and M-cone genotype, alanine at position 180 in the L cone gene (occurring approximately 56% of the time) and alanine at position 180 in the M cone gene (occurring 93% of the time) (Stockman et al. 1999). Obviously, if participants do not possess the most common genotype they may have cone

pigments with different spectral peaks and this will compromise isolation. Such effects were simulated by Huchzermeyer and Kremers who showed that an alteration of ± 6nm in the spectral peak of the L-cone opsin can lead to L-cone modulations of 1-8% by an erstwhile M-cone isolating stimulus (Huchzermeyer and Kremers 2016). Changes of that magnitude will certainly be noticed and may explain some of the reasons for incomplete M-cone isolation.

Although we have outlined the potential pitfalls of silent substitution, this method may still provide a useful measure of L and S cone function as well as a good measure of M cone function albeit with the possibility of less than perfect isolation when some variables are not controlled for in some subjects. In a more controlled environment such as the research lab, M cone isolation can be controlled, isolation is improved. Overall this method may not be useful for the definitive measures that are required in a clinical colour vision assessment. However, it has been shown to be a useful research tool in the cone interaction in both magnocellular and parvocellular pathways in the retina (Kamiyama et al. 1996; Scholl and Kremers 2000; Kremers and Link 2008; Kuchenbecker et al. 2014; Tsai et al. 2016).

Chapter 7

Final Discussion and Future work

7.1. Overview

In its basic form the electroretinogram (ERG) is the electrical response elicited from the retina in response to stimulation by light. By standardising retinal adaptation as well as stimulus luminance and temporal frequency, the electroretinogram has become an essential clinical tool for the objective assessment of retinal function (McCulloch et al. 2015). A key feature is its ability to selectively assay both the rod and cone system separately. In recent years, other non-standard test methods have been developed and these have proven to be useful in providing extra information about retinal function (Sieving and Nino 1988; Gouras and MacKay 1990; Viswanathan et al. 1999).

The central aim of the work in this thesis has been to extend the utility of the ERG from the perspectives of both applied clinical and basic research by investigating an alternative method, silent substitution (Estevez and Spekreijse 1982), as a means of generating ERGs from the human retina. The main advantage of this technique is that it allows ERGs from individual populations of photoreceptors to be recorded and studied in isolation. The results from this work can be considered under two broad themes: the first, concentrates on the isolation and characterisation of the non-dark adapted rod photoreceptor response, whilst the second, focusses on the analysis of responses from the L-, M- and S-cone photoreceptors. The following

sections summarise the main findings of this thesis and their relevance to the clinical assessment of the retina how the techniques may be usefully deployed in future work.

7.2. Rod Isolated ERGS

7.2.1 Validation of the rod isolating silent substitution stimulus

Rod ERGs are typically measured in the dark adapted eye using low intensity stimuli at scotopic levels of illumination (Gouras and Gunkel 1964; Stockman et al. 1995; Scholl and Kremers 2001; Bijveld et al. 2011a; Bijveld et al. 2011b). This allows the study of rod responses free from cone intrusions, which become increasingly more predominant as the stimuli increase to mesopic and photopic light levels (Stockman and Sharpe 2006; Zele and Cao 2014). In the first part of this thesis the objective was to record the rod ERG in the non-dark-adapted eye using the silent substitution paradigm. Current measures of rod function rely on the retina being fully dark adapted, a process which typically requires 20 minutes. Establishing a measure of rod function which doesn't require dark adaptation has the potential to be of major clinical benefit. The retinal illuminances of the stimuli used to elicit the rod responses, extended into the mesopic and photopic regions. Therefore, it was essential for us to ensure rod selectivity was maintained and that cone intrusions were minimised. Because of this, assessing the selective capability of the rod stimulus was one of the main aspects of the thesis. The data outlining the main verification process is

presented in chapter 3 but further validation of the rod selective nature of our ERG paradigm was provided in chapters 4 and 5.

The three experiments undertaken in chapter 3 focused on examining the response properties of ERGs elicited by rod isolating silent substitution stimuli in the context of known characteristics of the rod system, with emphasis on temporal frequency response characteristics, luminance response characteristics and post-bleach recovery time. The findings showed clear quantitative and qualitative similarities with previously published properties of rod mediated vision. Specifically, the rod ERG temporal frequency response characteristic was a low-pass function with no signal beyond 30Hz (Conner and MacLeod 1977), saturation of the rod ERG occurred around 1000ph Td (Aguilar and Stiles 1954) and the recovery time of the rod isolated ERG was significantly prolonged compared to the L cone ERG (Lamb and Pugh 2004). These findings are relevant as they are not only consistent with rod isolation, but they also demonstrate that the methods used for obtaining rod specific ERGs in these studies can be a legitimate means by which rod function can be assessed in the human retina. Studies which have used similar techniques of stimulation have used specific retinal disease models such as achromatopsia, RP or cone rod dystrophy as controls to demonstrate isolation (Cao et al. 2011; Mcanany et al. 2015; Park et al. 2015). However, given the relative rarity of some of these conditions, patients can often be difficult to recruit. Not only that but variable phenotype in patients with selective retinal pathology can lead to inconsistent outcomes.

In chapter 4, the same silent substitution technique was used to generate transient ERGs using stimuli with square–wave temporal profiles. This approach facilitated examination of rod mediated responses in the time domain and enabled characterisation of the morphology of the ERG waveform and its constituent components in the normal retina. A positive component at stimulus onset was identified (P_{Ri}), which exhibited a similar peak time to the rod b-wave. In addition to this, experiments using non-selective stimuli demonstrated changes in this response that arose as the result of cone photoreceptor stimulation. One important finding was that the pure rod isolated ERGs exhibited a clear reduction in the P_{Ri} response amplitude as stimulus intensity increased from mesopic to photopic levels. This response attenuation is not observed in ERGs elicited by stimuli that are not rod-selective and is critical because it provides a clear correlation with rod photoreceptor response properties which exhibit response saturation over the same illumination range.

In chapter 5 rod isolated responses were recorded from 3 participants with achromatopsia and two participants with CSNB1. The absence of cone from participants with achromatopsia and rod function from the participants with CSNB1 meant they constituted important control groups and allowed comparison with the results from chapters 3 and 4. Using the same rod stimulus as chapter 3, temporal response and luminance response characteristics were assessed in the achromat group. In relation to the temporal frequency response characteristics, the normal group and achromat groups exhibited similar low-pass functions and almost identical phase plots.

The retinal illuminance response function in the achromat group showed a broad resemblance to that of the normal trichromats. These findings are in agreement with other studies who used disease control models as a mode of verification (Mcanany et al. 2015; Park et al. 2015) and provide additional confirmation of the appropriateness of the methodological approach in the isolation of rod mediated retinal activity from the human retina. Supporting these findings are the results comparing the morphology of the transient rod response from normal trichromats with the achromat and CSNB1 group. These findings showed that both the onset and offset components previously described in the normal trichromat were also present in achromat group, therefore had to originate in the rod system. On the other hand the CSNB1 participants, who's ERG lack a rod b-wave, also lacked any obvious P_{Ri} component. This in turn also provided evidence that the origin of the P_{Ri} component, is the ON bipolar system, similar to the rod b-wave.

7.2.2. Clinical and research utility

The ability to elicit ERGs that selectively reflect the activity of rods plays a key role in the diagnosis and monitoring of conditions such as retinitis pigmentosa, congenital stationary night blindness (CSNB), vitamin A deficiency (Berson et al. 1968; Berson et al. 1969; Perlman et al. 1983; Scholl et al. 2001; Petzold and Plant 2006) and AMD (Owsley et al. 2000). Following on from the verification process, a further aim of this study was to assess the potential use of this stimulus as a clinical tool to assess rod function. Therefore we measured the degree of correlation between the rod

responses elicited using our methodology (non-dark adapted, 8 Hz silent substitution stimulus) and those obtained using current standard clinical protocols (ISCEV 0.01 cd.s.m^{-2} dark adapted rod response (DA0.01)) in normal trichromats. The findings of this experiment are presented in chapter 5 and showed a significant correlation ($r = 0.626$; $n = 18$; $p < 0.005$; $R^2 = 0.39$) between both measures. Following on from this, another important aspect to assess was the ability of the rod isolating stimulus to differentiate between participants with normal rod function from those with compromised rod function. To do this, data from participants with different retinal pathologies were added to the normal data. The correlation between both measures of rod function was further improved by this inclusion ($r = 0.6159$, $n = 28$; $p <0.001$; $R^2 = 0.62$). The findings demonstrated the ability of our silent substitution stimulus to clearly discriminate between the normal and pathological groups in most cases. A final verification measure which examined the correlation between the 8Hz rod isolated stimulus and the 30 Hz flicker was employed. As expected, no significant correlation between these measures was noted ($r = 0.38$; $n = 18$; $p = 0.881$; $R^2 = 0.0015$), further illustrating the selectivity of the rod stimulus.

Also presented in chapter 5 is a further piece of evidence which underpins the clinical utility of our rod isolating paradigm. As previously mentioned, transient rod ERGs were recorded on participants from the achromat and CSNB cohort to help gauge the level of rod isolation. As part of the clinical assessment, in-depth testing of the achromat group was performed using standard ISCEV ERG. One surprising finding which arose was that apart

from absent cone responses, the amplitude of the dark adapted 0.01 cd.s.m^{-2} and 3.0 cd.s.m^{-2} rod responses were also reduced to different degrees in each of the three participants. This is something which has been investigated within the thesis in section 5.5.2 and in particular it appears that the b-wave of these participants is selectively disproportionality affected. By examining the transient rod response from these participants, it was clear that these changes were also present in the P_{Ri} component and also reflected the changes noted in both ISCEV 0.01 and 3.0 rod b-wave amplitudes. This links back to the previous correlation plots and suggests that most of the signal from the 8Hz rod isolated response may originate from the P_{Ri} component. An advantage of this is that while the correlation between the rod isolated 8Hz response and the dark adapted 0.01 response was a positive finding, some of the post analysis techniques such as Fast Fourier Transform (FFT) do not easily lend themselves to a clinical environment. The transient rod response, like the ISCEV measures, requires no complicated post analysis beyond measuring the amplitude of the P_{Ri} component and therefore provides a simple measure of rod function. This offers a significant clinical advantage in that it allows a quick (less than 2 minutes) assessment of rod function without the need for time-consuming dark adaptation. The clinical aspect of the data was somewhat limited by time, therefore the sample provided in this thesis merely provides an indication of its utility as a clinical tool. It is not a substitute for the current standard testing. However, by further characterisation of rod ERGs elicited by silent substitution stimuli across a wider range of retinal pathologies may prove to be of additional benefit. Handheld ERG systems are being used in clinics by ophthalmologists to

provide a quick measure of cone function in children (Grace et al. 2016) and adults. Obtaining a measure of rod function in clinical situation will often not be feasible due to time constraints. However it is conceivable that a paradigm such as the one utilised in these studies that does not require dark adaptation may enable a more time efficient assessment of rod function.

7.3. Cone Isolated ERGs

In the second theme of this thesis (Chapter 6) the focus shifted to the examination of ERGs elicited by the L-, M- and S-cone photoreceptors. The use of cone isolated ERGs has introduced a new level of precision, allowing the independent assessment of photoreceptoral and post receptoral contributions from L-, M- and S-cones. Specifically, the transient ON/OFF presentation has the advantage of eliciting an ERG waveform whereby the individual components can be identified and measured. This allows the analysis of both receptoral and post-receptoral contributions to both the onset and offset states (Kuchenbecker et al. 2014). One area where this technique might be of benefit is in the objective assessment of acquired colour vision deficiencies (CVDs). The most common type of CVD is a red green defect. The loss of the L- or M-cone opsin gene will result in either a failure to produce L-cones (protanopia) or M-cones (deuteranopia) respectively. This affects approximately ~1% and 1.27% of the population respectively (Hagstrom et al. 2000; Neitz and Neitz 2011), with anomalous trichromacy (occurring as a result of the presence of a hybrid opsin rather than the loss of an opsin) affecting almost ~6% of the population (protanomalous ~1%, deuteranomalous 4.67%) (Neitz and Neitz 2000; Neitz

and Neitz 2011). Changes in the morphology of transient cone isolating responses in dichromats compared to trichromats have been previously demonstrated (Kremers et al. 2014; McKeefry et al. 2014) but with limited data. Therefore the need for a more complete characterisation of L- and M-cone ERGs in the different forms of CVD was the reason for the initial experiments in this chapter.

In contrast to protan and deutan defects, congenital tritan deficiencies are comparatively rare (Van Norren and Went 1981). Changes in the transient S-cone ERG have been shown in the past to be associated with pathology affecting S cone function also, these include some forms of RP (Swanson et al. 1993), type 1 and type 2 diabetes (Yamamoto et al. 1996; Mortlock et al. 2005), glaucoma (Drasdo et al. 2001; Maeda et al. 2001), and ocular hypertension (Aldebasi et al. 2004; North et al. 2010). However, amongst the multiple studies which have recorded S cone ERGs exists a degree of variation in the amplitude and timing of the S cone ERG b-wave component. Presumably, this is as a result of different methods in obtaining the response. As a result of these inconsistencies a better characterisation of the normal S-cone ERG was required, as well as better description of the L- and M-cone mediated responses. To this end, the main aim of chapter 6 was to expand the characterisation of the individual ERG recordings elicited using transient L-, M- and S-cone stimulation in normal trichromats. Throughout the chapter the scope is further expanded to encompass the characterisation of these responses in participants with specific retinal pathologies. By doing so, the work took on a secondary aim which was to focus on the use of L-, M- and S-

cone isolating stimuli as potential stimuli for the clinical assessment of cone mediated vision.

7.3.1. L- and M-cone ERGs and VEPs

In the first two experiments (sections 6.2 & 6.7), cone isolated transient stimuli were used to characterise the main morphological features of L- and M- cone ERGs (experiment 1) as well as simultaneously recorded VEPs (experiment 2) in normal trichromats and dichromats. The overarching aim of these experiments was to examine whether specific colour vision deficiencies, generated characteristic changes in the response morphology of cone isolated ERGs and VEPs. The main findings from the first experiment characterising L and M cone ERGs were as follows:

1. Transient L- and M-cone stimuli in normal trichromats produced ERG responses with both an onset and offset component.
2. Both responses exhibited different morphologies.
3. L- and M-cone ERGs, recorded from the normal trichromat have reversed onset/offset responses i.e. the L cone onset response resembles the M cone offset response and the L cone offset response resembles the M cone onset response.
4. The reversed onset/offset response outlined in the normal trichromats was not observed in dichromats.

5. The L-cone ERG morphology was repeatable across normal participants and the L-cone isolating stimulus did not elicit a response from the protan and protanomalous participants.

6. The M-cone ERG morphology was more variable across normal participants and in some cases the M-cone isolating stimulus did elicit a response from deutan and deuteranomalous participant.

The main findings from the second experiment, characterising the L- and M-cone transient VEP responses were similar to those described for the ERGs:

1. In normal trichromats the L- and M-cone VEPs exhibited different morphologies.

2. The responses consisted of both onset and offset components, which were more complex (dual peaked) compared to the ERG.

3. Some evidence of reversal was present i.e. the L cone onset resembles the M cone offset and the L cone offset resembles the M cone onset, but not as obvious compared to ERG responses.

4. The L-cone VEP morphology was generally reproducible in normal trichromats and the L-cone isolating stimulus failed to elicit VEPs in the protanope and protanomalous participants.

5. The M-cone VEP morphology was less reproducible across participants and in some cases the M-cone stimulus did elicit VEP in deutan and deuteranomalous participants.

6. Overall, L and M cone VEPs were not as well formed and reproducible across participants compared to the L and M cone ERGs.

In theory, given that the structural makeup of L- and M-cones is nearly identical, exhibiting a homology of 98% (Neitz and Neitz 2011) one might expect similar ERG responses. However, the morphologies of the L- and M-cone transient ERGs differ quite significantly. This is something that had been previously described (McKeefry et al. 2014) but which we wanted to expand on. One particular difference is the 180^0 phase shift that occurs in the ERG elicited in trichromats using transient ON/OFF M-cone stimuli compared to the response elicited using L-cone stimuli. This was previously described by McKeefry et al. who found that that an L-cone excitation increment elicits an L ON response and an L-cone decrement elicits an OFF response. Conversely, an M-cone increment produces an OFF response and an M-cone decrement produces and ON response. A possible explanation for this is that it is an electrical manifestation of the L- and M-cone opponent process (Kremers et al. 2014; McKeefry et al. 2014). The results in section 6.4.1, replicate this phase shift and it is particularly obvious in the averaged responses. The notion that this polarity reversal between onset and offset responses is a reflection of cone opponency in the human retina is supported by the results shown in sections 6.4.2 and 6.4.3 which describe the morphology of the L- and M-cone ERG in participants with protan and deutan deficiencies. In this cohort, the phase reversal observed in the normal trichromats is no longer evident, reflecting a breakdown in the L/M cone opponent mechanism.

In section 6.7 the L and M cone VEP is examined. The findings from this section are not unlike those noted for the ERG data. Firstly, the onset/offset reversal between L and M cone stimuli previously observed in the ERG, was present in the L and M cone VEP data (Figure 6.8). This is interesting because if indeed this phase reversal is a reflection of opponent processing, than these findings suggest that we are able to record evidence of this over the V1 region of the cortex. Secondly, the L and M cone VEP data from the dichromats also lacked evidence of the phase reversal. In fact L-cone stimulation in deuteranopes and M cone stimulation in protanopes exhibited VEP responses that looked almost identical to a VEP response recorded using a non-isolated luminance stimulus (Figure 6.13). This further suggests that, like the ERG data, dichromats lack the mechanism for L/M opponent processing and instead the output responses are more in-keeping with those generated by the luminance system.

The idea that cone isolated transient responses are a pure representation of cone opponent pathways in the trichromat may provide a simple explanation to describe the ERG and VEP data. The processing of luminance and red/green chromatic information takes place across two parallel channels in the retina, the magnocellular and parvocellular respectively. The parvocellular pathway receives opponent input from L- or M -cones making one to one connections with single midget bipolar cells, which in turn will synapse with single midget ganglion cell (Wässle 2004). The magnocellular system consists of diffuse bipolar cells with multiple additive L and M cone inputs and synapses with parasol ganglion cells (Wässle 2004). As a result,

both systems exhibit a strong influence on the morphology of the ERG and VEP. Full-field stimulation was used in both ERG and VEP experiments; therefore both the central retina and the far periphery were being stimulated. It is therefore more likely that, when testing the normal trichromat participants that, at any one time, both the opponent (parvocellular) and luminance (magnocellular) are being stimulated. In this case the response that is being recorded either by the ERG or VEP contains contributions from both mechanisms. The theory that the reverse morphology that was described between the L and M cone responses from trichromats (certainly in the ERG data) may be a direct result of the overall majority the absolute number of the midget ganglion cell population (Perry et al. 1984; Shapley and Perry 1986). This would also explain why the contribution from the magnocellular system which contains less ganglion cells relative to the parvocellular system is more obvious in dichromats. Previous studies which have examined L and M cone ERG as a function of retinal eccentricity showed that beyond 35^0 eccentricity, the L and M cone ERG response reversal was not as obvious, signifying a loss in cone opponency (Tsai et al. 2016). This is supported by similar findings using psychophysical techniques which reported a loss of opponent behaviour beyond 30^0 (Mullen et al. 2005). This is likely related to the relatively paucity of M cones in the far periphery (Kuchenbecker et al. 2008). The L and M VEP onset response may also provide evidence for this theory, in that the dual peaked onset and offset noted in the trichromat retina might represent the activation of both mechanisms. While the relative simplicity (single positive peak) of the waveform noted in the dichromats, potentially representing the luminance system only.

The second aim of this chapter was to assess the suitability of our silent substitution cone isolating stimuli as an objective measure of cone mediated colour vision. This aspect of the study yielded variable outcomes. The results showed the L-cone stimulus to be effective in assessment of protan CVDs. Both the L cone ERG and VEP responses elicited were typically well formed and reproducible across the normal trichromat group. This finding was complimented by the fact that the L cone ERG response was absent in the protan participants while only background EEG (alpha rhythm) was present in VEPs generated from the same group. This suggests that no modulation was detected by the L cone system to elicit a VEP. These results suggest that ERGs and VEPs generated by L-cone isolating stimuli have the potential to provide the basis for objective diagnostic tests for protan deficiencies. A relatively high degree of selectivity was evident in M-cone stimulus based on the fact that a robust M-cone ERG was recorded in the trichromats and that in the majority of individuals with a deutan deficiency, ERGs were largely absent. However, evidence of a residual ERG response was noted in the averaged response from the deutan participants, indicating a lack of M cone isolation. This lack of complete isolation revealed by the M-cone responses leads to a reduced level of confidence in the ability of the M cone stimulus to differentiate between normal and deutan deficient participants. It is not 100% clear why this was the case for M-cones but not for L-cones. This topic is discussed in detail in the general discussion (section 6.17), where possible reasons include polymorphisms within the L cone opsin and pre-receptoral filtering, both of which have been shown to specifically affect M-cone selectivity more so than L-cone (Huchzermeyer and Kremers 2016). In

essence, because silent substitution is based on the cone fundamentals there will always be the potential for errors among the anomalous trichromat population. It is difficult to account for this, specifically in a clinical setup and as the majority of individuals with a CVD are deuteranomalous (Neitz and Neitz 2011), this technique may not offer the sensitivity required for an objective clinical test.

7.3.2. S cone ERG

The main aim of the experiment described in this section (6.12) was to characterise the normal S-cone ERG using triple silent substitution. To accomplish this aim we recorded the S-cone ERG from a group of normal trichromats. S cone ERGs were also recorded in participants with selected retinal pathology. This contributed to the validation of the response as well as expanding the characterisation of the response to encompass specific cone dysfunction syndromes (dichromacy and BCM) and ESCS. Strictly speaking, the use of triple silent substitution has not been previously employed to isolate the S cone ERG. The more common approach has been the use of double silent substitution with a sufficiently high luminance to saturate the rod response (Drasdo et al. 2001; Scholl and Kremers 2001; Kuchenbecker et al. 2014). The use of triple silent substitution offers the advantage that by using a four primary ganzfeld stimulator the net excitation in all four photoreceptor types can be controlled. This negates the use of a high luminance adapting light used to supress the rod system, which can introduce post receptoral non linearities which cannot be accounted for. This

may be particularly relevant in the case of S-cone isolation as the S-cones and rods share a common post receptoral pathway (Field et al. 2009). The findings from the normal group revealed a waveform consisting of a small a-wave, comparatively larger b-wave and a prominent negative PhNR. The timing and amplitude of these components were in-keeping with the findings of some previous studies (Drasdo et al. 2001; Chiti et al. 2003; Marmor et al. 2004; Mortlock et al. 2005) but differed from others. The studies that differed either had earlier b-wave peak times varying from 31-46ms (Gouras and MacKay 1990; Horiguchi et al. 1995; Simonsen and Rosenberg 1995; Kuchenbecker et al. 2014) or much later b-wave peak times 60-80ms (Sawusch et al. 1987). The later b-wave can most likely be explained by rod intrusion (Arden et al. 1999) however, the shorter peak times are more difficult to account for. One study in particular exhibited a b-wave 10ms faster than ours (Kuchenbecker et al. 2014). Higher luminance stimuli may explain some shortening of the peak time.

Examining how the morphology of S-cone ERG is affected in two forms of hereditary retinal pathology, namely; blue cone monochromatism (BCM) and enhanced S-cone syndrome (ESCS) represented an important control group for S cone isolation. The participant diagnosed with BCM only possessed functioning S-cones and rods. Therefore, under photopic conditions the ERG is theoretically free from intrusion from L- and M-cones and as such provides a true indication of S-cone ERG morphology. The participant with ESCS has a mutation which causes rod photoreceptors to differentiate into S-cones, resulting in an increase of S-cones in the retina. Although there are

functional L- and M-cones, their contributions to the ERG are very much reduced (Hood et al. 1995; Audo et al. 2008). S-cone stimulation has shown that short wavelength cones dominate the retina in ESCS, with a 4-6 fold increase noted in the a-wave amplitude of the S cone ERG (Hood et al. 1995). Therefore examining the morphology of the S-cone ERG from the ESCS participant using our triple silent substitution stimulus should display characteristic changes if indeed this stimulus does reflect S-cone mediated visual function.

The results from the participant with BCM showed that the S cone ERG morphology was similar to that recorded from the normal trichromats. This is an important finding as it indicates that the S cone stimulus is selective in terms of reflecting S-cone function. The fact that there is only one functioning cone population within the retina of the BCM participant means that comparisons made with the S cone ERG elicited from this individual were a good indicator of potential intrusion from other photoreceptors. Based on these findings it would appear that not accounting for individual variations caused by macular pigment, for example, did not lead to any notable photoreceptor intrusions. Simulation studies have indicated that in the most extreme circumstances macular pigment density and lens absorption introduce rod modulation of ~5% (Huchzermeyer and Kremers 2017). However, should this occur, little change would be expected as the rod system will not respond in such a photopic environment (Aguilar and Stiles 1954).

Using long duration onset and offset isolated stimuli has the advantages of being able to separate both the ON and OFF cellular contributions to the ERG. An unexpected finding was that the offset response from the BCM and ESCS participants were very different compared to each other and to the normal S cone response. S-cone ERGs recorded from the participant with ESCS revealed a large positive OFF component. Although not novel, this is particularly interesting and is consistent with previous results (Román and Jacobson 1991; Audo et al. 2008a). The significance of the more prominent S-cone offset responses in ESCS may be related to retinal remodelling, where it is hypothesised that peripheral S cones make synaptic connections to both ON and OFF bipolar cells (Bonilha et al. 2009). This is something that is likely given the highly disorganised retinal structure associated with this disease (Audo et al. 2008a). In contrast, the S-cone ERG offset response in the BCM subject consists of a negative component (Figure 6.19). Almost 180^0 out of phase with the OFF response noted in ESCS participant. On the whole, the S cone off response is a controversial topic. While evidence of cells which exhibited an OFF response to S cone stimulation was demonstrated in the primate LGN (Valberg et al. 1986), establishing the retinal origins of this response has been difficult. However, recent research has confirmed the presence of an S-cone OFF pathway in the macaque, constituting S-cone inputs to an OFF midget bipolar, connected to an off midget ganglion cell. Although the S OFF pathway has not been detailed within the human retina, it is suggested that this is the mechanism used to convey S off signals (Dacey et al. 2014; Dacey et al. 2017). Functional evidence of the existence of this pathway has been described in humans

with the use of psychophysical techniques employing S cone stimuli (Shinomori and Werner 2012). In particular they showed that the temporal response of the S OFF response was slower compared to the S ON. This is an interesting finding as it raises the question, can evidence of this be also found using non-invasive electrophysiology? The lack of L and M cone photoreceptors in participants diagnosed with BCM, combined with the triple silent substitution technique may provide an opportunity to investigate this further.

7.4. Limitations of Silent Substitution

Whilst the experiments described in this thesis clearly show that it is possible to generate photoreceptor specific driven ERGs from the human retina, as researchers we always have to be aware of potential limitations of the methods we employ. One of the main criticisms of the silent substitution technique is that the calculations are based on standard sets of cone fundamental data (Stockman and Sharpe 2000). Therefore, anything that leads to a change in these standard measurements may affect the level of isolation. Such factors that have to be considered include: age-related lenticular pigmentation, macular pigment optical density and individual variations in spectral sensitivity caused by polymorphisms in the opsin genes. Simulations carried out using a four primary system to generate triple silent substitution stimuli have shown that rods and S-cones are preferentially more vulnerable to L- and M- cone intrusion (~5% in the most extreme simulation) as a result of individual variation in macular and lenticular pigment densities (Huchzermeyer and Kremers 2017). However

the stimulus being used was full-field, taking into account that macular pigment affects the central 3-5 degrees, the chance of such an effect making a significant contribution is minimal. The same simulations also showed that M-cones are the more vulnerable to cone intrusion as a result of changes in the spectral peak of the L-cone opsin (up to 8.9% cone contrast in the most extreme case). Theoretically all of these factors can be measured on an individual basis and corrected for. However, in practical terms some of the psychophysical techniques employed in these measurements require training for naïve participants and are time consuming. Overall, such individual corrections may not be practical or possible in clinical settings.

Imperfect isolation of photoreceptoral responses was something that was certainly noticed in any experiment which involved recording M-cone isolated responses from deuteranopes. The expectation was that M-cone responses should not be recordable from deuteranopes. However, we recorded clear evidence of residual responses in a number of participants, indicating a possible failure of M-cone isolation. As mentioned previously, this is likely to be related to spectral peak differences in the L-cone opsin (Huchzermeyer and Kremers 2017). As none of the participants underwent any genetic or psychophysical testing this was an issue that ultimately could not be accounted for.

With regards to the rod ERG, the techniques used to optimise the parameters for isolation have been summarised in section 7.2.1 In brief, testing across wide temporal frequency and retinal illuminance ranges

allowed the elucidation of stimulus parameters which ensured maximum rod selectivity and minimised cone intrusions. The transient response contains a positive waveform which we have suggested has similar origins to the b-wave. Despite high mesopic/photopic stimuli being used there is no evidence of an equivalent rod a-wave using this method. This presents a major disadvantage of the rod isolated ERG using silent substitution as it is the unable to determine between receptoral and postreceptoral abnormalities.

Although such a wide range of parameter testing was not performed for the S-cone ERG, information obtained from previous studies (Huchzermeyer and Kremers 2017) indicated that changes in pre-retinal filtering typically resulted in rod modulation when recording the S-cone ERG. Therefore based on the overall luminance of the stimulus (8000ph Td) we were confident that this was more than enough to saturate any rod modulation present.

Other than introduce modulation from unwanted photoreceptors, there was also the concern that any unaccounted for macular pigment might result in a decrease in the overall amplitude of the S cone response, due to its absorption of short wavelength light. However, given the fact that the amplitude of the S-cone ERG was similar to that obtained in previous studies which did account for ocular media absorption (Mortlock et al. 2005; Kuchenbecker et al. 2014), it is unlikely that there was significant amplitude loss. Any potential amplitude loss occurring as a result of short wavelength light absorption in the central regions will be offset by the fall off in macular pigment outside of the central 8° degrees of the macula (Werner et al. 2000).

7.5. Future Work

7.5.1. Rod ERG

The majority of the experiments on the rod stimulus in this thesis focussed on characterising the normal rod isolated ERG. Some of the work undertaken however did focus on recording the rod isolated ERG in patients with retinal pathology. These experiments showed promising results, indicating the ability of the stimulus to assess rod function. Because of time constraints, much of the data recorded was limited to the use of the steady-state rod stimulus. The transient stimulus is a tool much more suited the clinical environment. The transient rod data recorded from the ACHM and CSNB participants exhibited interesting changes in morphology. These responses not only reflected amplitude changes observed in the ISCEV rod measures, but also, the comparisons between both measures provided insight into the origins of the rod isolated waveform components elicited by the silent substitution technique. Specifically, the comparisons suggest a link between the P_{Ri} component and the ON bipolar cells. The testing of this stimulus in other retinal pathologies is crucial to determining the clinical information provided by this waveform. For example, it would be interesting to observe changes in the morphology of the rod ERG in CSNB2, would there be a residual P_{Ri} component, for example? Also what kind of change would we expect to see in other rod related pathologies such as KCNV2 (cone dystrophy with super normal rod ERG). These are some of the questions we have yet to answer. Apart from assessing pathological changes, of course more normal data is required. This will be crucial in providing more accurate correlations with the ISCEV measures of rod function.

7.5.2. S cone ERG

The results from the S cone ERG experiments demonstrated that the triple silent substitution method can elicit a response which is representative of S cone function. Like the rod data, the S-cone ERG experiments concentrated on characterising the normal response. However some of the most interesting findings came from the patient with blue cone monochromacy. Firstly, this participant is interesting because genetic testing showed that this participant's condition was as a result of a novel mutation. Secondly, we showed that this participant exhibited an unusual offset response. One such avenue which we plan to investigate is a possible link between this patient's genotype and his offset response. Because this is an X-linked condition, there are several other affected males in the extended family. This provides an opportunity to conduct more in depth electrophysiological testing on all on individuals with this genotype for comparison. A second avenue to investigate is the actual origins of this offset response. The S-cone ERG OFF response is not a feature noted in normal trichromat. Yet its functional existence has been demonstrated using cone isolated psychophysical techniques (Shinomori and Werner 2012). One of the key findings of that study was that the OFF response exhibited slower temporal properties and was reduced with age. The combination S cone isolated stimuli and the lack of functioning L and M cones in the retina of the participants with BCM may provide an opportunity to examine this offset response in more detail from an electrophysiological perspective.

References

Abd-El-Barr, M. M., Pennesi, M. E., Saszik, S. M., Barrow, A. J., Lem, J., Bramblett, D. E., Paul, D. L., Frishman, L. J. and Wu, S. M. (2009) Genetic dissection of rod and cone pathways in the dark-adapted mouse retina. *Journal of neurophysiology* 102 (3), 1945-1955.

Aboshiha, J., Dubis, A. M., Carroll, J., Hardcastle, A. J. and Michaelides, M. (2015) The cone dysfunction syndromes. *British journal of ophthalmology*, bjophthalmol-2014-306505.

Aguilar, M. and Stiles, W. (1954) Saturation of the rod mechanism of the retina at high levels of stimulation. *Journal of modern optics* 1 (1), 59-65.

Ahnelt, P. and Kolb, H. (1994) Horizontal cells and cone photoreceptors in human retina: a Golgi-electron microscopic study of spectral connectivity. *Journal of comparative neurology* 343 (3), 406-27.

Ahnelt, P. K. (1998) The photoreceptor mosaic. Eye (Lond) 12 (Pt 3b), 531-40.

Aldebasi, Y. H., Drasdo, N., Morgan, J. E. and North, R. V. (2004) S-cone, L+ M-cone, and pattern, electroretinograms in ocular hypertension and glaucoma. *Vision research* 44 (24), 2749-2756.

Allen, A. E. and Lucas, R. J. (2016) Using Silent Substitution to Track the Mesopic Transition From Rod-to Cone-Based Vision in Mice Rod and Cone Activity at Mesopic Intensities. *Investigative ophthalmology & visual science* 57 (1), 276-287.

Alpern, M., Falls, H. F. and Lee, G. B. (1960) The enigma of typical total monochromacy. *American journal of ophthalmology* 50 (5), 996-1012.

Arden, G. and Brown, K. (1965) Some properties of components of the cat electroretinogram revealed by local recording under oil. *The journal of physiology* 176 (3), 429-461.

Arden, G., Wolf, J., Berninger, T., Hogg, C. R., Tzekov, R. and Holder, G. E. (1999) S-cone ERGs elicited by a simple technique in normals and in tritanopes. *Vision research* 39 (3), 641-650.

Asenjo, A. B., Rim, J. and Oprian, D. D. (1994) Molecular determinants of human red/green color discrimination. *Neuron* 12 (5), 1131-1138.

Audo, I., Michaelides, M., Robson, A. G., Hawlina, M., Vaclavik, V., Sandbach, J. M., Neveu, M. M., Hogg, C. R., Hunt, D. M. and Moore, A. T. (2008a) Phenotypic variation in enhanced S-cone syndrome. *Investigative ophthalmology & visual science* 49 (5), 2082-2093.

Audo, I., Robson, A. G., Holder, G. E. and Moore, A. T. (2008b) The negative ERG: clinical phenotypes and disease mechanisms of inner retinal dysfunction. *Survey of ophthalmology* 53 (1), 16-40.

Barlow, H. (1957) Increment thresholds at low intensities considered as signal/noise discriminations. *The journal of physiology* 136 (3), 469-488.

Baylor, D., Nunn, B. and Schnapf, J. (1984) The photocurrent, noise and spectral sensitivity of rods of the monkey Macaca fascicularis. *The journal of physiology* 357 (1), 575-607.

Berninger, T., Arden, G., Hogg, C. and Frumkes, T. (1989) Separable evoked retinal and cortical potentials from each major visual pathway: preliminary results. *British journal of ophthalmology* 73 (7), 502-511.

Berson, D. M., Dunn, F. A. and Takao, M. (2002) Phototransduction by retinal ganglion cells that set the circadian clock. *Science* 295 (5557), 1070-1073.

Berson, E. L., Gouras, P. and Gunkel, R. D. (1968) Rod responses in retinitis pigmentosa, dominantly inherited. *Archives of ophthalmology* 80 (1), 58-67.

Berson, E. L., Gouras, P., Gunkel, R. D. and Myrianthopoulos, N. C. (1969) Rod and cone responses in sex-linked retinitis pigmentosa. *Archives of ophthalmology* 81 (2), 215-225.

Bieber, M., Knoblauch, K. and Werner, J. (1997) Detecting colour vision deficiency in 4-and 8-week-old human infants. *Colour vision deficiencies XIII*. Springer. 277-282.

Biersdorf, W. R. and Armington, J. C. (1957) Response of the human eye to sudden changes in the wavelength of stimulation. *Journal of the optical society of America* 47 (3), 208-215.

Bijveld, M. M., Kappers, A. M., Riemslag, F. C., Hoeben, F. P., Vrijling, A. C. and van Genderen, M. M. (2011a) An extended 15 Hz ERG protocol (1): the contributions of primary and secondary rod pathways and the cone pathway. *Documenta ophthalmologica* 123 (3), 149-159.

Bijveld, M. M., Riemslag, F. C., Kappers, A. M., Hoeben, F. P. and van Genderen, M. M. (2011b) An extended 15 Hz ERG protocol (2): data of normal subjects and patients with achromatopsia, CSNB1, and CSNB2. *Documenta ophthalmologica* 123 (3), 161-172.

Bloomfield, S. A. and Dacheux, R. F. (2001) Rod Vision: Pathways and Processing in the Mammalian Retina. *Progress in retinal and eye research* 20 (3), 351-384.

Bloomfield, S. A. and Miller, R. F. (1982) A physiological and morphological study of the horizontal cell types of the rabbit retina. *Journal of comparative neurology* 208 (3), 288-303.

Bone, R. A., Landrum, J. T. and Cains, A. (1992) Optical density spectra of the macular pigmentin vivo andin vitro. *Vision research* 32 (1), 105-110.

Bonilha, V. L., Fishman, G. A., Rayborn, M. E. and Hollyfield, J. G. (2009) Retinal pathology of a patient with Goldmann-Favre Syndrome. *Ophthalmic genetics* 30 (4), 172-180.

Boycott, B. B. and Wassle, H. (1991) Morphological Classification of Bipolar Cells of the Primate Retina. *European journal of neuroscience* 3 (11), 1069-1088.

Brown, K. and Wiesel, T. (1961a) Analysis of the intraretinal electroretinogram in the intact cat eye. *The journal of physiology* 158 (2), 229.

Brown, K. and Wiesel, T. (1961b) Localization of origins of electroretinogram components by intraretinal recording in the intact cat eye. *The journal of physiology* 158 (2), 257.

Brown, K. T. (1968) The electroretinogram: its components and their origins. *Vision research* 8 (6), 633-IN6.

Brown, K. T. and Murakami, M. (1967) Delayed decay of the late receptor potential of monkey cones as a function of stimulus intensity. *Vision research* 7 (3), 179-189.

Brown, K. T. and Watanabe, K. (1962) Rod receptor potential from the retina of the night monkey. Nature.

Brown, K. T., Watanabe, K. and Murakami, M. (1965) The early and late receptor potentials of monkey cones and rods. *Cold spring harbor symposia on quantitative biology*. Vol. 30.

Brown, K. T. and Wiesel, T. (1959) Intraretinal recording with micropipette electrodes in the intact cat eye. *The journal of physiology* 149 (3), 537.

Burkhardt, D. A. (1993) Synaptic feedback, depolarization, and color opponency in cone photoreceptors. *Visual neuroscience* 10 (6), 981-989.

Bush, R. A. and Sieving, P. A. (1994) A proximal retinal component in the primate photopic ERG a-wave. *Investigative ophthalmology & visual science* 35 (2), 635-645.

Bush, R. A. and Sieving, P. A. (1996) Inner retinal contributions to the primate photopic fast flicker electroretinogram. Journal of optical of society of America 13 (3), 557-65.

Calkins, D. J. (2001) Seeing with S cones. *Progress in retinal and eye research* 20 (3), 255-287.

Cameron, A., Miao, L., Ruseckaite, R., Pianta, M. and Lamb, T. (2008) Dark adaptation recovery of human rod bipolar cell response kinetics estimated from scotopic b-wave measurements. *The journal of physiology* 586 (22), 5419-5436.

Cameron, M. A., & Lucas, R. J. (2009). Influence of the rod photoresponse on light adaptation and circadian rhythmicity in the cone ERG. *Molecular Vision*, *15*, 2209–2216.

Campbell, F. and Kulikowski, J. (1972) The visual evoked potential as a function of contrast of a grating pattern. *The journal of physiology* 222 (2), 345.

Cao, D., Lee, B. B. and Sun, H. (2010) Combination of rod and cone inputs in parasol ganglion cells of the magnocellular pathway. *Journal of vision* 10 (11), 4.

Cao, D., Pokorny, J. and Grassi, M. A. (2011) Isolated mesopic rod and cone electroretinograms realized with a four-primary method. *Documenta ophthalmologica* 123 (1), 29-41.

Carden, D., Kulikowski, J., Murray, I. and Parry, N. (1985) Human Occipital Potentials-Evoked by the Onset of Equiluminant Chromatic Gratings. *Journal of Physiology*-London. Vol. 369. Cambridge university press.

Carroll, J., Choi, S. S. and Williams, D. R. (2008) In vivo imaging of the photoreceptor mosaic of a rod monochromat. *Vision research* 48 (26), 2564-2568.

Carroll, J., Neitz, J. and Neitz, M. (2002) Estimates of L: M cone ratio from ERG flicker photometry and genetics. *Journal of vision* 2 (8), 1-1.

Castańo, J. A. and Sperling, H. G. (1982) Sensitivity of the blue-sensitive cones across the central retina. *Vision research* 22 (6), 661-673.

Chen, C., Zuo, C., Piao, C. and Miyake, Y. (2005) Recording rod ON and OFF responses in ERG and multifocal ERG. *Documenta ophthalmologica* 111 (2), 73-81.

Chiti, Z., North, R. V., Mortlock, K. E. and Drasdo, N. (2003) The S-cone electroretinogram: a comparison of techniques, normative data and age-related variation. *Ophthalmic and physiological optics* 23 (4), 370-376.

Cohen, A. I. (1968) New evidence supporting the linkage to extracellular space of outer segment saccules of frog cones but not rods. *The journal of cell biology* 37 (2), 424-444.

Cohen, A. I. (1972) Rods and cones. Physiology of Photoreceptor Organs. Springer. 63-110.

Conner, J. (1982) The temporal properties of rod vision. *The journal of physiology* 332, 139.

Conner, J. and MacLeod, D. (1977) Rod photoreceptors detect rapid flicker. *Science* 195 (4279), 698-699.

Crognale, M., Teller, D., Motulsky, A. and Deeb, S. (1998) Severity of color vision defects: electroretinographic (ERG), molecular and behavioral studies. *Vision research* 38 (21), 3377-3385.

Crognale, M. A., Switkes, E., Rabin, J., Schneck, M. E., Hægerström-Portnoy, G. and Adams, A. J. (1993) Application of the spatiochromatic visual evoked potential to detection of congenital and acquired color-vision deficiencies. *Journal of optical society of America* 10 (8), 1818-1825.

Curcio, C. A., Sloan, K. R., Kalina, R. E. and Hendrickson, A. E. (1990) Human photoreceptor topography. *Journal of comparative neurology* 292 (4), 497-523.

Dacey, D. M. (1999) Primate retina: cell types, circuits and color opponency. *Progress in retinal eye research* 18 (6), 737-63.

Dacey, D. M., Crook, J. D. and Packer, O. S. (2014) Distinct synaptic mechanisms create parallel S-ON and S-OFF color opponent pathways in the primate retina. *Visual Neuroscience* 31 (2), 139-151.

Dacey, D. M. and Lee, B. B. (1994) The'blue-on'opponent pathway in primate retina originates from a distinct bistratified ganglion cell type. *Nature* 367 (6465), 731-735.

Dacey, D. M., Lee, B. B., Stafford, D. K., Pokorny, J. and Smith, V. C. (1996) Horizontal cells of the primate retina: cone specificity without spectral opponency. *Science* 271 (5249), 656-9.

Dacey, D. M., Wool, L., Packer, O. and Wong, R. (2017) Confirmation of an S-OFF midget ganglion cell pathway using serial block-face scanning electron microscopy. *Journal of vision* 17 (7), 58-58.

Dacheux, R. F. and Raviola, E. (1986) The rod pathway in the rabbit retina: a depolarizing bipolar and amacrine cell. *The journal of neuroscience* 6 (2), 331-345.

De Valois, R., Smith, C., Kitai, S. and Karoly, A. (1958) Response of single cells in monkey lateral geniculate nucleus to monochromatic light. *Science*.

Demb, J. B. and Singer, J. H. (2012) Intrinsic properties and functional circuitry of the AII amacrine cell. *Visual neuroscience* 29 (01), 51-60.

Demontis, G. C. and Cervetto, L. (2002) Vision: how to catch fast signals with slow detectors. *Physiology* 17 (3), 110-114.

Derrington, A. M., Krauskopf, J. and Lennie, P. (1984) Chromatic mechanisms in lateral geniculate nucleus of macaque. *The journal of physiology* 357 (1), 241-265.

DeValois, R., Smith, C., Kitai, S. and Karoly, A. (1957) Responses from different layers of the monkey lateral geniculate-nucleus (LGN) to monochromatic light stimuli. *American psychologist. Vol. 12.*

Dhingra, A. and Vardi, N. (2012) mGlu receptors in the retina. *Wiley interdisciplinary reviews: membrane transport and signaling* 1 (5), 641-653.

Di Russo, F., Martínez, A., Sereno, M. I., Pitzalis, S. and Hillyard, S. A. (2002) Cortical sources of the early components of the visual evoked potential. *Human brain mapping* 15 (2), 95-111.

Dodt, E. (1951) Cone electroretinography by flicker. *Nature* 168:738-739.

Donner, K. and Rushton, W. (1959) Retinal stimulation by light substitution. *The journal of physiology* 149 (2), 288-302.

Dorgau, B., Herrling, R., Schultz, K., Greb, H., Segelken, J., Ströh, S., Bolte, P., Weiler, R., Dedek, K. and Janssen-Bienhold, U. (2015) Connexin50 couples axon terminals of mouse horizontal cells by homotypic gap junctions. *Journal of comparative neurology* 523 (14), 2062-2081.

Drasdo, N., Aldebasi, Y. H., Chiti, Z., Mortlock, K. E., Morgan, J. E. and North, R. V. (2001) The s-cone PHNR and pattern ERG in primary open angle glaucoma. *Investigative ophthalmology & visual science* 42 (6), 1266-1272.

Dryja, T. P., McGee, T. L., Berson, E. L., Fishman, G. A., Sandberg, M. A., Alexander, K. R., Derlacki, D. J. and Rajagopalan, A. S. (2005) Night blindness and abnormal cone electroretinogram ON responses in patients with mutations in the GRM6 gene encoding mGluR6. *Proceedings of the National Academy of Sciences of the United States of America* 102 (13), 4884-4889.

Dubra, A., Sulai, Y., Norris, J. L., Cooper, R. F., Dubis, A. M., Williams, D. R. and Carroll, J. (2011) Noninvasive imaging of the human rod

photoreceptor mosaic using a confocal adaptive optics scanning ophthalmoscope. *Biomedical optics express* 2 (7), 1864-1876.

Estevez, O. and Spekreijse, H. (1982) The "silent substitution" method in visual research. *Vision research* 22 (6), 681-91.

Estévez, O. and Spekreuse, H. (1974) A spectral compensation method for determining the flicker characteristics of the human colour mechanisms. *Vision research* 14 (9), 823-830.

Famiglietti Jr, E. and Kolb, H. (1975) A bistratified amacrine cell and synaptic circuitry in the inner plexiform layer of the retina. *Brain research* 84 (2), 293-300.

Farrow, K., Teixeira, M., Szikra, T., Viney, T. J., Balint, K., Yonehara, K. and Roska, B. (2013) Ambient illumination toggles a neuronal circuit switch in the retina and visual perception at cone threshold. *Neuron* 78 (2), 325-338.

Feigl, B., Cao, D., Morris, C. P. and Zele, A. J. (2011) Persons with age-related maculopathy risk genotypes and clinically normal eyes have reduced mesopic vision. *Investigative ophthalmology & visual science* 52 (2), 1145-1150.

Field, G. D., Greschner, M., Gauthier, J. L., Rangel, C., Shlens, J., Sher, A., Marshak, D. W., Litke, A. M. and Chichilnisky, E. (2009) High-sensitivity rod photoreceptor input to the blue-yellow color opponent pathway in macaque retina. *Nature neuroscience* 12 (9), 1159-1164.

Forrester, J. V. (2002) *The Eye*. second edition. W B Saunders.

Frishman, L. J. and Steinberg, R. (1989) Intraretinal analysis of the threshold dark-adapted ERG of cat retina. *Journal of neurophysiology* 61 (6), 1221-1232.

Frishman, L. J. and Steinberg, R. (1990) Origin of negative potentials in the light-adapted ERG of cat retina. *Journal of neurophysiology* 63 (6), 1333-1346.

Frumkes, T. E., Naarendorp, F. and Goldberg, S. H. (1986) The influence of cone adaptation upon rod mediated flicker. *Vision research* 26 (8), 1167-1176.

Fu, Y. and Yau, K. W. (2007) Phototransduction in mouse rods and cones. *Pflugers archives* 454 (5), 805-19.

Fulton, A. B. and Hansen, R. M. (2000) The development of scotopic sensitivity. *Investigative ophthalmology & visual science* 41 (6), 1588-1596.

Genead, M. A., Fishman, G. A., Rha, J., Dubis, A. M., Bonci, D. M. O., Dubra, A., Stone, E. M., Neitz, M. and Carroll, J. (2011) Photoreceptor structure and function in patients with congenital achromatopsia. *Investigative ophthalmology & visual science* 52 (10), 7298-7308.

Givre, S., Arezzo, J. and Schroeder, C. (1995) Effects of wavelength on the timing and laminar distribution of illuminance-evoked activity in macaque V1. *Visual neuroscience* 12 (02), 229-239.

Gouras, P. (1970) Symposium on Electrophysiology: Electroretinography: Some Basic Principles. *Investigative ophthalmology & visual science* 9 (8), 557-569.

Gouras, P. and Gunkel, R. D. (1964) The frequency response of normal, rod achromat and nyctalope ERGs to sinusoidal monochromatic light stimulation. *Documenta ophthalmologica* 18 (1), 137-150.

Gouras, P. and MacKay, C. (1990) Electroretinographic responses of the short-wavelength-sensitive cones. *Investigative ophthalmology & visual science* 31 (7), 1203-1209.

Gouras, P., MacKay, C. and Yamamoto, S. (1993) The human S-cone electroretinogram and its variation among subjects with and without L and M-cone function. *Investigative ophthalmology & visual science* 34 (8), 2437-2442.

Gouras, P. and MacKay, C. J. (1989) Growth in amplitude of the human cone electroretinogram with light adaptation. *Investigative ophthalmology & visual science* 30 (4), 625-630.

Grace, S. F., Capo, H. and Lam, B. (2016) Portable nonsedated electroretinogram evaluation of children with nystagmus in the pediatric ophthalmology clinic. *Journal of American association for pediatric ophthalmology and strabismus* 20 (4), e16.

Granit, R. (1950) Sensory mechanisms of the retina, London, 1947. Erg. *Physiology* 46, 31.

Granit, R. and Riddell, L. (1934) The electrical responses of light-and dark-adapted frogs' eyes to rhythmic and continuous stimuli. *The journal of physiology* 81 (1), 1.

Greenstein, V. C., Hood, D. C., Ritch, R., Steinberger, D. and Carr, R. E. (1989) S (blue) cone pathway vulnerability in retinitis pigmentosa, diabetes and glaucoma. *Investigative ophthalmology & visual science* 30 (8), 1732-1737.

Gurevich, L. and Slaughter, M. M. (1993) Comparison of the waveforms of the ON bipolar neuron and the b-wave of the electroretinogram. *Vision research* 33 (17), 2431-2435.

Hagstrom, S. A., Neitz, M. and Neitz, J. (2000) Cone pigment gene expression in individual photoreceptors and the chromatic topography of the retina. *Journal of the optical society of America* 17 (3), 527-537.

Hamilton, R. and Graham, K. (2016) Effect of shorter dark adaptation on ISCEV standard DA 0.01 and DA 3 skin ERGs in healthy adults. *Documenta ophthalmologica* 133 (1), 11-19.

Hansen, R. M., Moskowitz, A., Akula, J. D. and Fulton, A. B. (2017) The neural retina in retinopathy of prematurity. *Progress in retinal and eye research* 56, 32-57.

Hargrave, P. A. (2001) Rhodopsin structure, function, and topography the Friedenwald lecture. *Investigative ophthalmology and vision science* 42 (1), 3-9.

Hargrave, P. A. and McDowell, J. H. (1992) Rhodopsin and phototransduction: a model system for G protein-linked receptors. *Federation of American societies for experimental biology journal* 6 (6), 2323-31.

Hattar, S., Liao, H.-W., Takao, M., Berson, D. M. and Yau, K.-W. (2002) Melanopsin-containing retinal ganglion cells: architecture, projections, and intrinsic photosensitivity. *Science* 295 (5557), 1065-1070.

Haverkamp, S., Wässle, H., Duebel, J., Kuner, T., Augustine, G. J., Feng, G. and Euler, T. (2005) The primordial, blue-cone color system of the mouse retina. *Journal of neuroscience* 25 (22), 5438-5445.

Hecht, S. and Shlaer, S. (1936) Intermittent stimulation by light V. The relation between intensity and critical frequency for different parts of the spectrum. *The journal of general physiology* 19 (6), 965-977.

Hecht, S., Shlaer, S., Smith, E. L., Haig, C. and Peskin, J. C. (1948) The visual functions of the complete colorblind. *The journal of general physiology* 31 (6), 459-472.

Heckenlively, J. R. and Arden, G. B. (2006) *Principles and practice of clinical electrophysiology of vision*, 2nd Edition. MIT Press.

Heikkinen, H., Vinberg, F., Nymark, S. and Koskelainen, A. (2011) Mesopic background lights enhance dark-adapted cone ERG flash responses in the intact mouse retina: a possible role for gap junctional decoupling. *Journal of neurophysiology* 105 (5), 2309-2318.

Henkes, H. (1984) A history of human electroretinography. Special tests of visual function. Karger Publishers. 11-19.

Hess, R. and Nordby, K. (1986) Spatial and temporal limits of vision in the achromat. *The journal of physiology* 371 (1), 365-385.

Hood, D. C., Benimoff, N. I. and Greenstein, V. C. (1984) The response range of the blue-cone pathways: a source of vulnerability to disease. *Investigative ophthalmology & visual science* 25 (7), 864-867.

Hood, D. C. and Birch, D. G. (1990) The a-wave of the human electroretinogram and rod receptor function. *Investigative ophthalmology & visual science* 31 (10), 2070-2081.

Hood, D. C. and Birch, D. G. (1994) Rod phototransduction in retinitis pigmentosa: estimation and interpretation of parameters derived from the rod a-wave. *Investigative ophthalmology and visual science* 35 (7), 2948-2961.

Hood, D. C. and Birch, D. G. (1996) Assessing abnormal rod photoreceptor activity with the a-wave of the electroretinogram: Applications and methods. *Documenta ophthalmologica* 92 (4), 253-267.

Hood, D. C., Cideciyan, A. V., Roman, A. J. and Jacobson, S. G. (1995) Enhanced S cone syndrome: evidence for an abnormally large number of S cones. *Vision research* 35 (10), 1473-1481.

Horiguchi, M., Miyake, Y., Kondo, M., Suzuki, S., Tanikawa, A. and Koo, H. M. (1995) Blue light-emitting diode built-in contact lens electrode can record human S-cone electroretinogram. *Investigative ophthalmology & visual science* 36 (8), 1730-1732.

Hubel, D. H. and Wiesel, T. N. (1962) Receptive fields, binocular interaction and functional architecture in the cat's visual cortex. *The journal of physiology* 160 (1), 106-154.

Huchzermeyer, C. and Kremers, J. (2016) Perifoveal L-and M-cone-driven temporal contrast sensitivities at different retinal illuminances. *Journal of the optical society of America* 33 (10), 1989-1998.

Huchzermeyer, C. and Kremers, J. (2017) Perifoveal S-cone and rod-driven temporal contrast sensitivities at different retinal illuminances. *Journal of the optical society of America* 34 (2), 171-183.

Hurvich, L. M. and Jameson, D. (1957) An opponent-process theory of color vision. Psychological review 64 (6p1), 384.

Ives, H. E. (1922) Critical frequency relations in scotopic vision. *Journal of the optical society of America* 6 (3), 254-267.

Jacob, M. M., Pangeni, G., Gomes, B. D., Souza, G. S., da Silva Filho, M., Silveira, L. C. L., Maguire, J., Parry, N. R., McKeefry, D. J. and Kremers, J. (2015) The Spatial Properties of L-and M-Cone Inputs to Electroretinograms That Reflect Different Types of Post-Receptoral Processing. *PloS one* 10 (3), e0121218.

Jacobs, G. H., Deegan, J. F. and Neitz, J. (1998) Photopigment basis for dichromatic color vision in cows, goats, and sheep. *Visual neuroscience* 15 (03), 581-584.

Jacobs, G. H., Neitz, J. and Krogh, K. (1996) Electroretinogram flicker photometry and its applications. *Journal of the optical society of America* 13 (3), 641-648.

Kamiyama, M., Yamamoto, S., Nitta, K. and Hayasaka, S. (1996) Undetectable S cone electroretinogram b-wave in complete congenital stationary night blindness. *British journal of ophthalmology* 80 (7), 637-639.

Kanski, J. J. and Bowling, B. (2011) Clinical ophthalmology: a systematic approach. *Elsevier Health Sciences.*

Kaplan, E. and Shapley, R. M. (1986) The primate retina contains two types of ganglion cells, with high and low contrast sensitivity. *Proceedings of the national academy of sciences* 83 (8), 2755-2757.

Kelly, J. P., Crognale, M. A. and Weiss, A. H. (2003) ERGs, cone-isolating VEPs and analytical techniques in children with cone dysfunction syndromes. *Documenta ophthalmologica* 106 (3), 289-304.

Khan, N. W., Wissinger, B., Kohl, S. and Sieving, P. A. (2007) CNGB3 achromatopsia with progressive loss of residual cone function and impaired rod-mediated function. *Investigative ophthalmology & visual science* 48 (8), 3864-3871.

Klem, G. H., Lüders, H. O., Jasper, H. and Elger, C. (1999) The ten-twenty electrode system of the International Federation. *Electroencephalography clinical neurophysiology* 52 (3), 3-6.

Klistorner, A., Crewther, D. and Crewther, S. (1998) Temporal analysis of the chromatic flash VEP—separate colour and luminance contrast components. *Vision research* 38 (24), 3979-4000.

Knoblauch, K., Bieber, M. L. and Werner, J. S. (1998) M-and L-cones in early infancy: I. VEP responses to receptor-isolating stimuli at 4-and 8-weeks of age. *Vision research* 38 (12), 1753-1764.

Kohl, S., Marx, T., Giddings, I., Jägle, H., Jacobson, S. G., Apfelstedt-Sylla, E., Zrenner, E., Sharpe, L. T. and Wissinger, B. (1998) Total colourblindness is caused by mutations in the gene encoding the α-subunit of the cone photoreceptor cGMP-gated cation channel. *Nature genetics* 19 (3), 257-259.

Kohl, S., Varsanyi, B., Antunes, G. A., Baumann, B., Hoyng, C. B., Jägle, H., Rosenberg, T., Kellner, U., Lorenz, B. and Salati, R. (2005) CNGB3 mutations account for 50% of all cases with autosomal recessive achromatopsia. *European journal of human genetics* 13 (3), 302-308.

Kolb, H. (1970) Organization of the outer plexiform layer of the primate retina: electron microscopy of Golgi-impregnated cells. *Philosophical transactions of the royal society of London.* Series *B, biological Sciences*, 261-283.

Kolb, H. (1974) The connections between horizontal cells and photoreceptors in the retina of the cat: electron microscopy of Golgi preparations. *Journal of comparative neurology* 155 (1), 1-14.

Kolb, H. (1991) The neural organization of the human retina. Principles and Practices of *Clinical electrophysiology of vision*. Mosby Year Book Inc., St. Louis, 25-52.

Kolb, H. (1997) Amacrine cells of the mammalian retina: Neurocircuitry and functional roles. *Eye* 11 (6), 904-923.

Kolb, H. and Famigilietti, E. (1974) Rod and cone pathways in the inner plexiform layer of cat retina. *Science* 186 (4158), 47-49.

Kolb, H., Fernandez, E., Schouten, J., Ahnelt, P., Linberg, K. A. and Fisher, S. K. (1994) Are there three types of horizontal cell in the human retina? *Journal of comparative neurology* 343 (3), 370-386.

Kolb, H. and Nelson, R. (1983) Rod pathways in the retina of the cat. *Vision research* 23 (4), 301-312.

Kolb, H. and Nelson, R. (1996) Hyperpolarizing, small-field, amacrine cells in cone pathways of cat retina. *Journal of comparative neurology* 371 (3), 415-36.

Kolb, H., Nelson, R. and Mariani, A. (1981) Amacrine cells, bipolar cells and ganglion cells of the cat retina: A Golgi study. *Vision research* 21 (7), 1081-1114.

Kommanapalli, D., Murray, I. J., Kremers, J., Parry, N. R. and McKeefry, D. J. (2014) Temporal characteristics of L-and M-cone isolating steady-state electroretinograms. *Journal of the optical society of America* 31 (4), A113-A120.

Kraft, T., Schneeweis, D. and Schnapf, J. (1993) Visual transduction in human rod photoreceptors. *The journal of physiology* 464 (1), 747-765.

Kremers, J. (2003) The assessment of L-and M-cone specific electroretinographical signals in the normal and abnormal human retina. *Progress in retinal and eye research* 22 (5), 579-605.

Kremers, J., Czop, D. and Link, B. (2009) Rod and S-cone driven ERG signals at high retinal illuminances. *Documenta ophthalmologica* 118 (3), 205-216.

Kremers, J. and Link, B. (2008) Electroretinographic responses that may reflect activity of parvo-and magnocellular post-receptoral visual pathways. *Journal of vision* 8 (15), 11-11.

Kremers, J. and Meierkord, S. (1999) Rod–cone-interactions in deuteranopic observers: models and dynamics. *Vision research* 39 (20), 3372-3385.

Kremers, J. and Pangeni, G. (2012) Electroretinographic responses to photoreceptor specific sine wave modulation. *Journal of the optical society of America* 29 (2), A306-A313.

Kremers, J., Pangeni, G., Tsaousis, K. T., McKeefry, D., Murray, I. J. and Parry, N. R. (2014) Incremental and decremental L-and M-cone driven ERG responses: II. Sawtooth stimulation. *Journal of the optical society of America* 31 (4), A170-A178.

Kremers, J., Rodrigues, A. R., de Lima Silveira, L. C. and da Silva Filho, M. (2010) Flicker ERGs representing chromaticity and luminance signals. *Investigative ophthalmology & visual science* 51 (1), 577-587.

Kremers, J., Scholl, H. P., Knau, H., Berendschot, T. T., Usui, T. and Sharpe, L. T. (2000) L/M cone ratios in human trichromats assessed by psychophysics, electroretinography, and retinal densitometry. *Journal of the optical society of America* 17 (3), 517-526.

Kremers, J., Stepien, M. W., Scholl, H. P. and Saito, C. (2003) Cone selective adaptation influences L-and M-cone driven signals in electroretinography and psychophysics, by Kremers, Stepien, Scholl & Saito. *Journal of vision* 3 (2), 3.

Kremers, J., Usui, T., Scholl, H. and Sharpe, L. T. (1999) Cone signal contributions to electroretinograms [correction of electrograms] in dichromats and trichromats. *Investigative ophthalmology & visual science* 40 (5), 920-930.

Kuchenbecker, J. A., Greenwald, S. H., Neitz, M. and Neitz, J. (2014) Cone-isolating ON–OFF electroretinogram for studying chromatic pathways in the retina. *Journal of the optical society of America* 31 (4), A208-A213.

Kuchenbecker, J. A., Sahay, M., Tait, D. M., Neitz, M. and Neitz, J. (2008) Topography of the long-to middle-wavelength sensitive cone ratio in the human retina assessed with a wide-field color multifocal electroretinogram. *Visual neuroscience* 25 (03), 301-306.

Kulikowski, J. and Carden, D. (1989) Scalp VEPs to chromatic and achromatic gratings in macaques with ablated visual area 4. *Seeing contour and colour*, 586-590.

Lamb, T. (1981) The involvement of rod photoreceptors in dark adaptation. *Vision research* 21 (12), 1773-1782.

Lamb, T. and Pugh, E. (2004) Dark adaptation and the retinoid cycle of vision. *Progress in retinal and eye research* 23 (3), 307-380.

Lamb, T. and Pugh, E. N. (1992) A quantitative account of the activation steps involved in phototransduction in amphibian photoreceptors. *The journal of physiology* 449, 719.

Lamb, T. D. and Pugh, E. N. (2006) Phototransduction, dark adaptation, and rhodopsin regeneration the proctor lecture. *Investigative ophthalmology & visual science* 47 (12), 5138-5152.

Langlo, C. S., Patterson, E. J., Higgins, B. P., Summerfelt, P., Razeen, M. M., Erker, L. R., Parker, M., Collison, F. T., Fishman, G. A. and Kay, C. N. (2016) Residual Foveal Cone Structure in CNGB3-Associated Achromatopsia. *Investigative ophthalmology & visual science* 57 (10), 3984-3995.

Lasater, E. M., Dowling, J. E. and Ripps, H. (1984) Pharmacological properties of isolated horizontal and bipolar cells from the skate retina. *The journal of neuroscience* 4 (8), 1966-1975.

Lee, B., Valberg, A., Tigwell, D. and Tryti, J. (1987) An account of responses of spectrally opponent neurons in macaque lateral geniculate nucleus to successive contrast. *Proceedings of the royal society of London b: biological sciences* 230 (1260), 293-314.

Lee, B. B., Smith, V. C., Pokorny, J. and Kremers, J. (1997) Rod inputs to macaque ganglion cells. *Vision research* 37 (20), 2813-2828.

Levin, L. A., Nilsson, S. F. E., Hoeve, J. V., Wu, S., Kaufman, P. L. and Alm, A. (2011) *Adler's physiology of the eye. Elsevier Health Sciences.*

MacLeod, D. I. (1972) Rods cancel cones in flicker. *Nature*.

Maeda, H., Nakamura, M. and Negi, A. (2001) Selective reduction of the S-cone component of the electroretinogram in Posner—Schlossman syndrome. *Eye* 15 (2), 163-167.

Maguire, J., Parry, N. R., Kremers, J., Kommanapalli, D., Murray, I. J. and McKeefry, D. J. (2016) Rod electroretinograms elicited by silent substitution stimuli from the light-adapted human eye. *Translational vision science & technology* 5 (4), 13-13.

Mahroo, O. and Lamb, T. (2004) Recovery of the human photopic electroretinogram after bleaching exposures: estimation of pigment regeneration kinetics. *The journal of physiology* 554 (2), 417-437.

Marmor, M. F., Cabael, L., Shukla, S., Hwang, J. C. and Marcus, M. (2004) Clinical S-cone ERG recording with a commercial hand-held full-field stimulator. *Documenta ophthalmologica* 109 (1), 101-107.

Martin, P. R. (1998) Colour processing in the primate retina: recent progress. *The journal of physiology* 513 (3), 631-638.

Martin, P. R., White, A. J., Goodchild, A. K., Wilder, H. D. and Sefton, A. E. (1997) Evidence that Blue-on Cells are Part of the Third Geniculocortical Pathway in Primates. *European journal of neuroscience* 9 (7), 1536-1541.

Maunsell, J. H. and Gibson, J. R. (1992) Visual response latencies in striate cortex of the macaque monkey. *Journal of neurophysiology* 68 (4), 1332-1344.

Mcanany, J. J., Park, J. C. and Cao, D. (2015) Rod-and cone-isolated flicker electroretinograms and their response summation characteristics. *Visual neuroscience* 32, E018.

McCulloch, D. L., Marmor, M. F., Brigell, M. G., Hamilton, R., Holder, G. E., Tzekov, R. and Bach, M. (2015) ISCEV Standard for full-field clinical electroretinography (2015 update). *Documenta ophthalmologica* 130 (1), 1-12.

McKeefry, D., Kremers, J., Kommanapalli, D., Challa, N. K., Murray, I. J., Maguire, J. and Parry, N. R. (2014) Incremental and decremental L- and M-cone-driven ERG responses: I. Square-wave pulse stimulation. *Journal of the optical society of America* 31 (4), A159-A169.

Meigen, T. and Bach, M. (1999) On the statistical significance of electrophysiological steady-state responses. *Documenta ophthalmologica* 98 (3), 207-232.

Miyake, Y., Yagasaki, K., Horiguchi, M., Kawase, Y. and Kanda, T. (1986) Congenital stationary night blindness with negative electroretinogram: a new classification. *Archives of ophthalmology* 104 (7), 1013-1020.

Mortlock, K. E., Chiti, Z., Drasdo, N., Owens, D. R. and North, R. V. (2005) Silent substitution S-cone electroretinogram in subjects with diabetes mellitus. *Ophthalmic and physiological optics* 25 (5), 392-399.

Moskowitz, A., Hansen, R. M., Akula, J. D., Eklund, S. E. and Fulton, A. B. (2009) Rod and rod-driven function in achromatopsia and blue cone monochromatism. *Investigative ophthalmology & visual science* 50 (2), 950-958.

Mullen, K. T., Sakurai, M. and Chu, W. (2005) Does L/M cone opponency disappear in human periphery? *Perception* 34 (8), 951-959.

Muller, F., Wassle, H. and Voigt, T. (1988) Pharmacological modulation of the rod pathway in the cat retina. *Journal of neurophysiology* 59 (6), 1657-1672.

Murray, I., Parry, N., Carden, D. and Kulikowski, J. (1987) Human visual evoked-potentials to chromatic and achromatic gratings. *Clinical vision sciences* 1 (3), 231-244.

Naka, K. and Rushton, W. (1966) An attempt to analyse colour reception by electrophysiology. *The journal of physiology* 185 (3), 556.

Nathans, J., Thomas, D. and Hogness, D. S. (1986) Molecular genetics of human color vision: the genes encoding blue, green, and red pigments. *Science* 232 (4747), 193-202.

Neitz, J. and Neitz, M. (2011) The genetics of normal and defective color vision. *Vision research* 51 (7), 633-651.

Neitz, M. and Neitz, J. (2000) Molecular genetics of color vision and color vision defects. *Archives of ophthalmology* 118 (5), 691-700.

Neitz, M., Neitz, J. and Jacobs, G. H. (1991) Spectral tuning of pigments underlying red-green color vision. *Science* 252 (5008), 971-975.

Nelson, R. (1977) Cat cones have rod input: A comparison of the response properties of cones and horizontal cell bodies in the retina of the cat. *The journal of comparative neurology* 172 (1), 109-135.

Norren, D. V. and Padmos, P. (1973) Human and macaque blue cones studied with electroretinography. *Vision research* 13 (7), 1241-1254.

North, R. V., Jones, A. L., Drasdo, N., Wild, J. M. and Morgan, J. E. (2010) Electrophysiological evidence of early functional damage in glaucoma and ocular hypertension. *Investigative ophthalmology and visual science* 51 (2), 1216-1222.

Nusinowitz, S., Ridder III, W. and Ramirez, J. (2007) Temporal response properties of the primary and secondary rod-signaling pathways in normal and< i> Gnat2</i> mutant mice. *Experimental eye research* 84 (6), 1104-1114.

Odom, J. V., Bach, M., Brigell, M., Holder, G. E., McCulloch, D. L., Mizota, A., Tormene, A. P. and Vision, I. S. f. C. E. o. (2016) ISCEV standard for clinical visual evoked potentials:(2016 update). *Documenta ophthalmologica* 133 (1), 1-9.

Odom, J. V., Reits, D., Burgers, N. and Riemslag, F. C. (1992) Flicker electroretinograms: a systems analytic approach. *Optometry and vision science* 69 (2), 106-116.

Owsley, C., Jackson, G. R., Cideciyan, A. V., Huang, Y., Fine, S. L., Ho, A. C., Maguire, M. G., Lolley, V. and Jacobson, S. G. (2000) Psychophysical evidence for rod vulnerability in age-related macular degeneration. *Investigative ophthalmology and visual science* 41 (1), 267-273.

Padmos, P. and Van Norren, D. (1971) Cone spectral sensitivity and chromatic adaptation as revealed by human flicker-electroretinography. *Vision research* 11 (1), 27-42.

Park, J. C., Cao, D., Collison, F. T., Fishman, G. A. and McAnany, J. J. (2015) Rod and cone contributions to the dark-adapted 15-Hz flicker electroretinogram. *Documenta ophthalmologica* 130 (2), 111-119.

Parry, N. R., McKeefry, D. J., Kremers, J. and Murray, I. J. (2016) A dim view of M-cone onsets. *Journal of the optical society of America* 33 (3), A207-A213.

Parry, N. R., Murray, I. J., Panorgias, A., McKeefry, D. J., Lee, B. B. and Kremers, J. (2012) Simultaneous chromatic and luminance human electroretinogram responses. *The journal of physiology* 590 (13), 3141-3154.

Paulus, W., Homberg, V., Cunningham, K. and Halliday, A. (1986) Colour and brightness coding in the central nervous system: theoretical aspects and visual evoked potentials to homogeneous red and green stimuli. *Proceedings of the royal society of London B: Biological sciences* 227 (1246), 53-66.

Peachey, N. S., Alexander, K. R. and Fishman, G. A. (1989a) The luminance-response function of the dark-adapted human electroretinogram. *Vision research* 29 (3), 263-270.

Peachey, N. S., Alexander, K. R., Fishman, G. A. and Derlacki, D. J. (1989b) Properties of the human cone system electroretinogram during light adaptation. *Applied optics* 28 (6), 1145-1150.

Pearring, J. N., Bojang, P., Shen, Y., Koike, C., Furukawa, T., Nawy, S. and Gregg, R. G. (2011) A role for nyctalopin, a small leucine-rich repeat protein, in localizing the TRP melastatin 1 channel to retinal depolarizing bipolar cell dendrites. *Journal of neuroscience* 31 (27), 10060-10066.

Penn, R. and Hagins, W. (1972) Kinetics of the photocurrent of retinal rods. *Biophysical journal* 12 (8), 1073.

Pepperberg, D. R., Birch, D. G. and Hood, D. C. (1997) Photoresponses of human rods in vivo derived from paired-flash electroretinograms. *Visual neuroscience* 14 (1), 73-82.

Perlman, I., Barzilai, D., Haim, T. and Schramek, A. (1983) Night vision in a case of vitamin A deficiency due to malabsorption. *British journal of ophthalmology* 67 (1), 37-42.

Perry, V., Oehler, R. and Cowey, A. (1984) Retinal ganglion cells that project to the dorsal lateral geniculate nucleus in the macaque monkey. *Neuroscience* 12 (4), 1101-1123.

Petzold, A. and Plant, G. T. (2006) Clinical disorders affecting mesopic vision. *Ophthalmic and physiological optics* 26 (3), 326-341.

Pokorny, J., Smith, V. C. and Lutze, M. (1987) Aging of the human lens. *Applied optics* 26 (8), 1437-1440.

Pokorny, J., Smithson, H. and Quinlan, J. (2004) Photostimulator allowing independent control of rods and the three cone types. *Visual neuroscience* 21 (03), 263-267.

Pugh, E. and Lamb, T. D. (2000) Phototransduction in vertebrate rods and cones: molecular mechanisms of amplification, recovery and light adaptation. *Handbook of biological physics* 3, 183-255.

Rabin, J., Switkes, E., Crognale, M., Schneck, M. E. and Adams, A. J. (1994) Visual evoked potentials in three-dimensional color space: correlates of spatio-chromatic processing. *Vision research* 34 (20), 2657-2671.

Rangaswamy, N. V., Shirato, S., Kaneko, M., Digby, B. I., Robson, J. G. and Frishman, L. J. (2007) Effects of spectral characteristics of ganzfeld stimuli on the photopic negative response (PhNR) of the ERG. *Investigative ophthalmology and visual science* 48 (10), 4818-4828.

Raviola, E. and Gilula, N. B. (1973) Gap junctions between photoreceptor cells in the vertebrate retina. *Proceedings of the national academy of sciences* 70 (6), 1677-1681.

Regan, D. (1966) Some characteristics of average steady-state and transient responses evoked by modulated light. *Electroencephalography and clinical neurophysiology* 20 (3), 238-248.

Remmer, M. H., Rastogi, N., Ranka, M. P. and Ceisler, E. J. (2015) Achromatopsia: a review. *Current opinion in ophthalmology* 26 (5), 333-340.

Robson, J. and Frishman, L. (1995) Response linearity and kinetics of the cat retina: the bipolar cell component of the dark-adapted electroretinogram. *Visual neuroscience* 12 (05), 837-850.

Robson, J. G. and Frishman, L. J. (1998) Dissecting the dark-adapted electroretinogram. *Documenta ophthalmologica* 95 (3-4), 187-215.

Robson, J. G. and Frishman, L. J. (2014) The rod-driven a-wave of the dark-adapted mammalian electroretinogram. *Progress in retinal and eye research* 39, 1-22.

Rodieck, R. W. (1972) Components of the electroretinogram—a reappraisal. *Vision research* 12 (5), 773-780.

Rodieck, R. W. (1998) The first steps in seeing. *Sinauer associates*.

Rodriguez-Carmona, M., Harlow, A., Walker, G. and Barbur, J. (2005) The variability of normal trichromatic vision and the establishment of the "normal" range. *Proceedings of 10th congress of the international colour association, Granada* (Granada, 2005).

Román, A. J. and Jacobson, S. G. (1991) S cone-driven but not S cone-type electroretinograms in the enhanced S cone syndrome. *Experimental eye research* 53 (5), 685-690.

Rushton, W. (1972) Review lecture. Pigments and signals in colour vision. *The journal of physiology* 220 (3), 1P.

Sawusch, M., Pokorny, J. and Smith, V. C. (1987) Clinical electroretinography for short wavelength sensitive cones. *Investigative ophthalmology and visual science* 28 (6), 966-974.

Schallek, J., Kardon, R., Kwon, Y., Abramoff, M., Soliz, P. and Ts'o, D. (2009) Stimulus-evoked intrinsic optical signals in the retina: pharmacologic dissection reveals outer retinal origins. *Investigative ophthalmology and visual science* 50 (10), 4873-4880.

Schneeweis, D. M. and Schnapf, J. L. (1995) Photovoltage of rods and cones in the macaque retina. *Science* 268 (5213), 1053.

Scholl, H. and Kremers, J. (2001) Electroretinograms in S-cone monochromacy using S-cone and rod isolating stimuli. *Color research and application* 26 (S1), S136-S139.

Scholl, H., Langrova, H., Weber, B., Zrenner, E. and Apfelstedt-Sylla, E. (2001) Clinical electrophysiology of two rod pathways: normative values and clinical application. *Graefe's archive for clinical and experimental ophthalmology* 239 (2), 71-80.

Scholl, H. P. and Kremers, J. (2000) Large phase differences between L-cone- and M-cone-driven electroretinograms in retinitis pigmentosa. *Investigative ophthalmology and vision science* 41 (10), 3225-33.

Schwartz, E. A. (1974) Responses of bipolar cells in the retina of the turtle. *The journal of physiology* 236 (1), 211-224.

Scoles, D., Sulai, Y. N., Langlo, C. S., Fishman, G. A., Curcio, C. A., Carroll, J. and Dubra, A. (2014) In Vivo Imaging of Human Cone Photoreceptor Inner SegmentsIn Vivo Imaging of Photoreceptor Inner Segments. *Investigative ophthalmology and visual science* 55 (7), 4244-4251.

Sergouniotis, P. I., Robson, A. G., Li, Z., Devery, S., Holder, G. E., Moore, A. T. and Webster, A. R. (2012) A phenotypic study of congenital stationary night blindness (CSNB) associated with mutations in the GRM6 gene. *Acta ophthalmologica* 90 (3), e192-e197.

Shapiro, A. G., Pokorny, J. and Smith, V. C. (1996) Cone–rod receptor spaces with illustrations that use CRT phosphor and light-emitting-diode spectra. *Journal of the optical society of America* 13 (12), 2319-2328.

Shapley, R., Kaplan, E. and Soodak, R. (1981) Spatial summation and contrast sensitivity of X and Y cells in the lateral geniculate nucleus of the macaque. *Nature* 292 (5823), 543-545.

Shapley, R. and Perry, V. H. (1986) Cat and monkey retinal ganglion cells and their visual functional roles. *Trends in neurosciences* 9, 229-235.

Sharbrough, F., Chatrian, G., Lesser, R., Lüders, H., Nuwer, M. and Picton, T. (1991) American Electroencephalographic Society guidelines for standard electrode position nomenclature. *Journal of clinical neurophysiology* 8 (2), 200-202.

Sharpe, L. T. and Stockman, A. (1999) Rod pathways: the importance of seeing nothing. *Trends in neurosciences* 22 (11), 497-504.

Sharpe, L. T., Stockman, A. and MacLeod, D. I. (1989) Rod flicker perception: scotopic duality, phase lags and destructive interference. *Vision research* 29 (11), 1539-1559.

Shinomori, K. and Werner, J. S. (2012) Aging of human short-wave cone pathways. *Proceedings of the national academy of sciences* 109 (33), 13422-13427.

Sieving, P. and Nino, C. (1988) Scotopic threshold response (STR) of the human electroretinogram. *Investigative ophthalmology and visual science* 29 (11), 1608-1614.

Sieving, P. A., Murayama, K. and Naarendorp, F. (1994) Push–pull model of the primate photopic electroretinogram: a role for hyperpolarizing neurons in shaping the b-wave. *Visual neuroscience* 11 (03), 519-532.

Simonsen, S. E. and Rosenberg, T. (1995) Reappraisal of a short-wavelength-sensitive (S-cone) recording technique in routine clinical electroretinography. *Documenta ophthalmologica* 91 (4), 323-332.

Slaughter, M. M. and Miller, R. F. (1981) 2-amino-4-phosphonobutyric acid: a new pharmacological tool for retina research. *Science* 211 (4478), 182-5.

Slaughter, M. M. and Miller, R. F. (1983) The role of excitatory amino acid transmitters in the mudpuppy retina: an analysis with kainic acid and N-methyl aspartate. *The journal of neuroscience* 3 (8), 1701-1711.

Smith, N. and Lamb, T. (1997) The a-wave of the human electroretinogram recorded with a minimally invasive technique. *Vision research* 37 (21), 2943-2952.

Smith, R. G., Freed, M. A. and Sterling, P. (1986) Microcircuitry of the dark-adapted cat retina: functional architecture of the rod-cone network. *The journal of neuroscience* 6 (12), 3505-3517.

Smith, V. C. and Pokorny, J. (1975) Spectral sensitivity of the foveal cone photopigments between 400 and 500 nm. *Vision research* 15 (2), 161-171.

Sterling, P., Freed, M. A. and Smith, R. G. (1988) Architecture of rod and cone circuits to the on-beta ganglion cell. *The journal of neuroscience* 8 (2), 623-642.

Stiles, W. and Burch, J. (1955) Interim report to the Commission Internationale de l'Eclairage, Zurich, 1955, on the National Physical Laboratory's investigation of colour-matching (1955). *Journal of modern optics* 2 (4), 168-181.

Stockman, A. (2008) Physiologically-based color matching functions. Color and Imaging Conference. Vol. 2008. *Society for imaging science and technology*.

Stockman, A., MacLeod, D. I. and Johnson, N. E. (1993) Spectral sensitivities of the human cones. *Journal of the optical society of America* 10 (12), 2491-2521.

Stockman, A. and Sharpe, L. T. (1998) Human cone spectral sensitivities: a progress report. *Vision research* 38 (21), 3193-3206.

Stockman, A. and Sharpe, L. T. (2000) The spectral sensitivities of the middle-and long-wavelength-sensitive cones derived from measurements in observers of known genotype. *Vision research* 40 (13), 1711-1737.

Stockman, A. and Sharpe, L. T. (2006) Into the twilight zone: the complexities of mesopic vision and luminous efficiency. *Ophthalmic and physiological optics* 26 (3), 225-239.

Stockman, A., Sharpe, L. T. and Fach, C. (1999) The spectral sensitivity of the human short-wavelength sensitive cones derived from thresholds and color matches. *Vision research* 39 (17), 2901-2927.

Stockman, A., Sharpe, L. T., Rüther, K. and Nordby, K. (1995) Two signals in the human rod visual system: a model based on electrophysiological data. *Visual neuroscience* 12 (05), 951-970.

Stockman, A., Sharpe, L. T., Zrenner, E. and Nordby, K. (1991) Slow and fast pathways in the human rod visual system: electrophysiology and psychophysics. *Journal of the optical society of America* 8 (10), 1657-1665.

Swanson, W. H., Birch, D. G. and Anderson, J. L. (1993) S-cone function in patients with retinitis pigmentosa. *Investigative ophthalmology and visual science* 34 (11), 3045-3055.

Tomita, T. (1950) Studies on the intraretinal action potential part i. Relation between the localization of micro-pipette in the retina and the shape of the intraretinal action potential. *The Japanese journal of physiology* 1, 110-117.

Tsai, T. I., Jacob, M. M., McKeefry, D., Murray, I. J., Parry, N. R. and Kremers, J. (2016) Spatial properties of L-and M-cone driven incremental (On-) and decremental (Off-) electroretinograms: evidence for the involvement of multiple post-receptoral mechanisms. *Journal of the optical society of America* 33 (3), A1-A11.

Tyler, C. W. and Hamer, R. D. (1990) Analysis of visual modulation sensitivity. IV. Validity of the Ferry–Porter law. *Journal of the optical society of America* 7 (4), 743-758.

Usui, T., Kremers, J., Sharpe, L. T. and Zrenner, E. (1998) Flicker cone electroretinogram in dichromats and trichromats. *Vision research* 38 (21), 3391-3396.

Valberg, A., Lee, B. B. and Tigwell, D. A. (1986) Neurones with strong inhibitory s-cone inputs in the macaque lateral geniculate nucleus. *Vision research* 26 (7), 1061-1064.

Van der Tweel, L. and Lunel, H. V. (1965) Human visual responses to sinusoidally modulated light. *Electroencephalography and clinical neurophysiology* 18 (6), 587-598.

Van Norren, D. and Went, L. (1981) New test for the detection of tritan defects evaluated in two surveys. *Vision research* 21 (8), 1303-1306.

Vincent, A., Robson, A. G. and Holder, G. E. (2013) Pathognomonic (diagnostic) ERGs A Review and Update. *Retina* 33 (1), 5-12.

Viswanathan, S., Frishman, L. J., Robson, J. G., Harwerth, R. S. and Smith, E. (1999) The photopic negative response of the macaque electroretinogram: reduction by experimental glaucoma. *Investigative ophthalmology and visual science* 40 (6), 1124-1136.

Völgyi, B., Deans, M. R., Paul, D. L. and Bloomfield, S. A. (2004) Convergence and segregation of the multiple rod pathways in mammalian retina. *The journal of neuroscience* 24 (49), 11182-11192.

Vos, J. and Walraven, P. (1971) On the derivation of the foveal receptor primaries. *Vision research* 11 (8), 799-818.

Wali, N. and Leguire, L. E. (1991) Dark-adapted luminance-response functions with skin and corneal electrodes. *Documenta ophthalmologica* 76 (4), 367-375.

Wässle, H. (2004) Parallel processing in the mammalian retina. *Nature reviews neuroscience* 5 (10), 747-757.

Wassle, H. and Boycott, B. B. (1991) Functional architecture of the mammalian retina. *Physiological reviews* 71, 447-480.

Wässle, H., Yamashita, M., Greferath, U., Grünert, U. and Müller, F. (1991) The rod bipolar cell of the mammalian retina. *Visual neuroscience* 7 (1-2), 99-112.

Werblin, F. S. and Dowling, J. E. (1969) Organization of the retina of the mudpuppy, Necturus maculosus. II. Intracellular recording. *Journal of neurophysiology* 32 (3), 339-355.

Werner, J. (2005) Night vision in the elderly: consequences for seeing through a “blue filtering” intraocular lens. *British journal of ophthalmology* 89 (11), 1518-1521.

Werner, J. S., Bieber, M. L. and Schefrin, B. E. (2000) Senescence of foveal and parafoveal cone sensitivities and their relations to macular pigment density *Journal of the optical society of America* 17 (11), 1918-1932.

Wiesel, T. N. and Hubel, D. H. (1966) Spatial and chromatic interactions in the lateral geniculate body of the rhesus monkey. *Journal of neurophysiology* 29 (6), 1115-56.

Witkovsky, P., Dudek, F. E. and Ripps, H. (1975) Slow PIII component of the carp electroretinogram. *The journal of general physiology* 65 (2), 119-134.

Wysecki, G. and Stiles, W. (1967) *Color science*. *Wiley, NY.*

Xu, X. and Karwoski, C. J. (1994) Current source density analysis of retinal field potentials II. Pharmacological analysis of the b-wave and M-wave. *Journal of neurophysiology* 72 (1), 96-105.

Yamamoto, S., Kamiyama, M., Nitta, K., Yamada, T. and Hayasaka, S. (1996) Selective reduction of the S cone electroretinogram in diabetes. *British journal of ophthalmology* 80 (11), 973-975.

Zeitz, C., Robson, A. G. and Audo, I. (2015) Congenital stationary night blindness: an analysis and update of genotype–phenotype correlations and pathogenic mechanisms. *Progress in retinal and eye research* 45, 58-110.

Zele, A. J. and Cao, D. (2014) Vision under mesopic and scotopic illumination. *Frontiers in Psychology* 5, 1594.

Zrenner, E. and Gouras, P. (1979) Blue-sensitive cones of the cat produce a rodlike electroretinogram. *Investigative ophthalmology and visual science* 18 (10), 1076-1081.

Zrenner, E., Nelson, R. and Mariani, A. (1983) Intracellular recordings from a biplexiform ganglion cell in macaque retina, stained with horseradish peroxidase. *Brain research* 262 (2), 181-185.

Appendix A

Reprint: Rod Electroretinograms Elicited by Silent Substitution Stimuli from the Light Adapted Human Eye

tvst

DOI: 10.1167/tvst.5.4.13

Article

Rod Electroretinograms Elicited by Silent Substitution Stimuli from the Light-Adapted Human Eye

John Maguire[1], Neil R. A. Parry[1–3], Jan Kremers[4], Deepika Kommanapalli[1], Ian J. Murray[5], and Declan J. McKeefry[1]

[1] Bradford School of Optometry and Vision Sciences, Bradford University, UK
[2] Vision Science Centre, Manchester Royal Eye Hospital, Central Manchester University Hospitals NHS Foundation Trust, Manchester Academic Health Science Centre, Manchester, UK
[3] Centre for Ophthalmology and Vision Sciences, Institute of Human Development, Faculty of Medical and Human Sciences, University of Manchester, UK
[4] Department of Ophthalmology, University Hospital Erlangen, Germany
[5] Faculty of Biology, Medicine & Health, University of Manchester, UK

Correspondence: Declan J. McKeefry; Bradford School of Optometry & Vision Sciences, University of Bradford, Bradford, BD7 1DP, W. Yorks, UK. e-mail: d.mckeefry@bradford.ac.uk

Received: 2 March 2016
Accepted: 16 June 2016
Published: 31 August 2016

Keywords: electroretinogram (ERG); rods; silent substitution

Citation: Maguire J, Parry NRA, Kremers J, Kommanapalli D, Murray IJ, McKeefry DJ. Rod electroretinograms elicited by silent substitution stimuli from the light-adapted human eye. Trans Vis Sci Tech. 5(4):13, doi:10.1167/tvst.5.4.13

Purpose: To demonstrate that silent substitution stimuli can be used to generate electroretinograms (ERGs) that effectively isolate rod photoreceptor function in humans without the need for dark adaptation, and that this approach constitutes a viable alternative to current clinical standard testing protocols.

Methods: Rod-isolating and non-isolating sinusoidal flicker stimuli were generated on a 4 primary light-emitting diode (LED) Ganzfeld stimulator to elicit ERGs from participants with normal and compromised rod function who had not undergone dark-adaptation. Responses were subjected to Fourier analysis, and the amplitude and phase of the fundamental were used to examine temporal frequency and retinal illuminance response characteristics.

Results: Electroretinograms elicited by rod-isolating silent substitution stimuli exhibit low-pass temporal frequency response characteristics with an upper response limit of 30 Hz. Responses are optimal between 5 and 8 Hz and between 10 and 100 photopic trolands (Td). There is a significant correlation between the response amplitudes obtained with the silent substitution method and current standard clinical protocols. Analysis of signal-to-noise ratios reveals significant differences between subjects with normal and compromised rod function.

Conclusions: Silent substitution provides an effective method for the isolation of human rod photoreceptor function in subjects with normal as well as compromised rod function when stimuli are used within appropriate parameter ranges.

Translational Relevance: This method of generating rod-mediated ERGs can be achieved without time-consuming periods of dark adaptation, provides improved isolation of rod- from cone-based activity, and will lead to the development of faster clinical electrophysiologic testing protocols with improved selectivity.

Introduction

The flash electroretinogram (ERG) is an electrical response elicited from the retina in response to stimulation by light. The ERG is generated by contributions from many different retinal cells types, but with appropriate manipulation of the temporal, chromatic, and luminance characteristics of the stimulus, as well as the subject's adaptational state, it is possible to selectively stimulate and assess the functional characteristics of discrete populations of retinal neurons.[1,2] In particular, the isolation of rod photoreceptor activity has long been considered important from a clinical perspective as many congenital and acquired visual disorders can differentially affect rod relative to cone function. The ability to elicit ERGs that selectively reflect the activity of rods has had a key role in the diagnosis and monitoring of conditions, such as retinitis pigmentosa, congenital stationary night blindness (CSNB), and vitamin A deficiency.[3–7] In age-related

macular degeneration (ARMD), some of the earliest pathological and functional changes occur in rod-mediated vision in geographically localized regions of the retina.[8] In addition, it has been shown that normal younger individuals who carry a high genetic risk of ARMD developing in later life exhibit subtle changes in rod-mediated mesopic vision.[9] Thus, there are compelling clinical reasons for methods that selectively assess rod function in humans.

The most frequently employed method of isolating rod function has centered on the use of stimuli of low light intensity after rod sensitivity has been maximized by a 20- to 30-minute period of dark adaption.[10] An alternative, but less frequently used, means of isolating ERGs from rods involves the method of silent substitution,[11,12] which is based on the principle of univariance.[13] The isolation of rod photoreceptor activity requires alternation between two stimuli which contain mixtures of wavelengths at different intensities. The alternation elicits no overall change in excitation in the L-, M-, and S-cone classes, but does elicit a change in rod excitation. The basic rule is that the isolation of 1 of n classes of photoreceptor requires a minimum of n primaries tuned to different wavelengths. Theoretically, any desired combination of photoreceptor excitation modulation can be achieved without changing the state of adaptation, a major advantage of this approach. With the increased commercial availability of light-emitting diode (LED) Ganzfeld stimulators containing at least 4 primaries, researchers now have the prospect of more precise control of ERG stimuli. This improved precision, coupled with our knowledge of cone and rod spectral characteristics, enables better control of photoreceptor excitation.[14] Stimuli based on the silent substitution method already have been applied in previous ERG studies of rod function.[15–19] However, despite the obvious advantages afforded by silent substitution, there is a clear need to demonstrate that the ERGs elicited by such rod-isolating stimuli do, in fact, selectively reflect rod function and are free from intrusions from cone photoreceptors, which normally predominate at higher mesopic and photopic light levels in the light-adapted human retina.[20,21]

The aim of this study was to demonstrate that stimuli generated using the silent substitution method enable the functional assessment of rods without the confounding effects of cone intrusion. Specifically, we examined ERGs obtained using rod-isolating stimuli in terms of temporal frequency and luminance characteristics. Rod vision has a lower temporal resolution limit than that mediated by cones.[22–28] At high scotopic levels of illumination rod temporal resolution can reach up to 28 Hz.[26–28] Cones, by comparison, can support a temporal resolution limit in excess of 60 Hz[28] and previous work has demonstrated that the cone flicker ERG can be recorded at frequencies up to 100 Hz in visually normal subjects.[29] Therefore, we wanted to exploit this difference to test the selectivity of our rod-isolating stimuli. We also assessed retinal illuminance response characteristics. Rod ERGs typically are measured using low intensity stimuli at scotopic levels of illumination.[30–34] This allows the study of rod responses free from the cone intrusions, which become increasingly more predominant as the stimuli increase to mesopic and photopic light levels.[20,21] However, in the light-adapted eye, stimuli of higher intensity must be used and this will require caution as we have to ensure rod selectivity is maintained and that cone intrusions are minimized. Measuring the ERG response as a function of retinal illuminance will help us to gauge the extent of such intrusions.

By examination of the temporal and retinal illuminance response characteristics we assessed the suitability of ERGs generated by silent substitution for the assessment of rod function in humans. In doing so, we attempted to define stimulus conditions for which rod responses can be optimized and identify parameter ranges beyond which the effects of cone intrusion can be demonstrated. Overall, this approach will lead to the development of better clinical testing protocols for the acquisition of rod-mediated ERGs for which there will be improved selectivity and reduced clinical testing times. To demonstrate this and assess the wider clinical applicability of our light-adapted silent substitution protocol, a second aim of this study was to compare the results to existing International Society for Clinical Electrophysiology of Vision (ISCEV) standard protocols in patient groups with normal and compromised rod function.

Methods

Stimuli

Sinusoidal, full-field flicker stimuli with temporal frequencies ranging between 5 and 100 Hz were presented using a ColorDome (Diagnosys LLC, Lowell, MA) four primary Ganzfeld stimulator with blue (460 nm), green (514 nm), amber (592 nm), and red (632 nm) LEDs. The spectral characteristics, chromaticities, and luminances of each class of LED

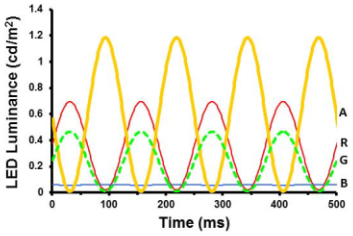

Figure 1. The luminance profiles and relative phases of the *blue* (*B*), *green* (*G*), *amber* (*A*) and *red* (*R*) LEDs that are required to generate a 63 Td, 8 Hz rod-isolating silent substitution stimulus. The modulation of rod excitation for the resultant stimulus = 0.25.

were measured and calibrated using a PR650 spectrophotometer (Photo Research, Inc., Chatsworth, CA). To obtain silent substitution stimuli photoreceptor excitations were calculated by multiplying the emission spectra of the LEDs with cone fundamentals and the V'_λ 10° function.[35,36] (see Appendix 1). Wavelength and intensity combinations produced no changes in net excitation in three of the four photoreceptor populations; thus, these were triple silent substitution stimuli.[11,12,37,38] Figure 1 shows how the luminance outputs of the four LEDs vary as a function of time to produce a silent substitution rod-isolating stimulus (8 Hz, 63 Td). Contrast was defined as the Michelson contrast of rod excitation and was set at 0.25 for all stimuli. Retinal illuminance varied between 1 and 12,000 photopic trolands (Td). We have used photopic as opposed to scotopic Tds throughout the study, since it would be arbitrary to change units when going from high to low stimulus intensities and also would confuse the examination of ERGs across mesopic-photopic illumination transitions. For the stimulus set used in this study, conversion from photopic to scotopic Tds is achieved by multiplying by a factor of 2.489.[36]

We also used L-cone isolating stimuli ($C = 0.25$) to compare ERGs mediated by the two photoreceptor populations. In addition, we also generated non-selective, non-isolating stimuli that elicited simultaneous excitation of rods and cones. These stimuli were generated by the same method described in Appendix 1, except that L- and M-cone modulations ($C = 0.3$) were added to the standard rod-isolating stimulus. Another non-selective "white" stimulus also was used and this was generated by modulating all of the LEDs in phase, the resultant stimulus produced the same excitation (0.25) across all four photoreceptors.

ERG Recording

Electroretinograms were recorded from the right eye using a silver/nylon corneal fiber electrode (Department of Physics and Clinical Engineering, Royal Liverpool University Hospital, UK) referenced to a 9-mm Ag/AgCl electrode (Biosense Medical, Chelmsford, UK) on the outer canthus; a similar electrode was affixed to the forehead to serve as ground. Impedance was maintained below 5 kΩ. Signals were recorded using the Espion E^2 system (Diagnosys LLC) which amplified and filtered (bandwidth = 1 to 300 Hz) the ERGs and digitized them at a rate of 1000 Hz. Retinal responses to the flicker stimuli were acquired over 4-second epochs with subsequent offline analysis being performed on an average of a minimum of 8 of these epochs. Participants viewed the stimuli monocularly and fixation was maintained on a central point which subtended approximately 0.5°. Participants underwent pupillary dilation (1% tropicamide); the mean (dilated) pupil diameter across the 7 subjects was 8 mm (SD = 1.78), and this value was used in the computation of retinal illuminance. Before each recording session they sat in the testing room, which had an illumination level of 500 lux, for 5 minutes.

Data Analysis

Following acquisition, the averaged traces were subjected to a two-stage offline analysis involving, firstly, resampling of the traces and then, secondly, subjecting these resampled traces to Fourier analysis. The first stage was necessary because the Espion system samples at 1000 Hz producing 4000 points over the recording epoch. To perform a Fast Fourier Transform (FFT) 2^n data points (where n = integer value) are required, so a method of interpolation was used to resample the averaged traces to give 4096 data points. The resampled traces then were imported into Signal software (version 2.16; Cambridge Electronic Design, Cambridge, UK) and subjected to a FFT. This analysis provided a measure of the amplitude and phase of the response at the stimulation frequency (i.e., the fundamental, F) as well as higher harmonics (2F). The phase values generated by the FFT can provide values that cycle in multiples of 360°. To "unwrap" these phase values we either added or subtracted multiples of 2π radians (360°) to minimize the phase differences measured between the adjacent sampled temporal frequencies.[38] Noise (N) was defined as the mean amplitude (A) of the response at the stimulus frequency minus 1 Hz and

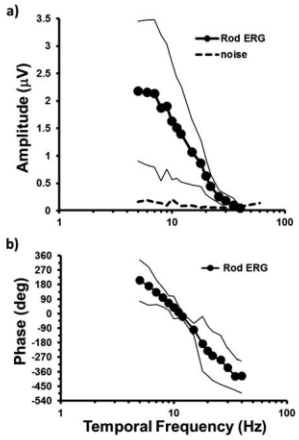

Figure 2. Electroretinogram (ERG) amplitude (a) and phase (b) of the fundamental component as function of temporal frequency obtained for a 63 Td rod-isolating silent substitution stimulus ($C = 0.25$). The data shown are the group ($n = 5$) averaged results and the *thin solid lines* represent ±1 SD from the mean. The *thick dashed line* (a) plots the measure of noise (see Methods).

plus 1 Hz:

$$N = \frac{A_{(F-1\mathrm{Hz})} + A_{(F+1\mathrm{Hz})}}{2} \qquad (1)$$

A response was considered significant if the measured ERG amplitude was a least 2.82 times greater than the computed noise amplitude for that frequency.[39]

Participants

In the first part of this study where the objectives were to characterize the response properties of the rod-mediated ERGs and optimize stimulus parameters, a total of 7 color normal trichromats (3 males; mean age, 28 years; age range, 35 years) were used. Color vision in all subjects was assessed using the City University Colour Vision Test (second edition), the Farnsworth Munsell 100 Hue test, and the HMC Anomaloscope (Oculus, Wetzlar, Germany). In the second part of the study we wanted to assess the wider clinical application of our techniques. As well as measuring responses to our 8 Hz 63 Td rod-isolating stimulus, we also measured rod- and cone (30 Hz) ERGs using standard ISCEV clinical protocols[10] in a cohort of 28 subjects (17 females; mean age, 36.8 years; age range, 52 years), 18 of whom had normal rod function and 10 of whom had compromised rod function (6 diagnosed with rod or rod/cone dystrophy, 2 with CSNB type 1, 2 with CSNB type 2). All participants gave informed consent before the commencement of the experiments, which were conducted in accordance with the Declaration of Helsinki and were approved by the University of Bradford Ethics Committee.

Results

Temporal Frequency Response Characteristics

Figure 2 shows the variation in ERG amplitude and phase as a function of temporal frequency for a 63 Td rod-isolating stimulus. The data shown are the group (vector) averaged responses ($n = 5$) and were obtained without dark adaptation. These results are similar to previous studies.[29] The data describe a low-pass temporal function and, consistent with psychophysically obtained estimates of the temporal resolution limit of rods,[26] the ERG amplitude relative to noise falls below significance between 26 and 30 Hz.

We compared the temporal frequency response functions obtained using silent substitution rod-isolating stimuli with those using non-isolating stimuli. Figure 3 shows the amplitude (Fig. 3a) and phase (Fig. 3c) of the ERG response fundamental obtained using a dim (63 Td) white light stimulus. Compared to those generated by the rod-isolating stimuli (also shown in Fig. 3) the temporal response functions elicited by the non-isolating stimuli are very different. In terms of amplitude, ERGs elicited by the dim white stimulus are reduced at low temporal frequencies (<15 Hz) while at frequencies normally considered beyond the range of rod photoreceptors (>30 Hz) responses still are obtainable well above noise levels. The phase plots show that beyond 18 Hz there is a discontinuity in response which is likely to reflect contributions from other (presumably cone-based) mechanisms at higher temporal frequencies. Figures 3b and 3d show the temporal response functions obtained from rod-isolating stimuli to which we have intentionally added L-cone modulation ($C = 0.30$), via manipulation of the luminance outputs and relative phases of the four LEDs. The addition of cone modulation to the erstwhile rod-isolating stimulus again has characteristic effects on the amplitude and phase responses as a function of temporal frequency. In terms of amplitude, the

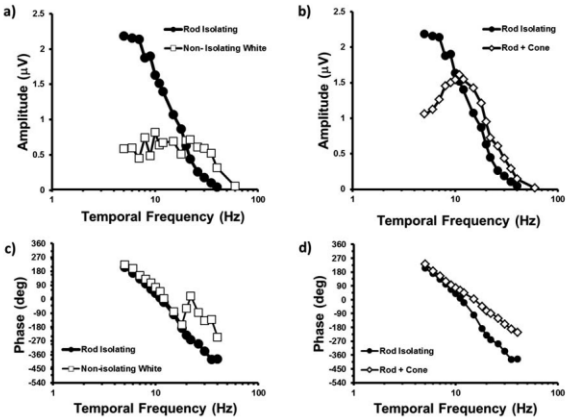

Figure 3. *Left*: Comparison between the variations in ERG (fundamental) amplitude (a) and phase (c) as function of temporal frequency obtained for a 63 Td rod-isolating (*filled circles*) and a 63 Td non-isolating white stimulus (*empty squares*). *Right*: Comparison between the variations in ERG (fundamental) amplitude (b) and phase (c) as function of temporal frequency obtained for a 63Td rod-isolating (*filled circles*) and a 63 Td stimulus which modulates rods (0.25) and L-cones (0.30; *empty diamonds*).

addition of cone modulation generates a more band-pass temporal response function, compared to the low-pass function obtained using a purely rod-isolating stimuli, with response amplitude being markedly reduced at low temporal frequencies. Similar reductions for combined rod/cone stimuli have been noted previously[19] and have been attributed to destructive interference between signals emanating from the different photoreceptor populations. The addition of cone modulation leads to a gradual phase advance of the response relative to that of the isolated rod response at higher temporal frequencies.

To eliminate intrusions from cones, rod ERGs typically have been elicited using low intensity scotopic stimuli.[32] To what extent does the use of silent substitution stimuli free the experimenter from this constraint? Figure 4 shows the amplitude and phase variation of the ERG fundamental as a function of temporal frequency obtained using rod-isolating stimuli with retinal illuminances extending well into the photopic range. Increasing the retinal illuminance of the stimulus up to 120 Td decreases the response amplitude at low temporal frequencies but the limit of temporal response is similar to that obtained at 63 Td as signal amplitude relative to noise falls below significance between 26 and 30 Hz. When stimulus illuminance is increased to high photopic

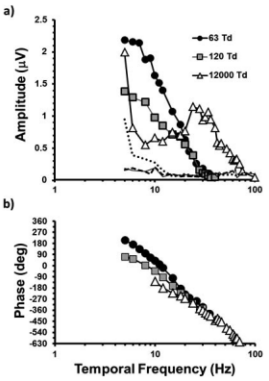

Figure 4. ERG temporal response functions for (s) amplitude and (b) phase of the fundamental obtained using rod-isolating stimuli at retinal illuminances equal to 63, 120, and 12,000 Td. The data represent the group vector average ($n = 5$). The *thick dashed line*, *solid thin line*, and *dotted line* represent the noise for 63, 120, and 12,000 Td conditions, respectively, and phase is plotted only for temporal frequencies where signal was 2.82× greater than noise.

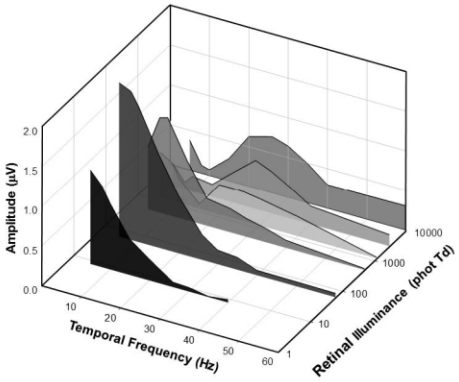

Figure 5. ERG (fundamental) temporal response functions obtained using rod-isolating stimuli at retinal illuminances: 8, 63, 500, 1200, 3000, and 10,000 photopic Td. The data represent vector averaged group ($n = 4$) responses.

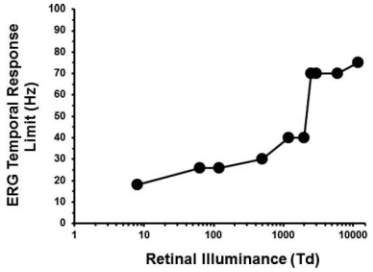

Figure 6. The temporal response limit of the ERG elicited by a rod-isolating stimulus as a function of retinal illuminance (see text for calculation).

illumination levels (12,000 Td) the temporal response function of the ERG takes on a very different form and becomes more band-pass in appearance, peaking at approximately 30 Hz. In addition the temporal response limit extends to higher frequencies. The function in effect becomes more like the cone temporal response function[29,30] and clearly indicates a loss of rod selectivity in the ERG at these light levels.

To examine more closely the stimulus intensity range over which the transition from rod- to cone-like temporal frequency response characteristic occurred, we measured a series of temporal response curves in four subjects. These were sampled less frequently in the temporal domain compared to the previous experiment, but used a larger range of retinal illuminances (8, 63, 500, 1200, 3000, and 10,000 photopic Td). The results are shown as a three-dimensional plot in Figure 5. The temporal functions generated by the stimuli of lower (8, 63, and 500 Td) and higher (1200, 3000, and 10,000 Td) illuminance are qualitatively very different; the former are low-pass in nature contrasting with the latter, which have more band-pass shape where responses still can be obtained for frequencies greater than 30 Hz.

In Figure 6, a measure of the temporal response limit of the ERG is plotted as a function of stimulus illuminance. This value was computed as the temporal frequency at which signal amplitude fell below the criterion for significance (i.e., 2.82 × noise amplitude). These temporal response functions were obtained for a single subject using rod-isolating stimuli ranging from 8 up to 12,000 Td and the ERG temporal response limit was calculated for each condition. The resultant plot shows that, at high illuminance levels (>2000 Td), the temporal response limit of the ERG is in excess of 60 Hz—a level that is incompatible with rod function but is more in keeping with the properties of cone photoreceptors.[33,34] Below 1000 Td the temporal response limit falls to 20 to 30 Hz, a value that is consistent with psychophysical measures of rod temporal properties obtained at higher scotopic illumination levels.[26–28]

The phase data plotted in Figure 4b for the 63, 120, and 12,000 Td stimuli are useful as they can provide information about the temporal characteristics of the neuronal mechanisms that underpin the generation of the response. Specifically, the slope of the function provides a measure of what is known as apparent latency and provides a measure of response delay.[40,41] Apparent latency (τ) is given by:

$$\tau = -\frac{1}{360} \times \left(\frac{\Delta\phi}{\Delta ft}\right) \quad (2)$$

where ϕ is response phase and ft the temporal frequency of the stimulation. In Figure 7, the apparent latency is plotted as a function of temporal frequency for the 63, 1200, and 12,000 Td "rod-isolating" stimuli. Each data point is calculated from the slope of a linear regression line fitted to 5 adjacent data points on the phase versus linear temporal frequency function. Constant values of apparent latency imply that physiologic mechanisms that underpin the generation of the response have similar

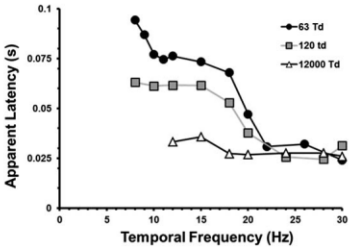

Figure 7. Apparent latency plotted as a function of temporal frequency for ERGs elicited by rod-isolating stimuli of retinal illuminance equal to 63, 1200, and 12,000 Td.

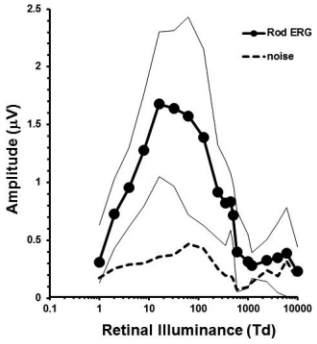

Figure 8. ERG (fundamental) response amplitude for an 8 Hz sinusoidal rod-isolating flicker stimulus plotted as a function of retinal illuminance (photopic Td). The *dashed line* plots the measure of noise as a function of stimulus illuminance. The data shown (*thick solid line filled circles*) are the group ($n = 5$) averaged data and the *thin solid lines* represent ±1 SD from the mean.

temporal response properties.[29] In this respect, the function derived from the 12,000 Td phase data is the simplest in that a relatively constant value for apparent latency is returned across the temporal frequency range tested. This suggests that a common mechanism with a short response delay (i.e., fast temporal response characteristics) underpins the ERG response to this stimulus. In view of the temporal response functions shown above for such high intensity stimuli, it would seem likely that cone-based mechanisms are the most likely generators of these responses. For the 120 and 63 Td stimuli, the apparent latency functions have two regions where a constant value is returned; the first is between 22 and 30 Hz where apparent latency values converge on a value similar to ERGs elicited by the 12,000 Td stimuli, implying that they are generated by mechanisms with common temporal response properties. A second constant region, indicating a different temporal mechanism, is found between 10 and 15 Hz. Between the two lies a transitional region (15–22 Hz) where the function has a non-zero slope. For the 63 Td stimuli, there also is an additional transitional region below 8 Hz which points to the possible existence of a third even slower mechanism (i.e., with increased apparent latency) that operates across low stimulus intensities and low temporal frequencies. The existence of multiple mechanisms with different temporal properties that contribute to the generation of rod-mediated ERG is consistent with previous studies.[26,28,31,42–44]

Retinal Illuminance Response Characteristics

Figure 8 shows the group averaged data where ERG amplitude measured with an 8 Hz rod-isolating stimulus is plotted as a function of retinal illuminance. Response amplitude increases as a function of illuminance reaching a peak between 10 and 100 Td where the response is significantly greater than noise. Response amplitude then falls towards noise levels at 1000 to 2000 Td; there may be a small increase for higher illuminances but this rarely exceeds our criterion for significance (>2.82 × noise).

By way of comparison, Figure 9 shows ERG amplitude as a function of retinal illuminance for an 8 Hz L-cone isolating stimulus of the same temporal frequency and with a cone contrast of 0.25. The data plotted were obtained from a subset ($n = 2$) of the main experimental group and demonstrate that the cone-mediated response behaves very differently from that of the rod ERG. Unlike the rod-mediated ERG the L-cone response exhibits an increase in response amplitude with increasing retinal illuminance showing no sign of the peak response between 10 and 100 Td. Another key point is that, in the region where the rod response reaches its maximum (~30 Td) the cone response barely rises above noise levels.

In addition to 8 Hz stimulation, we also examined ERG amplitude as a function of retinal illuminance (less densely sampled) at other stimulation frequencies. Figure 10 shows the averaged data from 4 subjects for rod-isolated ERGs elicited by stimulation frequencies of 5, 10, 15, and 30 Hz. For all but the highest stimulation frequency the responses are similar to the 8 Hz data in that the responses all

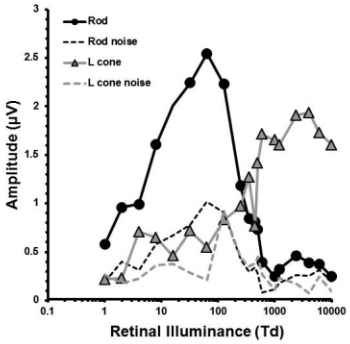

Figure 9. ERG (fundamental) response amplitude for 8 Hz sinusoidal rod (*black circles*) and L-cone (*gray triangles*) isolating flicker stimuli plotted as a function of retinal illuminance (photopic Td). The *dashed lines* plot the measure of noise as a function of stimulus illuminance. The data shown are averaged data from a subset of 2 subjects.

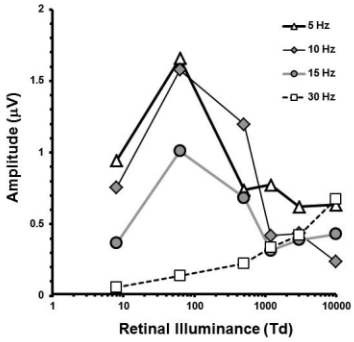

Figure 10. ERG (fundamental) response amplitude sinusoidal rod-isolating flicker stimuli plotted as a function of retinal illuminance (photopic Td) for stimuli of temporal frequency = 5, 10, 15, and 30 Hz. The data represent the group average from $n = 4$ subjects.

reach maximum amplitude at approximately 100 Td, then decrease with increasing illuminance. The data obtained from the 30 Hz stimulus follow a different response pattern; below 1000 Td it is barely recordable above noise levels but exhibits a steady increase in amplitude with increasing retinal illuminance, similar to the L-cone isolated response shown in Figure 9.

Comparison with Current Clinical Protocols

To assess the wider clinical applications of the silent substitution stimuli, we recorded ERGs in a group of normal participants ($n = 18$) using our 8 Hz rod-isolating stimulus and compared them to ERGs obtained from the same cohort using current ISCEV standard protocols[10] for isolating rod- (dark-adapted; 0.01 cd/s/m^2) as well as cone (light-adapted 3.0 cd/s/m^2 flicker [30 Hz])–mediated ERGs. Figure 11a plots the amplitude of the ERGs obtained using the 8 Hz silent substitution stimulus against those obtained for the ISCEV dark-adapted 0.01 protocol. There is a significant positive correlation between these two measures of rod function ($r = 0.626$, $n = 18$, $P < 0.005$, $R^2 = 0.39$). Figure 11b plots the correlation between the 8 Hz rod-isolating stimulus and the ISCEV light-adapted 3.0 cd/s/m^2 flicker response. These two measures would not be expected to exhibit a significant correlation as they purportedly separately assay rod and cone function, respectively. Our results demonstrated that this, indeed, is the case ($r = 0.38$, $n = 18$, $P = 0.881$, $R^2 = 0.0015$). However, when a similar analysis is performed for the data collected with the ISCEV dark-adapted 0.01 and light-adapted 3.0 flicker protocols a significant positive correlation is found ($r = 0.512$, $n = 18$, $P = 0.03$, $R^2 = 0.26$).

So far, we have considered the use of the silent substitution protocol in light-adapted participants with normal rod function. An important question is whether this new approach can be applied usefully in a clinical population with compromised rod function who may exhibit additional complications,, such as reduced visual acuity or nystagmus, for example. To address this issue we recorded ERGs from a cohort of 10 individuals, all of whom have compromised or severely reduced rod function due to rod/cone dystrophy ($n = 6$) or CSNB (type 1 [$n = 2$], type 2 [$n = 2$]). Figure 12a shows this group, now added to the normals previously shown in Figure 11a, where response amplitude for the 8 Hz rod-isolating is plotted against the ISCEV dark-adapted 0.01 protocol. Analysis, now including this patient group, demonstrates a stronger correlation ($r = 0.785$, $n = 28$, $P < 0.001$, $R^2 = 0.62$) between both measures of rod function.

Compared to the ISCEV clinical standard for generating rod ERGs, the absolute amplitude values are lower for our method. However, what is arguably more important than the absolute amplitude in this context is the signal-to-noise ratio (SNR). In Figure

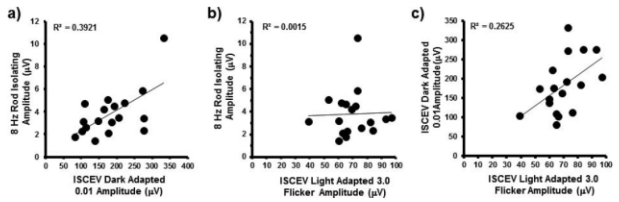

Figure 11. Correlation between ERG response amplitudes elicited by different testing protocols: (a) compares the amplitudes of the 8 Hz silent substitution rod-isolating (63 photopic Td) ERGs with those obtained for the ISCEV dark adapted 0.01 protocol, (b) compares the 8 Hz silent substitution with the ISCEV light adapted 3.0 flicker (30 Hz) response, and (c) compares the ISCEV dark-adapted and light-adapted responses. The data were collected from 18 normal participants.

12b the distributions of SNR are plotted for the normal and compromised rod function groups. Comparison of these distributions (Mann-Whitney U test) shows that the SNR ratio in the normal group is statistically significantly higher than in the group with abnormal rod function ($U = 0.0$, $P < 0.001$) and demonstrates that the rod-isolating silent substitution protocol has the potential to differentiate between subjects with normal and compromised rod function.

Discussion

In this study, we have demonstrated that, using silent substitution stimuli, it is possible to elicit ERGs with response characteristics that are consistent with known properties of rod-mediated vision. Rod ERGs are optimal for stimuli of temporal frequencies between 5 and 8 Hz and retinal illuminances between 10 and 100 photopic Td. Importantly, isolation of rod function can be achieved without prior dark adaptation and without the need for stimuli restricted to low scotopic light intensities. The low-pass, low resolution (<30 Hz) ERG temporal frequency response functions generated by rod-isolating stimuli constitute a key piece of evidence supporting the fact that silent substitution stimuli provide a selective assay of rod-mediated visual function.[30] Importantly, our measures of the temporal response limit of the rod ERG are consistent with psychophysical measures of rod function obtained at high scotopic light levels.[26,27] While this functional selectivity for rods is maintained for ERG responses elicited by silent substitution stimuli at mesopic and low photopic intensity levels, it is absent at levels of retinal illumination greater than 1000 Td. Above this level ERG temporal frequency response curves take on a more band-pass form and responses can be elicited by stimuli of frequencies in excess of 60 Hz. Such properties are incompatible with rod function. They are more consistent with their mediation by cone photoreceptors[28,30] and indicate that ERGs elicited beyond this parameter range are no longer rod-selective.

A number of studies have demonstrated the existence of separate pathways for the transmission of temporal information by rods (see prior review[44]). The existence of these pathways has been revealed by changes in the temporal resolution of the rod system with increasing stimulus intensity as well as phase-dependent interactions observed in psychophysical and electrophysiologic experiments.[20,26 29,42 45] These multiple processing pathways are based on the fact that rod signals have at least two, but probably more,[46] routes via which they can pass from outer to inner retina.[48] One route is via rod bipolar cells to AII amacrine cells.[48 50] This forms the so-called "slow" rod pathway, which operates over scotopic levels of

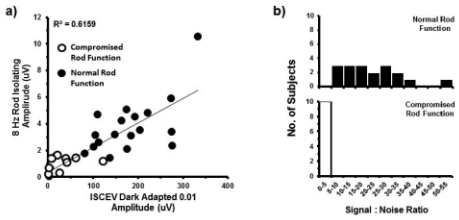

Figure 12. (a) Correlation between ERGs obtained with a standard ISCEV dark adapted 0.01 stimulus and those obtained with an 8Hz sinusoidal rod-isolating silent substitution stimulus. Recordings were made from 18 subjects with normal rod function (*filled circles*) and 10 subjects with compromised rod function. (b) Distribution of the signal-to-noise ratio calculated for the 8 Hz rod-isolating ERG data are shown for the normal (*upper panel*) and compromised (*lower panel*) rod function groups.

illumination. A "fast" rod pathway, which operates at higher intensity levels, is thought to be mediated anatomically by gap junctions that allow the passage of rod signals directly to cones and then via cone bipolar cells to ganglion cells.[49,51 53] A key question is whether ERGs elicited by silent substitution stimuli show evidence of similar temporal mechanisms. Examination of the apparent latency data (Fig. 7) would indicate that this is, indeed, the case. The plots of apparent latency versus temporal frequency exhibit distinct lobes for low intensity rod-isolating stimuli, indicating the existence of multiple generators of the ERG response with different temporal characteristics. Furthermore, an important transitional region between one mechanism and the other occurs between 15 and 20 Hz. This is consistent with psychophysical studies where the measurements of critical fusion frequency versus intensity also show this to be a key region in the transfer from slow to fast rod pathways.[44,54] Previous studies that have used silent substitution to generate rod-isolating stimuli have found that rod function can be assessed over a wider range of stimulus intensities than that which might be expected using non-isolating flash stimuli.[17,18] However, with the use of more intense stimuli comes the need for reassurance that, despite the employment of intensities that extend well beyond the scotopic range, rod selectively is maintained and is free of confounding contributions from cones. Hence, the emphasis in this study has been on defining parameter boundaries within which we can be confident about the selective stimulation of rod function. Our data showed that rod-isolating silent substitution stimuli generate ERGs that rise to a maximum amplitude between 10 and 100 Td, then decrease with increasing stimulus intensity. This "band-pass"–shaped function is similar to rod ERG amplitude versus intensity functions obtained in previous studies that have used either low intensity (scotopic) stimuli[32,33] or rod-isolating silent substitution stimuli[18] in dark-adapted participants. For comparison, in Figure 13 we have replotted rod ERG amplitude versus intensity functions obtained by Bijveld et al. Using a 15 Hz flickering stimulus, they measured ERGs in patients with either absent or reduced cone function (rod monochromats) or defective rod pathways (CSNB).[33,34] Alongside these data, we show 8 Hz amplitude versus intensity functions obtained in this study for rod- and L-cone isolating stimuli.

There are clear qualitative similarities between the different data sets. Importantly, the band-pass amplitude versus intensity function for the ERG

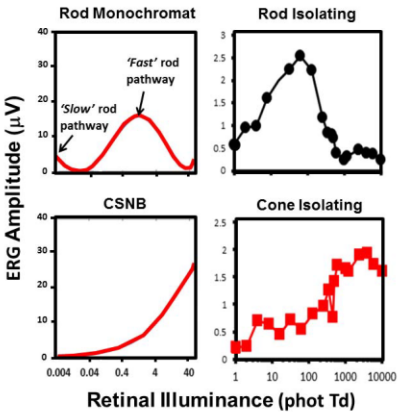

Figure 13. *Left column*: ERG amplitude as a function of stimulus intensity recorded from rod monochromats (*upper left panel*) and CSNB patients (*lower left panel*). These data are replotted from the study of Bijveld et al.[33] and were generated using 15 Hz flickering white light stimuli of low scotopic intensity. *Right hand column*: ERGs recorded from normal trichromats in this study which were elicited using an 8 Hz flickering rod-isolating stimulus (*upper right panel*) and an 8 Hz L-cone isolating stimulus (*lower right panel*).

obtained using rod-isolating silent substitution stimuli can be directly linked to rod activity on the basis that a similarly shaped response function is evident in ERG recordings from rod monochromats.[17,33,34] Rod ERGs obtained within this optimal intensity region are purported to reflect the activity of the fast rod pathway.[5,33,34] At higher illuminance levels our data showed a reduction in rod ERG amplitude where responses fall to a minimum at approximately 1000 Td. This minimum at higher intensities has been attributed to destructive interference between rod and cone signals.[33,34,42 44] The data from CSNB patients (who have dysfunctional rod signaling pathways) and normal trichromats using L-cone isolating ERG responses showed that cone responses behave in a different manner, clearly increasing in amplitude with increasing stimulus intensity. At higher intensities the temporal frequency response functions of the silent substitution rod ERGs become more "cone-like" in terms of their properties – that is, they take on a more temporally band-pass form and support high (> 60 Hz) temporal response limits. This increase in cone activation to ostensibly rod-isolating stimuli may arise from a number of possible sources. Firstly, the anatomy of the rod signaling pathway itself provides

multiple points of contact between the rod and cone systems. Studies have demonstrated a high degree of complexity in the extent to which rod signals can gain access to cone signaling pathways via direct photoreceptor coupling as well as via multiple connective pathways that are found in the inner retinal layers.[46,50] The increases observed in the ERG amplitude at the high stimulus intensities could, in theory, be mediated by any of these pathways. Secondly, increased cone contributions at high stimulus intensities could be the result of small departures from complete rod isolation by our stimuli. Such departures from isolation could arise as a result of interindividual variations in photoreceptor fundamentals and as well as differences in preretinal absorption characteristics.[14] The responses elicited at high stimulus intensities (>1000 Td), therefore, are not rod selective and are contaminated by intrusions from cone activation that potentially may be derived from a number of separate physical as well as physiologic sources.

The reduction in rod ERG amplitude for stimuli above 100 Td is interesting because it coincides with illumination levels over which rod saturation begins.[20,55,56] Earlier studies have referred to this as "rod insensitivity" at higher intensities.[18] But, what is the mechanism for this reduction? Previously, observed decreases in flicker ERG amplitude with increasing stimulus intensity have been modelled accurately on the basis of destructive interference and cancellation between rod and cone signals that are delayed with respect to each other.[42 44] Such interactions have been demonstrated clearly when ERGs have been elicited using non-isolating luminance flicker stimuli.[31] However, with the use of silent substitution stimuli to isolate rod function, the extent of cone modulation should be minimal. Thus, the potential for interference between rod and cone signals is likely to be reduced for silent substitution stimuli. Furthermore, the decrease in rod ERG for stimuli >10 to 100 Td is observed at all the temporal frequencies that we have tested (see Fig. 8). Stimulus frequencies at and around 7.5 Hz are important for revealing interactions between rods and cones because, at this frequency, the delay between rod and cone signals (66 ms) produces a 180° difference in phase between the rod and cone-mediated responses, leading to almost complete cancellation between the two signals.[42 44] However, at higher and lower temporal frequencies there should be constructive interference between the two signals which should augment the ERG signal. Figure 8 shows that, below 30 Hz, decreases in rod ERG amplitude occur regardless of the stimulation frequency suggesting that another mechanism must be responsible for this rod insensitivity at high illuminance levels. One possibility is that rod polarization remains essentially constant during the stimulus, therefore, generating no response to the silent substitution. Another is that the decrease in rod ERG amplitude is the result of a generalized suppression of rod activity that occurs abruptly with increasing illumination. Such a mechanism has been described in the mouse retina where a retinal circuit has been described, which mediates rapid switching from rod to cone-mediated vision at illumination levels where cone bipolars become activated.[57] We speculate that a similar suppression of rod function also may exist in the human retina and that the decreases in rod ERG amplitude that occur at high light intensities, regardless of the temporal frequency, may constitute an electrophysiologic correlate of this suppression in humans.

The assessment of rod-mediated visual function is becoming increasingly clinically relevant with the growing realization that some of the earliest pathological and functional changes that occur in ARMD are found in rod photoreceptors.[8] In addition, rod function also may constitute an important biomarker in the identification of individuals who carry a high genetic risk of ARMD developing in later life.[9] Thus, growing clinical demands are driving the need for the development and improvement of methods that selectively assess rod function in humans. Our data demonstrated that it is possible to elicit ERGs with response characteristics that are consistent with known properties of rod-mediated vision using silent substitution stimuli. Furthermore, we have delineated parameter ranges over which these responses can be optimized. From a clinical perspective, our approach offers potential advantages over current standard methods of assessing rod function. Importantly, the use of silent substitution stimuli provides an opportunity for the assessment of human rod function without the need for subjects having to undergo time-consuming periods of dark adaptation, offering the prospect of more time-efficient testing protocols. A second advantage is that the adaptation state is constant throughout the test session. Specifically, rods are maximally sensitive immediately following dark adaptation and begin to lose sensitivity following repeated stimulation. This can result in much larger responses at the beginning of the test session compared to the end. Excluding dark adaptation largely obviates this problem. Another advantage of

silent substitution stimuli is that they appear to provide better isolation of rod activity and, unlike current standard clinical protocols, do not exhibit a significant correlation with cone responses. The data presented here provide an important translational link between basic and clinical and demonstrate that silent substitution stimuli can efficiently and effectively isolate rod function in humans, providing an alternative approach to current standard clinical protocols.

Acknowledgments

Supported by the Manchester Biomedical Research Centre and the Greater Manchester Comprehensive Local Research Network (NRAP), and by Deutsche Forschungsgemeinschaft (DFG; KR1317/13-1) and Bundesministerium für Bildung und Forschung (BMBF; 01DN14009; JK).

References

1. Kremers J, Link B. Electroretinographic responses that may reflect activity of parvo- and magnocellular post-receptoral visual pathways. *J Vis*. 2008;85:1–14.
2. Parry NR, Murray IJ, Panorgias A, McKeefry DJ, Lee BB, Kremers J. Simultaneous chromatic and luminance human electroretinogram responses. *J Physiol*. 2012;590:3141–3154.
3. Berson EL, Gouras P, Gunkel RD, Myrianthopoulos NC. Rod and cone responses in sex-linked retinitis pigmentosa. *Arch Ophthalmol*. 1969;81:215–225.
4. Berson EL, Gouras P, Gunkel RD. Rod responses in retinitis pigmentosa, dominantly inherited. *Arch Ophthalmol*. 1968; 80:58–67.
5. Scholl HPN, Langrova H, Weber BH, Zrenner E, Apfelstedt-Sylla E. Clinical electrophysiology of two rod pathways: normative values and clinical application. *Graefes Arch Clin Exp Ophthalmol*. 2001;239:71–80.
6. Perlman I, Barzilai D, Haim T, Schramek A. Night vision in a case of vitamin A deficiency due to malabsorption. *Br J Ophthalmol*. 1983;67:37–42.
7. Petzold A, Plant GT. Clinical disorders affecting mesopic vision. *Ophthal Physiol Opt*. 2006;26:326–341.
8. Owsley C, Jackson GR, Cideciyan AV, et al. Psychophysical evidence for rod vulnerability in age-related macular degeneration. *Invest Ophthalmol Vis Sci*. 2000;41:267–273.
9. Feigl B, Cao D, Morris CP, Zele AJ. Persons with age-related maculopathy risk genotypes and clinically normal eyes have reduced mesopic vision. *Invest Ophthalmol Vis Sci*. 2011;52:1145–1150.
10. Marmor M, Fulton AB, Holder GE, Miyake Y, Brigell M, Bach M. ISCEV Standard for full-field clinical electroretinography (2008 update). *Doc Ophthalmol*. 2009;118:69–77.
11. Estevez O, Spekreijse H. Spectral compensation method for determining flicker characteristics of human color mechanisms. *Vis Res*. 1974;14:823–830.
12. Estevez O, Spekreijse H. The "silent substitution" method in visual research. *Vis Res*. 1982;22:681–691.
13. Rushton WA. Pigments and signals in colour vision. *J Physiol*. 1972; 220:1P–31P.
14. Kremers J. The assessment of L- and M-cone specific electroretinographical signals in the normal and abnormal human retina. *Prog Ret Eye Res*. 2003;22:579–605.
15. Kremers J, Czop D, Link B. Rod and S-cone driven ERG signals at high retinal illuminances. *Doc Ophthalmol*. 2009;118:205–216.
16. Cao D, Pokorny J, Grassi MA. Isolated mesopic rod and cone electroretinograms realized with a four-primary method. *Doc Ophthalmol*. 2011;123:29–41.
17. Kremers J, Pangeni G. Electroretinographic responses to photoreceptor specific sine wave modulation. *J Opt Soc Am A Opt Image Sci Vis*. 2012;29:A306–A313.
18. Park JC, Cao D, Collison FT, Fishman GA, McAnany JJ. Rod and cone contributions to the dark adapted 15 Hz flicker electroretinogram. *Doc Ophthalmol*. 2015;130:111–119.
19. McAnany JJ, Park JC, Cao D. Rod- and cone-isolated flicker electroretinograms and their response summation characteristics. *Vis Neurosci*. 2015;32:E018.
20. Stockman A, Sharpe LT. Into the twilight zone: the complexities of mesopic vision and luminous efficiency. *Ophthalmic Physiol Opt*. 2006;26:225–239.
21. Zele AJ, Cao D. Vision under mesopic and scotopic illumination. *Front Psychol*. 2015;5:1594.
22. Ives HE. Critical frequency relations in scotopic vision. *J Opt Soc Am Rev Sci Instrument*. 1922;6:254–268.

23. Hecht S, Shlaer S. Intermittent stimulation by light. V. The relation between intensity and cortical frequency for different parts of the spectrum. *J Gen Physiol.* 1936;19:965–979.
24. MacLeod DIA. Rods cancel cones in flicker. *Nature, London.* 1972; 235:173–174.
25. Odom JV, Reits D, Burgers N, Riemslag FC. Flicker electroretinograms - a systems analytic approach. *Optom Vis Sci.* 1992;69:106–116.
26. Conner JD, MacLeod DIA. Rod photoreceptors detect rapid flicker. *Science.* 1977;195:698–699.
27. Conner JD. The temporal properties of rod vision. *J Physiol.* 1982;332:139–155.
28. Hess RF, Nordby K. Spatial and temporal limits of vision in the achromat. *J Physiol.* 1986;371: 365–385.
29. Kommanapalli D, Murray IJ, Kremers JJ, Parry NRA, McKeefry D. Temporal characteristics of L and M-cone isolated steady-state ERGs. *J Opt Soc Am A Image Sci Vis.* 2014;31:A113–120.56.
30. Gouras P, Gunkel RD. The frequency response of normal, rod achromat and nyctalope ERGs to sinusoidal monochromatic light stimulation. *Doc Opthalmol.* 1964;18:137–150.
31. Stockman A, Sharpe LT, Ruther K, Norby K. Two signals in the human rod visual system: a model based on electrophysiological data. *Vis Neurosci.* 1995;12(5):951–970.
32. Scholl HPN, Kremers J. Electroretinograms in s-cone monochromacy using s-cone and rod isolating stimuli. *Color Res Appl.* 2001;26:S136–S139.
33. Bijveld MMC, Kappers AML, Riemslag FCC, Hoeben FP, Vrijling ACL, van Genderen MM. An extended 15 Hz ERG protocol (1): the contributions of primary and secondary rod pathways and the cone pathway. *Doc Ophthalmol.* 2011;123(3):149–159.
34. Bijveld MM, Riemslag FC, Kappers AM, Hoeben FP, van Genderen MM. An extended 15 Hz ERG protocol (2): data of normal subjects and patients with achromatopsia, csnb1 and csnb2. *Doc Ophthalmol.* 2011;123(3):161–172.
35. Stockman A, MacLeod DI, Johnson NE. Spectral sensitivities of the human cones. *J Opt Soc Am A Opt Image Sci Vis.* 1993;10(12):2491–2521.
36. Wyszecki G, Stiles WS. Color science. *In Concepts and methods, quantitative data and formulae,* 2nd ed. 1982. New York: Wiley.
37. Shapiro AG, Pokorny J, Smith VC. Cone-rod receptor spaces with illustrations that use CRT phosphor and light-emitting-diode spectra. *J Opt Soc Am A Opt Image Sci Vis.* 1996;13(12):2319–2328.
38. Strasburger H. The analysis of stead state evoked potentials revisited. *Clin Vis Sci.* 1987;1:245–256.
39. Meigen T, Bach M. On the statistical significance of electrophysiological steady-state responses. *Doc Opthalmol.* 1999;98(3):207–232.
40. Van Der Tweel LH, Lunel HF. Human visual responses to sinusoidally modulated light. *Electroenceph Clin Neurophysiol.* 1965;18:587–598.
41. Regan D. Some characteristics of average steady-state and transient responses evoked by modulated light. *Electroenceph Clin Neurophysiol.* 1966; 20:238–248.
42. Stockman A, Sharpe LT, Zrenner E, Nordby K. Slow and fast pathways in the human rod visual system: electrophysiology and psychophysics. *J Opt Soc Am A Opt Image Sci Vis.* 1991;8:1657–1665.
43. Sharpe LT, Stockman A, MacLeod DIA. Rod flicker perception: scotopic duality, phase lags and destructive interference. *Vis Res.* 1989;29: 1539–1559.
44. Sharpe LT, Stockman A. Rod pathways: the importance of seeing nothing. *Trends Neurosci.* 1999;22:497–504.
45. Hecht S, Shlaer S, Smith EL, Haig C, Peskin JC. The visual functions of the complete color-blind. *J Gen Physiol.* 1948;31:459–472.
46. Volgyi B, Deans MR, Paul DL, Bloomfield SA. Convergence and segregation of the multiple rod pathways in mammalian retina. *J Neurosci.* 2004; 24:11182–11192.
47. Bloomfield SA, Miller RF. A physiological and morphological study of the horizontal cell types in the rabbit retina. *J Comp Neurol.* 1982;208: 288–303.
48. Famiglietti EV, Kolb H. A bistratified amacrine cell and synaptic circuitry in the inner plexiform layer of the retina. *Brain Res.* 1975;84:293–300.
49. Dacheux RF, Raviola E. The rod pathway in the rabbit retina: a depolarizing bipolar and amacrine cell. *J Neurosci.* 1986;6:331–345.
50. Demb JB, Singer JH. Intrinsic properties and functional circuitry of the AII amacrine cell. *Vis Neurosci.* 2012;29:51–60.
51. Raviola E, Gilula NB. Gap junctions between photoreceptor cells in the vertebrate retina. *Proc Natl Acad Sci USA.* 1973;70:1677–1681.
52. Nelson R. Cat cones have rod input: a comparison of response properties of cones and horizontal cell bodies in the retina of the cat. *J Comp Neurol.* 1977;172:109–136.
53. Schneeweis DM, Schnapf JL. Photovoltages of rods and cones in the macaque retina. *Science* 1995;268:1053–1056.

54. Hess RF, Nordby K. Spatial and temporal properties of human rod vision in the achromat. *J Physiol*. 1986;371:387–406.
55. Hood DC, Finkelstein MA. Sensitivity to light. In: Boff K, Kaufman L, Thomas J, eds. *Handbook of Perception and Human Performance*, Vol. 1. New York: John Wiley & Sons; 1986:5-1–5-66.
56. Aguilar M, Stiles W. Saturation of the rod mechanism of the retina at high levels of stimulation. *J Mod Opt*. 1954;1:59–65.
57. Farrow K, Teixeira M, Szikra T, Viney TJ, Balint K, Yonehara K, Roska B. Ambient illumination toggles a neuronal circuit switch in the retina and visual perception at cone threshold. *Neuron*. 2013; 78:1–14.

Appendix 1

To generate silent substitution stimuli the spectral characteristics of the 4 LEDs were obtained using a PR650 spectrophotometer. These spectra then were multiplied by each of the four photoreceptor fundamentals,[34,35] integrating across the visible spectrum of wavelengths (see Equation A1). Equation A1 shows the calculation of the excitation of the rod photoreceptors by the red LED:

$$E_{r,R}(t) = F_R \times L_R(t) \times \sum_{\lambda} I_R(\lambda) A_r(\lambda) \qquad (A1)$$

where $E_{r,R}$ is the excitation of the rod by the red LED, changing as a function of time t. F_R is a conversion factor for the red LED relating to photometric measurements, L_R is the luminance of the red LED, $I_R(\lambda)$ is the emission spectrum of the red LED and $A_r(\lambda)$ is the V'_λ 10° function.[35] When the above calculation is carried out for all four photoreceptors for each of the individual LEDs the resultant is a 4×4 matrix, **A** (see Equation 2).

$$A = \begin{bmatrix} E_{l,R}(t) & E_{m,R}(t) & E_{s,R}(t) & E_{r,R}(t) \\ E_{l,G}(t) & E_{m,G}(t) & E_{s,G}(t) & E_{r,G}(t) \\ E_{l,B}(t) & E_{m,B}(t) & E_{s,B}(t) & E_{r,B}(t) \\ E_{l,A}(t) & E_{m,A}(t) & E_{s,A}(t) & E_{r,A}(t) \end{bmatrix} \qquad (A2)$$

The subscripts R, G, B, A represent the four LEDs (red, green, blue, and amber) and l, m, s, r the L-, M-, S-cone, and rod photoreceptors, respectively. To calculate maximal and minimal excitation and then cone or rod Michelson contrast from LED Michelson contrast a further step is required. With sine-wave stimuli, the maximal or minimal excitations coincide with the time-point t where LED luminance is maximal or minimal. Thus, from matrix A maximal and minimal excitations are calculated for each photoreceptor. From that we can calculate the photoreceptor contrast from LED contrast (RCd, GCd, BCd, and ACd, and so forth) which is matrix B.

As an example, let us say we wish to generate a rod-isolating stimulus that produces a 0.25 modulation of rod excitation. Our desired photoreceptor contrast setting (PC_d) would be 0% for L cone, 0% for M cone, 0% for S cone, and 25% for rods:

$$PC_d = \begin{bmatrix} L \\ M \\ S \\ r \end{bmatrix} = B \times \begin{bmatrix} RCd \\ GCd \\ BCd \\ ACd \end{bmatrix} PC_d = \begin{bmatrix} 0 \\ 0 \\ 0 \\ 0.25 \end{bmatrix} \qquad (A3)$$

We then can multiply our desired photoreceptor contrast with the inverse of B (B^{-1}), to obtain the desired LED contrast (LC_d) required to achieve our level of photoreceptoral isolation.

$$LC_d = PC_d \times B^{-1} \qquad (A4)$$

Appendix B

Reprint: The Morphology of Human Rod ERGs Obtained by Silent Substitution Stimulation

Doc Ophthalmol
DOI 10.1007/s10633-017-9571-4

ORIGINAL RESEARCH ARTICLE

The morphology of human rod ERGs obtained by silent substitution stimulation

J. Maguire · N. R. A. Parry · J. Kremers · I. J. Murray · D. McKeefry

Received: 30 August 2016 / Accepted: 5 January 2017

Abstract
Purpose To record transient ERGs from the light-adapted human retina using silent substitution stimuli which selectively reflect the activity of rod photoreceptors. We aim to describe the morphology of these waveforms and examine how they are affected by the use of less selective stimuli and by retinal pathology.
Methods Rod-isolating stimuli with square-wave temporal profiles (250/250 ms onset/offset) were presented using a 4 primary LED ganzfeld stimulator. *Experiment 1*: ERGs were recorded using a rod-isolating stimulus (63 ph Td, rod contrast, $C_{rod} = 0.25$) from a group ($n = 20$) of normal trichromatic observers. *Experiment 2*: Rod ERGs were recorded from a group ($n = 5$) using a rod-isolating stimulus ($C_{rod} = 0.25$) which varied in retinal illuminance from 40 to 10,000 ph Td. *Experiment 3*: ERGs were elicited using 2 kinds of non-isolating stimuli; (1) broadband and (2) rod-isolating stimuli which contained varying degrees of L- and M-cone excitation. *Experiment 4:* Rod ERGs were recorded from two patient groups with rod monochromacy ($n = 3$) and CSNB (type 1; $n = 2$).
Results The rod-isolated ERGs elicited from normal subjects had a waveform with a positive onset component followed by a negative offset. Response amplitude was maximal at retinal illuminances <100 ph Td and was virtually abolished at 400 ph Td. The use of non-selective stimuli altered the ERG waveform eliciting more photopic-like ERG responses. Rod ERGs recorded from rod monochromats had similar features to those recorded from normal trichromats, in contrast to those recorded from participants with CSNB which had an electronegative appearance.
Conclusions Our results demonstrate that ERGs elicited by silent substitution stimuli can selectively reflect the operation of rod photoreceptors in the normal, light-adapted human retina.

Keywords Electroretinograms · Rod photoreceptors · Silent substitution

J. Maguire · N. R. A. Parry · J. Kremers · D. McKeefry (✉)
Bradford School of Optometry and Vision Sciences, University of Bradford, Bradford, W. Yorkshire BD7 1DP, UK
e-mail: d.mckeefry@bradford.ac.uk

N. R. A. Parry
Vision Science Centre, Manchester Royal Eye Hospital, Central Manchester University Hospitals NHS Foundation Trust, Manchester Academic Health Science Centre, Manchester, UK

N. R. A. Parry · I. J. Murray
Faculty of Biology, Medicine and Health, University of Manchester, Manchester, UK

J. Kremers
Department of Ophthalmology, University Hospital Erlangen, Erlangen, Germany

Published online: 13 January 2017

Introduction

The human electroretinogram (ERG), when elicited by a diffuse flash of light, constitutes a global electrical response from the retina which reflects the neural activity of a number of different retinal cell populations. However, with careful choice of the temporal, chromatic and luminance characteristics of the stimulus, it is possible to generate responses that have a greater degree of specificity in terms of the retinal cell populations from which they originate [1]. The isolation and selective stimulation of rod photoreceptor activity form an important part of clinical electrodiagnostic assessment routines. There is a variety of congenital and acquired visual pathologies that can differentially affect rod relative to cone function [2–7]. The International Society for Clinical Electrophysiology of Vision (ISCEV) has outlined a detailed set of standards governing all aspects of clinical electroretinography [8] which covers scotopic (and photopic) retinal assessment. However, in recent years, other non-standard test methods have been developed and these have proven to be useful in providing extra information about retinal function. One method that has become popular, following the wider availability of four and five primary LED stimulator systems, is silent substitution [9, 10]. This method provides a means by which ERGs from any one of the retinal photoreceptor populations can, in theory, be isolated from the other photoreceptor classes. In the case of rod isolation, four primary stimulators allow the creation of stimuli which, when modulated in time, produce a constant level of photoisomerisations in the three types of cone photoreceptors, but not in the rods [11, 12]. Thus, cone modulation is effectively kept at zero while the rods are selectively stimulated.

In a previous study, we demonstrated that it is possible to isolate rod-mediated steady-state (8 Hz) ERG responses using the silent substitution method without the need for dark adaptation [13]. We were able to show that ERGs elicited by this technique were selective for rods by the demonstration of a correspondence between temporal frequency and illuminance response characteristics and previously reported psychophysical properties of rod-mediated vision. In this study, we have used the same silent substitution technique to generate transient ERGs using stimuli with square-wave temporal profiles. This approach facilitates examination of rod-mediated responses in the time domain and enables characterisation of the morphology of the ERG waveform and its constituent components. The primary aim of this study was to describe the basic morphological features of the ERG associated with rod function in the normal trichromatic retina generated by silent substitution stimuli. In addition, we also wanted to explore how the rod ERG waveform morphology is affected by the use of less selective stimuli that modulate cone as well as rod photoreceptors. To this end, we compared rod-isolated ERGs, elicited by silent substitution, with responses obtained using non-selective broadband 'white' stimuli and stimuli to which we intentionally introduced varying degrees of cone modulation. Such stimulus manipulations allow us to identify key changes in the ERG waveform that might be attributable to the intrusion of cone activity. We also wanted to explore interactions between rod and cone responses using stimuli of varying intensities. Of particular interest is the way the rod ERG waveform is influenced by the use of stimuli that span the mesopic illumination range. This range is important as it marks the main transition between rod- and cone-mediated visual function, and it would be useful to ascertain whether the rod ERG reflects this transition in the human retina, as has been previously demonstrated in the mouse [14].

As well as examining rod-mediated ERGs from the normal trichromatic human retina, we also wanted to assess responses from individuals with specific retinal pathologies. In the context of this study, individuals with rod monochromacy constitute an important control group. Such individuals lack significant cone function and effectively only possess functioning rod photoreceptors. Thus, rod ERGs from these individuals can be compared to those responses obtained from normal trichromats (who still have functioning L-, M- and S-cones). If our silent substitution stimuli and recording conditions do effectively isolate rod function, then we would expect a high degree of correspondence between the morphological features of ERGs elicited from normal trichromats and those from rod monochromats. To facilitate this comparison, we recorded rod ERGs from subjects who have rod monochromacy caused by CNGB3 gene mutations. Such mutations result in completely or highly impaired cone function which results in abnormal colour vision, reduced visual acuity and nystagmus

[15–17]. Conversely, other retinal pathologies, such as the complete form of congenital stationary night blindness (CSNB1), for example, lead to severely compromised rod function but preserved cone function [18]. CSNB1 is associated with ON-bipolar cell dysfunction and leads to a characteristic set of full-field ERG abnormalities including abolished scotopic rod responses, electronegative mixed rod-cone responses and preserved, though abnormal, photopic responses [18–20]. In such cases, we would expect rod responses generated by silent substitution stimuli in participants with CSNB1 to be very different from those obtained from those with normal retinal function. The comparison of rod ERGs generated by silent substitution in participants with normal as well as pathological retinal function is useful as it will help us to gauge the extent to which our methodological approach leads to the effective and selective isolation of rod photoreceptoral function in humans.

Methods

Stimuli

Rod-isolating stimuli were presented using a ColorDome (Diagnosys LLC, Lowell, MA, USA) four primary ganzfeld stimulator with blue (460 nm), green (514 nm), amber (592 nm) and red (632 nm) LEDs. The spectral characteristics, chromaticities and luminances of each class of LED were calibrated using a PR650 spectrophotometer (Photo Research Inc., Chatsworth, CA, USA). In order to create silent substitution stimuli, photoreceptor excitations were calculated by multiplying the emission spectra of the LEDs with cone fundamentals and the V'_{λ} 10° function [22, 23] and integrating over a range of wavelengths (see: Ref. [13] for a fuller description of stimulus generation). The stimuli used in these experiments were triple silent substitutions in which intensity and wavelength combinations were used which produced no change in the net excitation of L-, M- or S-cones, but did produce excitation modulation of rod photoreceptors. Figure 1a illustrates an example of a rod-isolating stimulus. In these experiments, the modulation of rod excitation was kept constant at $C_{\mathrm{rod}} = 0.25$ (Michelson contrast) for all stimuli. The retinal illuminance produced by the stimuli was varied between 40 and 10,000 photopic trolands (ph Td). In order to obtain the stimuli with the lowest retinal illuminances (40, 63 ph Td), a 0.9 neutral density filter was placed in front of the stimulator which attenuated the stimuli to the required levels with little or no distortion of the spectral characteristics.

For consistency, we have used photopic as opposed to scotopic Troland units throughout this study rather than change units across the transitional mesopic–photopic illumination range within which the majority of our stimuli lie. Prior to the start of each experimental session, the participants underwent a 5-min adaptation period under ambient room illumination (500 lx). The stimuli were then delivered as continuous trains of pulses (only 1 cycle is shown in the Fig. 1 for clarity) with each waveform constituting the average response to 256 cycles (on–off presentations) of the stimulus.

In addition to the rod-isolating stimuli, we employed two other types of non-isolating stimuli which were designed to elicit excitation of both rod and cone photoreceptors. For one stimulus type, we introduced varying amounts of L- and M-cone modulation, ranging from 0.0–0.6, into our basic rod stimulus (Fig. 1b). The second kind of non-selective stimulus was produced by the modulation in phase of all four LEDs (Fig. 1c). This so-called 'white' stimulus (which actually appeared purple to the normal trichromats) produced the same modulation (0.25) across all four classes of photoreceptor.

ERG recording

ERGs were recorded from the right eye using a silver/nylon corneal fibre electrode (Dept. of Physics and Clinical Engineering, Royal Liverpool University Hospital, UK) referenced to a 9-mm Ag/AgCl electrode (Biosense Medical, Chelmsford, UK) on the outer canthus; a similar electrode was affixed to the forehead to serve as ground. Impedance was maintained below 5 kΩ. Signals were recorded using the Espion E^2 system (Diagnosys LLC, Lowell, MA, USA) which amplified and filtered (bandwidth = 1 to 300 Hz) the ERGs and digitised them at a rate of 1000 Hz. Retinal responses were acquired over 500 ms epochs with each response being composed of an average of a minimum of 256 epochs. Participants viewed the stimuli monocularly with a dilated pupil (1% Tropicamide) from a distance of 10 cm, and both a chin and head rest were used. Fixation was

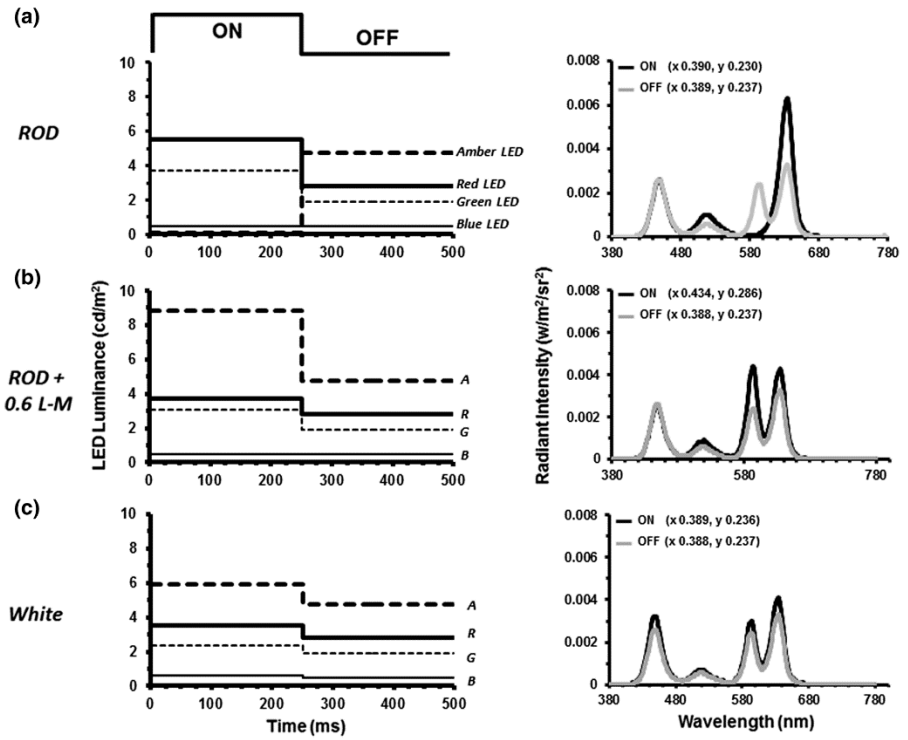

Fig. 1 Temporal profiles of the square-wave pulse stimulus used to generate rod ERGs. The plots on the *left* show the luminance variation of the four LED primaries required to generate: **a** the rod-isolating stimulus, **b** the mixed rod and L- and M-cone stimulus (cone modulation = 0.6) and **c** the 'white' stimulus. In each case, the initial 0–250 ms is the onset period followed by the offset period (250–500 ms). This sequence was then repeated with the stimuli presented as continuous trains of on–off pulses (256 cycles in total). The graphs on the *right-hand side* show the spectral characteristics of the onset (*black lines*) and offset (*grey lines*) phases of each of the stimuli. Also given are the 1931 CIE (xy) chromaticity co-ordinates for the onset and offset phases of each stimulus

maintained on a central point which subtended approximately 0.5°.

Participants

In experiment 1, a total of 20 normal trichromatic observers (mean age 31.5 years, age range 53 years) acted as participants, whilst in experiments 2 and 3 a subset of this cohort consisting of 5 colour normal trichromats (3 males; mean age: 32 years, age range 24 years) took part. Colour vision in all normal subjects was assessed using the City University Colour Test (2nd Edition) and the HMC Anomaloscope (Oculus, Wetzlar, Germany). In experiment 4, we recorded ERGs from 3 members of a family [RM1 (31 years), RM2 (38 years) and RM3 (34 years)] and with a homozygous p.T383fsX mutation in CNGB3 causing rod monochromacy. We also recorded ERGs from 2 patients [NB1 (17 years) and NB2 (27 years)] with congenital stationary night blindness (CSNB 1) who had severely compromised rod function caused by a NYX (Xp11.4) gene mutation.

Ethical approval for this study was obtained from the local ethics committee, and all participants gave

informed consent prior to the commencement of the experiments which were carried out in accord with the tenets of the Declaration of Helsinki.

Results

Experiment 1: Morphology of the transient rod ERG

Figure 2 shows ERGs obtained from 20 normal trichromatic observers in response to a silent substitution rod-isolating stimulus with a square-wave temporal profile comprising an onset (i.e. rod excitation increment) duration of 250 ms and a 250-ms offset (rod excitation decrement) period. Rod contrast, $C_{\mathrm{rod}} = 0.25$ and the stimulus had a mean retinal illuminance of 63 ph Td. In normal trichromats, the ERG produced by this stimulus had a consistent appearance across all participants exhibiting a waveform with an initial prominent positive peak, which we have termed P_{Ri}, which has a peak implicit time of 85.95 ms (±95% CI = 7.88 ms). The offset response is dominated by a negative component (termed N_{Rd}) which has a mean peak implicit time of 95.18 ms (±95% CI 7.85) after the offset of the stimulus.

Experiment 2: Rod ERGs as a function of retinal illuminance

ERGs mediated by rods are usually elicited from the dark-adapted eye [8] using low intensity (scotopic) stimuli [6, 8, 24–27]. However, the use of silent substitution stimuli to isolate rod activity potentially provides an opportunity to record rod responses at higher stimulus intensities. Examination of the responses elicited by stimuli that extend from mesopic to photopic levels of illumination, in particular, provide the opportunity to observe the effects of the ERG waveform as the transition from rod- to cone-mediated vision takes place. To this end, we generated a series of rod-isolating square-wave pulse stimuli which produced retinal illuminances ranging from 40 to 10,000 ph Td with a rod contrast of 0.25. Figure 3 shows the changing morphology of the averaged ($n = 5$) rod ERGs as a function of retinal illuminance. For the low intensity stimuli (40–100 ph Td), the ERGs have a distinct waveform similar to the responses shown in Fig. 2 with a prominent positive onset response (P_{Ri}) and a negative offset (N_{Rd}). As retinal illuminance increases from 100–1000 ph Td, the response becomes highly attenuated with hardly any discernible ERG waveform elicited by rod-isolating stimuli within this

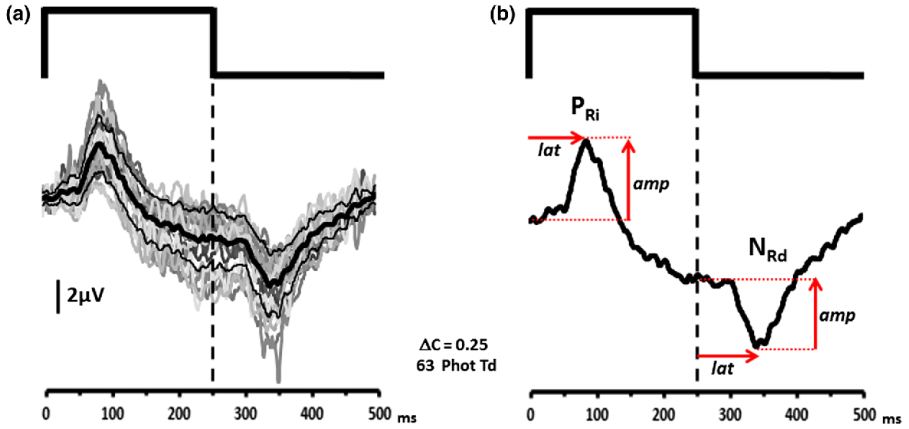

Fig. 2 **a** Shows the individual (*grey lines*) and group averaged (*thick black line*) ERGs elicited from 20 normal participants by a silent substitution rod-isolating stimulus. The thin *black lines* represent +/− 1 S.D. from the mean. For clarity, we have shown the group averaged rod ERG in **b**, this response consists of an initial positive peak (P_{Ri}) at stimulus onset followed by a negative response component (N_{Rd}) after stimulus offset

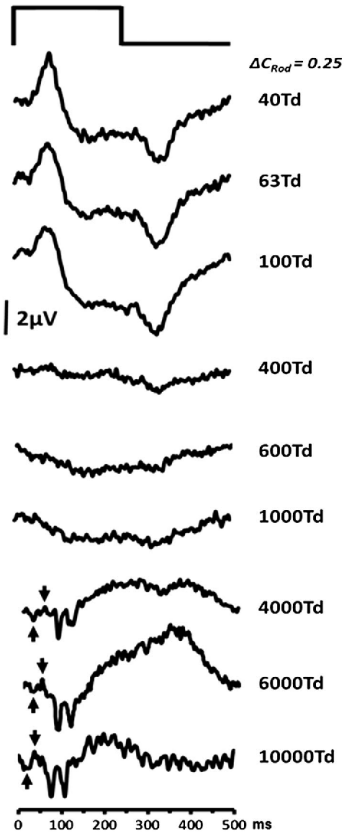

Fig. 3 Group averaged ($n = 5$) transient rod ERG as a function of retinal illuminance. For all stimuli, the modulation of rod excitation was 0.25

intensity range. At stimulus intensities above 1000 ph Td, a response does appear to re-emerge, but it has a very different morphology from that which is obtained at the lowest stimulus intensities. Under these conditions, the response exhibits a negative component (upward arrows in Fig. 3) with an implicit time of between 20–30 ms, followed by a small positive going peak at approximately 40 ms (downward arrows in Fig. 3). These components resemble those observed in the non-selective single flash photopic response. Later components (both positive and negative) are also observed between 75–100 ms and give the response obtained at these high illuminance levels a very different morphology to that which is observed for low illuminance levels.

Experiment 3: ERGs elicited with non-isolating stimuli

Having examined the morphology of the ERG generated by rod-isolating silent substitution stimuli, we wanted to examine the extent to which this waveform was affected by the use of non-selective stimuli that induce excitation of cone as well as rod photoreceptors. We employed two groups of stimuli: The first were broadband flash stimuli which modulated all photoreceptors to the same extent (0.25). These stimuli were presented over a range of different retinal illuminances. The second group comprised a series of nominally rod-isolating stimuli at 63 ph Td to which varying degrees of L- and M-cone modulation were added, ranging from 0% (i.e. rod isolating) to 60% cone modulation. All stimuli had the same temporal profile as those used in experiments 1 and 2 (see Fig. 1b, c).

Figure 4 shows the ERG responses elicited using the first non-isolating (white) group of stimuli. For comparison, the rod-isolating responses are also shown for the same stimulus intensities (grey traces). When we compare the rod-isolated responses with the non-isolated responses at similar stimulus intensities, we see that there are qualitative differences between the responses elicited by the different stimulus types. A key difference is that, at the lowest stimulus intensities, ERGs elicited by non-isolating stimuli do not exhibit the large positive component (P_{Ri}) that is present in the rod-isolating response. Instead, non-isolated responses are dominated by a broad negativity which is similar to the scotopic threshold response (STR) that has been previously reported in the dark-adapted ERG [28, 29]. This later and longer duration negativity, also observed in the response elicited by the silent substitution stimuli at low illuminance, has previously been attributed to inner retinal activity [28], and we speculate that a similar source is responsible for the generation of this component in both the non-isolated and rod-isolated ERGs.

As retinal illuminance increases, the non-isolated ERG starts to develop a prominent negative going

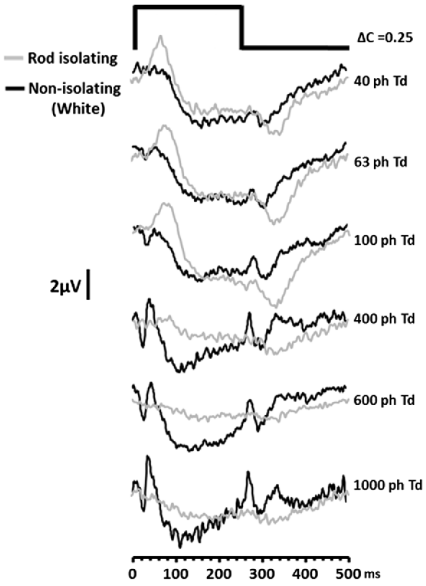

Fig. 4 ERGs elicited by a non-isolating (*white*) stimulus of increasing intensity (*black traces*). Also shown are the responses for the rod-isolating stimuli at the same levels of retinal illuminance (*grey traces*). The traces represent group averaged ($n = 5$) responses and for all stimuli the modulation of each photoreceptor class = 0.25

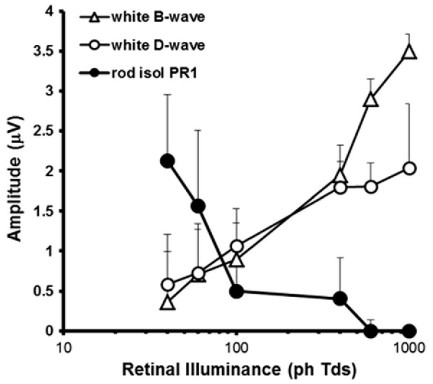

Fig. 5 Dependency of the ERG b- (*empty triangles*) and d-wave (*empty circles*) amplitude generated by a non-selective '*white*' stimulus plotted as a function of retinal illuminance. Also plotted for comparison is the amplitude of P_{Ri} (*filled circles*) of the rod-isolated ERG in the same participants across the same illuminance range. Data are the group averages ($n = 5$) and the *error bars* = +1 SD

a-wave and positive b-wave. Both these components have implicit times that are shorter than corresponding components found in the rod-isolated ERG. The development of these onset response components occurs in conjunction with the increased prominence of a positive d-wave offset response in the non-isolated ERG [30]. Figure 5 plots the variation in the amplitude of the b- and d-waves of the ERG generated in response to the non-isolating white stimulus as a function of retinal illuminance. As can be observed, both of these onset and offset components undergo an increase in amplitude with increasing stimulus intensity. Not unexpectedly, the waveform morphology to this non-selective stimulus takes on the appearance of the photopic on–off ERG that has been described previously (see Ref. [30], Fig. 9). In contrast, the amplitude of the P_{Ri} component of the rod-isolated ERG behaves very differently exhibiting a marked reduction in amplitude as a function of retinal illuminance beyond 400 ph Td.

ERGs elicited by the second group of non-isolating stimuli are shown in Fig. 6. The stimuli used in this experiment modulate L- and M-cones as well as rods. The extent of cone modulation varies across the stimuli from 0.0 (i.e. rod isolating) to 0.6. As the magnitude of cone modulation increases, there are clear changes in the ERG waveform morphology; there is an initial decrease in the P_{Ri} amplitude accompanied by increases in a- and d-wave amplitudes (see Fig. 7). At the highest levels of L- and M-cone modulation, the ERG waveforms elicited by these non-isolating stimuli are similar in appearance to those generated by the highest intensity white stimuli shown in Fig. 4.

Experiment 4: Transient rod ERGs from clinical patient groups

Figure 8 shows ERGs obtained using standard ISCEV protocols [8] from one of the rod monochromats (RM3) and one of the patients with CSNB type 1 (NB1). The ERGs shown are the light-adapted 30 Hz flicker (cone), the dark-adapted scotopic (rod) and the maximal (DA10) response. Normal responses (grey

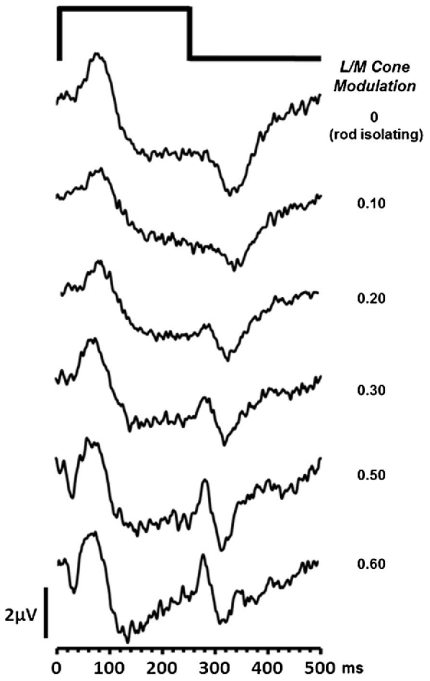

Fig. 6 ERGs elicited by stimuli which contain increasing amounts of L- and M-cone modulation. The ERGs in the uppermost trace were generated by a stimulus that produced no L- or M-cone excitation and were therefore rod isolating. Each stimulus has a retinal illuminance = 63 photopic Trolands

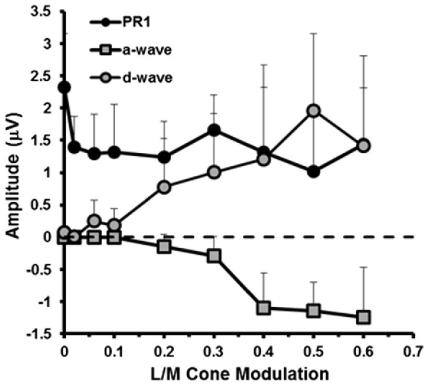

Fig. 7 Amplitude of the a-wave (*squares*), d-wave (*circles*) and P_{Ri} (*black circles*) components as a function of increasing amounts of L/M-cone modulation added to a rod-isolating stimulus. Data are the group averages ($n = 5$), and the *error bars* represent +1 SD

traces) are also shown for comparison. As can be observed from Fig. 8, the rod monochromat has negligible cone function, as indicated by the abolished 30 Hz flicker response, but has preserved (albeit reduced) rod function [31]. In contrast, the ERGs from the CSNB subject exhibit the opposite pattern, preserved (though again reduced) responses to the 30 Hz stimulus and abolished rod function with the characteristic electronegative maximal response [18, 19, 21, 32].

Figure 9 shows the group averaged ($n = 20$) ERG obtained from the normal trichromats in response to the silent substitution, rod-isolating stimulus. Also shown are the responses from the three rod monochromats and 2 CSNB subjects to the same stimulus. The responses elicited from the rod monochromats exhibit similar waveform morphologies to the normal rod response, with the P_{Ri} and N_{Rd} components being identifiable at stimulus onset and offset, respectively. However, response amplitudes vary across the three patients, and there is inter-subject variation in terms of the quality of waveform appearance. This is largely due to the fact that rod function is compromised in all of these individuals. The canonical view of rod monochromacy is that it primarily leads to cone dysfunction, leaving rod function intact (see Ref. [33]). However, Fig. 8 clearly demonstrates an attenuated ISCEV scotopic rod response for subject RM3 (the rod monochromat with the largest deficit in the rod response), and this is also the case for subjects RM1 and RM2 (data not shown), the latter subject being the least affected out of the three in terms of rod dysfunction. This secondary loss of rod response in rod monochromats is consistent with reports from previous studies [17, 34, 35].

In contrast, the ERGs generated by the rod-isolating stimuli from the CSNB patients are markedly different. The responses lack a prominent P_{Ri} component; instead, the waveform elicited by contrast increment (onset) is dominated by a prolonged negative component. The offset response is also very different in that it shows a small positivity rather than a large negativity.

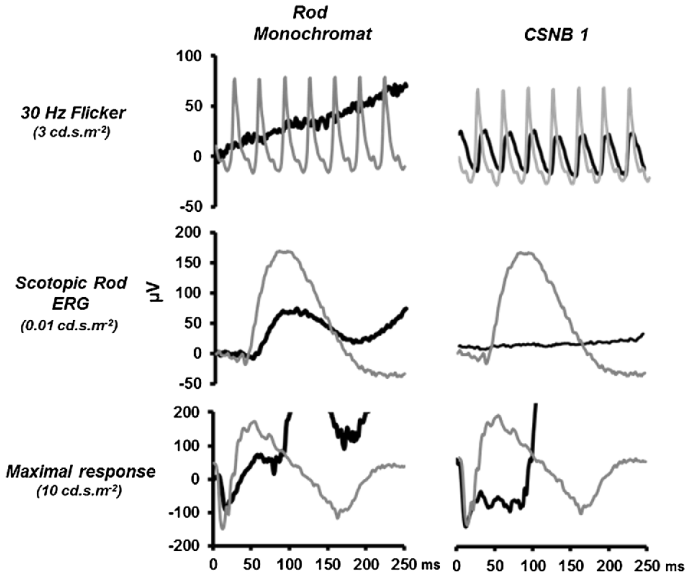

Fig. 8 ISCEV standard 30 Hz flicker, scotopic rod and maximal response ERGs recorded from one of the rod monochromats, RM3 (*left column*) and one of the patients with CSNB1, NB1 (*right column*). The *grey traces* show the responses from a normal trichromat to these stimuli

Discussion

In this study, we have used silent substitution stimuli to elicit transient ERGs from the light-adapted human retina in an attempt to generate retinal responses that selectively reflect rod-mediated visual function. We have characterised the morphology of this rod ERG waveform in the normal trichromatic retina and demonstrated how non-selective stimuli induce changes in this response that arise as the result of cone photoreceptor stimulation. Importantly, we have shown that rod ERGs generated by our methodology exhibit a clear reduction in response amplitude as stimulus intensity increases from mesopic to photopic levels. This response attenuation is not observed in ERGs elicited by stimuli that are not rod selective and is critical because it provides a clear correlation with rod photoreceptor response properties which exhibit response saturation over the same illumination range [36]. Complementing our observations from the normal human retina are the responses from participants with two contrasting kinds of inherited retinal pathology that have either selectively preserved (rod monochromacy), or compromised (CSNB) rod function. The similarity between the waveform morphologies of ERGs obtained by rod-isolating stimuli from normal trichromats and those from rod monochromats provides further verification that silent substitution stimuli can effectively isolate rod-mediated activity in the light-adapted trichromatic retina. Furthermore, the fact that key features of our 'normal' rod ERG waveform are absent in CSNB subjects who have compromised rod function, but preserved cone function, provides another indicator that this methodology does provide a selective assay of rod photoreceptor function.

Origins of on and off components in the Rod ERG

The human dark-adapted rod ERG, recorded under ISCEV standard conditions [8], typically comprises a positive b-wave of large amplitude with an implicit

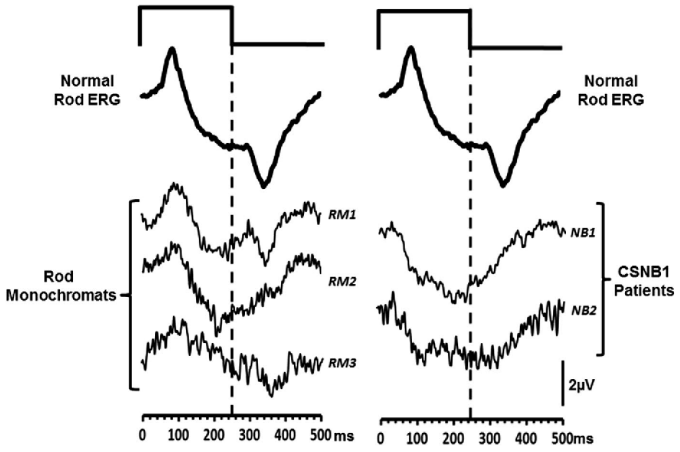

Fig. 9 ERGs elicited from normal trichromats and from patient groups. The *left-hand column* shows ERG waveforms, elicited by a 63 ph Td rod-isolating square-wave pulse stimulus (250/250 ms onset/offset), from normal trichromats (*upper trace*). This waveform is an average of $n = 20$ observers. The *lower three traces* are the responses obtained from the three rod monochromats (RM 1-3). Traces in the *right-hand column* again show the normal rod-isolated response (*upper trace*) and ERGs obtained from two patients with CSNB 1 (NB1-2) with the same stimulus

time of approximately 100 ms (see Fig. 8). The response is generated by a short duration broadband flash stimulus, and the resultant waveform is in effect a composite response of both onset and offset components (though heavily dominated by the former). In the mammalian retina, low scotopic vision is mediated by a pathway based upon rods which synapse with depolarising rod bipolar cells [30, 37–39] and numerous pharmacological studies point to the direct involvement of this pathway in the generation of the dark-adapted ERG b-wave [40–42]. ERGs elicited from the normal light-adapted human retina to the onset of a rod-isolating silent substitution stimulus (<400 ph Td) also are dominated by an initial positive component, P_{Ri}, with an implicit time of 85.95 ms (±95% CI 7.88 ms). We propose that the origin of this component is similar to that of the dark-adapted rod b-wave or the PII response [28, 43, 44] and is produced by the depolarisation of the rod ON-bipolar cells [28, 30]. Our recordings from participants with type 1 CSNB provide support for this view. This form of CSNB is the direct result of ON-bipolar cell dysfunction, and individuals with this condition have a characteristic set of full-field ERG abnormalities, abolished scotopic responses, electronegative scotopic bright flash ERGs as well as abnormalities in the morphology of the photopic a-wave [18–21]. The ERGs we have recorded from these individuals using the rod-isolating silent substitution stimuli lack any obvious P_{Ri} component but, in keeping with previous findings [e.g. 30], exhibit an electronegative waveform in response to the onset of a long duration rod-isolating stimuli. The rod ERGs obtained from the CSNB participants contrast with those elicited from rod monochromats and normal trichromats. The rod monochromats are members of a family with a homozygous pT383fsX mutation in the CNGB3 gene. This mutation generates deficits in critical parts of cone phototransduction cycle and leads to a loss of cone function. Individuals with this condition typically present with photophobia, nystagmus, reduced visual acuity and a total loss of colour vision but have preserved rod function [17, 31, 45, 46]. The fact that the silent substitution rod-isolating stimulus generates an ERG from these individuals that has the same basic morphology as the rod ERG obtained from the normal retina provides verification that this response does indeed reflect rod-mediated retinal function. This is

despite the fact that light-adapted trichromatic retina also contains functional cone as well as rod photoreceptors.

The temporally extended nature of our stimulus means that an offset response is also a feature of our rod ERG responses—something that is not usually observed in the ISCEV scotopic ERG. An intense, long duration stimulus typically evokes a positive potential or d-wave from cone-rich light-adapted retinas at stimulus offset [44, 47]. Examples of this offset response component can be seen in the ERGs recorded in response to high intensity white stimuli and stimuli which induce cone and rod excitation (see Figs. 4, 6). In comparison, offset responses elicited from dark-adapted, rod-dominated retinas comprise a negative component followed by a slower positive response [43, 44]. These morphological features are more in keeping with those observed in our rod-isolated ERGs which at stimulus offset exhibit a negative trough, N_{Rd}, that typically occurs at 95 ms post stimulus offset. The rod ERG offset response was first described when assessing retinal responses to long duration stimuli in rod dominant animal models and was described as a corneal negative wave occurring after stimulus offset [43, 48]. Brown originally suggested the offset response was a combination of the decay of ON-bipolar cells plus a dc component along with the recovery of the photoreceptors [42]. Further analysis in the cat confirmed that part of the negative trough is formed by repolarisation of the rod bipolar cells but that the slow positivity, immediately following it, originates in the more proximal regions of the retina [42]. The literature on the rod offset response in human retina is limited [49, 50]. In one study [49], the rod offset ERG was recorded in a patient with S-cone monochromacy using silent substitution. The resultant response is qualitatively similar to the offset ERGs reported in this study. A second study [50] used scotopic rapid on/off ramp stimuli and multifocal stimuli to record the rod onset and offset responses. The elicited waveform had a positive deflection at onset and a negative dip at offset. Our speculation is that the negative offset component observed in the rod-isolated ERGs recorded in this study is related to the recovery of the ON-bipolars, rather than an independent entity. The fact that a negative offset component is not observed in ERGs recorded from CSNB patients may provide further support for this notion. In these patients, the ON-bipolars are dysfunctional, and there is a lack of response at stimulus onset. As a consequence, there is no recovery following stimulus offset.

Rod ERGs as a function of retinal illuminance

A key feature of the ERGs generated by the silent substitution rod-isolating stimuli is that they exhibit a decrease in amplitude with increasing stimulus intensity, the responses becoming highly attenuated above 100 ph Td. This decrease is significant because it occurs across the range of mesopic illumination levels for which the saturation of rod responses is purported to begin [32, 51, 52]. This intensity-dependent decrease in amplitude for the isolate rod ERG is in stark contrast to the increase in amplitude of the responses elicited by non-selective stimuli which not only modulate rods but also cone photoreceptors (Figs. 3, 4, 5). This response behaviour provides another piece of evidence which points to the selective isolation of rod function by the current stimulation protocols. Similar intensity-dependent increases and decreases have been demonstrated in the mouse retina for cone and rod-mediated ERGs, respectively [14]. Interestingly, similar to the murine responses, human rod ERGs appear to undergo a similar abrupt reduction in amplitude across a relatively narrow range of retinal illuminance. The rapid nature of the rod response attenuation, which is coupled with an increase in the ERGs generated by cone photoreceptors [14], has prompted speculation about the existence of retinal mechanisms which control the switch from rod- to cone-mediated vision with increasing retinal illumination. One possibility is that rod response levels are moderated by the light intensity experienced by cones [53, 54]. Various mechanisms have been proposed as to how this suppression of rod function might be achieved, including mediation via gap junctions that exist between rods and cones [55] or via neural switching mechanisms involved cone bipolars [56]. These have, thus far, only been described in the mouse retina—but the behaviour of the rod-isolated ERGs shown here, suggesting that similar mechanisms involving the rapid suppression of rod responses by increasing cone activity exist in the human retina. The use of rod-isolating silent substitution stimuli may provide a means via which these mechanisms can be studied in humans.

Our results show that whilst there is a clear attenuation of the rod-isolated ERG for stimuli above 100 ph Td, some form of response does re-emerge at high stimulus illuminances (≥4000 ph Td). However, the morphology of these waveforms is clearly very different from that obtained using low illuminance stimuli (see Fig. 3). The early negative and positive components, occurring at approximately 20 and 40 ms, respectively, are similar in timing to the a- and b-waves observed in ERGs generated by non-selective stimuli. In addition, there is a later complex of negative and positive components, occurring between 75–110 ms that is observed in the high illuminance responses. This complex is completely absent from the responses elicited by the optimal (<100 ph Td) rod-isolating stimuli. In the light of these differences in waveform morphology, our view is that the ERGs elicited by rod-isolating stimuli of high illuminance no longer selectively reflect rod function and are the result of contamination from non-rod-mediated sources. Previous work has demonstrated that cone photoreceptors may form one potential source of these intrusions. This is based on the fact that the temporal response limit of these high illuminance ERGs far exceeds that supportable by the rod system and lies closer to temporal response limit of the cones [13]. These intrusions may be the result of the intrinsic anatomical connectivity that exists between the rod signalling pathway and cones [34, 57, 58]. The inadvertent stimulation of other photoreceptor populations may also arise as a result of departures in the degree rod isolation provided by our stimuli. Silent substitution calculations are based on representative photoreceptor fundamentals [22]. However, across individuals there are differences in these fundamentals, as well as variation in pre-retinal absorption characteristics. These factors are likely to increase the likelihood of stimulation of other photoreceptor classes which becomes more significant with increasing stimulus intensity. In addition to retinal-based sources of contamination, we also cannot rule out the possibility of myogenic contamination (due to blinks or blepharospasm) that is often induced by stimuli of high intensities. This could form a potential source, particularly for the later components observed in the ERGs elicited by high illuminance stimuli. Our results suggest that even with silent substitution stimuli, which in theory should elicit no cone excitation, rod isolation can no longer be assured for stimuli of illuminance above 1000 ph Td as a result of these potential physiological and physical sources of contamination.

In summary, we have described the key features of an ERG response, generated by silent substitution stimulation, which selectively reflect the operation of rod photoreceptors in the normal, light-adapted human retina. We have demonstrated how this rod ERG is affected by the use of stimuli that vary in the extent to which they selectively isolate rod function. In addition, we have also shown how this response is influenced by retinal pathologies that differentially affect rod and cone function in humans. We propose that our methodology will prove to be useful in the respect that it provides an opportunity for the examination of human rod function, in both the normal and abnormal retina, without having to subject participants to long periods of dark adaptation. Secondly, the use of rod-isolating stimuli, used in conjunction with carefully generated stimuli that are less selective in terms of their rod isolation, provides a means to study interactions between rods and cones in the normal and pathological retina, particularly in the context of the control of retinal sensitivity across mesopic illumination levels.

Acknowledgements NRAP's participation was facilitated by the Greater Manchester Comprehensive Local Research Network.

Funding Deutsche Forschungsgemeinschaft (DFG) (KR1317/13-1) and Bundesministerium für Bildung und Forschung (BMBF) (01DN14009) provided financial support for JK. The sponsor had no role in the design or conduct of this research.

Conflict of interest All authors certify that they have no affiliations with or involvement in any organisation or entity with any financial interest (such as honoraria; educational grants; participation in speakers' bureaus; membership, employment, consultancies, stock ownership, or other equity interest; and expert testimony or patent-licensing arrangements), or non-financial interest (such as personal or professional relationships, affiliations, knowledge or beliefs) in the subject matter or materials discussed in this manuscript.

Statement on Human Rights

Ethical approval All procedures performed in this study were carried out in accordance with the ethical standards of the institutional and/or national research committee and with the 1964 Helsinki declaration and its later amendments or comparable ethical standards.

Informed consent Informed consent was obtained from all individual participants included in the study.

References

1. Kremers J (2003) The assessment of L- and M-cone specific electroretinographical signals in the normal and abnormal human retina. Prog Ret Eye Res 22(5):79–605
2. Berson EL, Gouras P, Gunkel RD (1968) Rod responses in retinitis pigmentosa, dominantly inherited. Arch Ophthalmol 80:58–67
3. Berson EL, Gouras P, Gunkel RD, Myrianthopoulos NC (1969) Rod and cone responses in sex-linked retinitis pigmentosa. Arch Ophthalmol 81:215–225
4. Gouras P, Eggers HM, MacKay CJ (1983) Cone dystrophy, nyctalopia and supernormal rod responses. A new retinal degeneration. Arch Ophthalmol 101:718–724
5. Perlman I, Barzilai D, Haim T, Schramek A (1983) Night vision in a case of vitamin A deficiency due to malabsorption. Br J Ophthalmol 67:37–42
6. Scholl HPN, Langrova H, Weber BH, Zrenner E, Apfelstedt-Sylla E (2001) Clinical electrophysiology of two rod pathways: normative values and clinical application. Graefes Arch Clin Exp Ophthalmol 239(2):71–80
7. Petzold A, Plant GT (2006) Clinical disorders affecting mesopic vision. Ophthal Physiol Opt 26(3):326–341
8. Marmor M, Fulton AB, Holder GE et al (2009) ISCEV standard for full-field clinical electroretinography (2008 update). Doc Ophthalmol 118(1):69–77
9. Donner K, Rushton W (1959) Retinal stimulation by light substitution. J Physiol 149(2):288–302
10. Estevez O, Spekreijse H (1982) The "silent substitution" method in visual research. Vis Res 22(6):681–691
11. Shapiro AG, Pokorny J, Smith VC (1996) Cone–rod receptor spaces with illustrations that use CRT phosphor and light-emitting-diode spectra. J Opt Soc Am A 13(12):2319–2328
12. Cao D, Pokorny J, Grassi MA (2011) Isolated mesopic rod and cone electroretinograms realized with a four-primary method. Doc Ophthalmol 123(1):29–41
13. Maguire J, Parry NRA, Kremers J et al (2016) Rod electroretinograms elicited by silent substitution stimuli from the light adapted human eye. Trans Vis Sci Tech 5(4):10
14. Allen AE, Lucas RJ (2016) Using silent substitution to track the mesopic transition from rod- to cone-based vision in mice. Invest Ophthalmol Vis Sci 57:276–287
15. Alpern M, Falls HF, Lee GB (1960) The enigma of typical total monochromacy. Am J Ophthalmol 50:996–1012
16. Kohl S, Marx T, Giddings I et al (1998) Total colour blindness is caused by mutations in the gene encoding the alpha-subunit of the cone photoreceptor cGMP-gated cation channel. Nat Genet 19:257–259
17. Khan NW, Wissinger B, Kohl S, Sieving PA (2007) CNGB3 achromatopsia with progressive loss of residual cone function and impaired rod-mediated function. Invest Ophthalmol Vis Sci 48:3864–3871
18. Zeitz C, Robson AG, Audo I (2015) Congenital stationary night blindness: an analysis and update of genotype-phenotype correlations and pathogenic mechanisms. Prog Ret Eye Res 45:58–110
19. Miyake Y, Yagasaki K, Horiguchi M, Kawase Y, Kanda T (1986) Congenital stationary night blindness with negative electroretinogram. A new classification. Arch Ophthalmol 104:1013–1020
20. Dryja TP, McGee TL, Berson EL et al (2005) Night blindness and abnormal cone electroretinogram ON responses in patients with mutations in the GRM6 gene encoding mGluR6. Proc Natl Acad Sci USA 102:4884–4889
21. Sergouniotis PI, Robson AG, Li Z et al (2011) A phenotypic study of congenital stationary night blindness (CSNB) associated with mutations in the GRM6 gene. Acta Ophthalmol 90:192–197
22. Stockman A, MacLeod DI, Johnson NE (1993) Spectral sensitivities of the human cones. J Opt Soc Am A 10(12):2491–2521
23. Wyszecki G, Stiles WS (1982) Color science; concepts and methods, quantitative data and formulae, 2nd edn. Wiley, New York
24. Gouras P, Gunkel RD (1964) The frequency response of normal, rod achromat and nyctalope ERGs to sinusoidal monochromatic light stimulation. Doc Ophthalmol 18:137–150
25. Stockman A, Sharpe LT, Ruther K, Nordby K (1995) Two signals in the human rod visual system: a model based on electrophysiological data. Vis Neurosci 12(5):951–970
26. Bijveld MMC, Kappers AML, Riemslag FCC et al (2011) An extended 15 Hz ERG protocol (1): the contributions of primary and secondary rod pathways and the cone pathway. Doc Ophthalmol 123(3):149–159
27. Bijveld MM, Riemslag FC, Kappers AM, Hoeben FP, van Genderen MM (2011) An extended 15 Hz erg protocol (2): data of normal subjects and patients with achromatopsia, csnb1 and csnb2. Doc Ophthalmol 123(3):161–172
28. Robson JG, Frishman LJ (1998) Dissecting the dark-adapted electroretinogram. Doc Ophthalmol 95:187–215
29. Sieving PA, Frishman LJ, Steinberg R (1986) Scotopic threshold response of proximal retina in cat. J Neurophysiol 56:1049–1061
30. Sieving PA, Murayama K, Naarendorp F (1994) Push–pull model of the primate photopic electroretinogram: a role for hyperpolarizing neurons in shaping the b-wave. Vis Neurosci 11:519–532
31. Wang I, Khan NW, Branham K, Wissinger B, Kohl S, Heckenlively JR (2012) Establishing baseline rod electroretinogram values in achromatopsia and cone dystrophy. Doc Ophthalmol 125:229–233
32. Audo I, Robson AG, Holder GE, Moore AT (2008) The negative ERG: clinical phenotypes and disease mechanisms of inner retinal dysfunction. Surv Ophthalmol 53:16–40
33. Remmer MH, Rastogi N, Ranka MP, Ceisler EJ (2015) Achromatopsia: a review. Curr Opin Ophthalmol 26:333–340

34. Moskowitz A, Hansen RM, Akula JD, Eklund SE, Fulton AB (2009) Rod and rod-driven function in achromatopsia and blue cone monochromatism. Invest Ophthalmol Vis Sci 50:950–958
35. Genead MA, Fishman GA, Rha J, Dubis AM, Bonci DMO, Dubra A, Stone EM, Neitz M, Carroll J (2011) Photoreceptor structure and function in patients with congenital achromatopsia. Invest Ophthalmol Vis Sci 52:7298–7308
36. Stockman A, Sharpe LT (2006) Into the twilight zone: the complexities of mesopic vision and luminous efficiency. Ophthal Physiol Opt 26:225–239
37. Smith RG, Freed MA, Sterling P (1986) Microcircuitry of the dark-adapted retina: functional architecture of the rod-cone network. J Neurosci 6:3505–3517
38. Bloomfield SA, Dacheux RF (2001) Rod vision: pathways and processing in the mammalian retina. Prog Ret Eye Res 20:351–384
39. Sterling P, Freed M, Smith RG (1988) Architecture of rod and cone circuits to the On-beta ganglion cell. J Neurosci 8:623–642
40. Slaughter MM, Miller RF (1985) Characterization of an extended glutamate receptor of the ON bipolar neuron in the vertebrate retina. J Neurosci 5:224–233
41. Witkovsky P, Dudek FE, Ripps H (1975) Slow PIII component of the carp electroretinogram. J Gen Physiol 65:119–134
42. Frishman LJ, Steinberg R (1990) Origin of negative potentials in the light-adapted ERG of cat retina. J Neurophysiol 63:1333–1346
43. Brown KT (1968) The electroretinogram: its components and their origins. Vis Res 8:633–677
44. Granit R (1947) Sensory mechanisms of the retina. Oxford University Press, London
45. Eksandh L, Kohl S, Wissinger B (2002) Clinical features of achromatopsia in Swedish patients with defined genotypes. Ophthalmic Genet 23:109–120
46. Nishiguchi KM, Sandberg MA, Gorji N, Berson EL, Dryja TP (2005) Cone cGMP-gated channel mutations and clinical findings in patients with achromatopsia, macular degeneration, and other hereditary cone diseases. Hum Mutat 25:248–258
47. Brown KT, Murakami M (1967) Delayed decay of the late receptor potential of monkey cones as a function of stimulus intensity. Vis Res 7:179–189
48. Granit R, Riddell L (1934) The electrical responses of light- and dark-adapted frogs' eyes to rhythmic and continuous stimuli. J Physiol 81(1):1
49. Scholl HPN, Kremers J (2001) Electroretinograms in s-cone monochromacy using s-cone and rod isolating stimuli. Color Res Appl 26:S136–S139
50. Chen C, Zuo C, Piao C, Miyake Y (2005) Recording rod ON and OFF responses in ERG and multifocal ERG. Doc Ophthalmol 111:73–81
51. Hood DC, Finkelstein MA (1986) Sensitivity to light. In: Boff K, Kaufman L, Thomas J (eds) Handbook of Perception and Human Performance, vol 1. Wiley, New York, p 5-1–5-66
52. Aguilar M, Stiles W (1954) Saturation of the rod mechanism of the retina at high levels of stimulation. J Mod Opt 1:59–65
53. Cameron MA, Lucas RJ (2009) Influence of the rod photoresponse on light adaptation and circadian rhythmicity in the cone ERG. Mol Vis 15:2209–2216
54. Frumkes TE, Naarendorp F, Goldberg SH (1986) The influence of cone adaptation upon rod mediated flicker. Vis Res 26:1167–1176
55. Heikkinen H, Vinberg F, Nymark S, Koskelainen A (2011) Mesopic background lights enhance dark-adapted cone ERG flash responses in the intact mouse retina: a possible role for gap junctional decoupling. J Neurophysiol 105:2309–2318
56. Farrow K, Teixeira M, Szikra T et al (2013) Ambient illumination toggles a neuronal circuit switch in the retina and visual perception at cone threshold. Neuron 78:1–14
57. Volgyi B, Deans MR, Paul DL, Bloomfield SA (2004) Convergence and segregation of the multiple rod pathways in mammalian retina. J Neurosci 24:11182–11192
58. Raviola E, Gilula NB (1973) Gap junctions between photoreceptor cells in the vertebrate retina. Proc Natl Acad Sci USA 70:1677–1681

Appendix C

Reprint: CNGB3 Mutations Cause Severe Rod Dysfunction

OPHTHALMIC GENETICS
https://doi.org/10.1080/13816810.2017.1368087

CNGB3 mutations cause severe rod dysfunction

J. Maguire[a], M. McKibbin[b], K. Khan[b], S. Kohl[c], M. Ali[d], and D. McKeefry[a]

[a]School of Optometry and Vision Sciences, University of Bradford, Bradford, West Yorkshire, UK; [b]Department of Ophthalmology, St. James's University Teaching Hospital, Leeds, UK; [c]Molecular Genetics Laboratory, Institute of Ophthalmic Research, Centre of Ophthalmology, University Clinics Tubingen, Tubingen, Germany; [d]Section of Ophthalmology and Neuroscience, Leeds Institute of Biomedical and Clinical Sciences, University of Leeds, Leeds, UK

ABSTRACT

Purpose: Congenital achromatopsia or rod monochromatism is a rare autosomal recessive condition defined by a severe loss of cone photoreceptor function in which rods purportedly retain normal or near-to-normal function. This report describes the results of electroretinography in two siblings with *CNGB3*-associated achromatopsia.

Methods: Full field light- and dark-adapted electroretinograms (ERGs) were recorded using standard protocols detailed by the International Society for Clinical Electrophysiology of Vision (ISCEV). We also examined rod-mediated ERGs using series of stimuli that varied over a 6 log unit range of retinal illuminances (−1.9–3.5 log scotopic trolands).

Results: Dark-adapted ERGs in achromatopsia patients exhibited severely reduced b-wave amplitudes with abnormal *b:a* ratios (1.3 and 0.6). In comparison, the reduction in a-wave amplitude was less marked. The rod-mediated ERG took on an electronegative appearance at high-stimulus illuminances.

Conclusion: Although the defect that causes achromatopsia is primarily in the cone photoreceptors, our results reveal an accompanying disruption of rod function that is more severe than has previously been reported. The differential effects on the b-wave relative to the a-wave points to an inner-retinal locus for the disruption of rod function in these patients.

ARTICLE HISTORY
Received 8 February 2017
Revised 24 July 2017
Accepted 12 August 2017

KEYWORDS
Achromatopsia; electroretinogram; rods

Introduction

Complete achromatopsia (ACHM), also known as rod monochromacy, is a rare autosomal recessive congenital condition with a prevalence of 1:30,000, characterized by complete or partial loss of cone function (1). Clinically, patients present with photophobia, nystagmus, severely reduced visual acuity (20/200), and severe color vision deficits (2). Currently, six genes have been implicated in the generation of this disease, all of which encode crucial steps in the cone photo-transduction cycle. Two genes encoding for the cyclic nucleotide gated (CNG) channels alpha (α) and beta (β) (CNGA3, CNGB3) account for approximately 25% and 60% of the all mutations, respectively, with the rarer mutations found in the *GNAT2, PDE6C, PDE6H, ATF6* genes (1,3). Over 140 mutations have been discovered in the *CNGA3* and *CNGB3* genes, most of which result in a failure to produce α or β subunits. In the normal functioning retina, the CNG channels, located in the plasma membrane of the outer segment, are held open in darkness by cyclic guanosine monophosphate (cGMP), creating an inward positive current. When light causes hydrolysis of cGMP, the channels are closed causing a hyperpolarization of the cell; without functional subunits, CNG channels remain constantly closed, preventing cone hyperpolarization. In adults this can frequently result in the degeneration of cone photoreceptors. However, evidence of foveal disruption and hypoplasia has also been shown in young children (4–7). In a few cases, some residual cones may remain, although they too may later progressively decline (7–9).

In the light of the above findings, the canonical view of congenital ACHM has been that it is a condition that primarily leads to cone dysfunction, leaving rod photoreceptoral function largely intact (1,2,10–17). However, the phenotype is highly variable and a growing body of experimental evidence indicates that ACHM may not only lead to structural and functional abnormalities within the cone photoreceptor population but also may affect rod function as well. Rod dysfunction in ACHM, as assessed using ERG, has been noted in several studies, typically ranging from a mild (2,6,18–21) to a moderate reduction in the rod ERG amplitude (22–24). This can make discrimination between ACHM and cone–rod dystrophy (CORD) more difficult. Previously, the understanding was that the former was typically a stationary disease, associated with a normal rod ERG, whereas the latter was progressive in nature, affecting both rods and cones (25). An additional confounding factor is that both *CNGA3* and *CNGB3* genes have been implicated in autosomal recessive cone–rod dystrophy (arCORD) (22–27). In addition, structural changes more frequently associated with CORD, such as macular atrophy, have been reported in ACHM (14,21). In essence, the changes in amplitude noted to the rod ERG in ACHM generally remain in the sub-normal to

CONTACT D. McKeefry d.mckeefry@bradford.ac.uk School of Optometry and Vision Science, University of Bradford, Bradford, West Yorkshire BD7 1DP, UK.
Color versions of one or more of the figures in the article can be found online at www.tandfonline.com/iopg.

moderate category compared with severely reduced or abolished rod response found in CORD (12,24).

In this report, we present electro-retinographic results from two siblings with a homozygous 1148delC (Thr383fs) mutation in *CNGB3*. Interestingly, both of these siblings exhibit ERG findings which show severe disruption of the rod system, specifically confined to the inner retina, resulting in an electronegative ERG.

Materials and methods

Participants and clinical assessment

Two siblings from a consanguineous Pakistani family living in the U.K., both with molecularly confirmed *CNGB3*-associated ACHM were examined (see Table 1 for a summary of the main features). In brief, the patients were first examined at 1 year of age presenting with the classical features of ACHM —congenital nystagmus, reduced vision, and photophobia. Over three decades, changes in visual function have been minimal, with VA having remained constant. The most significant changes have been structural with progressive macular atrophy being noted on successive retinal examinations. The patients do not report any symptoms of nyctalopia and prefer conditions of low illumination.

At the time of this study, the patients were 31 years (Px1) and 38 years (Px 2) old, and full clinical history and assessment of the participants was performed which included Snellen visual acuity, color vision testing using the Color Assessment and Diagnosis (CAD) Test (City University, London), as well as ocular coherence tomography (OCT). In addition, Goldmann visual fields (Haag Streit, Bern, Switzerland) were assessed using the largest target on both ACHM patients (see Figure 1). The subjects gave informed consent prior to the commencement of the experiments and the study was conducted using a process that had been approved by the Leeds Research Ethics Committee and met the tenets of the Helsinki declaration.

Genetic assessment

One of the siblings (Patient 1) had previously been recruited to an earlier study investigating the molecular genetic basis for inherited retinal disease (IRD). As part of this study, patients' DNA was analyzed by Sanger sequencing of genes known at that

Table 1. Summary of the main clinical details of the ACHM patients.

Patient	Sex	Age	Symptoms	VA	Fundus
Px 1	Male	34 years	Nystagmus, photophobia, no color vision	CF (RE and LE)	Severe macular atrophy
Px 2	Female	38 years	Nystagmus, photophobia, no color vision	2/60 (RE and LE)	Severe macular atrophy

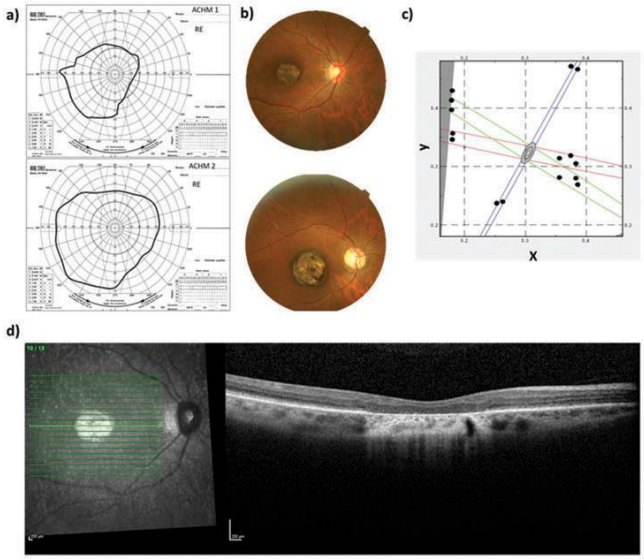

Figure 1. (a) Goldman visual field plots, and (b) fundus photographs for RE only of ACHM patients 1 and 2. (c) Color discrimination thresholds plotted on a CIE 1931 (xy) chromaticity diagram for 16 different colored targets along red, green, blue, and yellow color axes. Normal color discrimination thresholds (±1 SD) are indicated by the central grey ellipse. Both rod monochromats (only data from Patient 2 are shown) exhibit elevated discrimination thresholds consistent with severe L-, M-, and S-cone dysfunction. (d) OCT image of macular region of the RE of ACHM Patient 1.

time to be associated with ACHM in a step-by-step procedure. The proband was found to be homozygous for a null allele in *CNGB3* (NM_019098.4; c.1148delC, p.T383Ifs*13), the most frequently reported cause of ACHM in those of European ancestry (28). Segregation analysis confirmed that Patient 2 was also homozygous for the c.1148delC allele.

Electrophysiological assessment

Full-field ERGs were recorded using a ColorDome (Diagnosys LLC, Lowell, MA, USA) four primary ganzfeld stimulator and were obtained using standard protocols detailed by the International Society for Clinical Electrophysiology of Vision (ISCEV) (29). The light-adapted (LA) single flash and 30 Hz flicker stimuli (both 3.0 cd/s/m^2) were used to assess the cone system. Following a period of 20 min dark adaptation, 0.01 cd/s/m^2 (DA0.01) and 10.0 cd/s/m^2 (DA10.0) flash stimuli were used to elicit rod responses. In addition to the standard ISCEV stimuli, we also examined rod-mediated ERGs in our patient group and an age-matched control using series of stimuli that varied over a wider range (~6 log units) of retinal illuminance from −1.9 to 3.6 log scotopic trolands. ERGs were recorded using these stimuli which consisted of brief (4 ms) white flashes delivered after 20 min of dark adaptation.

ERGs were recorded from the right eye using a silver/nylon corneal fiber electrode (Department of Physics and Clinical Engineering, Royal Liverpool University Hospital, UK) referenced to a 9 mm Ag/AgCl electrode (Biosense Medical, Chelmsford, UK) on the outer canthus; a similar electrode was placed on the forehead to serve as ground. Impedance was maintained below 5 kΩ. Signals were recorded using the Espion E^2 system (Diagnosys LLC, Lowell, MA, USA) which amplified and filtered (bandwidth = 1–300 Hz) the ERGs and digitized them at a rate of 1000 Hz. Participants viewed the stimuli monocularly with a dilated pupil (1% Tropicamide).

Results

Figure 2 shows the standard ISCEV full-field ERG responses from the ACHM patients as well as a set of responses from a representative age-matched normal subject. The light-adapted single flash and the photopic flicker responses were undetectable in both ACHM patients, consistent with the severe cone dysfunction typically reported for this condition (22). The DA0.01 responses were also abnormal, with a severe loss of b-wave amplitude (Table 2). Patient 1's responses are reduced by 74%, while Patient 2 has lost 87% of their b-wave amplitude compared with our normal mean value. The DA10.0 waveforms also exhibit significant loss of b-wave amplitude, and for Patient 2 the waveforms are electronegative. A smaller reduction is noted in a-wave amplitude which may be explained by the loss of input from the dark-adapted cone system (30). Implicit times of the a- and b-waves are also increased compared with normative data (see Table 2).

Figure 3 shows the ERG waveforms for dark-adapted ERGs recorded as a function of retinal illuminance across a 6 log unit scale (−1.9–3.6 log scot trolands). The data show clear qualitative differences between the ERG waveforms obtained from an individual with normal rod function compared with those obtained from the two rod monochromats across the same illuminance range. In particular, the responses generated at low retinal illuminances (−1.9 to −0.9 log scot trolands) are markedly attenuated in the rod monochromats compared with the normal ERGs. In fact, b-wave amplitude is reduced across the whole illuminance range in the rod monochromats and again the development of the electronegative response in Patient 2 can be clearly observed beyond 1.1 log scot trolands.

In Figure 4 peak amplitudes and implicit times of the a- and b-waves have been plotted as a function of retinal illuminance for a normal control participant and the ACHM patients 1 and 2. As indicated by the waveforms in Figure 3, the greatest difference is in b-wave amplitude (Figure 4A). The illuminance response function from the normal subject exhibits an initial steep increase in

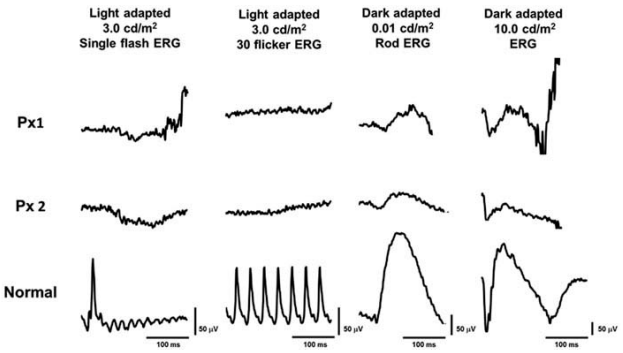

Figure 2. ISCEV standard full-field ERGs (RE only) recorded from two patients diagnosed with ACHM (rows I and II) plus a dataset from a representative of our normal control group (row III). Column 1: light adapted single flash response (3.0 cd/s/m^2); Column 2: 30 Hz flicker stimulus (3.0 cd/s/m^2); Column 3; dark-adapted (rod only) response (0.01 cd/s/m^2); Column 4: bright flash (10.0 cd/s/m^2).

Table 2. Summary of the amplitude (amp) and latency (lat) measurements for ERGs elicited by the standard ISCEV protocols.

Patients	Light adapted Single flash ERG	Light adapted Flicker ERG	Dark adapted 0.01 cd/s/m^2 ERG	Dark adapted 10.0 cd/s/m^2 ERG
Px 1				
a-wave amp	X	X	—	85.0
b-wave amp	X	X	42.16	114.37
a-wave lat	X	X	—	16.0
b-wave lat	X	X	114.0	57.0
Px 2				
a-wave amp	X	X	—	83.93
b-wave amp	X	X	21.25	44.39
a-wave lat	X	X	—	14.0
b-wave lat	X	X	90.0	57.0
Normal				
a-wave amp	17.95 ± 1.87	—	—	131.35 ± 10.92
b-wave amp	82.38 ± 7.85	47.17 ± 5.41	163.15 ± 15.88	271.01 ± 14.82
a-wave lat	15.15 ± 0.36	—	—	12.82 ± 0.53
b-wave lat	28.75 ± 0.37	26.24 ± 0.52	92.33 ± 3.02	50.66 ± 2.37

X denotes that no data could be obtained as the waveform component was undetectable, — denotes that no measurements were taken for that particular component. Normal values are based on n = 70 subjects assessed in the University of Bradford Electrodiagnostic Unit.

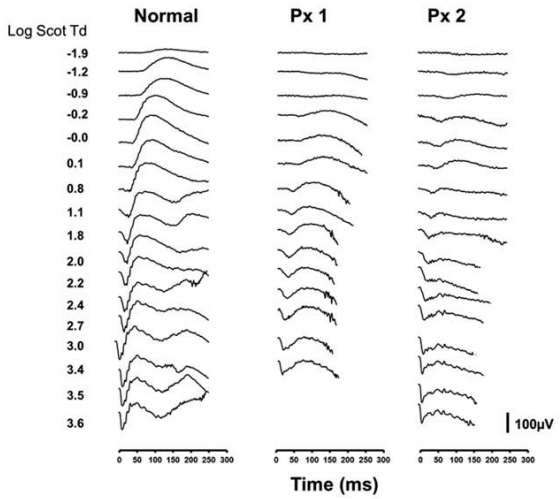

Figure 3. Dark-adapted ERGs generated by a series of stimuli of increasing retinal illuminance (−1.9–3.6 log scot trolands). ERGs from the age-matched normal control are shown in the first column with responses from the two ACHM patients shown in columns 2 and 3. ERG responses were not recorded to the two highest luminances for Px 1.

b-wave amplitude up to 1 log scot troland after which it reaches saturation. This saturating response function of the dark-adapted ERG has been described previously and is considered to be the result of an algebraic interaction between receptoral and post-receptoral retinal responses at higher illuminances (31,32). In contrast, the b-wave amplitude illuminance–response functions from the two monochromats are markedly different; with b-wave amplitude exhibiting a much shallower, monotonic increase with increasing retinal illuminance. The illuminance response of the a-wave (Figure 4C), by comparison, appears to be similar across the rod monochromats and the normal. In terms of a- and b-wave implicit times (Figure 4B and D) the biggest differences between the control subject and patients occur at low retinal illuminances (<1 log scot trolands) where the ERGs from the rod monochromats have considerably longer a- and b-wave implicit times. However, as retinal illuminance increases the differences in implicit times between the normal and the achromatopsic patients becomes less marked.

Discussion

In this case study, we have reported the results of visual electrophysiology in two siblings with *CNGB3*-associated ACHM and have demonstrated the existence of an unusually severe deficit of rod-mediated retinal function. As would commonly be expected in cases of complete ACHM,

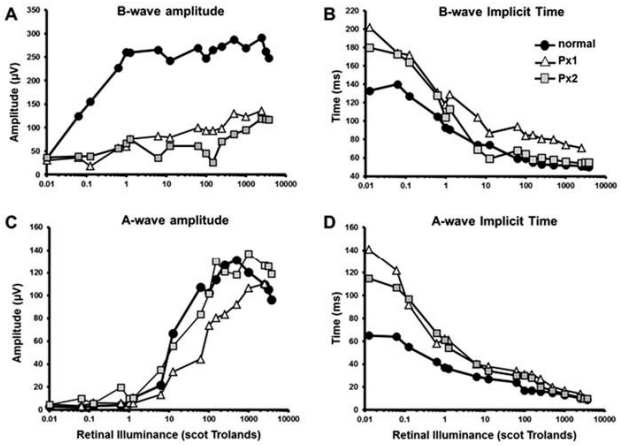

Figure 4. Plots of b-wave amplitude (A) and implicit time (B) and a-wave amplitude (C) and implicit time (D) as a function of retinal illuminance for the data shown in Figure 3 for the two-rod monochromats and the age-matched control subject.

electroretinography reveals a complete loss of cone function. However, this deficit is also accompanied by marked abnormalities of the rod-mediated dark-adapted b-wave ERG responses. While *CNGB3* mutations with moderate rod dysfunction have previously been reported in the literature (20–23), we are not aware of any cases demonstrating such severe rod involvement as exhibited by the individuals examined here. In particular, the electronegative appearance of the dark-adapted ERGs to more intense stimuli is a previously unreported finding for this specific mutation.

Rod function was assessed using standard ISCEV protocols. The dark-adapted (DA) rod stimulus (0.01 cd/s/m^2) elicits an ERG in the normal population that is typically dominated by a large positive component (the b-wave) with a peak occurring at approximately 100 ms after stimulus onset. This response reflects the activity of rod ON-bipolar cells from the inner nuclear layer of the retina (33,34). As the intensity of the stimulus is increased, the b-wave is preceded by a negative a-wave in the dark-adapted ERG, which predominantly reflects activity in the outer segments of the rod photoreceptors (30,34). The data presented here show that patients with *CNGB3*-associated ACHM have significant functional abnormalities in their rod system which accompanies severe cone dysfunction. This rod dysfunction in the ACHM patients is manifest in the severely attenuated b-wave amplitudes of the dark-adapted ERGs. In comparison, the a-waves of these responses are less drastically affected. While there is some reduction in a-wave amplitude across the illuminance range tested (something which is most likely attributable to the loss of contribution from the dark-adapted cones (30,34)), on the whole, a-wave amplitudes in the ACHM patients are comparable to normals. This differential effect on the b- and a-waves has not previously been reported and is significant because it points to a post-receptoral, inner retinal origin for this loss of rod function. It suggests that the deficit is at the level of the rod ON-bipolar cells, rather than at the level of the rod photoreceptors.

The reasons for the deficits in rod-mediated retinal function are not entirely clear. It is unlikely to be simply an age-related loss of rod function. The ages of the two ACHM patients in this study fall well within the range of previous study (5) where the ACHM patient cohort exhibits milder rod deficits than those reported here. Furthermore, the study by Moskowitz and colleagues (23) report rod deficits in a much younger group (median age 2.7 years) of ACHM patients. Genetic testing for the patients examined in this study was performed by successive Sanger sequencing of the following genes until a cause was identified (*CNGA3, CNGB3, GNAT2, PDE6C*). There remains the slim possibility that the family also segregate another monogenic retinopathy. However, the fact that the ERG shows a near normal a-wave with more severe b-wave reduction specifically suggests a predominantly inner retina dysfunction, which is not a classical feature associated with cone–rod dystrophy. A more likely explanation is that the environment created by degenerating cones may play a part in the generation of dysfunction in rod-mediated vision. Macular atrophy was an acquired feature in both patients suggesting there is some outer retinal degeneration at the macula and supporting the idea that rod dysfunction may be a secondary feature of cone death. In addition, work in mouse models has shown significant correlations between cone cell death and CNG channel abnormalities. A recent review of cone cell death in ACHM (35) has outlined several mechanisms that may contribute to cone apoptosis; stress markers associated with the endoplasmic reticulum are increased in CNGA3$^{-/-}$ and CNGA3$^{-/-}$ knockout mice. Abnormal levels of cellular $Ca2^{++}$ or cGMP often associated with ACHM have been shown to increase endoplasmic reticulum stress (36).

Recent advances in adaptive optics have made it possible to examine the structure of the both inner and outer segments of the photoreceptor layer *in vivo* using adaptive optics scanning laser ophthalmoscopy (AOSLO) (37,38). Imaging in patients with ACHM has shown significant loss and disruption of cone photoreceptors, but no real evidence of a decrease in the number of rods (5,7). However, changes in rod structure have been observed. Typically, the diameter of a rod photoreceptor in a healthy retina at 10° eccentricity is approximately 2.3 μm. Measurements of rod diameter in patients with ACHM in a similar region were shown to be on average 1 μm greater (4). This increase in diameter may be as a direct result of increased space in the retina which allows rods to expand following the loss of cone cells (23). Increases in rod diameter naturally occur in the ageing retina as the overall number of rod cells is reduced (39). It has been suggested that structural changes like these may well result in an alteration of the photo-transduction process and even post-receptoral connections (23).

In summary, we believe this report further adds to the evidence that ACHM associated with a homozygous mutation in the *CNGB3* gene can lead to abnormalities of rod-mediated vision as well cone dysfunction. More significantly, we have shown for the first time, the presence of an electronegative ERG that occurs as a consequence of this mutation. The deficits in the rod responses reported here are more severe than those that have been previously reported in ACHM patients. A key finding of this study is that it is the rod b-wave that is more severely affected, compared with the a-wave, which is relatively well preserved. This points to a post-receptoral/inner retinal site for the pathological changes in rod function found in these patients.

References

1. Remmer MH, Rastogi N, Ranka MP, Ceisler EJ. Achromatopsia: a review. Curr Opin Ophthalmol. 2015;26(5):333–40. doi:10.1097/ICU.0000000000000189.
2. Eksandh L, Kohl S, Wissinger B. Clinical features of achromatopsia in Swedish patients with defined genotypes. Ophthal Genet. 2002;23(2):109–20. doi:10.1076/opge.23.2.109.2210.
3. Kohl S, Zobor D, Chiang W-C, Weisschuh N, Staller J, Gonzalez Menendez I, et al. Mutations in the unfolded protein response regulator ATF6 cause the cone dysfunction disorder achromatopsia. Nat Genet. 2015;47(7):757–65. doi:10.1038/ng.3319.
4. Carroll J, Choi SS, Williams DR. In vivo imaging of the photoreceptor mosaic of a rod monochromat. Vis Res. 2008;48(26):2564–68. doi:10.1016/j.visres.2008.04.006.
5. Genead MA, Fishman GA, Rha J, Dubis AM, Bonci DMO, Dubra A, Stone EM, Neitz M, Carroll J. Photoreceptor structure and function in patients with congenital achromatopsia. Invest Ophthalmol Vis Sci. 2011;52(10):7298–308. doi:10.1167/iovs.11-7762.
6. Yang P, Michaels KV, Courtney RJ, et al. Retinal morphology of patients with achromatopsia during early childhood: implications for gene therapy. JAMA Ophthalmol. 2014;132:823–31. doi:10.1001/jamaophthalmol.2014.685.
7. Langlo CS, Patterson EJ, Higgins BP, Summerfelt P, Razeen MM, Erker LR, et al. Residual Foveal Cone Structure in CNGB3-Associated Achromatopsia. Invest Ophthalmol Vis Sci. 2016;57(10):3984–95. doi:10.1167/iovs.16-19313.
8. Thiadens AAHJ, Somervuo V, van den Born LI, Roosing S, van Schooneveld MJ, Kuijpers RWAM, van Moll-Ramirez N, Cremers FPM, Hoyng CB, Klaver CCW. Progressive loss of cones in achromatopsia: an imaging study using spectral-domain optical coherence tomography. Invest Ophthalmol Vis Sci. 2010;51(11):5952–57. doi:10.1167/iovs.10-5680.
9. Thomas MG, McLean RJ, Kohl S, Sheth V, Gottlob I. Early signs of longitudinal progressive cone photoreceptor degeneration in achromatopsia. Brit J Ophthalmol. 2012;96:1232–36. doi:10.1136/bjophthalmol-2012-301737.
10. Kohl S, Hamel CP. Clinical utility gene card for: achromatopsia. Eur J Hum Genet. 2011;19(6). doi:10.1038/ejhg.2010.231.
11. Ouechtati F, Merdassi A, Bouyacoub Y, Largueche L, Derouiche K, Ouragini H, et al. Clinical and genetic investigation of a large Tunisian family with complete achromatopsia: identification of a new nonsense mutation in GNAT2 gene. J Hum Genet. 2011;56:22–28. doi:10.1038/jhg.2010.128.
12. Saqib MA, Awan BM, Sarfraz M, Khan MN, Rashid S, Ansar M. Genetic analysis of four Pakistani families with achromatopsia and a novel S4 motif mutation of CNGA3. Jap J Ophthalmol. 2011;55:676–80. doi:10.1007/s10384-011-0070-y.
13. Wawrocka A, Kohl S, Baumann B, Walczak-Sztulpa J, Wicher K, Skorczyk-Werner A, Krawczynski MR. Five novel CNGB3 gene mutations in Polish patients with achromatopsia. Mol. 2014;20:1732–39.
14. Katagiri S, Hayashi T, Yoshitake K, Sergeev Y, Akahori M, Furuno M, et al. Congenital achromatopsia and macular atrophy caused by a novel recessive PDE6C Sutation (p.E591K). Ophthalmic Genet. 2015;36:137–44. doi:10.3109/13816810.2014.991932.
15. Liang X, Dong F, Li H, Yang L, Sui R. Novel CNGA3 mutations in Chinese patients with achromatopsia. Brit J Ophthalmol. 2015;99:571–76. doi:10.1136/bjophthalmol-2014-305432.
16. Kuniyoshi K, Muraki-Oda S, Ueyama H, Toyoda F, Sakuramoto H, Ogita H, et al. Novel mutations in the gene for alpha- subunit of retinal cone cyclic nucleotide-gated channels in a Japanese patient with congenital achromatopsia. Jap J Ophthalmol. 2016;60:187–97. doi:10.1007/s10384-016-0424-6.
17. Ueno S, Nakanishi A, Kominami T, Ito Y, Hayashi T, Yoshitake K, Kawamura Y, Tsunoda K, Iwata T, Terasaki H. In vivo imaging of a cone mosaic in a patient with achromatopsia associated with a GNAT2 variant. Jap J Ophthalmol. 2017;61:92–98. doi:10.1007/s10384-016-0484-7.
18. Doucette L, Green J, Black C, Schwartzentruber J, Johnson GJ, Galutira D, Young T-L. Molecular genetics of achromatopsia in Newfoundland reveal genetic heterogeneity, founder effects and the first cases of Jalili syndrome in North America. Ophthalmic Genet. 2013;34:119–29. doi:10.3109/13816810.2013.763993.
19. Kurent A, Stirn-Kranjc B, Brecelj J. Electroretinographic characteristics in children with infantile nystagmus syndrome and early-onset retinal dystrophies. Eur J Ophthalmol. 2015;25:33–42. doi:10.5301/ejo.5000493.
20. Nishiguchi KM, Sandberg MA, Gorji N, Berson EL, Dryja TP. Cone cGMP-gated channel mutations and clinical findings in patients with achromatopsia, macular degeneration, and other hereditary cone diseases. Hum Mutat. 2005;25:248–58. doi:10.1002/humu.20142.
21. Sundin OH, Yang JM, Li Y, Zhu D, Hurd JN, Mitchell TN, Silva ED, Hussels Maumenee I. Genetic basis of total colour blindness among the Pingelapese islanders. Nat Genet. 2000;25:289–29. doi:10.1038/77162.
22. Khan NW, Wissinger B, Kohl S, Sieving PA. CNGB3 achromatopsia with progressive loss of residual cone function and impaired rod-mediated function. Invest Ophthalmol Vis Sci. 2007;48:3864–71. doi:10.1167/iovs.06-1521.
23. Moskowitz A, Hansen RM, Akula JD, Eklund SE, Fulton AB. Rod and rod-driven function in achromatopsia and blue cone monochromatism. Invest Ophthalmol Vis Sci. 2009;50:950–58. doi:10.1167/iovs.08-2544.
24. Li S, Huang L, Xiao X, Jia X, Guo X, Zhang Q. Identification of CNGA3 mutations in 46 families: common cause of achromatopsia and cone-rod dystrophies in Chinese patients. JAMA Ophthalmol. 2014;132:1076–83. doi:10.1001/jamaophthalmol.2014.1032.
25. Michaelides M, Aligianis IA, Ainsworth JR, Good P, Mollon JD, Maher ER, Moore AT, Hunt DM. Progressive cone dystrophy associated with mutation in CNGB3. Invest Ophthalmol Vis Sci. 2004;45:1975–82. doi:10.1167/iovs.03-0898.

26. Thiadens AA, Roosing S, Collin RW, van Moll-Ramirez N, van Lith-Verhoeven JJ, van Schooneveld MJ, et al. Comprehensive analysis of the achromatopsia genes CNGA3 and CNGB3 in progressive cone dystrophy. Ophthalmol. 2010;117:825–30.e1. doi:10.1016/j.ophtha.2009.09.008.
27. Shaikh RS, Reuter P, Sisk RA, Kausar T, Shahzad M, Maqsood MI, et al. Homozygous missense variant in the human CNGA3 channel causes cone-rod dystrophy. Eur J Hum Genet. 2015;23:473–80. doi:10.1038/ejhg.2014.136.
28. Kohl S, Varsanyi B, Antunes GA, Baumann B, Hoyng CB, Jägle H, et al. CNGB3 mutations account for 50% of all cases with autosomal recessive achromatopsia. Eur J Hum Genet. 2005;13 (3):302–08. doi:10.1038/sj.ejhg.5201269.
29. McCulloch DL, Marmor MF, Brigell MG, Hamilton R, Holder GE, Tzekov R, Bach M. ISCEV Standard for full-field clinical electroretinography (2015 update). Doc Ophthalmol. 2015;130 (1):1–12. doi:10.1007/s10633-014-9473-7.
30. Robson JG, Frishman LJ. The rod-driven a-wave of the dark-adapted mammalian electroretinogram. Prog Ret Eye Res. 2014;39:1–22. doi:10.1016/j.preteyeres.2013.12.003.
31. Peachey NS, Alexander KR, Fishman GA. The luminance-response function of the dark-adapted human electroretinogram. Vis Res. 1989;29(3):263–70. doi:10.1016/0042-6989(89)90075-8.
32. Wali N, Leguire LE. Dark-adapted luminance-response functions with skin and corneal electrodes. Doc Ophthalmol. 1989;76 (4):367–75. doi:10.1007/BF00142675.
33. Stockton RA, Slaughter MM. b-Wave of the electroretinogram: a reflection of ON bipolar cell activity. J Gen Physiol. 1989;93:101–22. doi:10.1085/jgp.93.1.101.
34. Robson JG, Frishman LJ. Dissecting the dark-adapted electroretinogram. Doc Ophthalmol. 1998;95(3–4):187–215. doi:10.1023/A:1001891904176.
35. Carvalho LS, Vandenberghe LH. Understanding cone photoreceptor cell death in achromatopsia. In: Bowes Rickman C, LaVail M, Anderson RE, Grimm C, Hollyfield J, Ash J, editors. Retinal Degenerative Diseases: Mechanisms and Experimental Therapy. New York: Springer; 2016: p. 231-36.
36. Thapa A, Morris L, Xu J, Michalakis S, Biel M, Ding XQ. Endoplasmic reticulum stress-associated cone degeneration in cyclic nucleotide-gated channel deficiency. Invest Ophthalmol Vis Sci. 2012;53(14):4282–4282.
37. Dubra A, Sulai Y, Norris JL, Cooper RF, Dubis AM, Williams DR, Carroll J. Noninvasive imaging of the human rod photoreceptor mosaic using a confocal adaptive optics scanning ophthalmoscope. Biomed Opt Exp. 2011;2(7):1864–76. doi:10.1364/BOE.2.001864.
38. Scoles D, Sulai YN, Langlo CS, Fishman GA, Curcio CA, Carroll J, Dubra A. In vivo imaging of human cone photoreceptor inner segments. Invest Ophthalmol Vis Sci. 2014;55(7):4244–51. doi:10.1167/iovs.14-14542.
39. Werner J. Night vision in the elderly: consequences for seeing through a "blue filtering" intraocular lens. Brit J Ophthalmol. 2005;89(11):1518–21. doi:10.1136/bjo.2005.073734.

Appendix D

Reprint: Human S-cone Electroretinograms Obtained by Silent Substitution Stimulation

Research Article Vol. 35, No. 4 / April 2018 / Journal of the Optical Society of America A B11

Journal of the Optical Society of America A
OPTICS, IMAGE SCIENCE, AND VISION

Human S-cone electroretinograms obtained by silent substitution stimulation

J. Maguire,[1] N. R. A. Parry,[1,2,3] J. Kremers,[1,4] I. J. Murray,[3] and D. McKeefry[1,*]

[1]School of Optometry and Vision Sciences, University of Bradford, Bradford, UK
[2]Vision Science Centre, Manchester Royal Eye Hospital, Manchester University NHS Foundation Trust, Manchester Academic Health Science Centre, Manchester, UK
[3]Faculty of Biology, Medicine & Health, University of Manchester, Manchester, UK
[4]Department of Ophthalmology, University Hospital Erlangen, Erlangen, Germany
*Corresponding author: d.mckeefry@bradford.ac.uk

Received 2 November 2017; revised 19 December 2017; accepted 27 December 2017; posted 3 January 2018 (Doc. ID 312491); published 29 January 2018

We used triple silent substitution stimuli to characterize human S-cone electroretinograms (ERGs) in normal trichromats. Short-wavelength-cone (S-cone) ERGs were found to have different morphological features and temporal frequency response characteristics compared to ERGs derived from L-cones, M-cones, and rod photoreceptors in normal participants. Furthermore, in two cases of retinal pathology, blue cone monochromatism (BCM) and enhanced S-cone syndrome (ESCS), S-cone ERGs elicited by our stimuli were preserved and enhanced, respectively. The results from both normal and pathological retinae demonstrate that triple silent substitution stimuli can be used to generate ERGs that provide an assay of human S-cone function.

OCIS codes: (330.1720) Color vision; (330.5020) Perception psychology; (330.5310) Vision - photoreceptors; (330.5510) Psychophysics.

https://doi.org/10.1364/JOSAA.35.000B11

1. INTRODUCTION

The human electroretinogram (ERG) is a response that provides a measure of the global electrophysiological activity of the retina in response to light stimulation. Responses to diffuse flashes of light of the kind typically used in the clinical assessment of human ERGs [1] contain contributions from all the main classes of cone [long- (L), middle- (M), and short-wavelength (S) sensitive] and rod photoreceptors. While such stimuli have undoubtedly proven to be useful in assessing retinal function in a global, non-selective manner, there has also been a great deal of interest in attempting to record ERGs that reflect the activity of individual photoreceptor populations.

The ERG that arises from isolated S-cone photoreceptors has been of particular interest. From a clinical perspective, this is driven primarily by the suggestion that S-cones are more vulnerable to damage in congenital and acquired retinal, as well as systemic, pathologies [2–8]. For example, several studies have demonstrated selective or more severe changes in S-cone-mediated ERGs, compared to L- and M-cone responses, in certain forms of retinitis pigmentosa [9], type 1 and type 2 diabetes [6,7], glaucoma [10], and ocular hypertension [11,12]. Interest in isolating responses from S-cones has also been driven by the fact that the S-cone system forms part of a visual pathway that has several distinctive properties that set it apart from vision mediated by L- and M-cones [13]. For example, S-cones have different evolutionary origins from L- and M-cones [2,14]. The gene for the S-cone opsin is located on chromosome 7, rather than on the *X* chromosome, as it is for the L- and M-cone opsins [15]. S-cones also have distinctive anatomical [16–20] and functional [21] properties compared to L- and M-cones.

In the light of the special status of S-cone mediated vision, numerous attempts adopting different methodologies have been made at isolating ERGs that reflect their operation. In some studies, S-cone isolation was achieved via chromatic adaptation [22–28]. This technique relies upon the use of a short-wavelength incremental flash stimulus, superimposed on a high-luminance broadband or longer-wavelength background to which L-cones, M-cones, and rods are adapted. In other studies, silent substitution techniques [29] were employed to isolate responses from S-cones [7,9,28,30–32]. The isolation of S-cone activity via silent substitution requires alternation between two stimuli that contain mixtures of wavelengths at different intensities, which elicit no overall change in excitation in the L-cones, M-cones, and rods, but do elicit changes in S-cone excitation. The isolation of one out of *n* classes of photoreceptor requires a minimum of *n* primaries

tuned to different wavelengths. Therefore, to isolate human S-cones, a triple silent substitution stimulus is needed, which necessitates generation by a four-primary system. Although two previous studies have used double silent substitution combined with sufficiently high background luminances to suppress the rods [31,32], none have, as yet, recorded an isolated S-cone ERG using triple silent substitution.

The aim of this study was to generate human S-cone ERGs using triple silent substitution stimuli generated on a four-primary Ganzfeld stimulator. First, we wanted to characterize the morphology of the S-cone ERG in normal trichromats and compare it to the waveforms generated by L-cone-, M-cone-, and rod-isolating stimuli. Second, we wanted to examine how the morphology of the S-cone ERG is affected in two kinds of hereditary retinal pathology; blue cone monochromatism (BCM) and enhanced S-cone syndrome (ESCS). Both pathologies have relevance to S-cone-mediated vision. BCM is an *X*-linked congenital cone dysfunction syndrome caused by L- and M-cone opsin gene array mutations that result in non-functional photopigments. This leads to an absence of L- and M-cone function in affected individuals, who are left with only preserved S-cone and rod function [33–38]. As a result, color discrimination is severely impaired in subjects with BCM, but there is some preservation of tritan discrimination [37,39]. ESCS is a rare genetic disease associated with an increase in the number and sensitivity of S-cones within the retina [40–44]. The ERG in individuals with ESCS is dominated by the S-cone response with reduced contribution from the L- and M-cones [40,42,45]. By comparing the responses elicited from patients with these pathologies with those from normal trichromats, we wanted to verify whether the S-cone ERGs generated by our triple silent substitution technique can provide responses that selectively reflect S-cone-mediated visual function in the human retina.

2. METHODS

A. Stimuli

Photoreceptor-isolating stimuli were presented on a ColorDome (Diagnosys LLC, Lowell, Massachusetts, USA) four-primary Ganzfeld stimulator. The four light-emitting diodes (LEDs) had the following peak wavelengths: blue [460 nm ± 15 nm (half-bandwidth at half height)], green (514 nm ± 20 nm), amber (590 nm ± 8 nm) and red (635 nm ± 10 nm). The spectral characteristics, chromaticities, and luminances of each class of LED were calibrated using a PR650 spectrophotometer (Photo Research Inc., Chatsworth, California, USA). The stimuli used in these experiments comprised triple silent substitutions whereby responses from rods, L-, M-, or S-cone photoreceptor populations were obtained in isolation using temporal modulations of color and luminance of the four LEDs [29,46]. Stimulus contrast (i.e., photoreceptor modulation) was defined as the Michelson contrast [Eq. (1)] of rod or cone excitation (E) and was set at 0.25 for all stimuli:

$$\text{Contrast} = (\text{Emax} - \text{Emin})/(\text{Emax} + \text{Emin}). \quad (1)$$

To create silent substitution stimuli, photoreceptor excitations were calculated by multiplying the emission spectra of the LEDs with cone fundamentals and the $V'\lambda 10°$ function [47,48] and integrating over a range of wavelengths (see: Ref. [49] for a fuller description of stimulus generation).

Two forms of temporal stimulation were used in this study; transient and steady-state. For the former, the luminance of the LEDs was modulated with a square-wave temporal profile (250 ms on, 250 ms off) to generate L-cone-, M-cone-, S-cone-, and rod-isolating stimuli (see Fig. 1). For the steady-state stimuli, the luminance of the four LEDs was modulated with sinusoidal profiles ranging from 5 to 70 Hz. These stimuli allowed assessment of the temporal frequency response characteristics of the photoreceptor-isolated ERGs. The modulation of photoreceptor excitation was kept constant at 0.25 for all stimuli. The retinal illuminance produced by each of the cone-isolating stimuli was 8000 photopic trolands (phot Td). The retinal illuminance of the rod-isolating stimuli was 63 phot Td.

B. ERG Recording

ERGs were recorded from the right eye using a silver/nylon corneal fiber electrode (Dept. of Physics and Clinical Engineering, Royal Liverpool University Hospital, UK) referenced to a 9 mm Ag/AgCl electrode (Biosense Medical, Chelmsford, UK) on the outer canthus; a similar electrode was affixed to the forehead to serve as ground. Impedance was maintained below 5 kΩ. Signals were recorded using the Espion E^2 system (Diagnosys LLC, Lowell, Massachusetts, USA), which amplified and filtered (bandwidth = 1 to 300 Hz) the ERGs and digitized them at a rate of 1000 Hz. Retinal responses were acquired over 500 ms

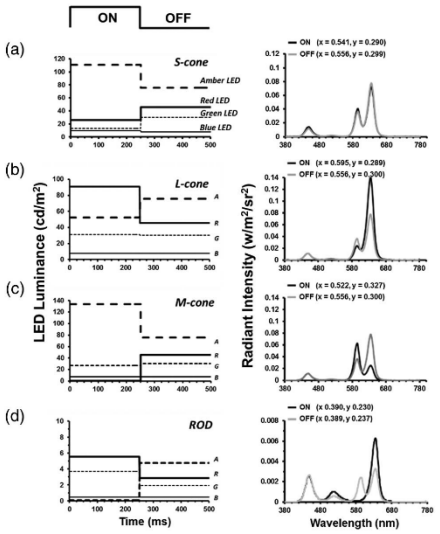

Fig. 1. Left-hand column: LED luminance profiles used to generate the (a) S-cone-, (b) L-cone-, (c) M-cone-, and (d) rod-isolating transient ERGs. The right-hand column shows the spectral characteristics of the onset and offset phases of the same stimuli along with the CIE (1931) *xy* chromaticity coordinates of the onset and offset phases.

epochs with each response being composed of a minimum of 256 repetitions. Participants viewed the stimuli monocularly with a dilated pupil (1% Tropicamide) and both a chin- and head-rest were used. Fixation was maintained on a central point that subtended approximately 0.5°.

C. Data Analysis

The averaged steady-state ERGs were subjected to a two-stage offline analysis involving: first, resampling of the traces, and second, Fourier analysis. ERG responses were recorded using a sampling rate of 1000 Hz with an epoch of 4000 ms, but because the fast Fourier transform (FFT) uses a sampling rate of 1024 Hz, a simple interpolation was required to produce 4096 samples. The resampled traces were imported into Signal software (version 2.16; Cambridge Electronic Design, Cambridge, UK) and subjected to a FFT. This analysis provided a measure of the amplitude at the fundamental (stimulating) frequency. Noise (N) was defined as the mean amplitude (A) of the response ±1 Hz from the stimulation frequency (F):

$$N = (A(F-1) + A(F+1))/2. \quad (2)$$

A response was considered significant if the measured ERG amplitude was a least 2.82 times greater than the computed noise amplitude for that frequency [50].

D. Participants

A total of 16 color-normal trichromats (5 males, 11 females; mean age: 33 yrs; age range: 20–60 yrs) participated in this study. In addition, two participants diagnosed with blue cone monochromacy (BCM) and one participant diagnosed with enhanced S-cone syndrome (ESCS) were tested. The participants with BCM have an L opsin gene, with a novel point mutation p. Pro196Ala, predicted to account for the phenotype. The participant with ESCS has bi-allelic loss of function mutations in *NRL*. This is a transcription factor that positively regulates *NR2E3*, and the loss of function is likely to cause the phenotype. Color vision in all subjects (except the participant with ESCS) was assessed using the CAD color test (City University, UK). The 16 trichromats had normal red/green and yellow/blue color thresholds. The BCM subjects had highly elevated red/green thresholds (BCM1 35.78 × normal; BCM2 38.80 × normal). Their yellow/blue thresholds were also slightly elevated compared to the normals (BCM1 3.96 × normal; BCM2 3.51 × normal).

All subjects gave informed consent prior to the commencement of the experiments, which were conducted (both in terms of stimulation and use of the recording electrodes) in accordance with the Declaration of Helsinki and were approved by the University of Bradford Ethics Committee.

3. RESULTS

A. Morphology of the Transient S-cone ERG in Normal Trichromats

Figure 2 shows ERGs obtained from 16 trichromats in response to a silent substitution S-cone isolating stimulus with a square-wave temporal profile comprising an onset (i.e., S-cone excitation increment) duration of 250 ms and a 250 ms offset (S-cone excitation decrement) period. The S-cone ERG elicited by this

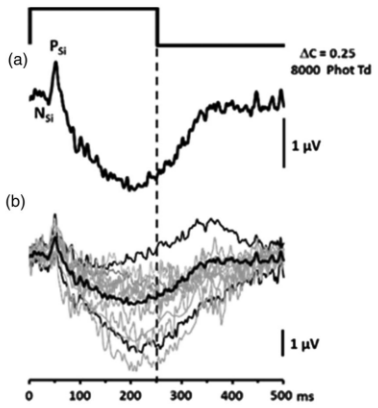

Fig. 2. (a) The group-averaged ($n = 16$) S-cone ERG. The onset response consists of an initial negative peak (N_{Si}) followed by a positive component (P_{Si}) after which there is a large negativity. At stimulus offset there is no discernible d-wave, and the response returns to baseline levels. (b) To illustrate the response variability across the subject cohort, individual (gray lines) and group-averaged (thick black line) ERGs elicited from 16 normal participants by a silent substitution S-cone-isolating stimulus are plotted. The thin black lines represent ±1 standard deviation (S.D.) from the mean. S-cone contrast = 0.25, and the stimulus had a retinal illuminance of 8000 photopic trolands.

stimulus has a waveform with an initial negative a-wave (which we have termed N_{Si}), which has a peak implicit time of 31.36 ms (s.d. = 5.95 ms). This negativity is followed by a b-wave component (termed here P_{Si}) with a peak implicit time of 53.8 ms (s.d. = 5.36 ms). Following these main onset components, the S-cone ERG then appears to be dominated by a large negativity. Following stimulus offset, the S-cone ERG exhibits a slow recovery of the negativity back to baseline approximately 350 ms after the stimulus onset.

In order to compare the S-cone ERGs with responses derived from the other photoreceptor populations, Fig. 3 shows the group-averaged ($n = 16$) S-cone responses with those elicited by the L-cone, M-cone, and rod silent substitution stimuli. As can be observed, the ERGs from the four photoreceptor populations have different morphological features. The ERGs elicited using the S-cone-isolating stimuli have the smallest amplitudes compared to the other photoreceptors, with b-waves (P_{Si}) typically of the order of approximately 1 μV. There are also differences in terms of the peak implicit times of the main onset response components. For example, the S-cone a- and b-waves (N_{Si} and P_{Si} in our nomenclature) are longer (31.36 ms and 53.8 ms, respectively) than those for the equivalent components [and in the L-cone isolated ERG {N_{Li} = 20.1 ms (s.d. = 1.449 ms)}; P_{Li} = 39.4 ms (s.d. = 3.34 ms)]. By comparison, the rod b-wave (P_{Ri}) has the longest implicit time at 85.95 ms (s.d. = 6.88 ms) and has no discernible a-wave under these recording conditions. Another distinctive feature of the S-cone

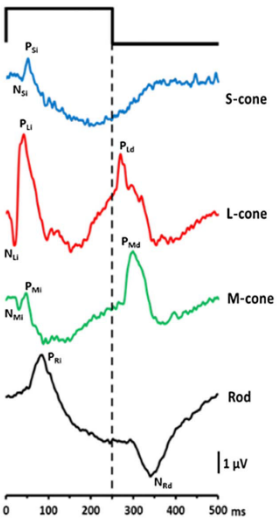

Fig. 3. Comparison of the ERGs elicited from the four classes of human photoreceptors using silent substitution stimuli. Each of the traces is group averaged ($n = 16$) from trichromatic observers. For all stimuli, photoreceptoral modulation was 0.25. The L-cone-, M-cone-, and S-cone-isolating stimuli resulted in a mean retinal illuminance of 8000 photopic Trolands. The rod-isolating stimulus resulted in a retinal illuminance of 63 photopic Trolands.

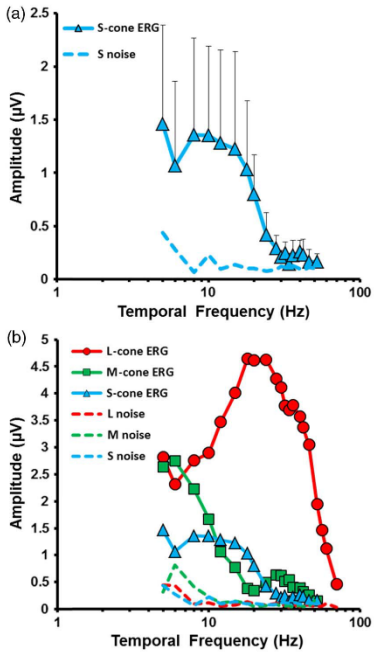

Fig. 4. (a) Temporal frequency response function for the fundamental of the S-cone ERG. The dashed line represents noise levels (see methods for definition). The data represent the group averaged responses ($n = 4$). (b) For comparison, the temporal frequency response functions for all cone-isolating stimuli (L-, M-, and S-cones) are plotted together. For all stimuli, photoreceptor modulation = 0.25. The retinal illuminance of the L-cone-, M-cone-, and S-cone-isolating stimuli = 1000 ph Td.

ERG is the lack of any prominent positive d-wave following stimulus offset. This contrasts with the L- and M-cone ERGs, which exhibit a clear offset response component (P_{Ld} and P_{Md}). The rod-mediated ERG appears to exhibit a prominent negative response (N_{Rd}) to stimulus offset.

B. Temporal Response Properties of the S-cone ERG

Figure 4 shows the ERG temporal response functions obtained using steady-state (sinusoidally modulated) L-cone-, M-cone-, and S-cone-isolating stimuli. The S-cone ERG function [Fig. 4(a)] is low-pass in appearance and response amplitude falls below our threshold criterion (<2.82 × noise) beyond 28 Hz. Figure 4(b) shows the S-cone ERG temporal response function along with those obtained for the L-cone- and M-cone-isolating stimuli under the same conditions. The L-cone ERG has the largest magnitude, and the function has a band-pass appearance with peak responses obtained between 20–25 Hz. Even at the highest stimulation rates tested (70 Hz), the L-cone ERG remains above the threshold criterion. The M-cone ERG exhibits response amplitudes at the lowest stimulation frequencies that are comparable to the L-cone responses. However, beyond 10 Hz, the M-cone ERG falls to a minimum value, and then the temporal response function exhibits a secondary peak at 30 Hz. The response falls below threshold above 46 Hz.

C. S-cone ERG in BCM and ESCS

ERG recordings from BCM patients in response to our silent substitution cone-isolating stimuli have the potential of providing us with a means of checking the suitability of these stimuli in eliciting selective responses from the different human photoreceptor classes. Individuals with BCM only have one operational population of cones contributing to photopic vision, the S-cones. Hence, the prediction is that S-cone ERGs should be preserved in these individuals but there would be negligible responses to L- and M-cone stimulation. Figure 5 shows the ERGs obtained from the two participants with BCM in response to L-, M-, and S-cone isolating stimuli, alongside the group averaged responses from normal trichromats to the same stimuli. In line with predictions, there is little or no discernible response to L- and M-cone stimulation. However, there does appear to be a response in both BCM patients to S-cone stimulation—consistent with the preserved S-cone

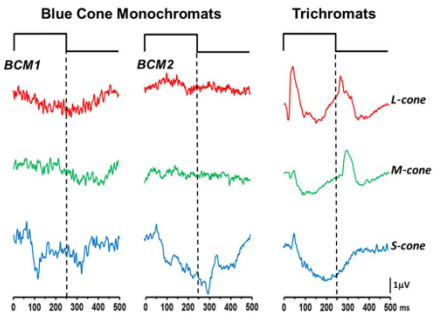

Fig. 5. L-, M-, and S-cone ERGs recorded from two blue cone monochromats (BCM1 and BCM2). Also shown are the group averaged ($n = 16$) responses from normal trichromatic observers to the same stimuli. For all stimuli, photoreceptoral modulation = 0.25. The L-cone-, M-cone-, and S-cone-isolating stimuli had a retinal illuminance of 8000 photopic Trolands.

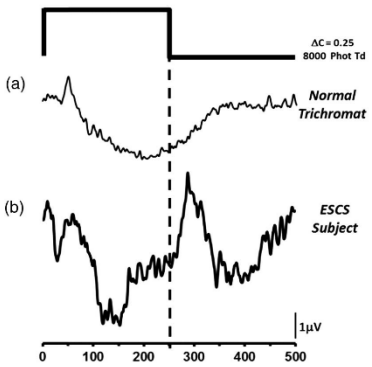

Fig. 6. (a) The group-averaged ($n = 16$) S-cone ERG obtained from normal trichromats. (b) The S-cone ERG obtained from a participant with enhanced S-cone syndrome (ESCS). All of the responses were elicited using a stimulus with S-cone contrast = 0.25 and a retinal illuminance of 8000 photopic trolands.

photoreceptors in this condition. In terms of the ERG response components to S-cone onset, there are similarities between the waveforms obtained from normal trichromats and those from the BCM patients. Both groups have ERGs with clear b-waves (P_{Si}) occurring between 50–60 ms post-stimulus onset. However, there are some differences between the responses from the normals and BCM patients. For example, the descending portion of the P_{Si} in the BCM ERGs exhibits a steep decline followed by a broad, low amplitude positivity. This is contrary to the typical response from the normal group, which consists of a gradual decline into a broad negativity. The offset response is also different, consisting of a more prominent d-wave compared to the slower recovery phase of the response in the trichromats.

Figure 6 shows the S-cone ERG elicited from a single participant with ESCS using the triple silent substitution stimulus. Also shown is the group averaged ERG response obtained from the normal trichromats to the same stimulus. This response is very different compared to the normal S-cone response from the trichromatic group. The first unique feature of the S-cone response in ESCS is the large a-wave and b-wave, with peak amplitudes of 1.41 μV and 1.28 μV, respectively. The ESCS a-wave is four times the amplitude of the a-wave obtained from the trichromatic group. The second feature is the d-wave (peak amplitude 2.56 μV) at stimulus offset, a feature that is not usually present in the normal S-cone ERG.

4. DISCUSSION

In this study we have used triple silent substitution stimuli to elicit ERGs that selectively reflect S-cone function in the normal trichromatic human retina. We have described the basic morphology of the S-cone response and have shown that the use of silent substitution stimuli enables the generation of responses from each of the rods, L-, and M-cone photoreceptor classes that have different morphological features and temporal frequency response characteristics. We have been able to validate the selective nature of our S-cone stimulation paradigm by the examination of responses from patients with genetically verified blue cone monochromatism (BCM). The preservation of the S-cone response in these subjects, coupled with the abolition of the L- and M-cone ERGs, is consistent with the fact that the S-cones are the only functional group of cone photoreceptors in BCM. In addition, the S-cone ERG in ESCS exhibits changes in response amplitude and waveform morphology that are consistent with previous reports [42,51,52]. Overall, these findings demonstrate that our triple silent substitution stimuli provide a clinically useful means via which we can assay human S-cone mediated visual function.

Strictly speaking, the use of triple silent substitution has not been previously employed to isolate the S-cone ERG. More commonly, double silent substitution stimuli have been employed with sufficiently high luminances to saturate the rod response [10,31,32]. The use of triple silent substitution stimuli, generated by a four-primary stimulator, offers the advantage of maintaining net excitation in all four photoreceptor types at a constant level. This negates the use of a high-luminance adapting light used to suppress the rod system, which can introduce post receptoral nonlinearities. This may be particularly relevant in the case of S-cone isolation as the S-cones and rods share a common post-receptoral pathway [53]. The S-cone ERG elicited by our paradigm is broadly consistent with previous results [7,10,28,32] and comprises a small a-wave with a larger b-wave. Overall, the S-cone ERG is of smaller amplitude than those generated by rod, L- and M-cone isolating stimuli of the same photoreceptoral contrast. The average peak implicit timings of the S-one ERG a- and b-wave components (31 ± 2 and 52 ± 2 ms, respectively) are longer than for other cone types and consistent with some earlier studies [7,10,27,28,45] but not others [26,30,32,54,55].

Where longer b-wave implicit times have been noted, it has been postulated that this is most likely to be related to rod intrusions [27]. However, some studies have shown that the S-cone ERG b-wave implicit time is up to 10 ms earlier that reported in this study [32]. Differences in stimulus intensities used across studies may partially explain these discrepancies, but intrusions from L- and M-cones have also been suggested as a reason for some of the earlier S-cone b-wave implicit times reported [32]. These intrusions are minimized in our measurements.

In contrast to L- and M-cone ERGs, the S-cone ERG elicited by our triple silent substitution method exhibits no obvious d-wave offset component in normal trichromats. This is consistent with previous S-cone ERG studies [10,28,30,32,56,57]. The absence of an offset d-wave response in the S-cone ERG has been traditionally interpreted as providing evidence for a lack of direct S-cone input to an OFF pathway [56,57]. This tended to corroborate the notion of a poorly established S-cone OFF pathway in the primate retina (e.g., Ref. [58]). In fact, the presence/absence of an S-cone offset response in the ERG has been previously employed as an indicator of S-cone isolation and a measure of L- or M-cone intrusion into the S-cone ERG [10,32,56]. However, subsequent anatomical studies have established the presence of an S-cone OFF pathway in the macaque, based on S-cone inputs to an OFF midget bipolar, which in turn are connected to OFF midget ganglion cells [59]. Although the S-OFF pathway has not been described in the human retina, it is postulated that a similar physiological substrate exists to convey S-off signals [60–63], presumably forming the basis of a mechanism for the detection of S-cone decrements which has been psychophysically established [64]. While this OFF midget bipolar, OFF midget ganglion cell circuitry might exist in the central fovea, in the retinal periphery OFF midget ganglion cells receive most of their input from L- and M-cones. Thus, S-cone OFF midget ganglion cells are something of a rarity in the peripheral retina [65]. This lack of access to an S-cone OFF pathway in the periphery may be the reason for the reduced d-wave offset response in our S-cone ERGs, which are generated by spatially extensive stimuli, which extend to a retinal eccentricity of approximately 60°–70°.

S-cone ERGs from patients diagnosed with BCM have previously been used to characterize S-cone responses that are free of intrusions from L- and M-cones [26,54,55]. The results from the participants with BCM presented in this study show a clear preservation of the S-cone ERG with abolished L- and M-cone mediated responses. This is an important finding as it provides validation of the selective nature of our cone-isolating stimuli. Nevertheless, while the morphology and timing of the onset b-waves (P_{Si}) are similar to the S-cone ERG elicited from normal trichromats, there are features of the S-cone responses in BCM that are clearly very different. First, the descending portion of the b-wave (P_{Si}) as it develops into the PhNR is steeper and larger compared to the gradual decline seen in the S-cone ERG elicited from the normal trichromats. Second, the response following the steep decline is positive compared to a gradual negative trough in the trichromats. A similar response was recorded in two patients with BCM using a chromatic adaptation paradigm [55]. Several studies in primates have shown that the second-order neurons, particularly hyperpolarizing bipolar cells and horizontal cells, contribute to the negative trough following the b-wave [66–68]. The presence of what clearly resembles an offset response in both BCM patients is unusual. The fact that this component is not present in the normal trichromats demonstrates that this is not an artifact of our methodology. Furthermore, the fact that the offset response was reproducible in both subjects, on two separate recording sessions, suggests that it is a genuine physiological response. Currently, we are unsure of its origins but speculate whether it may be related to an S-OFF pathway, where in the absence of functioning L- and M-cones in BCM, the S-OFF midget pathway is the only viable OFF mechanism present in these patients.

The S-cone ERG recorded from the participant with ESCS using the triple silent substitution stimulus also appears to exhibit morphological features consistent with those that have been previously described for this condition (e.g., Refs. [51,52,69]). ESCS is a rare inherited degenerative retinal condition that, in addition to other retinal changes, is associated with increased S-cone sensitivity [45] resulting from an increased number of S-cones in the retina compared to normals [42–44]. Although there are functional L- and M-cones, their contributions to the ERG are very much reduced [42,52]. A consequence of this S-cone domination of the retina is that individuals with ESCS exhibit supra-normal ERGs mediated largely by the S-cone system [42]. Consistent with this increase in S-cones, the response elicited from the ESCS subject using the S-cone-isolating triple silent substitution stimulus is of greater amplitude than that found in normals. In line with previous studies, there is a prominent, large amplitude a-wave component [42].

Another feature of the S-cone ERG recorded from the participant with ESCS that is not found in normal trichromats is a large positive d-wave component generated following stimulus offset. This has been previously reported in ESCS [51,52], and the presence of a prominent positive offset response forms a possible electrophysiological correlate of the re-organization of post-receptoral circuitry that is purported to take place in this condition [42,43]. As noted above, the normal retina S-cones in the central retina have connections with both ON- and OFF-bipolar neurons, while peripheral S-cones are largely restricted to ON-bipolars [65]. The presence of an OFF response in ESCS clearly suggests that the outputs of the more numerous S-cones have access to both ON and OFF response pathways just like L- and M-cones do in the normal trichromatic retina [70]. Given the highly disorganized retinal structure associated with this pathology, such re-organization of S-cone outputs remains a possibility [52]. Interestingly, the S-cone ERG offset response in the BCM subjects consists of an initial negative component, almost 180° out of phase with the OFF response observed in the ESCS participant, suggesting differences in post-receptoral re-organization across the two pathologies.

In addition to transient ERGs, we also recorded cone-isolating steady-state responses from L-, M-, and S-cones in normal trichromats. This was in an attempt to ascertain whether S-cone ERGs could be differentiated from L-cone- and M-cone-mediated responses on the basis of their temporal

frequency response characteristics. Each of the cone photoreceptor populations generated ERG temporal response functions with different features. The S-cone ERG exhibits a low-pass temporal frequency response function with a resolution limit lower than that obtained for either the L- or M-cone responses. This would appear to be in keeping with traditional views of the S-cone system, which characterize it as a temporally sluggish system [71,72] compared to vision mediated by the L- and M-cones. This reduced temporal resolution may reflect limitations on the S-cone signal imposed by an anatomically segregated processing pathway that has its origins in the retina [13,18,60] and is maintained in retino-cortical projections via the koniocellular processing pathway [73]. One theory that has been advanced is that the slow temporal responsiveness of the S-cone system is the result of response delays between ON and OFF responses at the ganglion cell level [74]. The fact that this temporal limitation is manifest in the steady-state ERG appears consistent with its imposition on the S-cone system at a relatively early retinal level.

In summary, we have demonstrated in this study that triple silent substitution stimuli provide an effective means via which we can selectively investigate S-cone function. The responses we have elicited from the S-cone population exhibit different morphological features and have different temporal frequency response characteristics compared to ERGs derived from L-cone, M-cone, and rod photoreceptors. Furthermore, in cases of retinal pathology, which either isolate or enhance S-cone function, the responses elicited by our stimuli provide an appropriate assay of the functional integrity of the S-cone system.

Funding. Deutsche Forschungsgemeinschaft (DFG) (KR1317/13-1); Bundesministerium für Bildung und Forschung (BMBF) (01DN14009).

Acknowledgment. N. R. A. P.'s participation was facilitated by the Greater Manchester Comprehensive Local Research Network.

REFERENCES

1. M. Marmor, A. Fulton, G. Holder, Y. Miyake, M. Brigell, and M. Bach, "ISCEV standard for full-field clinical electroretinography (2008 update)," Doc. Ophthalmol. **118**, 69–77 (2009).
2. J. Mollon, "A taxonomy of tritanopias," Doc. Ophthalmol. Proc. Ser. **33**, 87–101 (1982).
3. E. Zrenner, "Electrophysiological characteristics of the blue sensitive mechanism: test of a model of cone interaction under physiological and pathological conditions," Doc. Ophthalmol. Proc. Ser. **33**, 103–125 (1982).
4. D. Hood, N. Benimoff, and V. Greenstein, "The response range of the blue-cone pathways: a source of vulnerability to disease," Invest. Ophthalmol. Visual Sci. **25**, 864–867 (1984).
5. V. Greenstein, D. Hood, R. Ritch, D. Steinberger, and R. Carr, "S (blue) cone pathway vulnerability in retinitis pigmentosa, diabetes and glaucoma," Invest. Ophthalmol. Visual Sci. **30**, 1732–1737 (1989).
6. S. Yamamoto, M. Kamiyama, K. Nitta, T. Yamada, and S. Hayasaka, "Selective reduction of the S cone electroretinogram in diabetes," Br. J. Ophthalmol. **80**, 973–975 (1996).
7. K. Mortlock, Z. Chiti, N. Drasdo, D. Owens, and R. North, "Silent substitution S-cone electroretinogram in subjects with diabetes mellitus," Ophthalmic Physiol. Opt. **25**, 392–399 (2005).
8. A. Schatz, M. Fischer, K. Schommer, E. Zrenner, K. U. Bartz-Schmidt, F. Gekeler, and G. Willmann, "Attenuation of S-cone function at high altitude assessed by electroretinography," Vis. Res. **97**, 59–64 (2014).
9. W. Swanson, D. Birch, and J. Anderson, "S-cone function in patients with retinitis pigmentosa," Invest. Ophthalmol. Visual Sci. **34**, 3045–3055 (1993).
10. N. Drasdo, Y. Aldebasi, Z. Chiti, K. Mortlock, J. Morgan, and R. North, "The s-cone PHNR and pattern ERG in primary open angle glaucoma," Invest. Ophthalmol. Visual Sci. **42**, 1266–1272 (2001).
11. Y. Aldebasi, N. Drasdo, J. Morgan, and R. North, "S-cone, L + M-cone, and pattern, electroretinograms in ocular hypertension and glaucoma," Vis. Res. **44**, 2749–2756 (2004).
12. R. North, A. Jones, N. Drasdo, J. Wild, and J. Morgan, "Electrophysiological evidence of early functional damage in glaucoma and ocular hypertension," Invest. Ophthalmol. Visual Sci. **51**, 1216–1222 (2010).
13. D. Calkins, "Seeing with S cones," Prog. Retinal Eye Res. **20**, 255–287 (2001).
14. D. Hunt and L. Piechl, "S cones: evolution, retinal distribution, development, and spectral sensitivity," Visual Neurosci. **31**, 115–138 (2014).
15. J. Nathans, D. Thomas, and D. Hogness, "Molecular genetics of human color vision: the genes encoding blue, green, and red pigments," Science **232**, 193–202 (1986).
16. P. Ahnelt, C. Keri, and H. Kolb, "Identification of pedicles of putative blue sensitive cones in human and primate retina," J. Comp. Neurol. **293**, 39–53 (1990).
17. P. Ahnelt, H. Kolb, and R. Pflug, "Identification of a subtype of cone photoreceptor, likely to be blue sensitive, in the human retina," J. Comp. Neurol. **255**, 18–34 (1987).
18. D. Dacey, "Primate retina: cell types, circuits and color opponency," Prog. Retinal Eye Res. **18**, 737–763 (1999).
19. D. Williams, D. MacLeod, and M. Hayhoe, "Foveal tritanopia," Vis. Res. **21**, 1341–1356 (1981).
20. H. Hofer, J. Carroll, J. Neitz, M. Neitz, and D. Williams, "Organization of the human trichromatic cone mosaic," J. Neurosci. **25**, 9669–9679 (2005).
21. H. Smithson, "S-cone psychophysics," Visual Neurosci. **31**, 211–225 (2014).
22. P. Gouras, "Symposium on electrophysiology: electroretinography: some basic principles," Invest. Ophthalmol. Visual Sci. **9**, 557–569 (1970).
23. D. Van Norren and P. Padmos, "Human and macaque blue cones studied with electroretinography," Vis. Res. **13**, 1241–1254 (1973).
24. P. Padmos, D. van Norren, and J. Faijer, "Blue cone function in a family with an inherited tritan defect, tested with electroretinography and psychophysics," Invest. Ophthalmol. Visual Sci. **17**, 436–441 (1978).
25. P. Gouras and C. MacKay, "Electroretinographic responses of the short wavelength-sensitive cones," Invest. Ophthalmol. Visual Sci. **31**, 1203–1209 (1990).
26. P. Gouras, C. MacKay, and S. Yamamoto, "The human S-cone electroretinogram and its variation among subjects with and without L and M-cone function," Invest. Ophthalmol. Visual Sci. **34**, 2437–2442 (1993).
27. G. Arden, J. Wolf, T. Berninger, C. Hogg, R. Tzekov, and G. Holder, "S-cone ERGs elicited by a simple technique in normals and in tritanopes," Vis. Res. **39**, 641–650 (1999).
28. Z. Chiti, R. North, K. Mortlock, and N. Drasdo, "The S-cone electroretinogram: a comparison of techniques, normative data and age-related variation," Ophthal. Physiol. Opt. **23**, 370–376 (2003).
29. O. Estevez and H. Spekreijse, "The 'silent substitution' method in visual research," Vis. Res. **22**, 681–691 (1982).
30. M. Sawusch, J. Pokorny, and V. Smith, "Clinical electroretinography for short wavelength sensitive cones," Invest. Ophthalmol. Visual Sci. **28**, 966–974 (1987).
31. H. Scholl and J. Kremers, "Electroretinograms in S-cone monochromacy using S-cone and rod isolating stimuli," Color Res. Appl. **26**, S136–S139 (2001).
32. J. Kuchenbecker, S. Greenwald, M. Neitz, and J. Neitz, "Cone-isolating ON-OFF electroretinogram for studying chromatic pathways in the retina," J. Opt. Soc. Am. A **31**, A208–A213 (2014).

33. J. Nathans, T. Piantanida, R. Eddy, T. Shows, and D. Hogness, "Molecular genetics of inherited variation in human color vision," Science **232**, 203–210 (1986).
34. J. Nathans, C. Davenport, I. Maumenee, R. Lewis, J. Hejtmancik, M. Litt, E. Lovrien, R. Weleber, B. Bachynski, and F. Zwas, "Molecular genetics of human blue cone monochromacy," Science **245**, 831–838 (1989).
35. J. Nathans, I. H. Maumenee, E. Zrenner, B. Sadowski, L. T. Sharpe, R. A. Lewis, E. Hansen, T. Rosenberg, M. Schwartz, and J. R. Heckenlively, "Genetic heterogeneity among blue-cone monochromats," Am. J. Human Genet. **53**, 987–1000 (1993).
36. M. Michaelides, D. Hunt, and A. Moore, "The cone dysfunction syndromes," Br. J. Ophthalmol. **88**, 291–297 (2004).
37. M. Michaelides, S. Johnson, M. Simunovic, K. Bradshaw, G. Holder, J. Mollon, and A. Moore, "Blue cone monochromatism: a phenotype and genotype assessment with evidence of progressive loss of cone function in older individuals," Eye **19**, 2–10 (2005).
38. J. Gardner, M. Michaelides, G. Holder, N. Kanuga, T. Webb, J. Mollon, A. Moore, and A. Hardcastle, "Blue cone monochromacy: causative mutations and associated phenotypes," Mol. Vision **15**, 876–884 (2009).
39. E. Berson, M. Sandberg, B. Rosner, and P. Sullivan, "Color plates to help identify patients with blue cone monochromatism," Am. J. Ophthalmol. **95**, 741–747 (1983).
40. S. Jacobson, M. Marmor, C. Kemp, and R. Knighton, "SWS (blue) cone hypersensitivity in a newly identified retinal degeneration," Invest. Ophthalmol. Visual Sci. **31**, 827–838 (1990).
41. U. Kellner, E. Zrenner, B. Sadowski, and M. Foerster, "Enhanced S cone sensitivity syndrome: long-term follow-up, electrophysiological and psychophysical findings," Clin. Vis. Sci. **8**, 425–434 (1993).
42. D. Hood, A. Cideciyan, A. Roman, and S. Jacobson, "Enhanced S cone syndrome: evidence for an abnormally large number of S cones," Vis. Res. **35**, 1473–1481 (1995).
43. V. Greenstein, Q. Zaidi, D. Hood, B. Spehar, A. Cideciyan, and S. Jacobson, "The enhanced S cone syndrome: an analysis of receptoral and post-receptoral changes," Vis. Res. **36**, 3711–3722 (1996).
44. C. Ripamonti, J. Aboshiha, B. Henning, P. Sergouniotis, M. Michaelides, A. Moore, A. Webster, and A. Stockman, "Vision in observers with enhanced S-Cone syndrome: an excess of S-Cones but connected mainly to conventional S-Cone pathways," Invest. Ophthalmol. Vis. Sci. **55**, 963–976 (2014).
45. M. Marmor, S. Jacobson, M. Forester, U. Kellner, and R. Weleber, "Diagnostic findings of a new syndrome with night blindness, maculopathy, and enhanced S cone sensitivity," Am. J. Ophthalmol. **110**, 124–134 (1990).
46. A. Shapiro, J. Pokorny, and V. Smith, "Cone-rod receptor spaces with illustrations that use CRT phosphor and light-emitting-diode spectra," J. Opt. Soc. Am. A **13**, 2319–2328 (1996).
47. A. Stockman, D. MacLeod, and N. Johnson, "Spectral sensitivities of the human cones," J. Opt. Soc. Am. A **10**, 2491–2521 (1993).
48. G. Wyszecki and W. Stiles, *Color Science; Concepts and Methods, Quantitative Data and Formulae*, 2nd ed. (Wiley, 1982).
49. J. Maguire, N. Parry, J. Kremers, D. Kommanapalli, I. Murray, and D. McKeefry, "Rod electroretinograms elicited by silent substitution stimuli from the light adapted human eye," Transl. Vis. Sci. Technol. **5**, 13 (2016), doi: 10.1167/tvst.5.4.13.
50. T. Meigen and M. Bach, "On the statistical significance of electrophysiological steady-state responses," Doc. Ophthalmol. **98**, 207–232 (1999).
51. A. Román and S. Jacobson, "S cone-driven but not S cone-type electroretinograms in the enhanced S cone syndrome," Exp. Eye Res. **53**, 685–690 (1991).
52. I. Audo, M. Michaelides, A. Robson, M. Hawlina, V. Vaclavik, J. Sandbach, M. Neveu, C. Hogg, D. Hunt, A. Moore, A. Bird, A. Webster, and G. Holder, "Phenotypic variation in enhanced S-cone syndrome," Invest. Ophthalmol. Visual Sci. **49**, 2082–2093 (2008).
53. G. Field, M. Greschner, J. Gauthier, C. Rangel, J. Shlens, A. Sher, D. Marshak, A. Litke, and E. Chichilnisky, "High-sensitivity rod photoreceptor input to the blue-yellow color opponent pathway in macaque retina," Nat. Neurosci. **12**, 1159–1164 (2009).
54. M. Horiguchi, Y. Miyake, M. Kondo, S. Suzuki, A. Tanikawa, and H. Koo, "Blue light-emitting diode built-in contact lens electrode can record human S-cone electroretinogram," Invest. Ophthalmol. Visual Sci. **36**, 1730–1732 (1995).
55. S. Simonsen and T. Rosenberg, "Reappraisal of a short-wavelength-sensitive (S-cone) recording technique in routine clinical electroretinography," Doc. Ophthalmol. **91**, 323–332 (1995).
56. E. Zrenner and P. Gouras, "Blue-sensitive cones of the cat produce a rod-like electroretinogram," Invest. Ophthalmol. Visual Sci. **18**, 1076–1081 (1979).
57. H. Evers and P. Gouras, "Three cone mechanisms in the primate electroretinogram: two with, one without off-center bipolar responses," Vis. Res. **26**, 245–254 (1986).
58. F. De Monasterio, "Asymmetry of on- and off-pathways of blue-sensitive cones of the retina of macaques," Brain Res. **166**, 39–48 (1979).
59. K. Klug, S. Herr, I. Ngo, P. Sterling, and S. Schein, "Macaque retina contains an S-cone OFF midget pathway," J. Neurosci. **23**, 9881–9887 (2003).
60. D. Dacey, J. Crook, and O. Packer, "Distinct synaptic mechanisms create parallel S-ON and S-OFF color opponent pathways in the primate retina," Vis. Neurosci. **31**, 139–151 (2014).
61. D. Dacey, L. Wool, O. Packer, and R. Wong, "Confirmation of an S-OFF midget ganglion cell pathway using serial block-face scanning electron microscopy," J. Vis. **17**(7), 58 (2017).
62. A. Sher and S. Devries, "A non-canonical pathway for mammalian blue-green color vision," Nat. Neurosci. **15**, 952–953 (2012).
63. S. Chen and W. Li, "A color-coding amacrine cell may provide a blue-Off signal in a mammalian retina," Nat. Neurosci. **15**, 954–956 (2012).
64. K. Shinomori and J. Werner, "Aging of human short-wave cone pathways," Proc. Natl. Acad. Sci. USA **109**, 13422–13427 (2012).
65. K. Miyagishima, U. Grunert, and W. Li, "Processing of S-cone signals in the inner plexiform layer of the mammalian retina," Vis. Neurosci. **31**, 153–163 (2014).
66. P. Sieving, K. Murayama, and F. Naarendorp, "Push-pull model of the primate photopic electroretinogram: a role for hyperpolarizing neurons in shaping the b-wave," Vis. Neurosci. **11**, 519–532 (1994).
67. N. Rangaswamy, S. Shirato, M. Kaneko, B. Digby, J. Robson, and L. Frishman, "Effects of spectral characteristics of Ganzfeld stimuli on the photopic negative response (PhNR) of the ERG," Invest. Ophthalmol. Visual Sci. **48**, 4818–4828 (2007).
68. J. Schallek, R. Kardon, Y. Kwon, M. Abramoff, P. Soliz, and D. Ts'o, "Stimulus-evoked intrinsic optical signals in the retina: pharmacologic dissection reveals outer retinal origins," Invest. Ophthalmol. Visual Sci. **50**, 4873–4880 (2009).
69. H. Newman, S. Blumen, I. Braverman, R. Hanna, B. Tiosana, I. Perlman, and T. Ben-Yosef, "Homozygosity for a recessive loss-of-function mutation of the NRL gene is associated with a variant of enhanced S-cone syndrome," Invest. Ophthalmol. Visual Sci. **57**, 5361–5371 (2016).
70. V. Bonilha, G. Fishman, M. Rayborn, and J. Hollyfield, "Retinal pathology of a patient with Goldmann-Favre syndrome," Ophthalmic Genet. **30**, 172–180 (2009).
71. G. S. Brindley, J. J. Du Croz, and W. A. Rushton, "The flicker fusion frequency of the blue-sensitive mechanism of colour vision," J. Physiol. **183**, 497–500 (1966).
72. J. J. Wisowaty and R. M. Boynton, "Temporal modulation sensitivity of the blue mechanism: measurements made without chromatic adaptation," Vis. Res. **20**, 895–909 (1980).
73. S. H. Hendry and R. C. Reid, "The koniocellular pathway in primate vision," Annu. Rev. Neurosci. **23**, 127–153 (2000).
74. E. J. Chichilnisky and D. A. Baylor, "Receptive-field microstructure of blue-yellow ganglion cells in primate retina," Nat. Neurosci. **2**, 889–893 (1999).